A Numerical Side Impact Model to Investigate Thoracic Injury in Lateral Impact Scenarios

By

Brett M. Campbell

A thesis
presented to the University of Waterloo
in fulfillment of the
thesis requirement for the degree of

Master of Applied Science

in

Mechanical Engineering

Waterloo, Ontario, Canada, 2009

I hereby declare that I am the sole author of this thesis. This is a true copy of the thesis, including any required final revisions as accepted by my examiners.

I understand that my thesis may be made electronically available to the public.

Brett M. Campbell

Abstract

Although there have been tremendous improvements in crash safety there has been an increasing trend in side impact fatalities, rising from 30% to 37% of total fatalities from 1975 to 2004 (NHTSA, 2004). Between 1979 and 2004, 63% of AIS≥4 injuries in side impact resulted from thoracic trauma (NHTSA, 2004). Lateral impact fatalities, although decreasing in absolute numbers, now comprise a larger percentage of total fatalities. Safety features are typically more effective in frontal collisions compared to side impact due to the reduced distance between the occupant and intruding vehicle in side impact collisions. Therefore, an increased understanding of the mechanisms governing side impact injury is necessary in order to improve occupant safety in side impact auto crash.

This study builds on an advanced numerical human body model with focus on a detailed thoracic model, which has been validated using available post mortem human subject (PMHS) test data for pendulum and side sled impact tests (Forbes, 2005). Crash conditions were investigated through use of a modified side sled model used to reproduce the key conditions present in full scale crash tests. The model accounts for several important factors that contribute to occupant response based on the literature. These factors are; the relative velocities between the seat and door, the occupant to door distance, the door shape and compliance.

The side sled model was validated by reproducing the crash conditions present in FMVSS 214 and IIHS side impact tests and comparing the thoracic compression, velocity, and Viscous Criterion (VC) response determined by the model to the response of the ES-2 dummy used in the crash tests. Injury was predicted by evaluating VCmax, selected for its ability to predict rate-sensitive soft tissue injury during thoracic compression (Lau & Viano, 1986). The Ford Taurus FMVSS 214 and Nissan Maxima IIHS tests were selected from side impact crash test data found in the NHTSA database

because they included factors not present in standard side impact test procedures. These factors were; the presence of door accelerometers used to provide input velocities to the side impact model and the use of a ES-2 (rather than the SID) to facilitate comparison of VC response to the human body model. Also, the two crash test procedures (FMVSS 214 & IIHS) were selected to ensure accurate side impact model response to different impact scenarios. The side impact model was shown to closely reproduce the timing and injury response of the full-scale FMVSS 214 side impact test of a Ford Taurus, as well as the IIHS side impact test of a Nissan Maxima.

The side impact model was then used to investigate the effects of door to occupant spacing, door velocity profile, armrest height, seat foam, restraint system, and arm position. It was found that the VCmax was controlled by both the first and second peaks typically found in door velocity profiles, but the effect of each varies depending on the situation.

This study found that VCmax was reduced by 73-88% when door intrusion was eliminated compared to the VC response incurred by an intruding door. Also, the presence of a deformable door based on physical geometry and material characteristics rather than a simplified rigid door reduced VCmax by 16% in this study.

The study on seat foam determined that significant effects on VC response can be made by modest adjustments in foam properties. Low stiffness seat foam was found to increase VCmax by 41% when compared to the VC response when using high stiffness foam.

Arm position has been proven to be a relevant factor in side impact crash. Positioning the arms parallel to the thorax, in the “down” position, caused a 42% increase in VCmax when compared to the VC response determined with the arms positioned at 45 degrees.

Finally, although restraint systems have limited influence on side impact crash safety compared to front and rear impacts, this study found that the presence of a pre-tensioning

restraint system reduced VCmax by 13% when compared to the VC response of an un-belted occupant.

It should be noted that the current study was limited to velocity profiles obtained from a specific FMVSS 214 test and therefore results and observations are restricted to the confines of the input conditions used. However, the side impact model developed is a useful tool for evaluating factors influencing side impact and can be used to determine occupant response in any side impact crash scenario when the appropriate input conditions are provided.

Acknowledgements

I would like to thank several people for their encouragement, support, and patience during the course of my Master's at the University of Waterloo.

I wish to thank my supervisor, Duane Cronin, for the opportunity he has presented to work in the field of crash safety and biomechanics. I appreciate your encouragement and guidance provided throughout my research. I would also like to thank Christopher Salisbury and Christian Kaufmann for their expertise and guidance in material testing.

I am grateful for the support of Dr. Yih-Charng Deng and General Motors of Canada Limited (GMCL), the Premier's Research Excellence Award (PREA), the Partners for the Advancement of Collaborative Engineering Education (PACE), the Ontario Graduate Scholarship (OGS) Program, the University of Waterloo, and the Department of Mechanical Engineering for their financial support during my studies.

I would like to thank my friends Cam, Katelyn, Tom, Leanne, Brent, and "the guys" for providing a link to reality over the course of my research. Your friendship will always be deeply appreciated. I would also like to thank my officemates, Ken and Chris, for their company in model tinkering and thesis writing.

I wish to thank Nicole for her constant motivation and support. I am truly grateful for your unwavering encouragement in all my endeavors.

Finally, I would like to thank my parents, Harry and Diane, as well as my sisters, Jenna and Breanne, who endlessly encourage me in everything I do. I am eternally grateful for your support, encouragement, and patience, without which, my accomplishments would not have been possible.

Thank you.
B.M.C

Table of Contents

List of Figures

List of Tables

List of Acronyms and Symbols

Acronyms:

AAAM	Association for the Advancement of Automotive Medicine
AD	Door to Occupant Distance
AIS	Abbreviated Injury Scale
ATD	Anthropometric Test Devices
BioSID	Bio Side Impact Dummy
EEVC	European Experimental Vehicles Committee
EuroSID	European Side Impact Dummy
FEA	Finite Element Analysis
FEM	Finite Element Model
FMVSS	Federal Motor Vehicle Safety Standard
GM	General Motors
H-Model	Human Body Model
HUMOS	Human Model for Safety
IIHS	Insurance Institute for Highway Safety
ISO	International Standards Organization
MADYMO	MAthematical DYnamic MOdels
MAIS	Maximum Abbreviated Injury Scale
MDB	Moving Deformable Barrier
NHTSA	National Highway Traffic Safety Administration
PMHS	Post Mortem Human Subject
PSHPB	Polymeric Split Hopkinson Pressure Bar
SID	Side Impact Dummy
TTI	Thoracic Trauma Index
VC	Viscous Criteria
VIP	Very Important People
WSU	Wayne State University
WorldSID	World Side Impact Dummy

Symbols:

C(t)	Normalized Chest Compression
Mass	Subject Mass
M_{std}	Standard mass of 50^{th} percentile male (75 kg)
RIBY	Max Absolute Value of Rib on Struck Side in Lateral Direction
T12Y	Max Absolute Value of the Twelfth Thoracic Vertebrae in the Lateral Direction
V(t)	Velocity Response

-- CHAPTER 1 --

Introduction

1.1 Background

Automotive safety research is a relatively new area of study that has become of primary interest to automotive designers over the last 40 years. The high number of injuries and fatalities incurred in auto crash has led to a considerable amount of research in order to improve safety and minimize the substantial societal costs associated with automotive collisions.

Researching human trauma at the levels experienced in auto crash is a difficult task as it cannot be performed with live human subjects. As a result, researchers began to evaluate injury mechanisms and tolerances by subjecting post mortem human subjects (PMHS) to a variety of impact conditions. These tests produced valuable insight and provided the basis for several injury criteria. However, PMHS testing has a wide range of variability and limitations. PMHS testing provides researchers with a test subject that is both geometrically and mechanically accurate. However, due to the destructive nature of the impact conditions, PMHS are often irreversibly damaged and cannot be reused in subsequent tests. Therefore, researchers are often required to perform experiments on several PMHS that vary in height, mass, and age, thus introducing a significant degree of inconsistency between test subjects.

In order to minimize the challenges present in PMHS testing, researchers began to develop Anthropomorphic Test Devices (ATD's) capable of producing human body response in a representative and repeatable manner. Currently ATD's are used in crash testing to assess vehicle safety under a variety of impact conditions. ATD's provide a consistent and reusable test subject standardized for use in side impact (EuroSID, ES-2, SID, and SID II), rear impact (RID), and frontal impact conditions (Hybrid III). However, crash tests performed have a high cost associated with them as they often involve the destruction of the vehicle.

Automotive research is a challenging field due to the complexity and cost associated with full-scale vehicle testing. Recent efforts have focused on the development of advanced finite element models of vehicles and occupants capable of reproducing the response present in crash scenarios in order to provide insight into injury under traditional, as well as non-traditional loading.

This thesis provides an overview of thoracic anatomy, injury criteria, side impact test methodologies, and the developments in crash safety research that has led up to this study.

1.2 Justification of Work

The total economic cost of automotive collisions in the United States in 2000 was $230.6 billion dollars (Blincoe et al., 2000). These figures include the lifetime economic cost for each fatality & injury, lost productivity, property damage, medical costs, travel delays, legal costs, and emergency services. Medical costs as a direct result of injuries were $32.6 billion dollars and lost workplace productivity costs totaled $61 billion dollars, representing 14% and 26% of the total cost respectively. The total costs are approximately 2.3% of the U.S Gross Domestic Product.

The introduction of safety systems such as seatbelts and airbags has greatly reduced the number of fatalities and serious injuries, as well as the associated costs. Blincoe et al. suggest that the use of safety belts saved 135,000 lives and prevented 3.8 million serious nonfatal injuries between 1975 and 2000, saving $585 billion dollars in total.

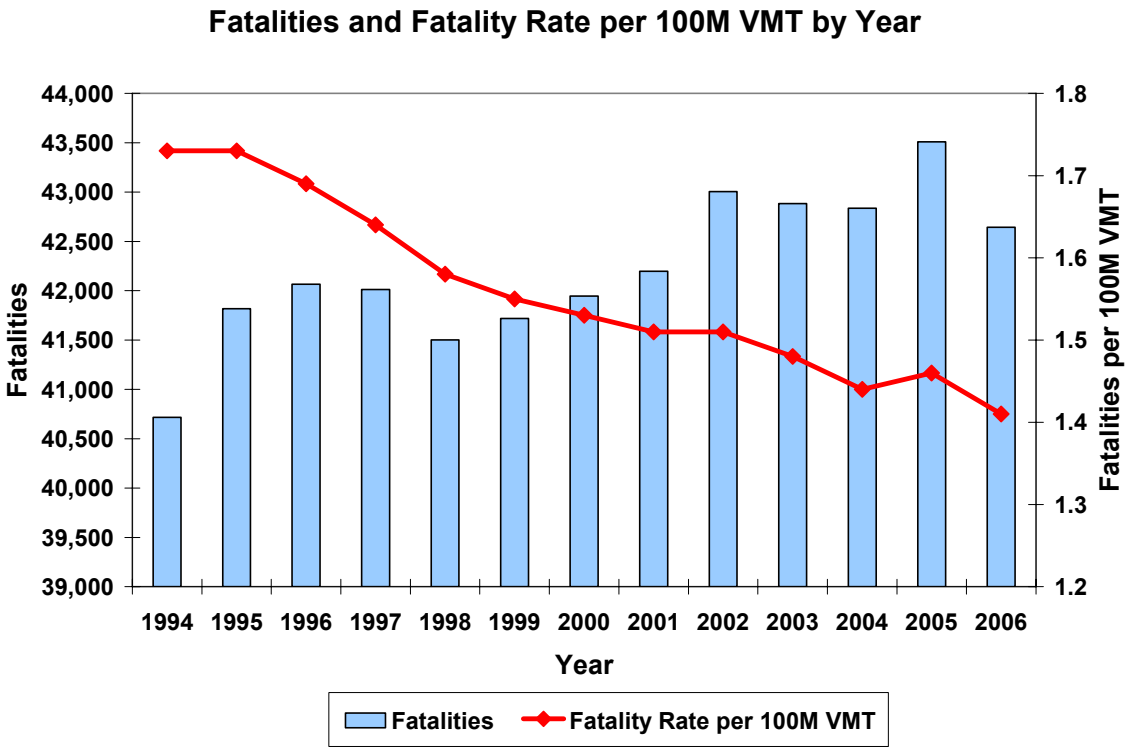

Figure 1.1 US Fatalities and Fatality Rate by Year (NHTSA, 2006)

Although there have been tremendous improvements in crash safety there is an increasing trend in side impact fatalities, rising from 30% to 37% of total fatalities from 1975 to 2004 (Figure 1.2) (NHTSA, 2004). Safety features such as seat belts and airbags are far more effective in frontal collisions than in side impact due to the small distance between the occupant and intruding vehicle in side impact collisions. Lateral impact fatalities, although decreasing in absolute numbers, now comprise a larger percentage of total fatalities.

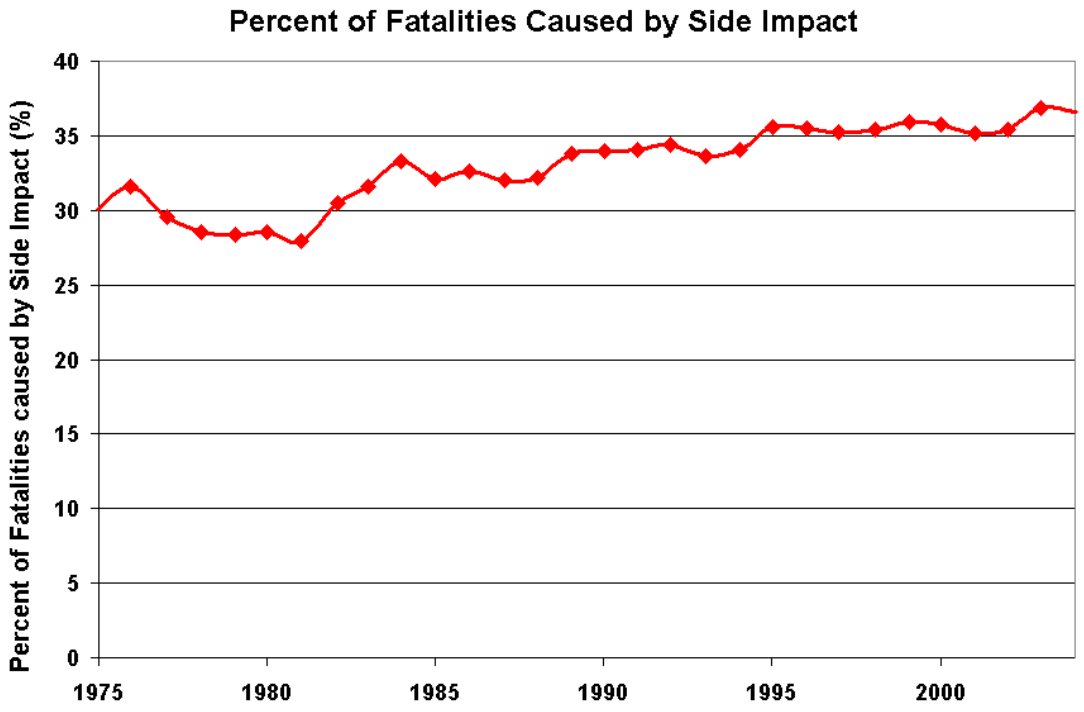

Figure 1.2 Percent of Fatalities Caused by Side Impact (NHTSA, 2004)

Finally, between 1979 and 2004, 63% of AIS≥4 injuries were caused by thoracic trauma (NHTSA, 2004). The substantial loss of life, as well as high economic costs associated with side impact crash demands further research in the area. Understanding side impact crash and the factors influencing thoracic trauma may lead to improved safety features and a decrease in fatalities and injuries.

1.3 Research Goals and Approach

This research was intended to provide a detailed understanding of thoracic trauma resulting from side impact crash using a previously developed numerical human body model (Forbes, 2005; Chang, 2001; Deng et al., 1999). The first goal of this research was to develop and validate a side impact model capable of reproducing the conditions present in full scale crash testing. The second goal of this research was to perform a parametric study varying conditions in the side impact model to provide an understanding of loading and its effect on thoracic trauma in side impact collisions.

Chapter 2 provides the background information prerequisite to this study, including the biomechanics of thoracic trauma, thoracic injury criteria, history of ATD's and numerical human body models, and side impact test methods. The development and validation of the numerical human body model used in this study is discussed in Chapter 3. The development of the side impact model is presented in Chapter 4. This chapter includes seat model development and foam characterization for varying rates of strain, door model development, and restraint system development. Chapter 5 presents the validation of the side impact model by applying input conditions present in two full scale crash tests. Input conditions for the side impact model were obtained from the NHTSA database for two full scale side impact tests; a FMVSS 214 test of a Ford Taurus and an IIHS test of a Nissan Maxima. Validation of the side impact model presented was performed by integrating the detailed human body model in the side impact simulation and comparing the thoracic response obtained to that found in the full scale crash tests.
Chapter 6 presents the results of the parametric study performed to investigate the effect of door to occupant distance, door intrusion velocity profile, seat foam, restraint systems, arm placement, and armrest height on thoracic trauma. Finally, Chapter 7 presents the conclusions found from the parametric study and recommendations for future research.

-- CHAPTER 2 --

Literature Review

2.1 Introduction

Investigating thoracic trauma in side impact automotive collisions is a topic of considerable complexity. First, there is a required understanding of the crash conditions; this includes vehicle velocity-time profiles, door intrusion velocity-time profiles, door-to-occupant offset, and door stiffness. Velocity profiles can be determined from the integration of accelerometer data obtained in side impact crash tests performed by the National Highway Traffic Safety Administration (NHTSA). The literature has shown that there is a complex relationship between thoracic trauma and door intrusion characteristics. Second, an understanding of thoracic response and the mechanisms governing injury is vital. Several injury criteria have been developed to estimate injury using globally measurable responses (Forbes, 2005). These injury criteria were developed by researchers that correlated specific levels of trauma to corresponding, typically simplified, load conditions.

The intent of this chapter is to introduce the prerequisite information necessary to understand the relevance of side impact collision research and the methodology used to further understand thoracic trauma in side impact scenarios. Also, current methods of side impact crash testing will be discussed, along with various injury criteria and thresholds.

2.2 Biomechanics of Thoracic Trauma

Thoracic trauma is a frequent occurrence in automotive collisions, ranking second only to head injury in terms of overall fatalities and serious injuries experienced (Nahum & Melvin, 2002). Injury to the human body can be induced in a number of ways, but they often possess the common mechanism of deforming biological tissues beyond their recoverable limit to produce anatomical damage (Viano et al., 1989a). Blunt trauma sustained during an automotive crash can be a result of aggressive contact with the vehicle interior, including restraint systems, the steering wheel, instrument panel, door panel, and airbags (Nahum & Melvin, 2002). This section presents the thoracic anatomy and potential thoracic injuries that can be induced as a result of automotive collisions.

2.2.1 Anatomy of the Thorax

The thorax functions as the structure used to house and protect internal organs, while it is still compliant to allow for breathing. The thorax is described as the superior part of the trunk between the neck and the abdomen consisting of the rib cage and its contents (Moore & Dalley, 2006). The thoracic cavity houses the organs of the respiratory and cardiovascular systems and is bound by the diaphragm, separating the thoracic contents from the abdominal contents (Nahum & Melvin, 2002).

Thoracic Cage

The thoracic cage (Figure 2.1) includes 12 pairs of ribs, 12 thoracic vertebrae (T1 through T12), and the sternum. There are three types of ribs (Moore & Dalley, 2006):

- True (vertebrocostal) ribs (1^{st}-7^{th} ribs): attach directly to the sternum through their own costal cartilages.
- False (vertebrochondral) ribs (8^{th}, 9^{th}, and usually 10^{th} ribs): cartilages are connected to the cartilage of the rib above them; thus their connection with the sternum is indirect.
- Floating (vertebral, free) ribs (11^{th}, 12^{th}, and sometimes 10^{th}): rudimentary cartilages of these ribs do not connect even indirectly with the sternum; instead they end in the posterior abdominal musculature.

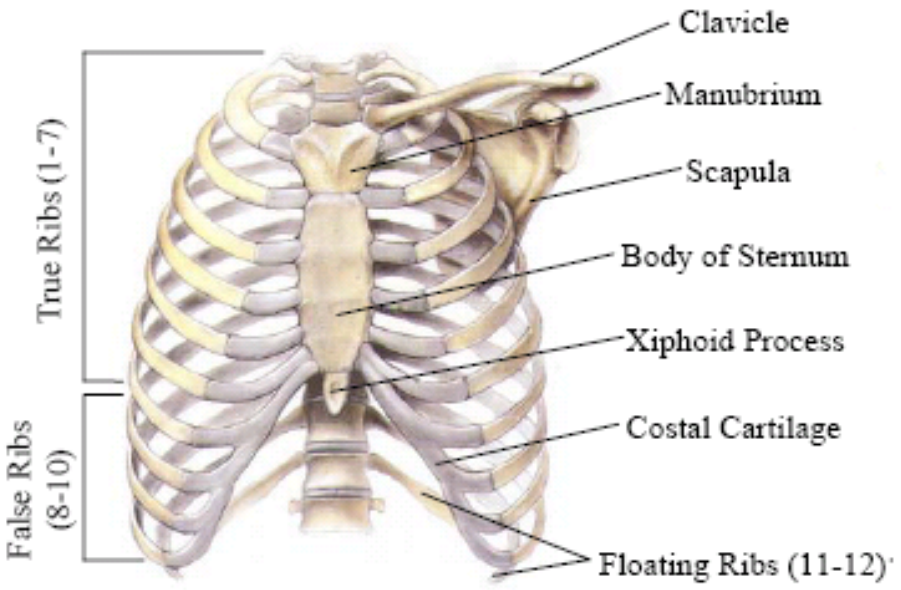

Figure 2.1 Thoracic Skeleton Anatomy (Moore & Dalley, 2006)

Lungs and Pleurae

The lungs function to oxygenate the blood by bringing air in close relation with the venus blood in the pulmonary capillaries (Moore & Dalley, 2006). Each lung is enclosed in a pleural sac consisting of two continuous membranes; the parietal and visceral pleura. The parietal pleura lines the pulmonary cavity including the thoracic wall, mediastinum, diaphragm, and encloses the structures in the middle of thorax. The visceral pleura is a membrane which closely covers the lung, enabling it to move freely on the parietal pleura (Moore & Dalley, 2006).

The left lung consists of two lobes, the upper and lower, while the right lung consists of three lobes, the upper, middle, and lower (Figure 2.2).

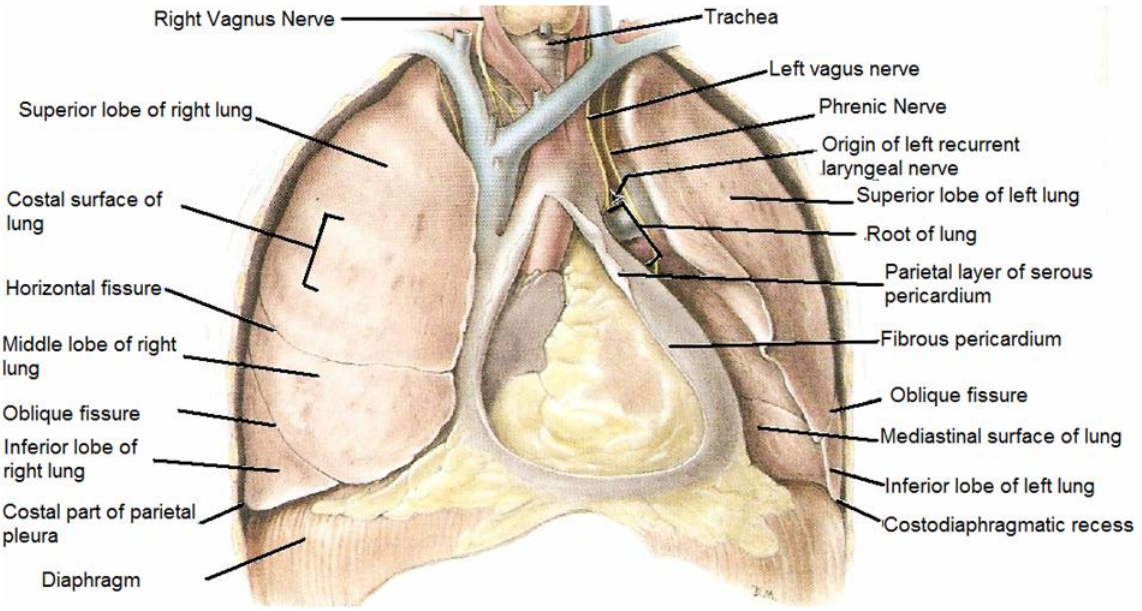

Figure 2.2 Anatomy of the Lungs (Moore & Dalley, 2006)

The mediastinum is the central region of the thoracic cavity containing the heart and its great vessels, thymus gland, esophagus and the lower portion of the trachea, the thoracic

duct and lymph nodes, as well as nerves passing through the thorax (Nahum & Melvin, 2002).

Heart and Great Vessels

The heart is a muscular organ found in the middle of the mediastinum that facilitates the circulation of blood throughout the body. The heart and the roots of its great vessels are covered by a fibroserous membrane known as the pericardium. The heart is divided into four chambers, left and right atria, and left and right ventricles (Figure 2.3). The right atrium receives the returning deoxygenated blood from the body which is then pumped by the right ventricle to the lungs through the pulmonary artery to be re-oxygenated. The oxygenated blood returns from the lungs to the left atrium and is pumped through the aorta to the rest of the body except the lungs (Nahum & Melvin, 2002).

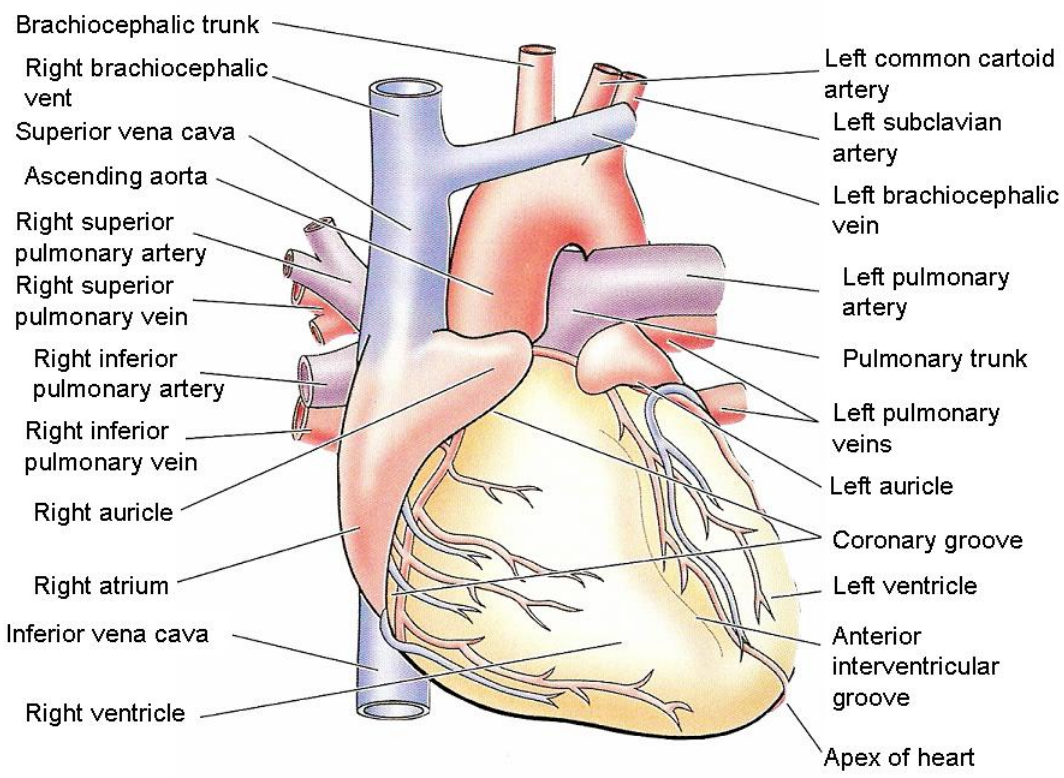

Figure 2.3 Anatomy of the Heart and its Great Vessels (Moore & Dalley, 2006)

2.3 Thoracic Injury

This section describes potential thoracic injuries that may be incurred by blunt impacts experienced in traffic accidents as a result of aggressive contact between an occupant and the steering wheel, dashboard, door, or other vehicle interior components. The injuries as a result of blunt trauma can be categorized as skeletal or soft tissue injury.

Rib fractures are common injuries in blunt trauma, but single fractures are relatively minor (Table 2.2). However, the severity of injury rises as the number of fractures and potential for complications increase. Ribs most likely fail in bending on the tensile side at the point of maximum curvature, but fracture is possible at any location (Nahum & Melvin, 2002). Multi-rib fracture may cause the thoracic cavity to lose its stability, a condition known as flail chest, which may result in respiratory problems.

Thoracic compression can result in lung contusion with or without the presence of rib fractures. Unlike rib fracture which depends highly on the amount of compression, lung contusion is a rate dependant injury (Nahum & Melvin, 2002). Rib fractures may also cause the laceration or perforation of the lung tissue resulting in hemothorax and pneumothorax. Hemothorax occurs when the pleural cavity fills with blood and pneumothorax when the pleural cavity fills with air. Hemopneumothorax is a condition that occurs when the pleural cavity fills with both blood and air.

Blunt impact may also result in the contusion and laceration of the heart. Contusion and laceration may occur due to a high level of compression, or high rate of loading. High rates of loading may also cause arrhythmia, fibrillation, or arrest (Nahum & Melvin, 2002).

2.3.1 The Abbreviated Injury Scale

The abbreviated injury scale (AIS) is an anatomically based injury scale and is the standard method used to classify human trauma as developed by the Association for the Advancement of Automotive Medicine (AAAM) (States, 1969; Nahum & Melvin, 2002). It was introduced as a means of quantifying injury sustained in automotive collisions, but is currently used in triage assessments during emergency medical situations, as well as research regarding injury prediction.

The AIS is a numerical rating system that ranges from 0 (no injury) to 6 (maximal/untreatable), where increasing AIS levels coincide with increased mortality (Nahum & Melvin, 2002). The scale is strictly used as an immediate indicator of injury and does not account for long term effects as a result of injuries. Table 2.1 and Table 2.2 show the ranking codes and typical skeletal and soft tissue injuries as categorized by the AIS respectively (AIS, 2005).

Table 2.1 AIS Ranking Codes (AIS, 2005)

AIS LEVEL	INJURY SEVERITY
1	Minor
2	Moderate
3	Serious (not life threatening)
4	Severe (life threatening but survivable)
5	Critical (survival uncertain)
6	Maximal (currently untreatable)

Table 2.2 Examples of Skeletal and Soft Tissue Injuries to the Thorax Ranked by the Abbreviated Injury Scale (AIS, 2005)

AIS LEVEL	THORACIC CAGE INJURY	THORACIC SOFT TISSUE INJURY
1	1 rib fracture	Heart Contusion
2	2 rib fractures sternum fracture	Pericardium Laceration Pleura Laceration Unilateral Lung Contusion, minor*
3	3 or more rib fractures Unilateral flail chest	Unilateral Lung Contusion, major* Bilateral Lung Contusion, minor* Unilateral Lung Laceration, minor* Hemothorax
4		Bilateral Lung Contusion, major* Bilateral Lung Laceration, minor* Aortic Laceration, minor Heart Contusion, major
5	Bilateral flail chest	Bilateral Lung Laceration, major* Tension Pneumothorax Aortic Laceration, major
6		Aortic Laceration with hemorrhage, not confined to

Note: Minor means < 1 lobe, Major means 1 or more lobes, at least on one side

2.4 Thoracic Injury Criteria

Thoracic injury criteria were developed to provide convenient indicators of thoracic trauma in order to relate globally available thoracic measures to injury risk. There have been many widely used injury criteria developed to predict and describe thoracic trauma. Often these approaches quantify injury by evaluating thoracic force, acceleration, velocity, and compression by comparing these measurements to levels of injury found during PMHS experiments. PMHS experiments are performed using a variety of methods. First, input conditions such as the impact velocity are controlled and measurable outputs such as chest deflection are recorded. Secondly, local injuries such as rib fractures and lung contusion are determined by autopsy and statistically correlated to the measured outputs. Thereby, allowing researchers to predict local injury using globally measured criteria. However, predicting actual human trauma using globally measurable factors is an extremely difficult task. Correlating global measurements to

specific levels of injury by use of PMHS experiments depends highly on the range and diversity of the subjects tested. That being said, there is evidence to support and discredit many of the common injury criteria for different impact scenarios.

This section describes several methods of predicting thoracic trauma using global measurements.

2.4.1 Acceleration Criteria

Initial developments of the acceleration injury criteria were developed by Stapp (1951,1957,1970) to reduce injury and the loss of life in military aviation. Stapp realized that travel at high speeds risked large decelerative forces applied over a relatively short duration, capable of fatally injuring an occupant. Stapp performed rocket-propelled sled tests on human and chimpanzee subjects to investigate the decelerative tolerance levels of restrained occupants (Stapp, 1957). The current human tolerance for severe thoracic injuries in frontal and lateral impacts is determined by the peak spinal acceleration sustained for a minimum of 3ms.

Eiband (1959) later analyzed the data provided by the Stapp tests and showed that the deceleration tolerance was reduced as the duration of exposure was increased. The thoracic acceleration tolerance of a stunt man diving from varying heights onto a thick mattress was investigated by Mertz and Gadd (1971). Their research concluded that no discomfort was experienced as a result of a 50g thoracic acceleration over a duration of 100ms (Mertz & Gadd, 1971; Nahum & Melvin, 2002). The authors also concluded that a 60g acceleration with a duration of 100ms be recommended as a thoracic tolerance level. This tolerance level was later introduced by the Federal Motor Vehicle Safety Standard (FMVSS) 208 as an occupant chest injury criterion in frontal collisions.

2.4.2 Force Criteria

Patrick et al. (1965) initiated force criterion research to improve the design of interior vehicle components, such as the steering wheel. Sled tests were performed using unrestrained PMHS to determine loads encountered in front impact collisions with velocities between 4.47 and 8.94 m/s (Figure 2.4). Padded load cells were used to determine the impact forces of the head, chest, and knees.

Figure 2.4 Frontal Sled Test (Patrick et al, 1965)

This data was used as the foundation in the design of an energy-absorbing steering wheel and produced initial force tolerance levels for loads applied to the sternum (3.3 kN) and applied to the chest and shoulders (8.0 kN) (Gadd & Patrick, 1968; Nahum & Melvin, 2002).

Pendulum tests were performed by Viano (1989) to determine the thoracic force tolerances under lateral loading. Through these experiments, Viano indicated a 25% probability of an AIS≥4 injury due to a lateral force of 5.5 kN.

2.4.3 Compression Criteria

Numerous blunt thoracic impact experiments (Patrick et al., 1967; Kroell et al., 1971, 1974) have been performed over the years using PMHS to better understand thoracic injury (Figure 2.5). Through these experiments, researchers have determined that the acceleration and force criterion do not correlate well with AIS (r=.524) and that chest compression was a better predictor of injury (r=.730) (Nahum & Melvin , 2002). Although acceleration and force criteria have been shown to predict injury for whole-body motions, they tend to underestimate the effects of local loading essential for understanding injury (Forbes, 2005). The equation relating AIS to chest compression is as follows:

$$AIS = -3.78 + 19.56C \qquad (2.1)$$

Where C is the chest deformation divided by the chest depth.

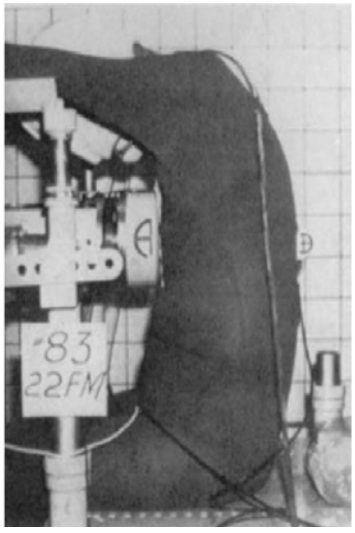

Figure 2.5 Frontal Blunt Thoracic Impact Test (Kroell et al., 1971)

The PMHS data obtained through experiments performed by Kroell et al. (1971,1974) were investigated by Neathery et al. (1974) and revealed that a maximum allowable compression of 75 mm was recommended to limit chest injury to AIS 3 with 25% probability (Nahum & Melvin, 2002).

The PMHS data was later analyzed by Viano and Lau (1988) using Logist analysis to produce more extensive injury tolerance levels. Their research revealed a 25% probability of severe (AIS≥4) injury at a compression of 35%, and a 50% probability of severe injury at a compression of 37.86% (Figure 2.6).

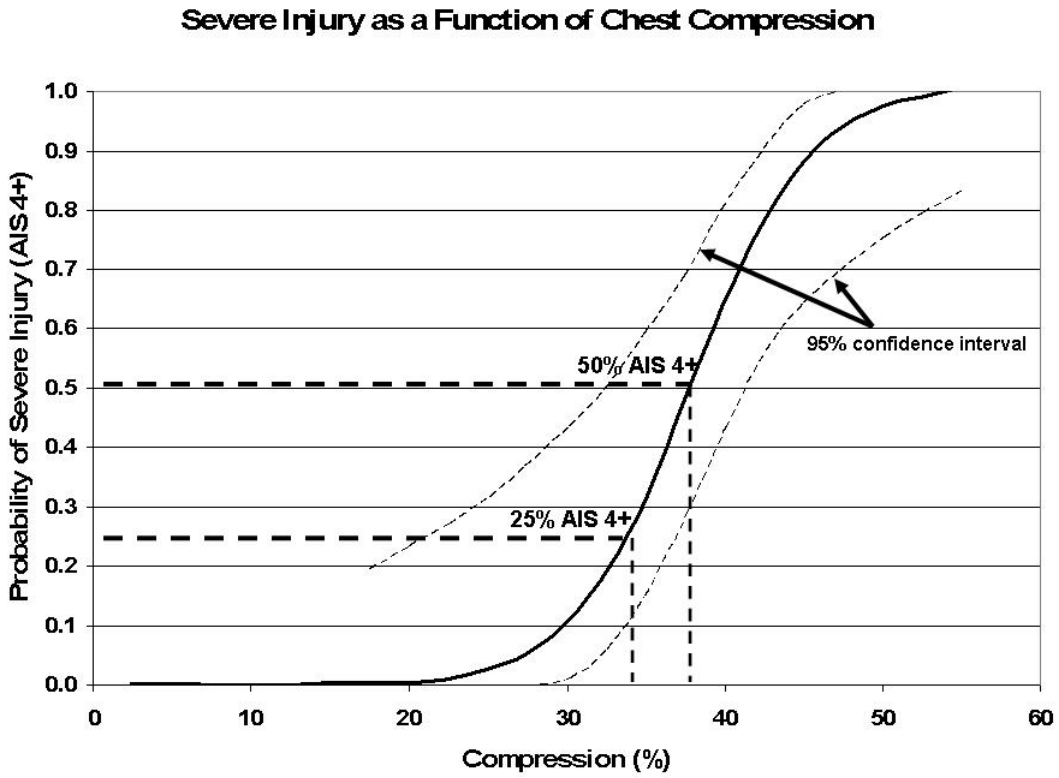

Figure 2.6 Severe injury risk as a function of chest compression (Viano & Lau, 1988)

Viano continued to develop a lateral compression criterion by subjecting PMHS to blunt lateral impacts at velocities of 4.5, 6.7, and 9.4 m/s with a 23.4 kg pendulum (Viano, 1989a). Through these experiments Viano et al. indicated a 25% probability of an AIS≥4 injury due to a lateral chest compression of 38.4%, and a 50% probability of AIS≥4 injury at a compression of 39.8% (Viano et al., 1989b). Current European Side Impact Standards impose a ES-2 half thoracic deflection threshold of 42mm, equivalent to 30% compression given a half thoracic chest width of 140mm.

The results of compression experiments are summarized in Table 2.3.

Table 2.3 Thoracic Compression Criteria (Forbes, 2005)

INJURY LEVEL	25% PROBABILITY	50% PROBABILITY
Frontal C_{max}		
AIS≥3 (Neathery et al. 1974)	34%	*
AIS≥3 (Viano & Lau, 1988)	35%	37.9%
Lateral C_{max}		
MAIS≥3 (Viano, 1989a)	*	33.9%
MAIS≥3 (Viano et al., 1989b)	38.4%	39.8%
*Data not provided.		

2.4.4 Thoracic Trauma Index

The Thoracic Trauma Index (TTI) is an acceleration based injury criterion developed using data from numerous side impact PMHS sled tests to measure thoracic response in side impact scenarios (Eppinger et al., 1984, Morgan et al., 1986). This injury criterion was adopted by FMVSS 214 and is the current criteria used to measure trauma for side impact protection. TTI relates spine and rib acceleration to injury, while considering the body mass of the subject as defined in the following equation (Morgan et al., 1986):

$$TTI = 1.4Age + .5(RIBY + T12Y)\frac{MASS}{M_{std}} \tag{2.2}$$

Where:

TTI = Thoracic Trauma Index

Age = Age of the test subject (in years)

RIBY = Max absolute value of rib acceleration on struck side in lateral direction

T12Y = Max absolute value of the twelfth thoracic vertebrae acceleration in the lateral direction

Mass = Subject mass

M_{std} = Standard mass of 50^{th} percentile male (75 kg)

Using data from PMHS side impact experiments, Morgan et al. (1986) developed the following curves summarizing injury severity versus TTI (Figure 2.7). The results of these experiments are further summarized in Table 2.4.

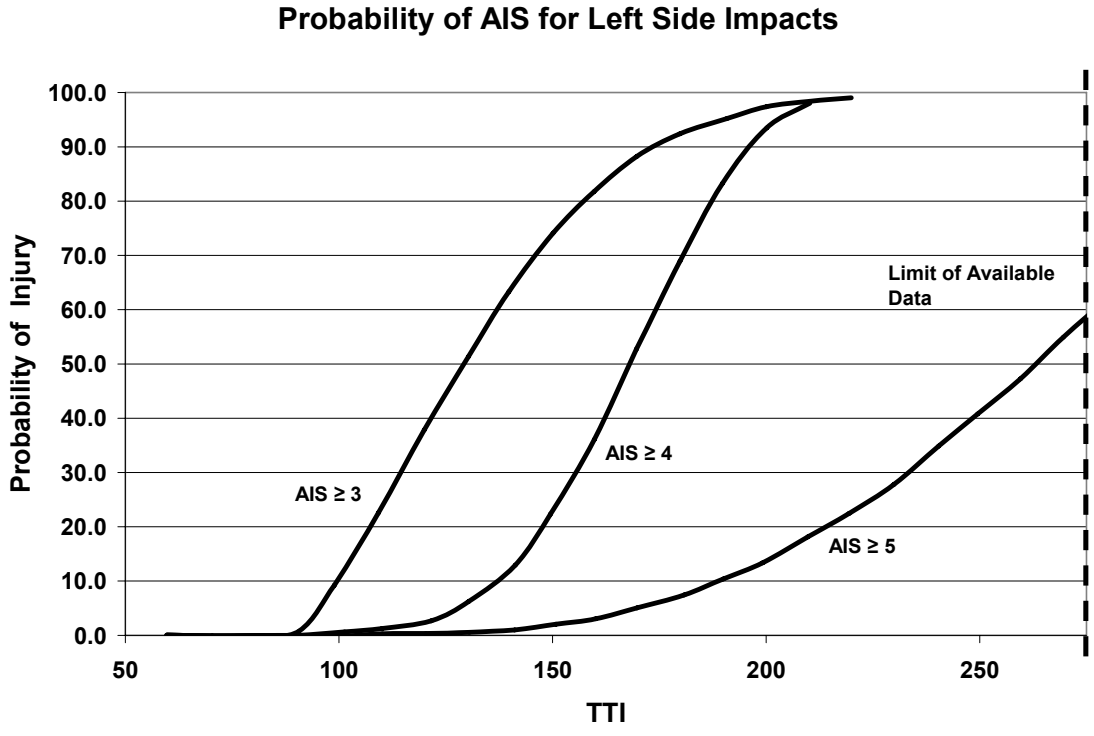

Figure 2.7 Probability of AIS for Left Side Impacts (Morgan et al., 1986)

Table 2.4 TTI Criteria Results for the Thorax (Morgan et al., 1986; Forbes, 2005)

INJURY LEVEL	25% PROBABILITY	50% PROBABILITY
	TTI (G's)	
AIS≥3	110	130
AIS≥4	150	168
AIS≥5	223	265

Current FMVSS 214 Side Impact Standards require TTI < 85 g for 4-door vehicles and TTI <90 g for 2-door vehicles.

It should be noted that injury criteria based on whole-body acceleration do not completely explain the mechanisms governing thoracic injury (Viano & Lau, 1988). Viano (1987) evaluated the TTI, stating "it is an acceleration-based criterion which averages the maximum near-side rib and spinal acceleration irrespective of differences in times of occurrence". Viano explained that the TTI was evaluated in the first milliseconds of impact, far too early for human injuries to be sustained. Therefore, it is possible that TTI may indicate a safe exposure when the full events of impact indicate a significant risk of injury (Viano, 1987).

2.4.5 Viscous Criterion

It has been found that soft tissue injury is dependant on chest compression, as well as the rate of chest compression (Viano & Lau, 1988). Although the compression criterion has been validated as an adequate predictor of injury, it is only applicable for speeds of deformation less than 3 m/s (Viano & Lau, 1988). For speeds of deformation greater than 3 m/s the compression and rate of deformation are required to adequately measure the body's viscous response to injury. The rate-sensitive response to injury, whereby an acceptable level of thoracic compression at low rates can be life threatening at higher rates of compression, has led to the development of the Viscous Criterion (Viano & Lau, 1988).

The interrelationship of thoracic compression and velocity was investigated through blunt impact experiments on male swine by Kroell et al. (1981). Kroell et al. found that high velocity impacts produced higher levels of injury despite having low levels of compression. Lau & Viano (1981) further reinforced the findings of Kroell et al. by performing abdominal impact tests of varying velocity on rabbits. In these tests, a constant level of compression was produced by a pneumatic impactor at velocities between 5 and 20 m/s. The authors found that for the same level of compression, minor injuries were produced at low impact velocities and extensive deep lacerations of the liver and hemoperitoneum were found at high impact velocities (Lau & Viano, 1981).

On the basis of numerous thoracic impact experiments, Lau & Viano (1986) proposed the concept of the Viscous Criterion be defined as "any generic biomechanical index of injury potential for soft tissue defined by rate sensitive torso compression." Lau & Viano defined the viscous response (VC) as "a time function formed by the product of the velocity of deformation, V(t), and the instantaneous normalized compression, C(t)."

$$VC(t) = V(t)xC(t) \tag{2.3}$$

Where $C(t) = \frac{D(t)}{D_o}$ and $V(t) = \frac{d[D(t)]}{dt}$

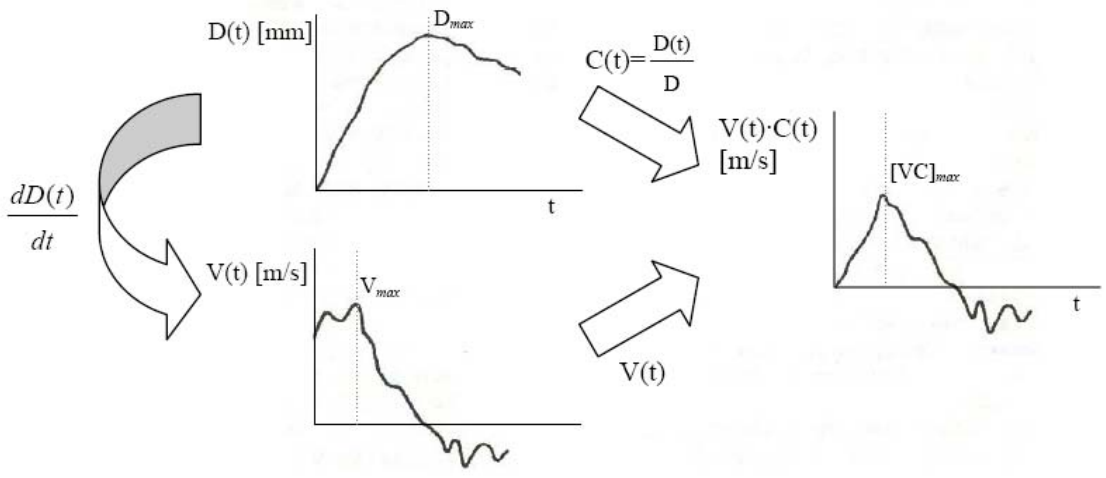

Figure 2.8 The Viscous Criterion Defined by The Instantaneous Deformation (Lau & Viano, 1986)

Using the PMHS data provided by Kroell et al. (1971, 1974), Viano & Lau (1988) developed VC_{max} values for frontal injury. Further research performed by Viano (Viano, 1989a; Viano et al., 1989b) provided insight into the viscous response of PMHS in lateral impacts (Figure 2.9).

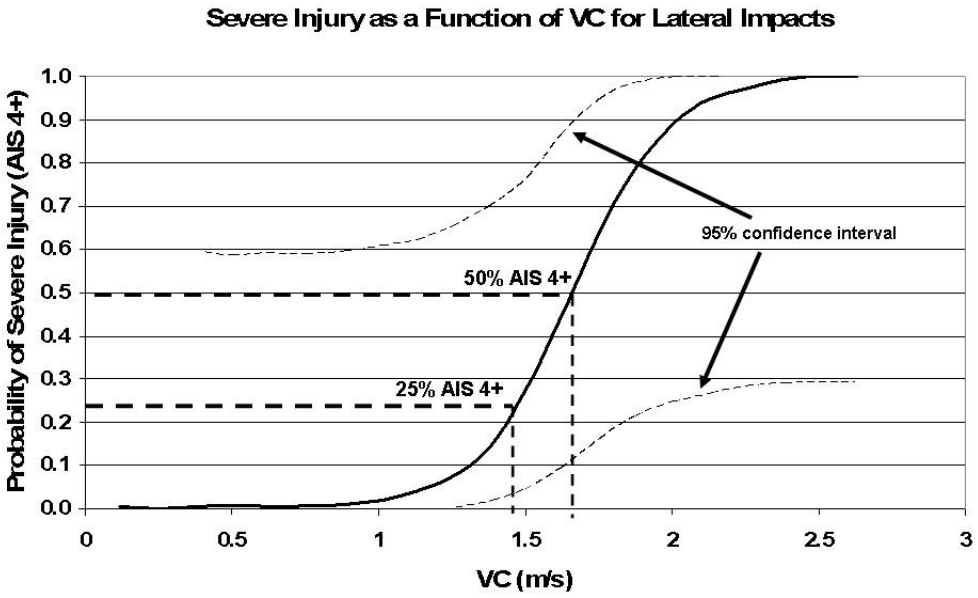

Figure 2.9 Severe injury risk as a function of Viscous Criterion (Viano & Lau, 1989b)

Studies have shown (Lau & Viano, 1986) that Viscous Criterion is most applicable as an indicator of soft tissue injury for velocities of deformation between 3 and 30 m/s. As stated previously, compression criteria is a good predictor of injury for rates of deformation less than 3 m/s. At these low velocities injury is produced by crushing the tissue and the rate of deformation has little to no effect on injury. At velocities greater than 30 m/s, impact velocity begins to completely govern injury as is seen in blast trauma. Figure 2.10 shows the range of validity for the Viscous Criterion as a function of the velocity of deformation.

The results of compression experiments are summarized in Table 2.5.

Table 2.5 Viscous Criteria Results for the Thorax (Forbes, 2005)

INJURY LEVEL	25 % PROBABILITY	50% PROBABILITY
Frontal VC_{max} (m/s)		
AIS≥4 (Viano & Lau, 1988)	1.00	1.08
LateralVC_{max} (m/s)		
AIS≥3 (Viano et al., 1989b)	*	1.00
AIS≥4 (Viano et al., 1989b)	1.47	1.65
*Data not provided.		

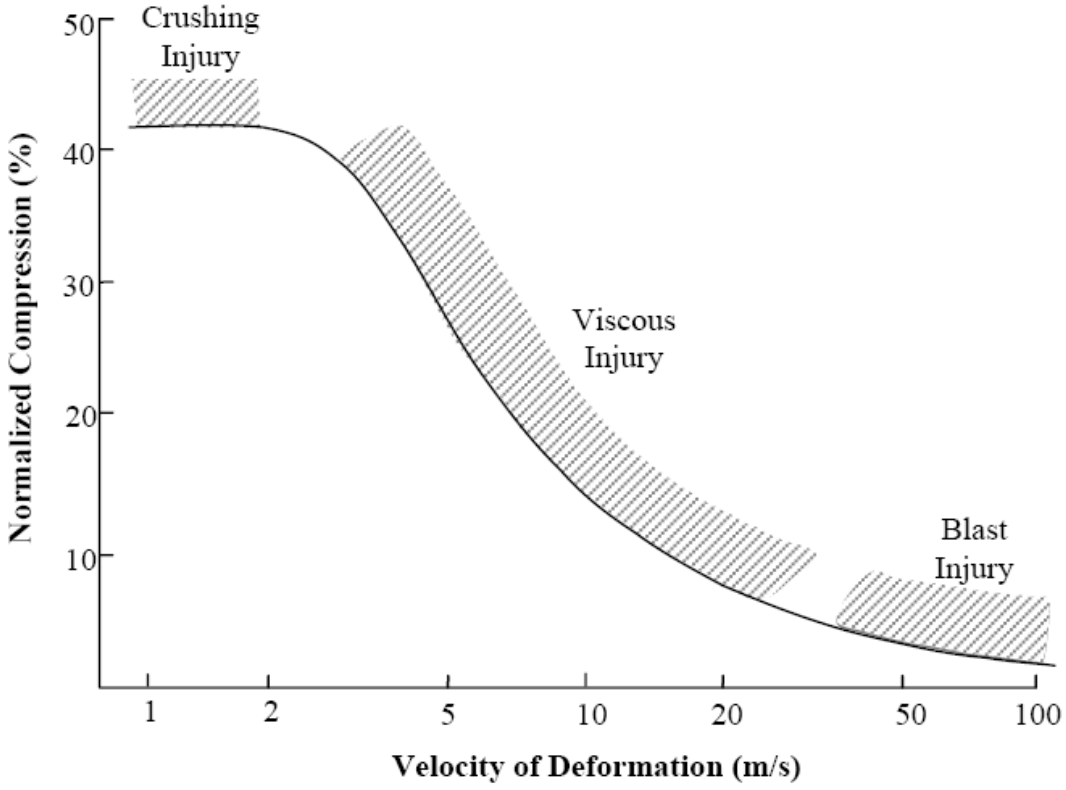

Figure 2.10 Range of Validity for the Viscous Criterion (Lau & Viano, 1986)

Current European Side Impact Standards implement an ES-2 VC threshold of 1 m/s.

2.4.6 Current Side Impact Criteria and Thresholds

There has been an ongoing discussion regarding the best predictor of thoracic injury over the past 20 years. For this reason, differing opinions on injury criteria exist and differing standards are currently imposed in North America and Europe. However, the New FMVSS 214 standard will use the ES-2re side impact dummy and determine injury using deflection and VC, as done in the current European standard. Table 2.6 displays the criteria and tolerance levels used by North American and European standards.

Table 2.6 Current Side Impact Criteria and Thresholds

CRITERIA	**NORTH AMERICA**			**EUROPE**
	FMVSS 214	**New FMVSS 214**	**IIHS**	**ECE95**
ATD	SID (50^{th})	ES-2re ($50^{th}/5^{th}$)	SID II (5^{th})	ES-2
Chest Compression	N/A	44 mm	34 mm [b]	42 mm
VC	N/A	1 m/s	1 m/s [b]	1 m/s
TTI	85/90 g [a]	N/A	N/A	N/A

a – 85 g's for 4-door vehicles and 90 g's for 2-door vehicles
b – Maximum value to produce 'good' response according to IIHS standards

2.5 Predicting Thoracic Response

2.5.1 History of Anthropomorphic Test Devices

Anthropomorphic Test Devices (ATDs), commonly known as crash test dummies, have been used to assess the potential for injury in automotive collisions since the late 1940's. Dummies are designed to be biofidelic and have been developed to mimic human responses of trajectory, velocity, acceleration, deformation, and articulation when exposed to specific loading conditions (Nahum & Melvin, 2002). ATDs are classified according to size, age, sex, and impact direction and are instrumented to measure acceleration and deformation at specific locations to calculate injury criteria.

The first crash test dummy used to evaluate automotive crashworthiness was originally developed by Sierra Engineering in 1949 to assess the occupant impact of seat ejection by the U.S. Air Force. The dummy, dubbed Sierra Sam, consisted of a laminated plastic and fiberglass skeleton with stainless steel joints covered in a poly-vinyl chloride to represent flesh. These dummies represented the 95th percentile male in terms of shape and weight and were used to test restraint systems in frontal collisions. Sierra Stan was later created to represent a 50th percentile male in 1967 and Sierra Susie was developed to represent the 5th percentile female in 1970.

Alderson Research Laboratories released the VIP (very important people) 5th percentile female and 50th and 95th percentile male dummy in 1966 for frontal impact use by General Motors (GM) and Ford. The release of the VIP models encouraged Sierra Engineering to release Sierra Stan and Susie as competitors to the VIP dummies.
GM recognized the need to improve the biofidelity of the current models and developed the Hybrid I, II, and III dummies between 1971 and 1976. The Hybrid III model has undergone continual improvements and is currently in use for evaluating the crashworthiness of vehicles in frontal collisions (FMVSS 208). Vehicle safety in frontal collisions has been greatly improved upon as a result of the data produced by the Hybrid III dummy (Figure 2.11).

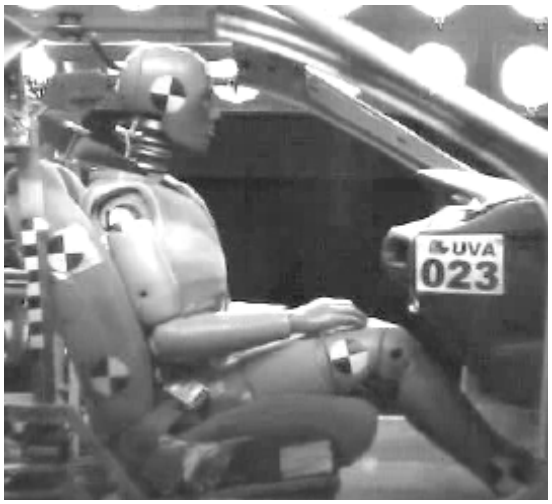

Figure 2.11 Hybrid III Dummy (Forman et al., 2006)

Although the Hybrid III functions well in front impact situations it has not been developed to assess injury as a result of lateral loading. This lack of lateral biofidelity initiated research in side impact dummy design, starting in 1979 with NHTSA's Side Impact Dummy (SID). The SID is a modified Hybrid III with an improved chest design for side impact loading and is currently used in the US side impact compliance tests (FMVSS 214). The European Experimental Vehicles Committee (EEVC) developed the EuroSID in 1989 to evaluate side impact requirements in Europe, while the BioSID was simultaneously developed by GM. Recently, the International Standards Organization (ISO) released an internationally accepted side impact dummy considered to be the most biofidelic dummy for lateral impact tests known as the WorldSID. According to the ISO/TR9790 rating scale, the WorldSID is far more biofidelic in comparison to other side impact dummies in use (Figure 2.12).

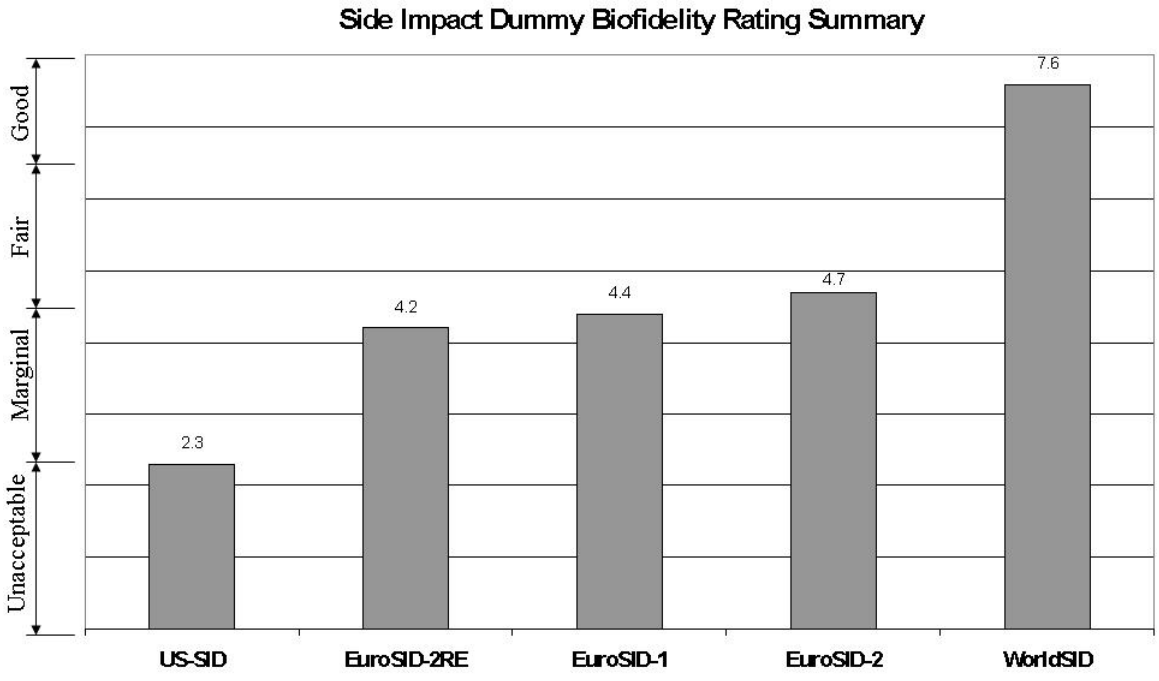

Figure 2.12 Lateral Impact Biofidelity Rating (WorldSID Home Page)

Although ATDs have provided significant insight into occupant injury in automotive collisions, they are limited in their biofidelity. This lack of biofidelity has led researchers to develop more advanced methods of predicting injury through numerical modeling.

2.5.2 History of Numerical Human Body Models

Automotive research is a challenging field due to the complexity and cost associated with full-scale vehicle testing. Recent efforts have focused on the development of advanced finite element models of vehicles and occupants capable of reproducing the response present in crash scenarios. Several methods have been used to aid investigators in their research on injury in crash scenarios. First, analytical models were developed using a series of masses, springs, and dampers to represent thoracic response (Figure 2.13). Model validation was often done using PMHS impact data and provided much of the information required in the development of ATD's.

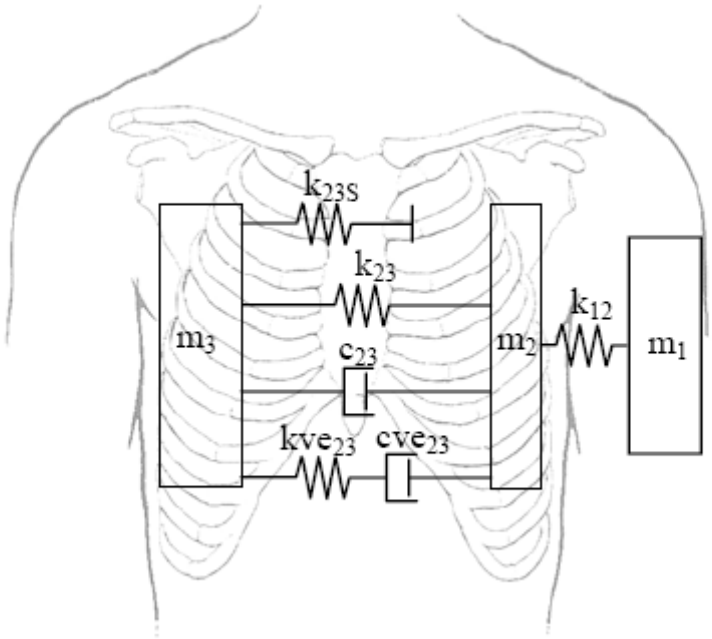

Figure 2.13 Lobdell Thoracic Lumped-Mass Model (Lobdell, 1973; Viano, 1988)

Second, rigid body models have been used to investigate the kinematic and dynamic motion of human response by modeling the body as several rigid components with a prescribed mass and moment of inertia. Components are connected using rotational joints with a predetermined response to loading. Cheng (1994) developed the Generator of Body Data (GEBOD) program to produce a rigid body model using several ellipsoids, each with its own specific geometry and mass. However, rigid body models do not provide significant insight into the mechanisms of injury or the response of human anatomy to crash.

Figure 2.14 GEBOD Model

Finally, researchers have developed thoracic finite element models to predict thoracic trauma under applied loads. An early thoracic finite element model was developed by Andriacchi et al (1974), consisting of the vertebrae, sternum, and ribs modeled as rigid bodies connected by spring and beam elements representing the intervertebral discs, joints, costal cartilages, and ligaments (Figure 2.15). A more robust model including the ribs, cartilages, sternum, vertebra, intervertebral discs, muscles, lung, and heart was developed by Sundaram and Feng (1977) using similar methods. However, to reduce computational requirements, Sundaram and Feng developed a half thoracic model and submitted it to a concentrated load.

Figure 2.15 Andriacchi Lumbar Spine and Skeletal Thorax Model (a) Anterior (b) Lateral (Andriacchi et al., 1974)

Advances in computer processing permitted Plank and Eppinger (1989) to develop a 7-rib thoracic model to analyze dynamic thoracic response in crash. Further improvements were made to include 12 ribs with improved geometry and the addition of an abdominal mass (Plank & Eppinger, 1991). The force-displacement response of the model was validated against PMHS experimental corridors. The model was later used in the analysis of thorax-restraint system interaction (Plank & Eppinger, 1994).

Huang et al. (1994) developed a side impact finite element model using MADYMO to predict injury and gross motion of human cadavers. The model included deformable ribs, spine, shoulder, visceral contents, and pelvis. Although the model did not include detailed internal organs, the model response agreed well with PMHS pendulum and side impact sled testing (Figure 2.16).

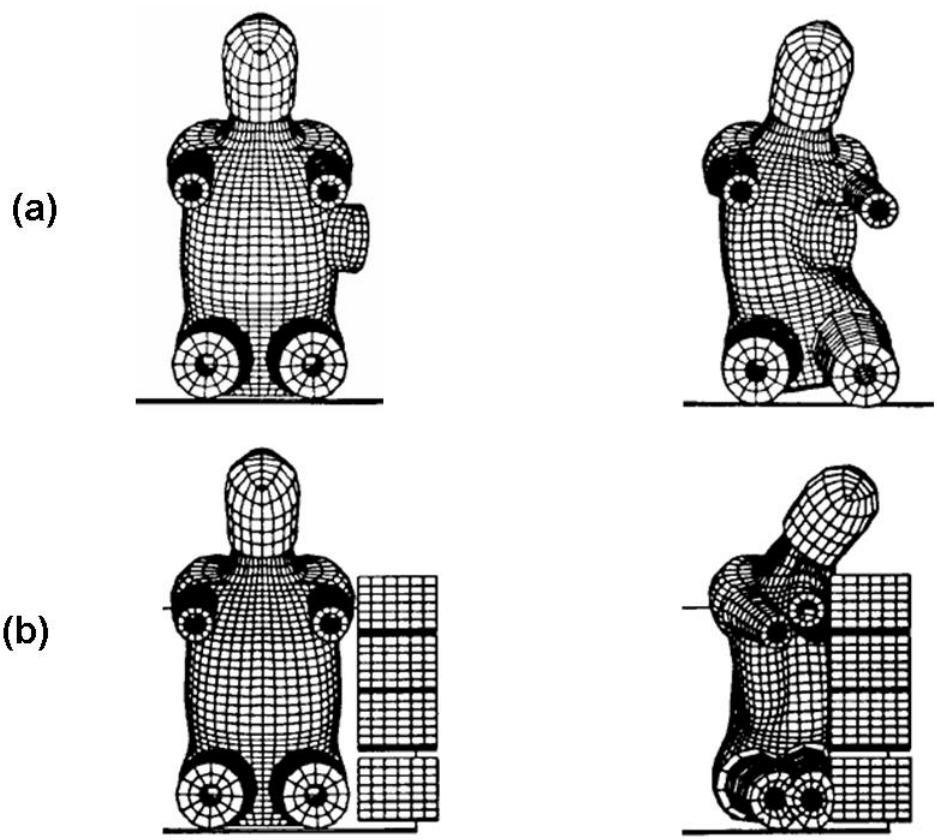

Figure 2.16 Huang Model During (a) Side Pendulum Impacts (b) Side Sled Impacts (Huang et al., 1994)

A more detailed thoracic model was developed by Wang (1995) which included internal organs such as the lungs and heart, as well blood vessels including the aorta, vena cava, pulmonary arteries and veins. Shah et al (2001) improved upon Wang's model to predict modes of loading likely to produce aortic rupture. Wang modeled the aorta as a hollow tube using shell elements without the presence of blood and assumed linear and isotropic material properties. Shah et al included fluid elements representing blood and validated aortic injury predicted by the model against the literature for frontal and lateral impacts. Iwamoto (2000) also improved upon Wang's model by incorporating a detailed shoulder model to improve injury prediction in lateral impacts (Figure 2.17).

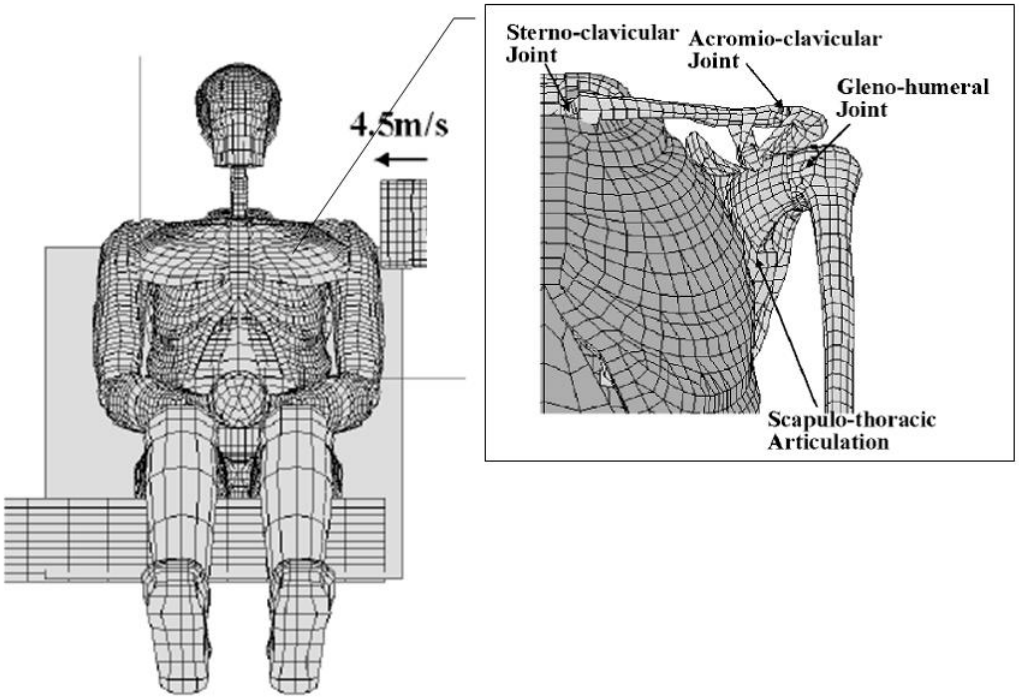

Figure 2.17 Wang Thoracic Model with Iwamoto Shoulder Model (Iwamoto et al, 2000)

TNO Automotive developed a human body model for frontal and rearward loading based on the 50th percentile male using the MADYMO software package (Happee et al., 1998). Model validation was performed for frontal, lateral, and rear impact scenarios with focus on the biofidelity of the head, neck, shoulder, thorax, and abdominal regions (de Lange et al., 2005).

The skeleton was modeled as a series of rigid and flexible components connected by kinematic joints. The inertial properties of the rigid bodies and the joint translational and rotational properties were based on biomechanical data found in the literature (de Lange et al., 2005). The thoracic and abdominal area were modeled using flexible bodies to represent characteristic deformations in impact scenarios. All components in the model used a multi-body approach (Figure 2.18).

Figure 2.18 The MADYMO Mid Size Male Occupant Model (de Lange et al., 2005)

The THUMS (Total Human Model for Safety) FEM, developed by Toyota Inc., represents a 50th percentile male in a seated posture and includes skeletal structures, joints, ligaments, and internal organs (Oshita et al., 2002). Bones were modeled using solid elements to represent cancellous bone and shell elements to represent the cortical bone. The THUMS joints consisted of ligaments modeled as shell or beam elements and sliding contact interfaces defined between bones. Internal organs were modeled as single continuum parts with solid elements.

Figure 2.19 THUMS Model (Oshita et al., 2002)

The EU BRITE-EURAM program launched the HUMOS (Human Model for Safety) to develop an accurate numerical human body model (Behr et al., 2003). The HUMOS model included similar components as the THUMS model, but included detailed models of the heart, lungs, kidneys, and liver (HUMOS, 2001).

Ford Motor Company developed a detailed numerical human body model to predict injury response in crash scenarios. The model was based on Wang's model (1995), but included major improvements to geometry, articulating joints between the ribs and spine, and internal organs (Ruan et al., 2003). The model was validated using front and side pendulum impact tests and showed good correlation with PMHS force and deflection responses.

Figure 2.20 Numerical Human Body Models (a) Sagital Section of Humos Upper Body (HUMOS, 2001) (b) Ford Motor Company Human Body Finite Element Model (Ruan et al., 2003)

Finite element models of common ATD's have also been developed and used to investigate injury response under various load conditions including full-scale vehicle simulations, sled tests, and pendulum impact tests. These models can provide further insight into the loading observed in crash conditions, as well as additional information regarding the anatomical response, but provide less detail than human body models.

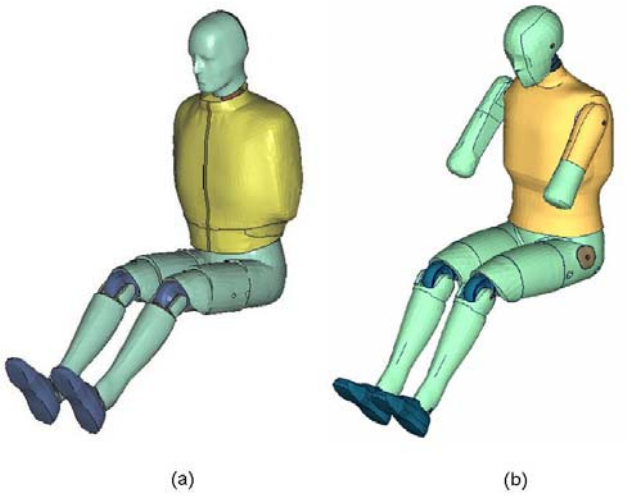

Figure 2.21 Finite Element Models of Side Impact Models (a) US SID (b) ES-2

2.6 Side Impact Test Methods and Compliance Tests

In the past, safety has been investigated by subjecting PMHS or ATD's to crash conditions representative of full body automotive collisions. Historically this has been done with full vehicle crash testing or sled testing for various types of collisions. However, there has been a surge in research, driven by advances in computer technology, where researchers can recreate crash conditions through numerical modeling. This section provides a brief overview of the current methods of safety research.

2.6.1 Full Vehicle Side Impact Tests

Side impact standards are currently in place to ensure vehicles meet basic safety requirements for occupant injury. The North American (FMVSS 214) and the European (ECE-R95) procedures are dynamic tests using a stationary test vehicle struck by a moving deformable barrier (MDB) representing the striking vehicle. Although the tests are similar in their approach, historically they differ in test procedure, MDB, dummies, and injury criteria used (Samaha, et al., 1998).

The FMVSS 214 test represents a side impact collision in which the striking vehicle is traveling at 48.3 km/h into a target vehicle traveling at 24.2 km/h. The 1367 kg MDB impacts with a crab angle of 27 degrees and a closing speed of 54 km/h (Figure 2.22). A 50th percentile SID is used to evaluate injury using the TTI injury criterion. Future FMVSS 214 tests will replace the SID with the ES-2re, to evaluate crash safety by measuring chest deflection and viscous criteria, as opposed to the historical acceleration based injury criteria provided by the SID.

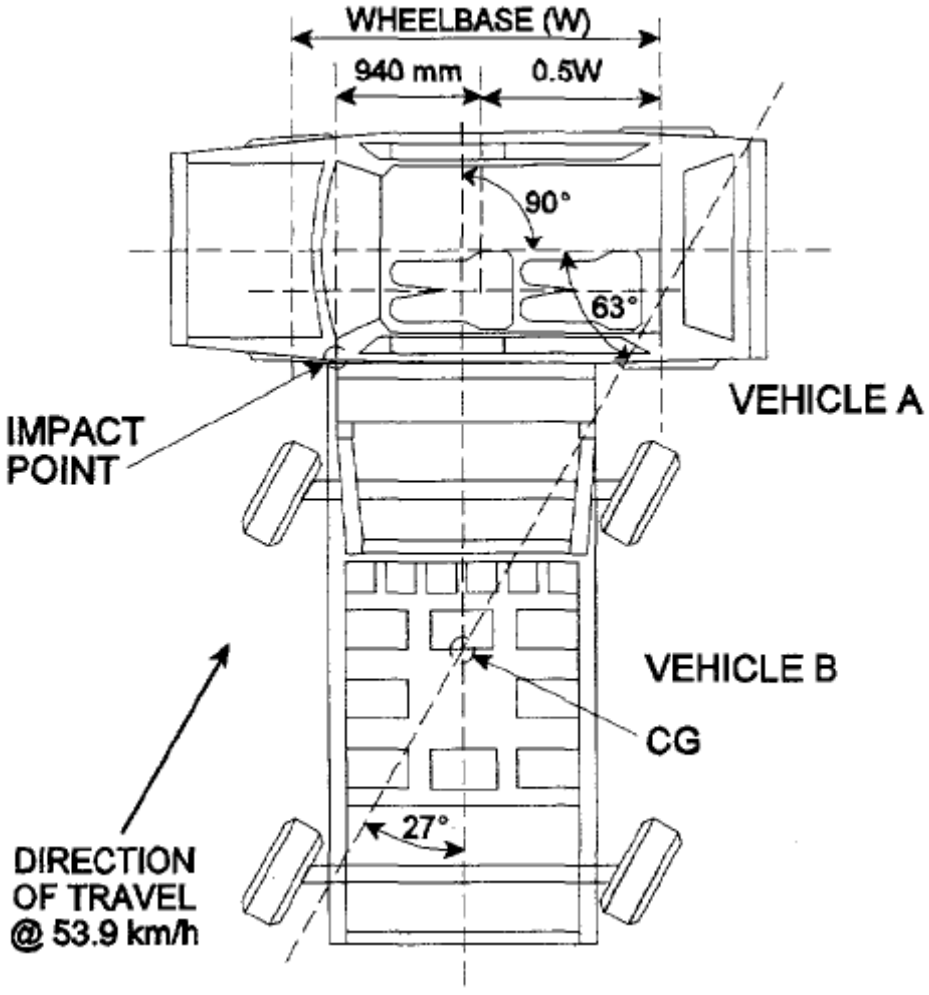

Figure 2.22 FMVSS 214 Test Configuration

In the European test, a 950 kg MDB impacts the target vehicle at 50 km/h with no crab angle (Figure 2.23). Injury is evaluated using an ES2-re to determine chest deflection and viscous criterion.

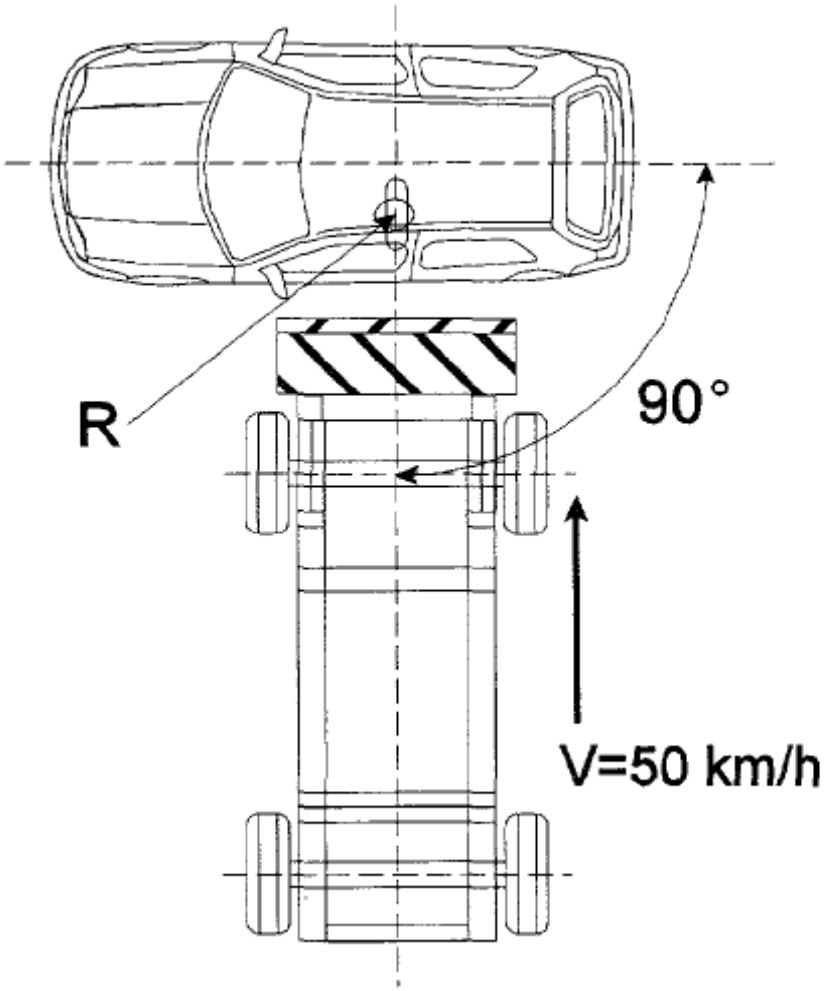

Figure 2.23 ECE-R95 Test Configuration

The Insurance Institute for Highway Safety (IIHS) performs a test similar to the European standard, but uses a MDB representative of a large vehicle such as a SUV or pickup truck. The test is conducted using a 1500 kg MDB at 50 km/h with no crab angle. A 5th percentile SID-II is placed in the front and rear driver side seats to determine occupant injury.

The tests methods described can be reproduced and applied to finite element models of vehicles to investigate vehicle and occupant response during crash. These simulations can provide information that is unavailable in crash reports and can further the understanding of crash factors in side impact collisions. An example of a simulated Ford Taurus FMVSS 214 test is shown in Figure 2.24 (Teng et al., 2007).

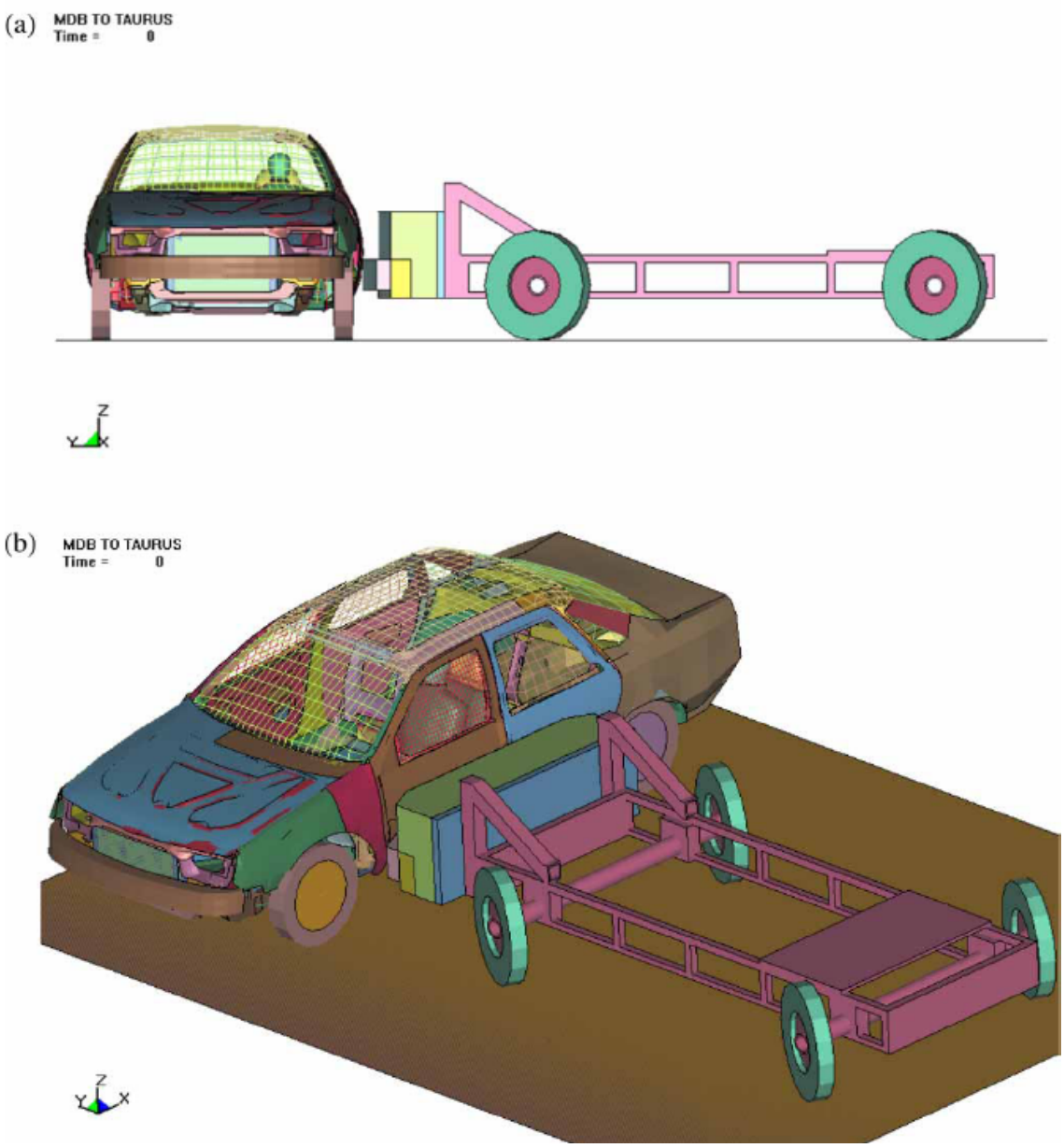

Figure 2.24 Finite Element Model of FMVSS 214 test

Full-scale side impact tests typically produce door intrusion velocity profiles that consist of three common characteristics; first peak, valley, and second peak as seen in Figure 2.25 (Morris et al., 1998). The first peak occurs immediately after the barrier contacts the door causing the door velocity to rapidly increase to its initial peak. The door velocity then decreases to its valley as the vehicle side structure transfers load to the main structure of the vehicle (Payne et al, 1997). The second peak in door velocity is caused by stiffening of the barrier prior to slowing to its final velocity. It has been found that the overall kinematics of the door is essentially unaltered by the interaction with the occupant (Chung et al., 1997).

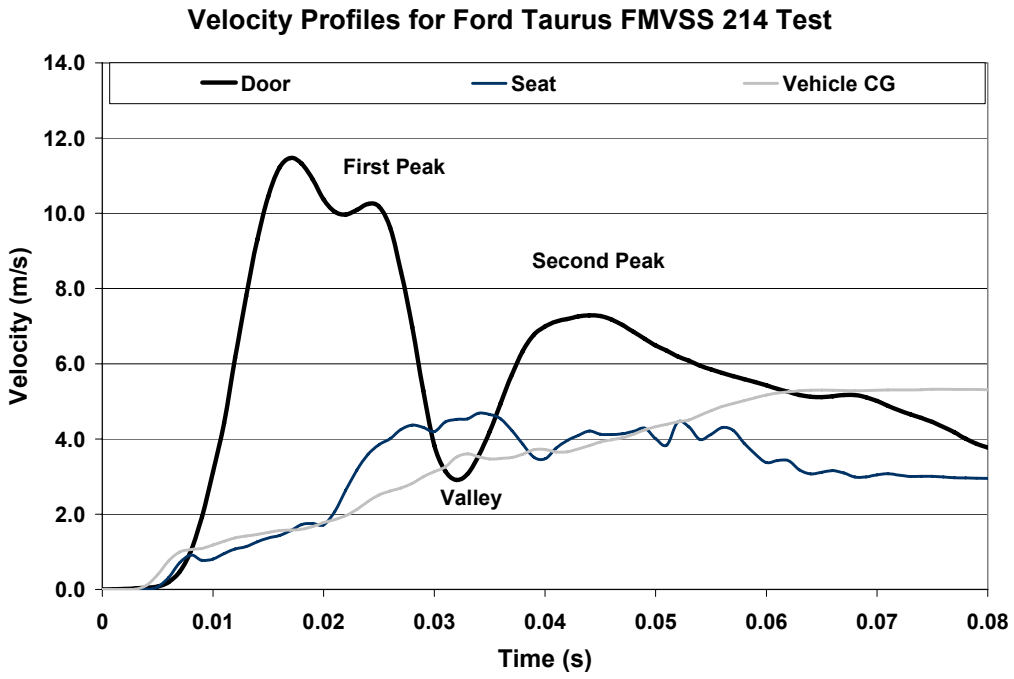

Figure 2.25 Typical Velocity Profiles for Experimenal FMVSS 214 Crash Test (MGA Research Corporation, 2001)

2.6.2 Sled Testing

As previously discussed, sled testing is often used to predict injury under specific load conditions using PMHS and ATD's. Unlike full scale vehicle tests, sled tests provide the flexibility to vary the influential factors on occupant safety. The NHTSA and WSU sled tests are simplified cases approximating the impact velocity present in side impact collisions. However, these simple cases do not account for important factors such as door intrusion, door velocity profile, door compliance/shape, and occupant to door spacing.

Several test methods have been developed to more accurately reproduce crash conditions. Morton (1995) developed a sled test which consisted of a reinforced vehicle door and seat mounted on a sled carriage. A honeycomb structure representing the striking vehicle was accelerated into the door. Although this method is a closer representation of a physical collision, it did not accurately reproduce the door velocity profile necessary to ensure a realistic occupant response (Aekbote et al., 1999). A system developed by MIRA simulated the entire door velocity profile, but used a simplified rigid door which does not account for the door compliance and shape on occupant response (Aekbote et al., 1999). Aekbote et al. (1999) developed a sled test which reproduced the door velocity profile while accounting for the door compliance and shape (Figure 2.26). The sled operates in four phases. First, a pre-crushed door is mounted on a sled and is accelerated by the HYGE representing the first characteristic peak of the door velocity profile. The door sled is then decelerated by a honeycomb block mounted on a base sled, simulating the "valley" in the velocity profile in the second phase. In the third phase the door and base sleds are accelerated by the HYGE to simulate the second peak in the velocity profile. Finally, the door and base sleds are decelerated until door-dummy separation.

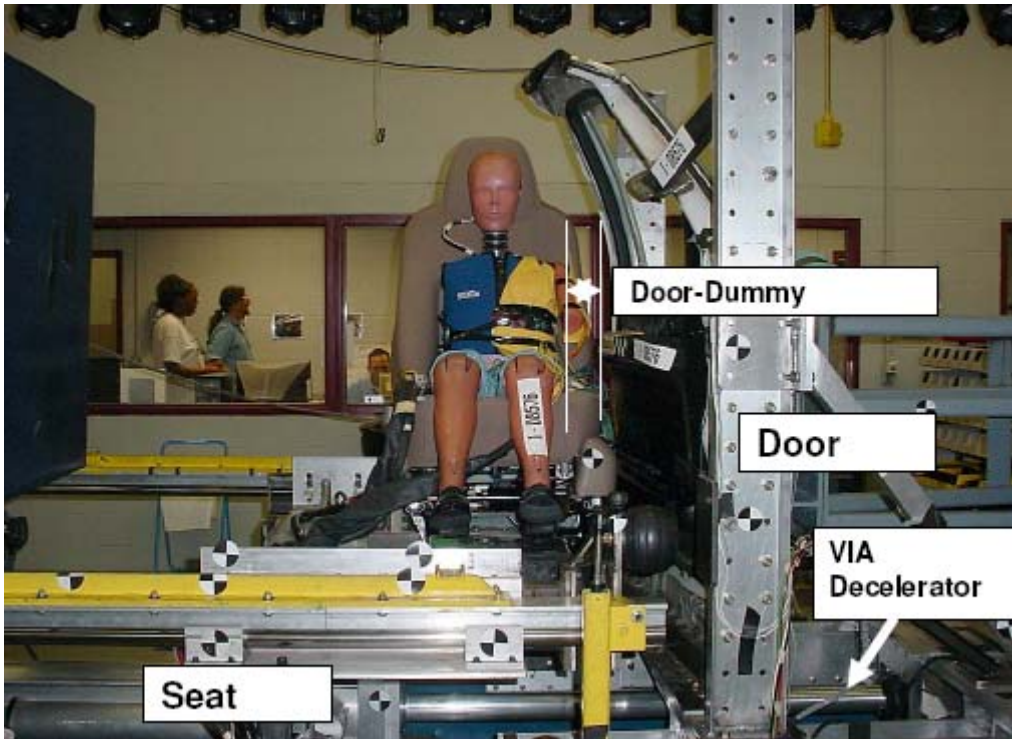

Figure 2.26 Aekbote Sled-to-Sled Test Apparatus (Aekbote et al, 2007)

As in the case of full vehicle testing, sled tests have also been developed as finite element models (FEM) for the purpose of crash investigation. An early side sled FEM was developed by Huang et al. (1994), which subjected a simple human body model to conditions similar to the WSU sled tests (Figure 2.27). The model was used to investigate occupant reaction to rigid and padded wall impacts as well as the effects of shoulder engagement.

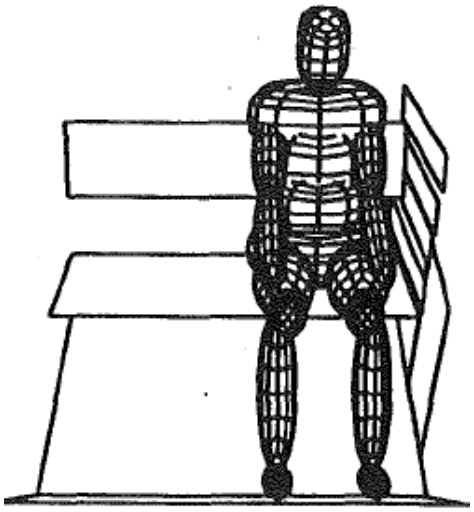

Figure 2.27 Side Impact MADYMO Model (Huang et al., 1994)

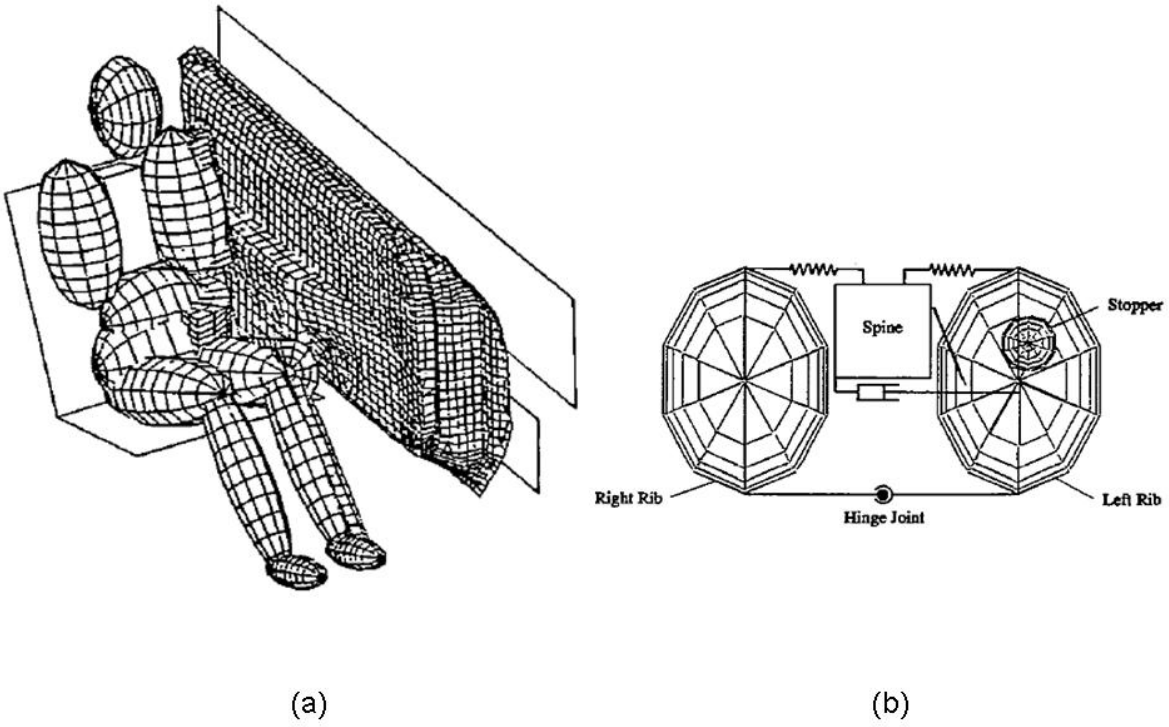

Figure 2.28 Side Impact Model (a) Sled (b) Thorax (Deng & Tzeng, 1996)

Deng and Tzeng (1996) developed a side impact model to simulate occupant response in FMVSS 214 tests (Figure 2.28). This model included a door model which included the armrest, door trim, inner/outer panels, and side airbags. The occupant model used was a simple model representative of a SID and consisted of 13 segments. The thorax was modeled by 3 segments representing the spine and left and right ribs. Springs and dampers were used to connect the ribs to the spine. The model used a MDB to impact the door with a prescribed velocity as determined from FMVSS 214 data. The effect of door padding, a crushable armrest, and side airbags were investigated for an unrestrained occupant using TTI and pelvis acceleration as injury criteria.

Another side impact FEM was developed by Morris et al., (1998) to examine the effects of door to occupant spacing, padding, and door velocity profile. The MADYMO model included a door structure, seat, and SID model (Figure 2.29). Door and seat acceleration profiles were determined by accelerometers positioned on the inner door panel and seat track in FMVSS 214 tests. The door geometry was based on the driver's door of a 4-door sedan and force-deflection characteristics were determined by quasi-static testing.

Figure 2.29 Side Impact Model (Morris et al., 1998)

The models response was evaluated using both TTI and viscous criterion for varying input profiles as shown in Figure 2.30.

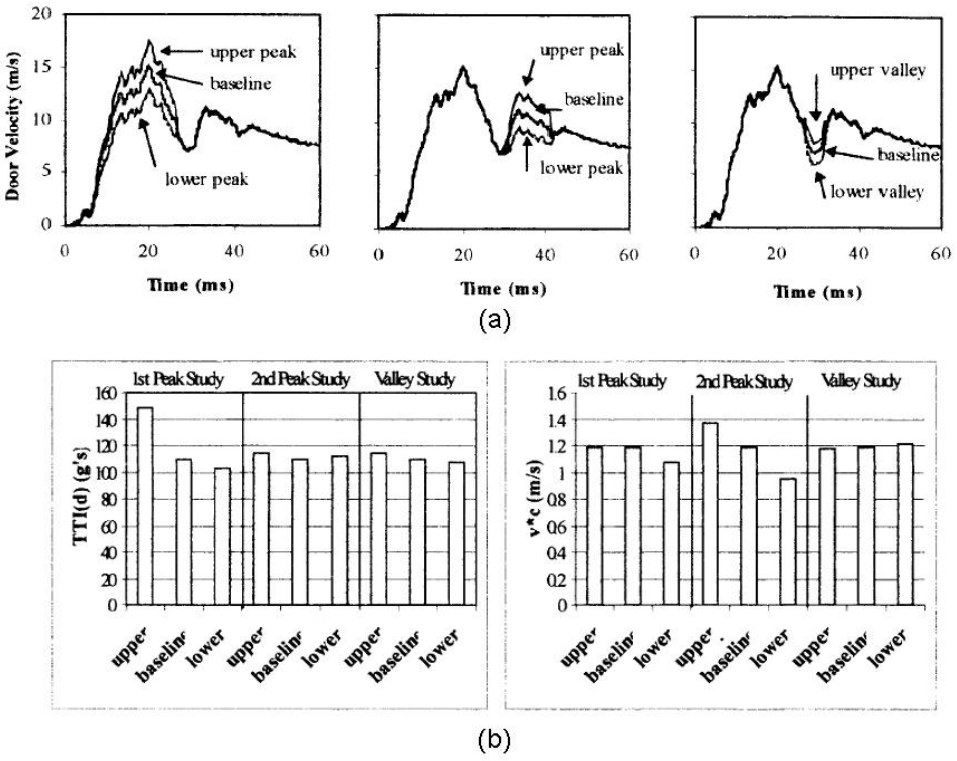

Figure 2.30 Side Impact Study (a) Input Profiles (b) Results (Morris et al., 1998)

The results shown in this study provide interesting insight into two commonly disputed injury criteria. Figure 2.30b shows that TTI is highly sensitive to variations in first peak, but relatively unchanged by variations in the valley and second peak variations. This is an expected result as the highest accelerations occur early in the collision. In contrast, VC shows a high degree of sensitivity to the second peak variations and minimal sensitivity to the first peak and valley variations. Although the model uses a SID developed to measure TTI, values of VC can be produced with the FE SID. However, results may not be entirely accurate as the models response was validated based on acceleration and TTI, and was not validated to experimental data based on VC.

Schönpflug et al. (2004) developed numerical simulations providing insight into crash dynamics using a modified NHTSA side sled test as well as full vehicle simulations based on EuroNCAP side impact tests methods (Figure 2.31). These studies compared a human body model (H-Model) to the EuroSID 1 to estimate the benefits of using numerical human body models in future studies.

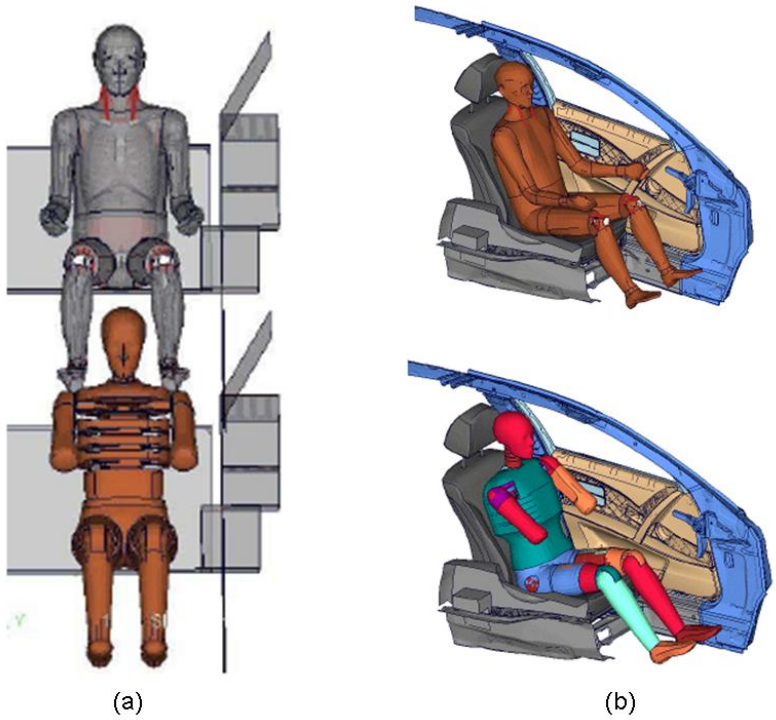

Figure 2.31 H-model and EuroSID Comparison (a) Side Sled Test (b) Full Vehicle Test (Schönpflug et al., 2004)

Schönpflug et al. also examined the effects of pelvic offset on rib deflection and VC and found that injury can be significantly reduced by pelvic offset (Figure 2.32).

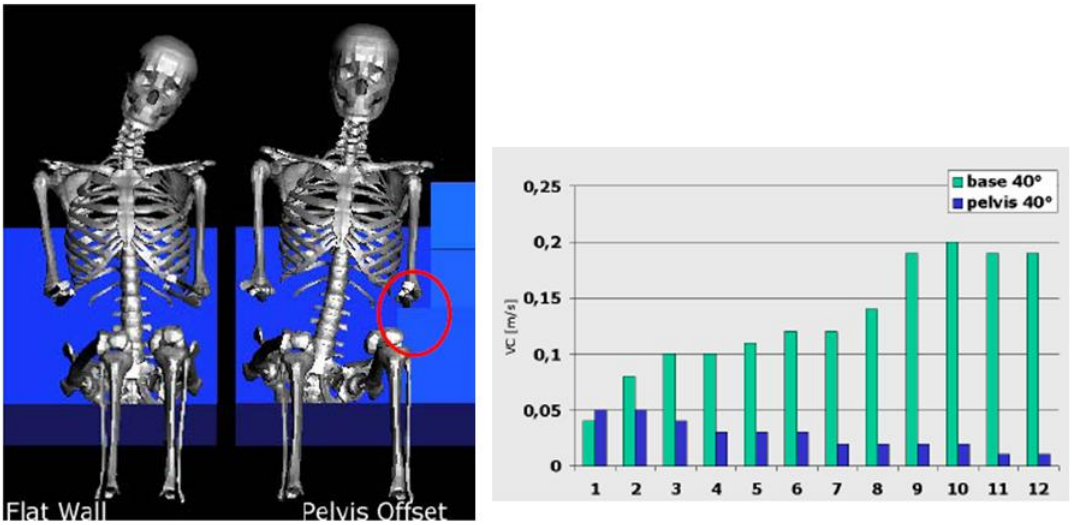

Figure 2.32 Effect of Pelvic Offset on all 12 ribs (Schönpflug et al., 2004)

Teng et al. (2007) developed a side sled model based on the BASIS side sled system (Figure 2.33). The BASIS system uses a computer controlled braking system to reproduce the acceleration profile of a struck vehicle. Velocity profiles are applied to the door and seat models based on information gathered from FMVSS 214 testing (Figure 2.34).

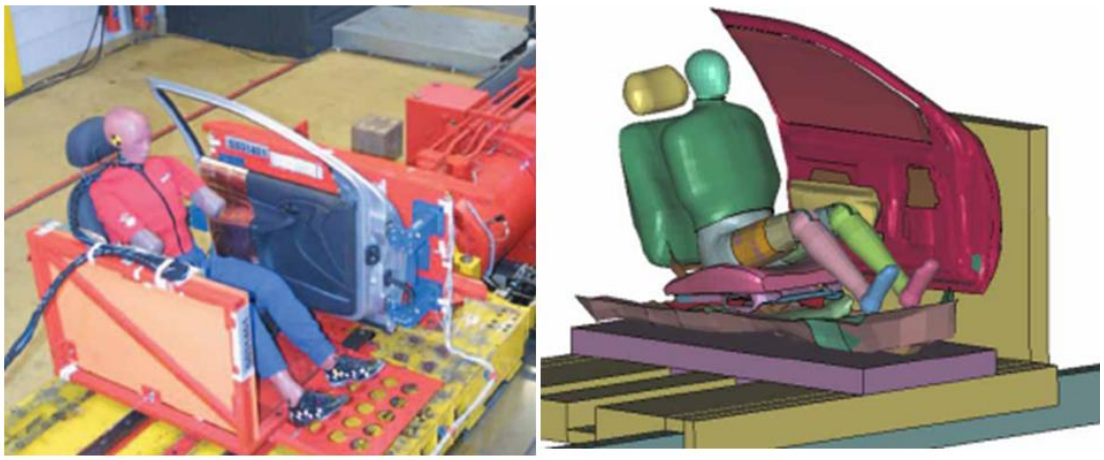

Figure 2.33 Side Sled Test (a) BASIS system (b) Numerical Model (Teng et al., 2007)

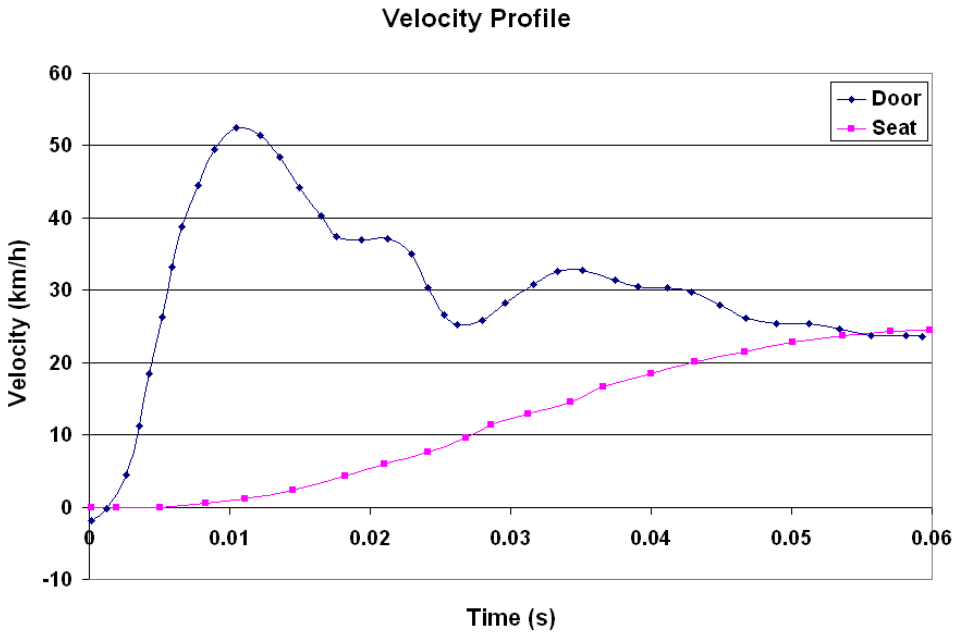

Figure 2.34 Velocity Profile of Side Sled Model (Teng et al., 2007)

The numerical model developed by Teng et al. uses a SID model and compares TTI and pelvic acceleration to values obtained in full scale FMVSS 214 tests. Simulated side sled results for TTI and pelvic acceleration compare reasonably well to experimental data differing by 2.6% and 13% respectively (Table 2.7).

Table 2.7 Comparison of Experimental and Simulated Sled Test (Teng et al., 2007)

AREA OF OCCUPANT	EXPERIMENTAL RESULTS (g)	SIDE SLED SIMULATION (g)
Lower Spine	83.5	75
Upper Rib	59.2	77.1
Lower Rib	70.5	76.14
Pelvis	115.2	100
TTI	78	76

Figure 2.35 Impact Sequence of Side Sled Test (a) t=.015 s (b) t=.027 s (a) t=.043 s (b) t=.060 s (Teng et al., 2007)

Although the numerical human body models discussed are capable of producing responses which closely correlate to experimental data gathered from PMHS testing, they are often computationally expensive (Forbes, 2005). As a result, it is difficult to accurately model representative crash scenarios such as frontal and side sled tests due to the high computational costs associated with these models. In order to overcome the challenges associated with these human body models Forbes (2005) developed a detailed numerical human body model with focus on the thorax, while implementing simplified models of the remaining body regions.

-- CHAPTER 3 --

University of Waterloo Human Body Model Development and Validation

3.1 Introduction

Forbes (2005) developed a detailed numerical human body model validated to produce thoracic response in correlation with response corridors of pendulum and side sled tests to tests performed on PMHS. Computational time has been improved relative to other numerical human body models through focus on a detailed thorax, while implementing simplified models of the remaining body regions. The human body model displayed *good* to *reasonable* correlation with the response corridors of pendulum and side sled tests to tests performed on PMHS.

This study has implemented the human body model developed by Forbes (2005) in crash scenarios representing FMVSS 214 side impact testing. The low computational costs and high thoracic biofidelity of the human body model make it a practical and accurate option for the modeling of thoracic trauma in side impact crash. The development and validation of the University of Waterloo Human Body Model (Forbes, 2005) is discussed in detail in this chapter.

3.2 Human Body Model Development

The thoracic model used in this research was originally developed by Deng et al. (1999), and included three-dimensional models of the spine, ribs, heart, lungs, and major blood vessels (Figure 3.1, Figure 3.2). Component geometry was gathered from a commercial data package of human geometry (Viewpoint Data Labs, Orem, Utah).

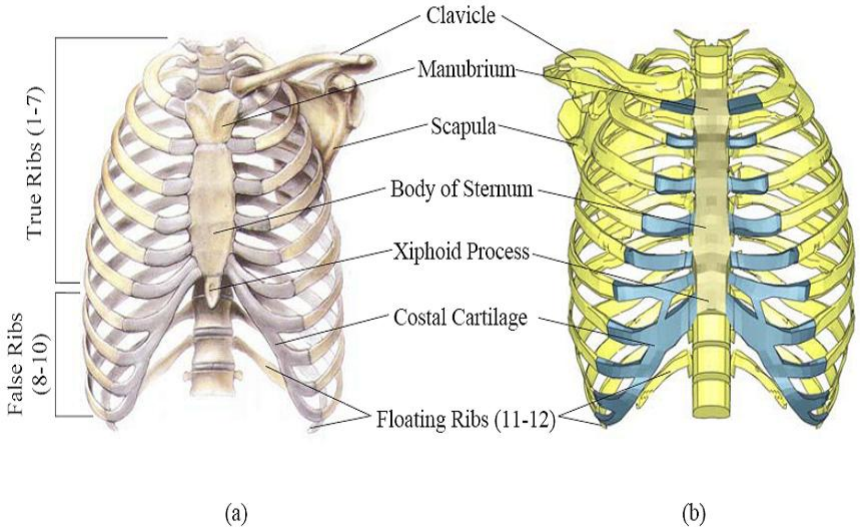

Figure 3.1 Thoracic Cage (a) Anatomical (b) Model (Moore and Dalley, 1999; Forbes, 2005)

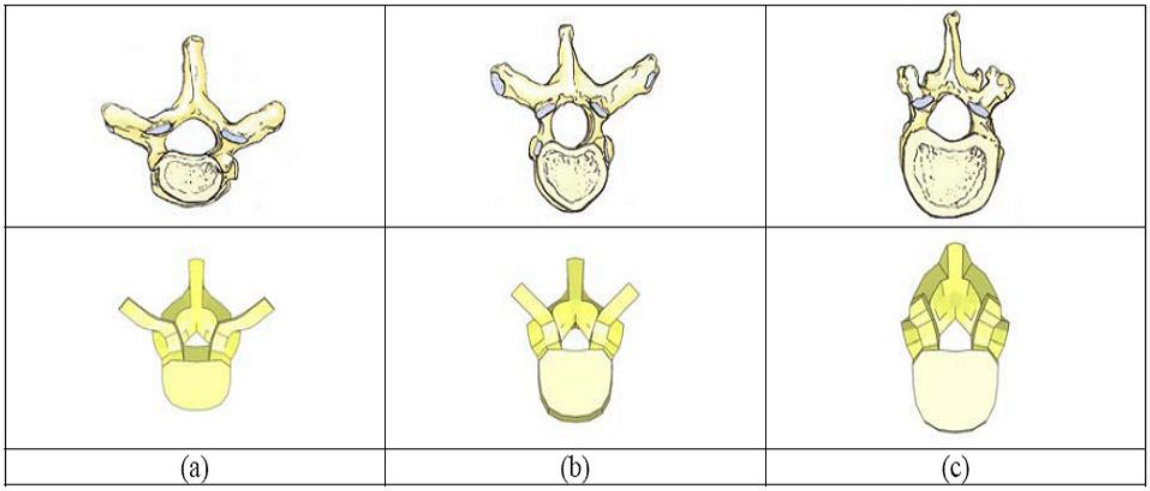

Figure 3.2 Thoracic Vertebrae, anatomical vs. model (a) T1 (b) T6 (c) T12 (Forbes, 2005)

Each rib was modeled with lengths and cross-sectional areas representative of human geometry and was submitted to bending tests to confirm that the mesh density, geometry, and material model were acceptable. The costal cartilage, connecting the ribs to the sternum, was modeled using the elastic material properties found by Viano (1986) and the connection between the ribs and the vertebrae were modeled using a single spherical joint. All vertebrae were modeled as rigid components with uniform material properties to represent the trabecular and cortical bone as determined by Yamada (1971).

For simplicity the lungs were modeled as a continuous solid material used to produce general response under load conditions observed in auto crash. Figure 3.3 shows the original lung model developed by Deng et al. (1999) based on geometry provided by ViewPoint Data Labs. The material properties were based on modeling developed by Fung et al. (1978) and Vawter et al. (1980) which used a strain-energy equation to account for both the air interaction and the surface energy present in the lung.

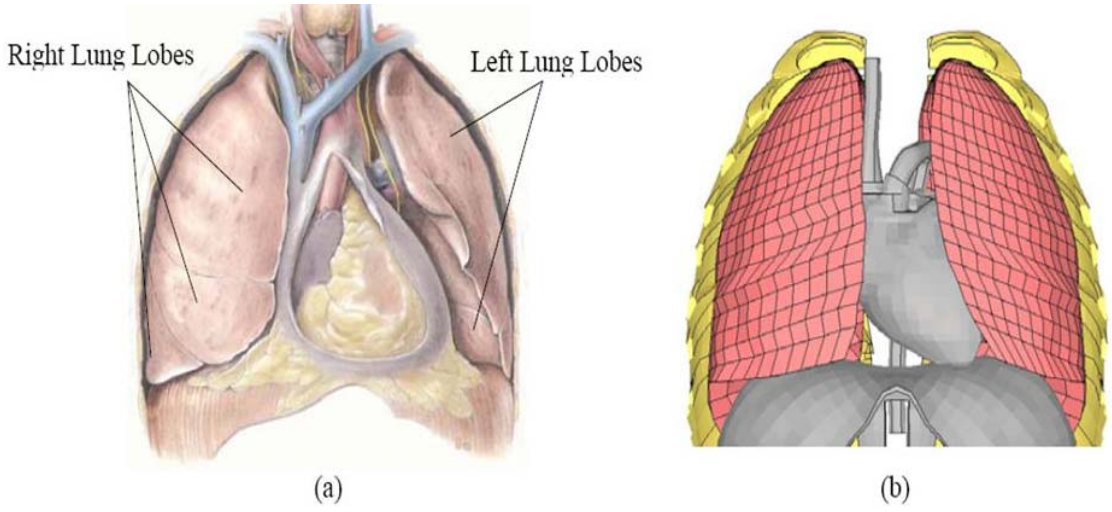

Figure 3.3 Lungs (a) Anatomical (b) Model (Moore and Dalley, 1999; Forbes, 2005)

Although the lungs are not modeled to the degree necessary to predict pneumothorax or hemothorax, the presence of fractured ribs intruding into the lungs is sufficient to infer such injuries. Current research is focused on the development of a lung model and criteria capable of predicting contusion (Yuen, 2008)

The heart and aorta have been modeled and filled with a linear elastic fluid material to represent blood. The model is capable of predicting laceration, rupture, and gross motion. As in the case of the lungs, contusion is a common injury. However, contusion is a form of injury the current model is unable to predict. Deng et al. applied the modeling approaches of Guccione et al. (1991), Guccione and McCulloch (1991), and McCulloch and Omens (1991) to represent heart properties. The model makes use of a single material model to represent the three layers of the heart using only the myocardium tissue coefficients, as the myocardium composes a majority of heart tissue (Forbes, 2005).

Figure 3.4 Heart (a) Anatomical (b) Model (Moore and Dalley, 1999; Forbes, 2005)

Chang (2001) performed the second iteration of the thoracic model which focused on the addition of rib cage surface muscles and upper limbs, as well as improving various constitutive models. Thoracic and arm tissue was added to the thoracic model and used the same material properties used to represent the heart. Although, this material provided reasonable results in pendulum tests, Forbes (2005) found that it was inadequate in side impact sled tests due to its lack of rate dependency. Forbes applied experimental data for various rates (Van Sligtenhorst, 2003; McElhaney 1966) to a rate dependant hyperelastic material model developed by Du Bois (2003) to model the hyperelastic and

viscoelastic properties of the thoracic tissue. Improvements were also made to the original mesh density to more closely match the mesh densities of the underlying components.

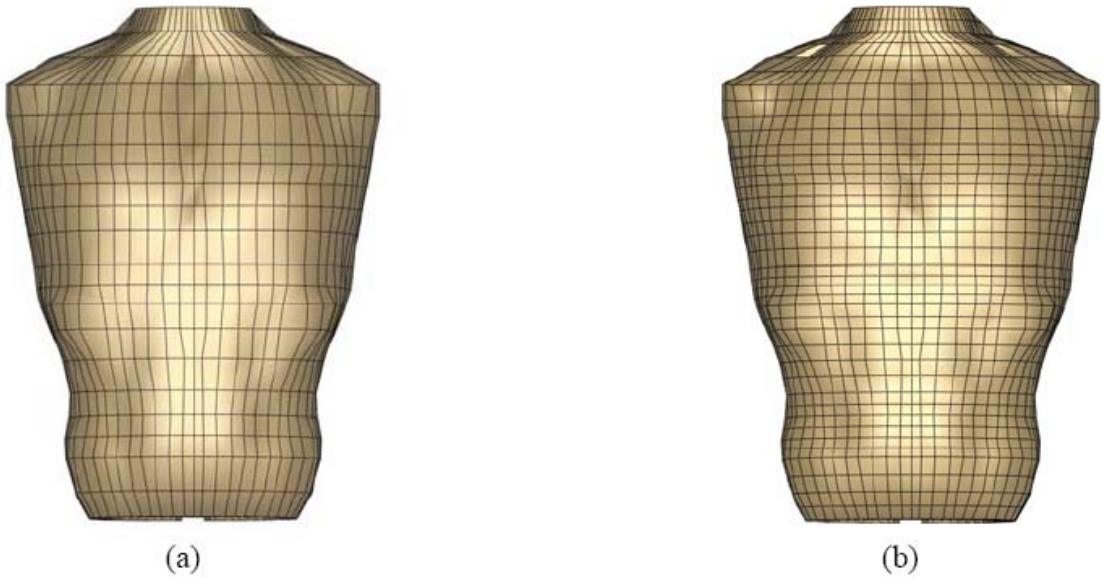

Figure 3.5 Thoracic Muscle Tissue (a) Old Mesh (b) New Mesh (Forbes, 2005)

The shoulder acts as a means of energy absorption, and therefore limits the load experienced by the thorax in side impact crash. Chang developed a shoulder model which provided a realistic kinematic response for front and side thoracic pendulum tests. However, Forbes (2005) found that the shoulder model did not perform adequately in shoulder pendulum impact tests. Forbes improved the shoulder model by providing new attachment and insertion points for beam muscles, adding new beam muscles not present in the original model, and replacing the material models for solid and beam elements with more appropriate models.

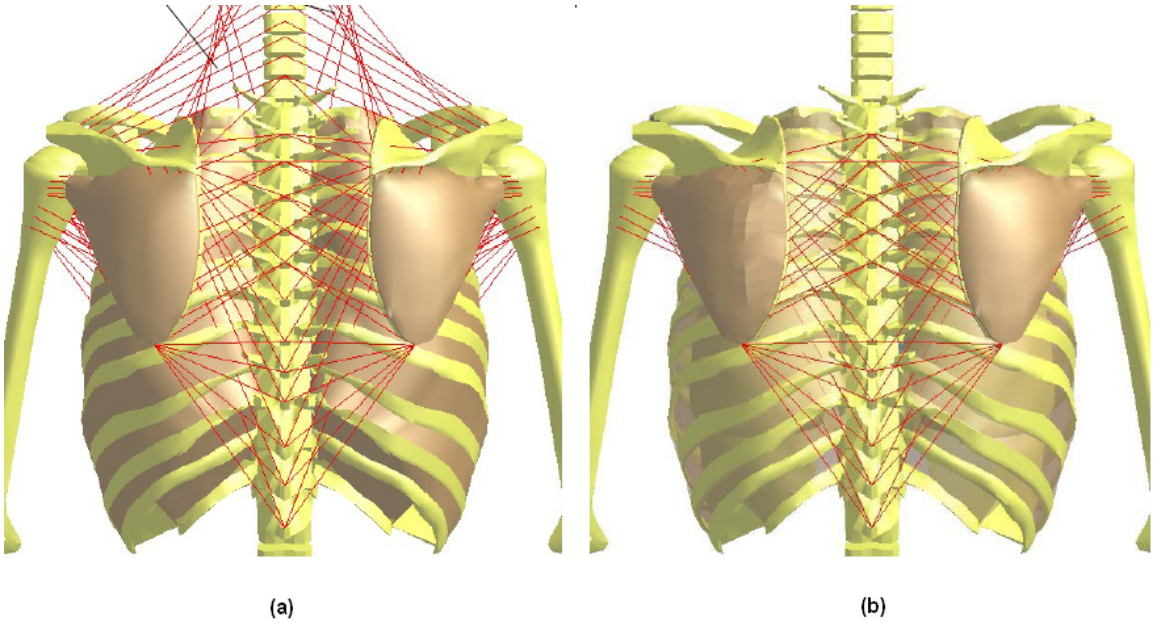

Figure 3.6 Shoulder (a) New Model (b) Chang Model (Forbes, 2005)

In order to predict global body response, Forbes developed simplified pelvic, abdominal, leg, and head models. Side pelvic and abdominal pendulum tests were performed and compared to PMHS data to confirm the models response. Figure 3.7 shows the full body model after the iterations performed by Forbes (2005), Chang (2001), and Deng (1999).

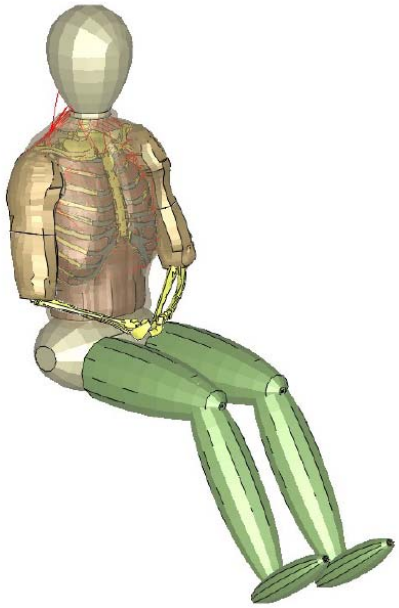

Figure 3.7 Full Body Model (Forbes, 2005)

3.3 Human Body Model Validation

The biofidelity of the model was validated by the use of pendulum and side sled impact simulations compared to experimental results of PMHS testing. Pendulum impact tests were performed to isolate the performance of the thoracic region without influence of neighboring regions. On the other hand, side sled simulations were performed and compared to PMHS testing to determine the response of the entire human body model to load conditions present in auto crash scenarios. The following terms were used to describe the qualitative measures used to assess the model response and were based on ISO methods for testing side impact dummies:

- *Good* Falling within the corridor of the experimental data.
- *Reasonable* Falling outside the corridor of the experimental data, but within one corridor width.
- *Poor* Falling outside the corridor by more than one corridor width.

To validate the models response to loading, the following results were compared to PMHS experiments:

- Force Impact force between impactor and body.
- Compression Deflection divided by initial thoracic depth as measured at the 6^{th} rib anteriorly
- VC Viscous injury criterion; rate of deflection multiplied by compression
- Injury Number of Rib Fractures.

3.3.1 Pendulum Impact Tests

The model's frontal response was validated using pendulum impact tests performed by Kroell et al. on thirty-seven PMHS (Figure 3.8). However, the validation only uses tests that had a male subject that underwent impact of a 23.4 kg impactor at 6.7 m/s providing a sample size of five PMHS.

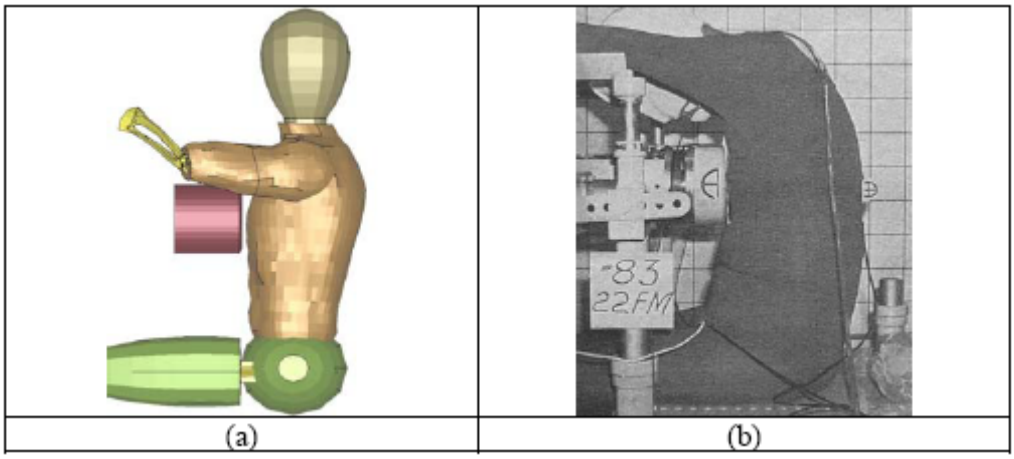

Figure 3.8 Front Thoracic Pendulum Impact Test (a) Simulation (b) Experiment (Kroell et al., 1971)

Figure 3.9 shows the response of the thorax at various times during a frontal pendulum impact.

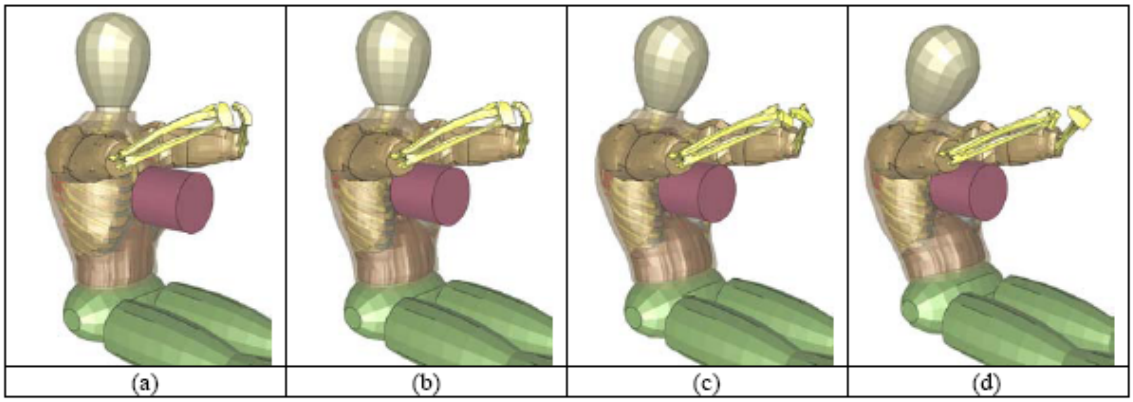

Figure 3.9 Front Thoracic Impact Simulation (a) t=0 sec (b) t=0.015 sec (c) t=0.030 sec (d) t=0.045 sec (Forbes, 2005)

The front pendulum simulation results are shown below (Figure 3.10).

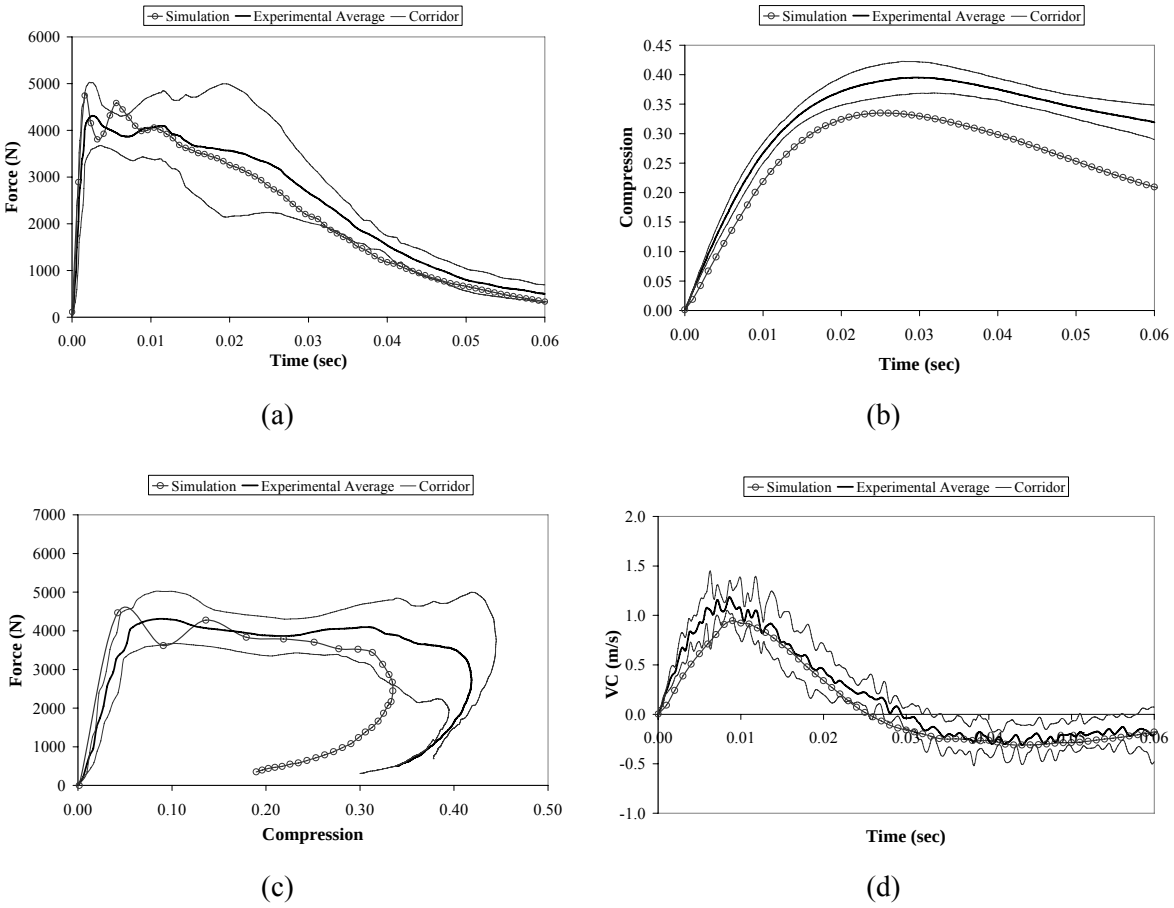

Figure 3.10 Front Thoracic Impact Simulation Results (a) Force (b) Compression (c) Force-Compression (d) VC (Forbes, 2005)

The results are further summarized in Table 3.1.

Table 3.1 Front Thoracic Impact Correlation Summary (Forbes, 2005)

MEASUREMENT	IMPACT PHASE	CORRELATION
Force	Loading	*Good*
	1st Peak	*Good*
	Plateau/2nd Peak	*Reasonable*
	Unloading	*Good*
Compression	Loading	*Reasonable*
	Peak	*Reasonable*
	Unloading	*Poor*
VC	Loading	*Good*
	Peak	*Good*
	Unloading	*Good*

The model's side impact response has been validated by pendulum impact tests performed by Chung et al. on four PMHS using a 50 kg wood impactor of 152.4 mm diameter centered over the 6th rib (Figure 3.11). However, the validation only uses tests that had a male subject providing a sample size of five PMHS. The impact force and chest deflection were measured using a load cell in the impactor and a chest band respectively.

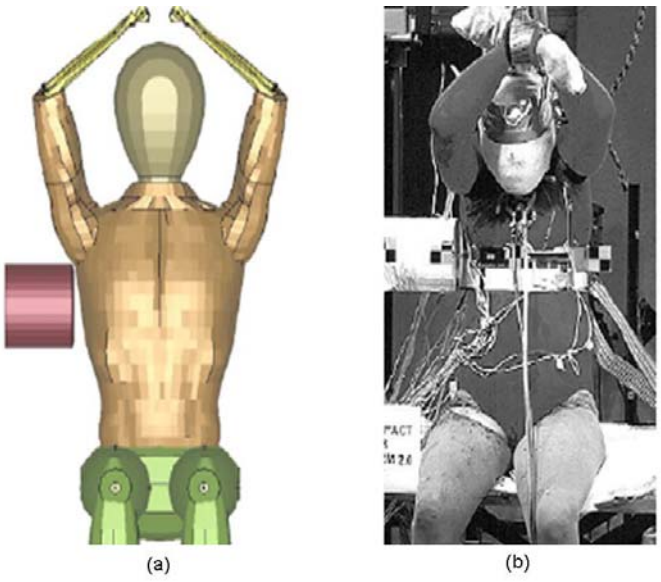

Figure 3.11 Side Thoracic Pendulum Impact Test (a) Simulation (b) Experiment (Chung et al., 1999)

Figure 3.12 shows the response of the thorax at various times during a lateral pendulum impact.

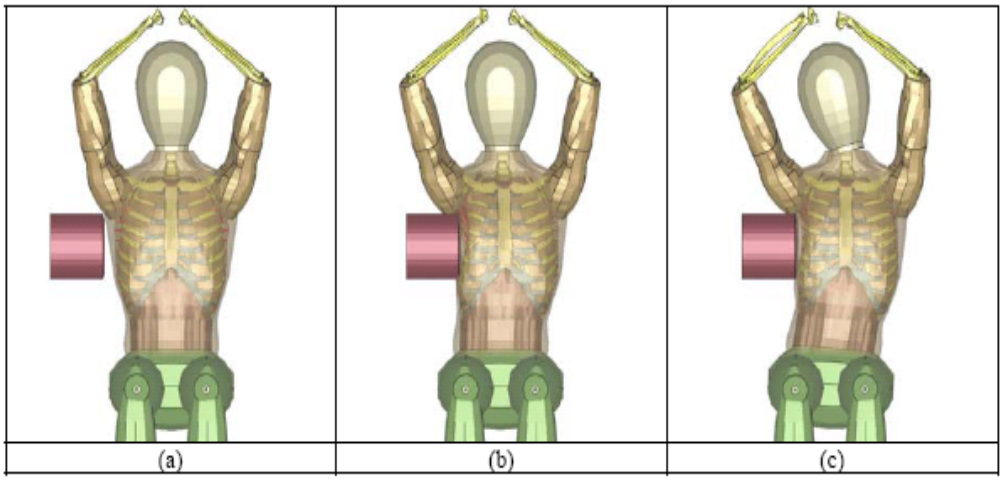

Figure 3.12 Side Thoracic Impact Simulation (a) t=0 sec (b) t=0.015 sec (c) t=0.030 sec (Forbes, 2005)

The side pendulum simulation results are shown below (Figure 3.13) and the results are further summarized in Table 3.2.

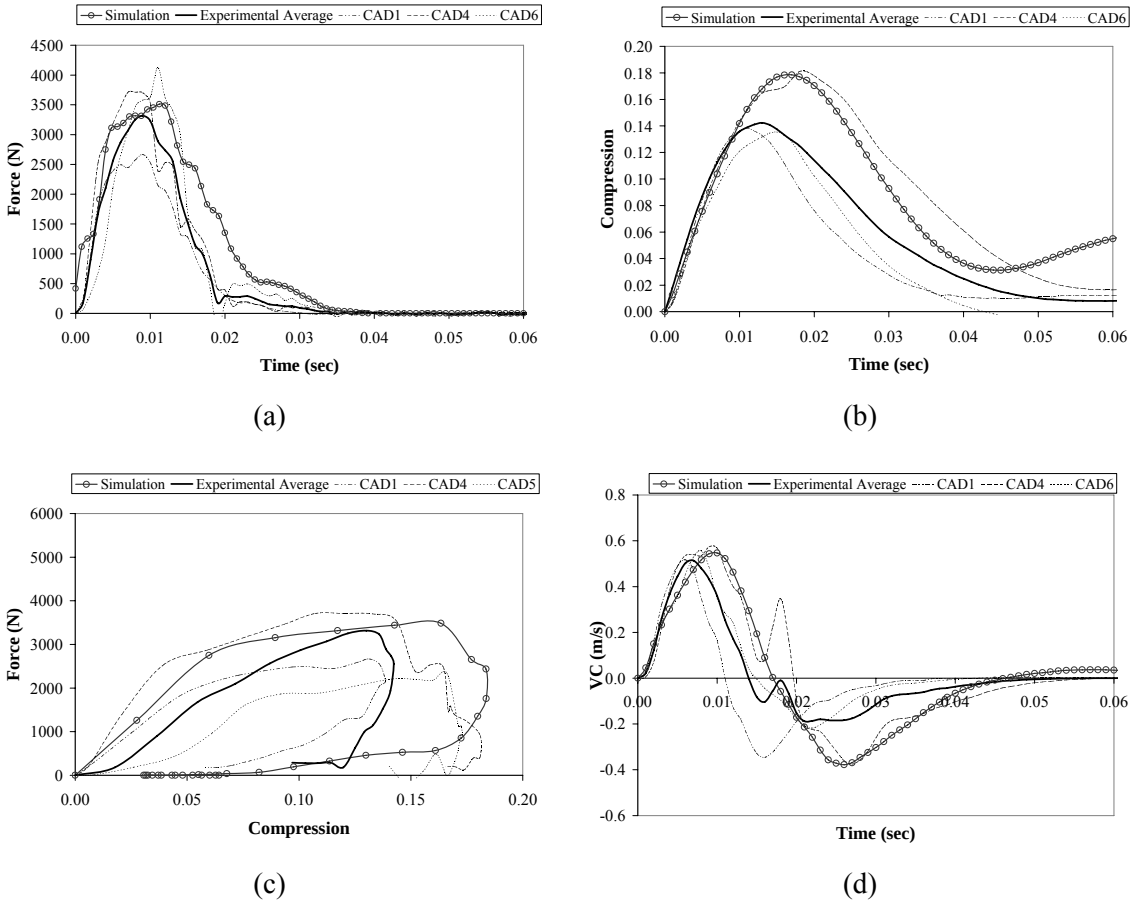

Figure 3.13 Side Thoracic Simulation Results (a) Force (b) Compression (c) Force-Compression (d) VC (Forbes, 2005)

Table 3.2 Side Thoracic Impact Correlation Summary (Forbes, 2005)

MEASUREMENT	IMPACT PHASE	CORRELATION
Force	Loading	*Good*
	Peak	*Good*
	Unloading	*Good/Reasonable*
Compression	Loading	*Good*
	Peak	*Good*
	Unloading	*Good*
VC	Loading	*Good*
	Peak	*Good*
	Unloading	*Good*

3.3.2 Side Sled Tests

Whole body response was validated using side sled impact tests performed to provide information on the interaction of all body regions and their influence on injury. Two types of side sled impact tests, NHTSA and Wayne State University (WSU), were used to validate the model. First, Pintar et al. (1997) conducted 26 PMHS side sled impact tests based on the NHTSA sled (Kaillieris et al., 1981). The apparatus consisted of a 1.3 m long bench accelerated to 6.67 m/s or 8.89 m/s and then suddenly decelerated to 0 m/s causing the PMHS to travel into a rigid wall at 6.67 m/s or 8.89 m/s. Figure 3.14 and Figure 3.15 show the NHTSA side sled wall and side sled test setup respectively.

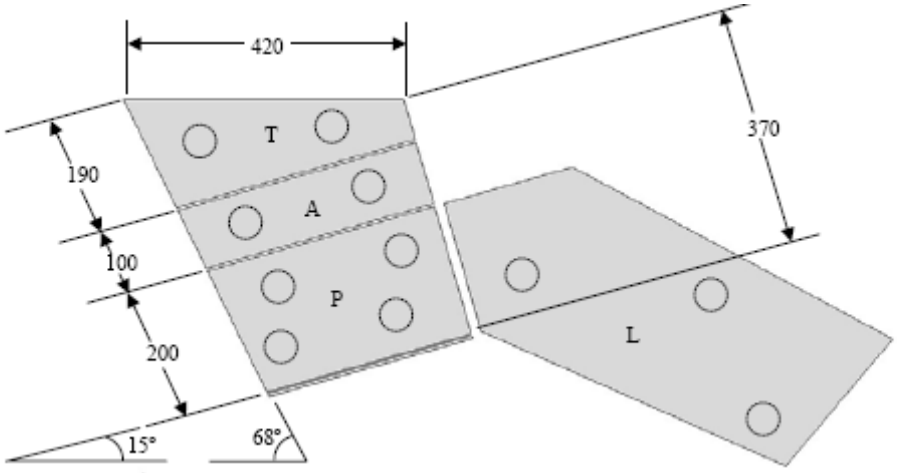

Figure 3.14 NHTSA Side Sled Device Dimensions (Pintar et al., 1997; Forbes, 2005)

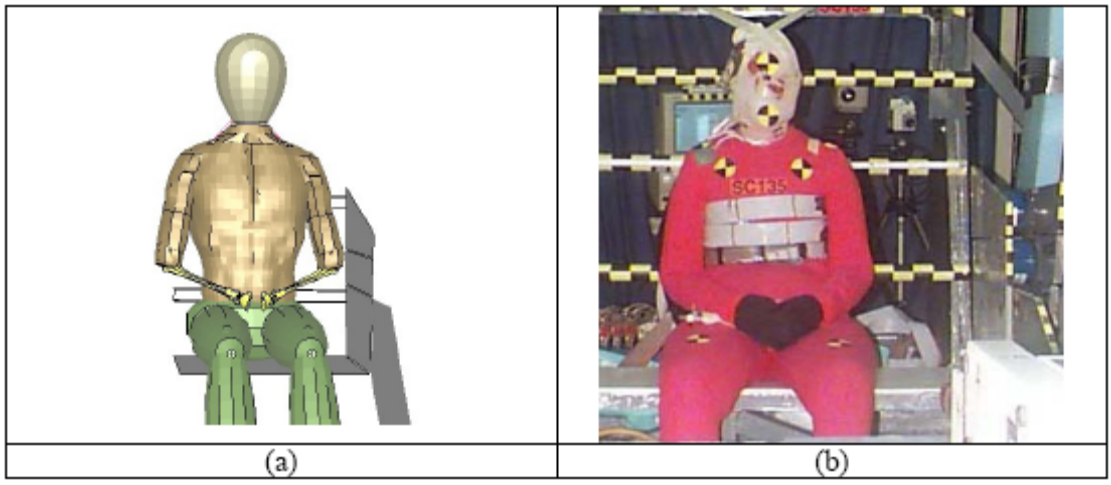

Figure 3.15 NHTSA Side Sled Test (a) Simulation (b) Experiment (Pintar and Yoganandan, 2001; Forbes, 2005)

The impact force was measured by impact plates instrumented with load cells and chest deflection was measured using chest bands at the 4th rib, xiphoid processs, and 10th rib termed the upper, middle, and lower bands respectively.

The second type of PMHS side sled impact tests were conducted on 31 PMHS at WSU and were based on the Heidleberg sled with modifications to the plate orientation (Cavanaugh et al., 1990). As in the case of Pintar's work, the PMHS were impacted into a rigid wall at 6.67 and 8.89 m/s. Figure 3.16 and Figure 3.17 show the WSU side sled wall and side sled test setup respectively.

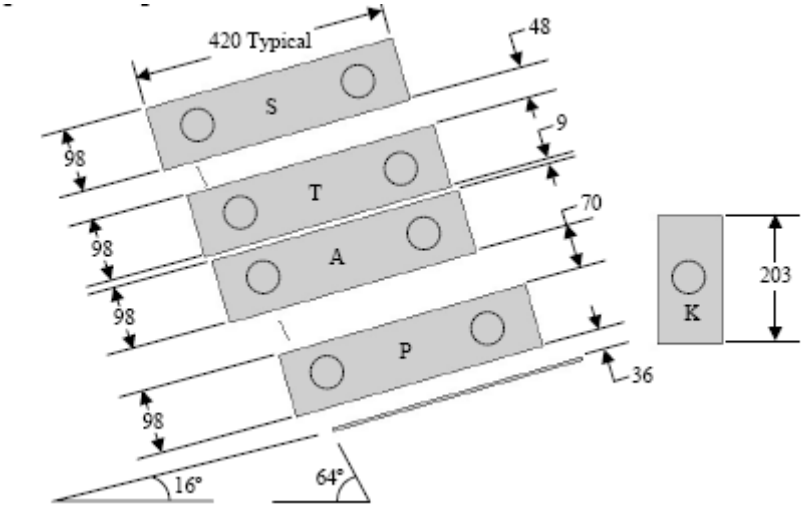

Figure 3.16 WSU Side Sled Device Dimensions (Cavanaugh et al., 1990)

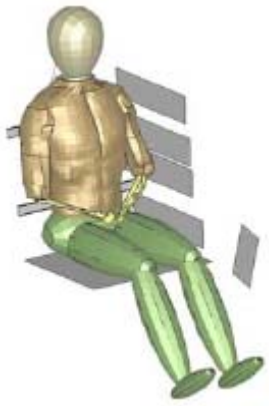

Figure 3.17 WSU Side Sled Test Simulation (Forbes, 2005)

Again, the impact plates were equipped with load cells to measure the impact force. However, the chest deflection was measured by tracking targets placed on the PMHS sternum at the T5 level.

The NHTSA tests had three male test subjects impacted at 6.67 m/s and five subjects at 8.89 m/s. WSU PMHS tests provided three male tests at 6.67 m/s and two tests at 8.89 m/s.

The following responses were used to compare the NHTSA and WSU side sled impact tests to simulated results:

- Timing — Timing of Impact Evaluated by the onset of force at each plate.
- Force — Impact force between rigid wall and body.
- Impulse — Impulse measured throughout impact to account for the total body impact.
- Compression — Full width thoracic compression measurements made for NHTSA sled test and half width compression measurements made for WSU sled tests
- VC — Viscous injury criterion; rate of deflection multiplied by compression
- Injury — Number of Rib Fractures.

Figure 3.18 shows the human body model response versus the PMHS response at various times during a NHTSA side sled impact.

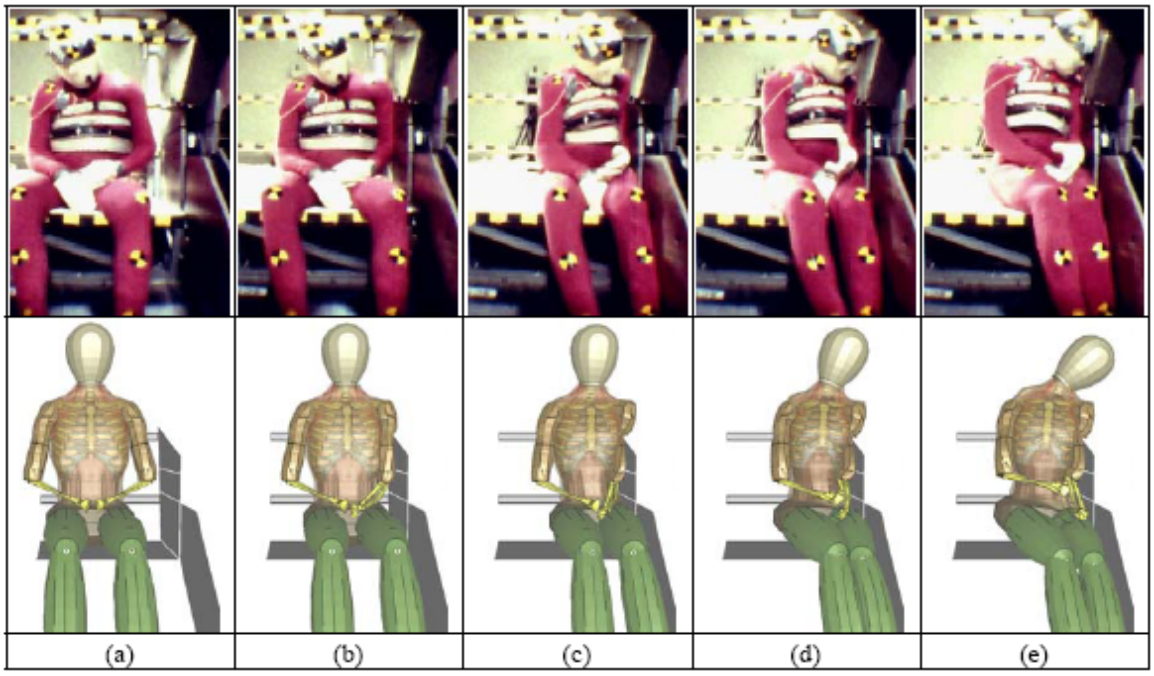

Figure 3.18 NHTSA Side Sled Impact Simulation (a) t=0 sec (b) t=0.015 sec (c) t=0.030 sec (d) t=.045 sec (e) t=.060 sec (Forbes, 2005)

The VC response for the upper and lower bands is shown below for the NHTSA side sled impact simulation. The upper and lower VC response displays *good* and *reasonable* correlation to PMHS data respectively (Figure 3.19).

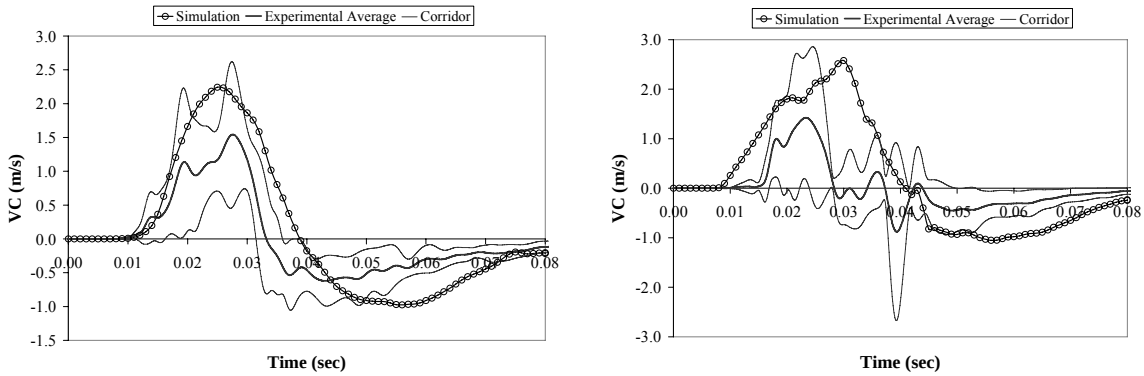

Figure 3.19 NHSTA Sled Test VC Response (8.89m/s) (a) Upper Band (b) Lower Band (Forbes, 2005)

The pendulum and side impact sled tests provided useful insight into the biofidelity of the human body model. Comparison of human body model simulated results to PMHS testing showed *good* correlation to thoracic impact and *good* or *reasonable* correlation to whole body response.

This study further validates the human body model using load conditions experienced in side impact auto crash and investigates the collision factors affecting thoracic trauma. Current side impact test methods and numerical modeling efforts are discussed in the following chapter.

-- CHAPTER 4 --

Side Impact Model Development

This chapter discusses the development of a side impact model implementing some of the methodology previously summarized in order to further validate the human body model using realistic crash conditions.

4.1 Side Impact Model Development

The side impact model is a simplified model used to reproduce the key conditions present in full scale crash tests. The model accounts for several important factors that contribute to occupant response based on the literature. These factors are; the relative velocities between the seat and door, the occupant to door distance, the door shape, and door compliance. Although some components were simplified in terms of geometry, they were based on geometries found in typical vehicles and material characteristics determined by experiment or found in the literature.

The side impact model consists of several components modeled as rigid materials, including the seatbelt anchors, sled base, and outer door. The seat, seatbelts, and door

were based on representative geometries and material properties determined by experimental testing and data from the literature.

The seat pan, sled base, and door had velocity profiles applied for the duration of the simulation. Velocity profiles were obtained from the NHTSA database for crash testing. Although rotational velocities do exist in full scale crash testing, rotation tends to occur after the maximum thoracic response is observed and can therefore be omitted for the purposes of this study (Watson et al., 2009). Therefore, the side sled is constrained in the X and Z directions to prevent rotations and to allow focus entirely on the effects of side impact in the Y direction.

4.2 Seat Model

Automotive seats consist of two major components; structural frame members and non-structural seat material (Severy et al., 1976). Structural frame members are often constructed from tubular steel or stamped sheet metal, while non-structural seat material consists of seat foam, springs, and upholstery. This section discussing the development of a simplified seat model used to represent the seat frame and foam based on representative geometries and material characteristics determined through experimental testing and data found in the literature.

4.2.1 Seat Foam Materials and Properties

Energy absorbing and comfort enhancing foam materials have been utilized by the automotive industry for many years. In particular, low density open cell polyurethane-based foams are commonly used in automotive seating applications. Although a wide range of mechanical properties can be achieved through varying the material density and processing conditions, many automotive seat foams fall into a relatively narrow range in terms of density and mechanical properties. Automobile seats typically incorporate a metallic frame, wires and springs to act as a support system, and a foam pad to support the occupant. These components are then enclosed with soft trim (fabric) that may pre-

compress the foam, making automotive seat performance challenging to model and design. Although there are many aspects to automotive seat performance, the focus of this study is the characterization of typical automotive seat foams and implementation of these properties into appropriate numerical constitutive models that can account for the non-linear material responses and rate effects.

To accurately represent the interaction between an occupant and vehicle an appropriate model of the seat, including representative material properties, is required. Foam is one of the main components of a seat and the mechanical properties have a significant influence on occupant response in the event of a collision. Foam used for automotive applications is manufactured from soft polyurethanes and typically has a density between 20-60 kg/m^3 and a Poisson's Ratio of approximately zero. The mechanical properties of foams depend on their geometric structure (i.e. size and shape of the cell) and the intrinsic properties of the cell wall material (Du Bois, 2004).

Mechanical property characterization of soft materials is challenging since we often require properties for large deformations across a range of deformation rates from quasi-static/relaxation response to intermediate rates in auto crash and high rates in impact scenarios. This necessitates the use of several test apparatuses to achieve the desired range of rates.

For the current study, this has been accomplished using three types of testing. First, low rate stress-strain data was measured using quasi-static compression apparatus. Second, intermediate strain rates were obtained using direct impact pendulum testing. Finally, high rate properties were determined using a unique Polymeric Split Hopkinson Pressure Bar (PSHPB), previously used and validated for a variety of materials including elastomers, foams, and biological soft tissues (Du Bois, 2004, Cronin et al, 2006, Doman et al 2006, Van Slightenhorst et al, 2003).

Foam Characterization Results

Five open-cell polyurethane foam materials, commonly used in automotive seating applications have been characterized. Material densities can be seen in Table 4.1, where materials 4 and 5 had a similar density but different tear strengths attributed to a difference in material processing. This highlights the wide range of mechanical properties that may be achieved even for a relatively narrow range of foam density.

Table 4.1 Density of Automotive Seat Foam

PHYSICAL PROPERTY	**SAMPLE 1**	**SAMPLE 2**	**SAMPLE 3**	**SAMPLE 4**	**SAMPLE 5**
Density Kg/m^3	48.1	39.2	38.5	27.3	27.3

Quasi-static Testing

Quasi-static compression tests were performed to acquire low rate stress-strain data. Foam samples were cut into cylinders approximately 54 mm in length and 54 mm in diameter, and tested in a hydraulic compression machine. It should be noted that all specimens were removed from the core of larger foam samples so that the material in the specimen was relatively consistent in cell size and density. The outer skin generally present on foam components was not investigated in this study. Figure 4.1 shows typical specimens. Although every effort was made to make the samples consistent in size, some variability was present. However, this was accounted for by using the actual specimen dimensions to calculate the stress-strain curves.

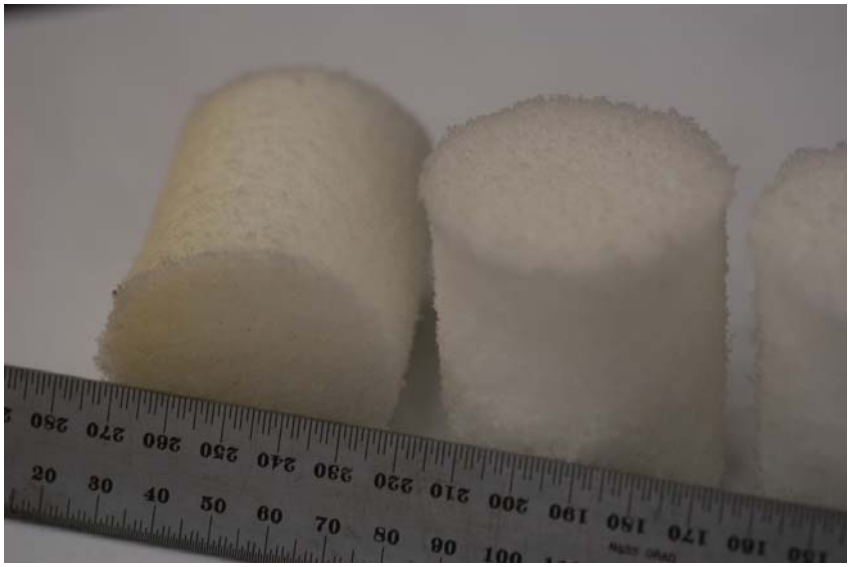

Figure 4.1 Quasi-static Foam Samples (Dimensions in mm)

The quasi-static test apparatus is shown in Figure 4.2 below:

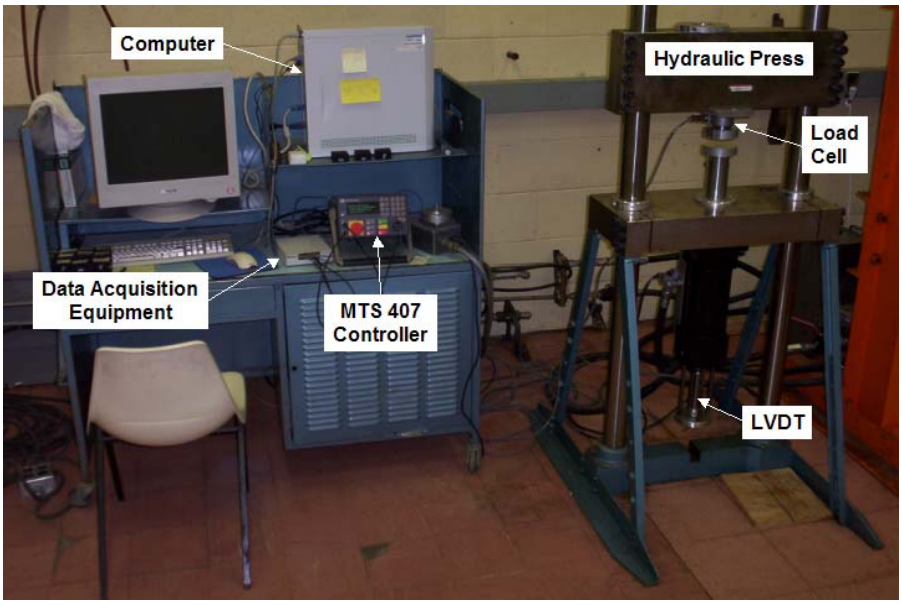

Figure 4.2 Quasi-static Test Apparatus

Experiments were conducted at a strain rate of 0.01 s^{-1} up to 95% compression for the five materials. Three tests on each material were performed to ensure that consistent results were obtained. Figure 4.3 and Figure 4.4 show typical results from the quasi-static compression tests on each of the five foams. The material stiffness generally increased with increasing density, as expected. This is not the case for Foam1, where the stiffness was lower, and Foam 5, where the stiffness was higher than suggested by the material density. Figure 4.5 and Figure 4.6 show three repeat tests on Foam 1 indicating the measured response was very consistent between samples.

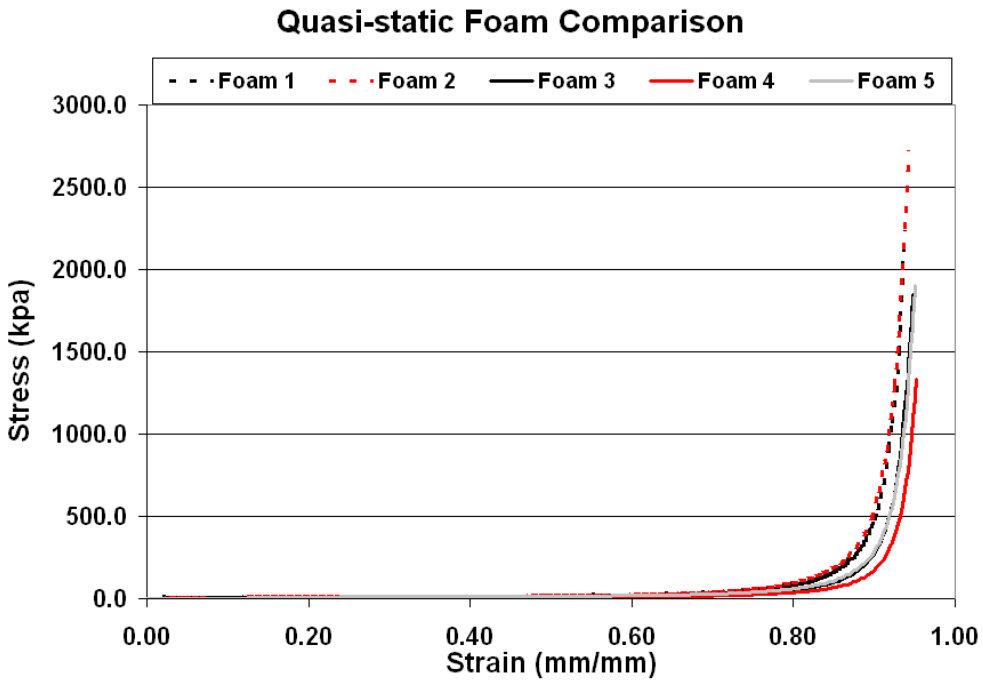

Figure 4.3 Quasi-static Compression Test Data

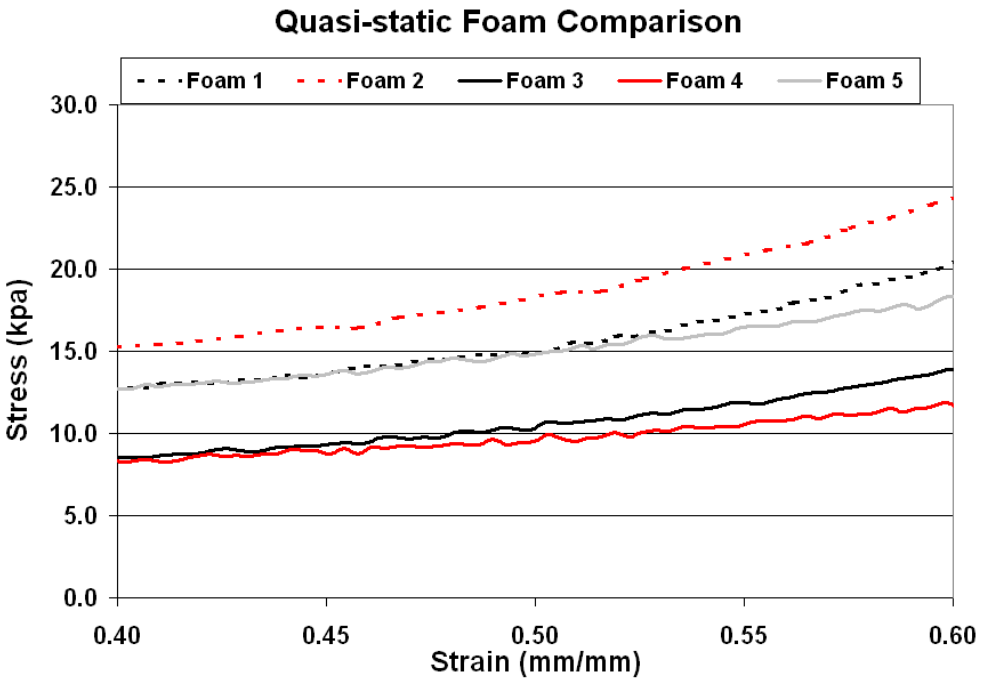

Figure 4.4 Quasi-static Compression Test Data

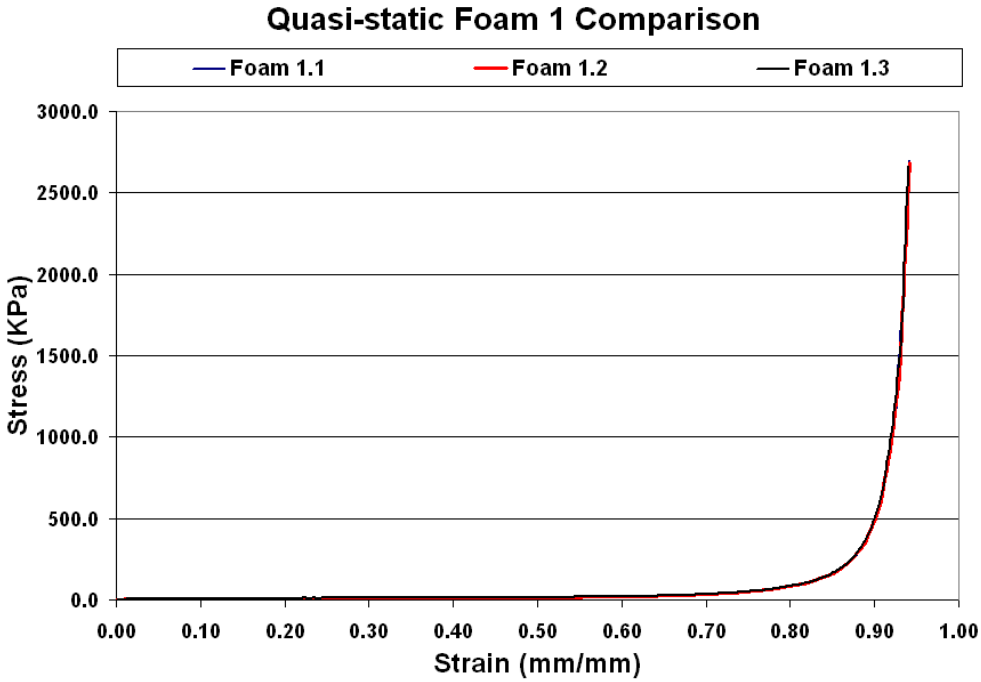

Figure 4.5 Repeat Quasi-static Test Results for Foam 1

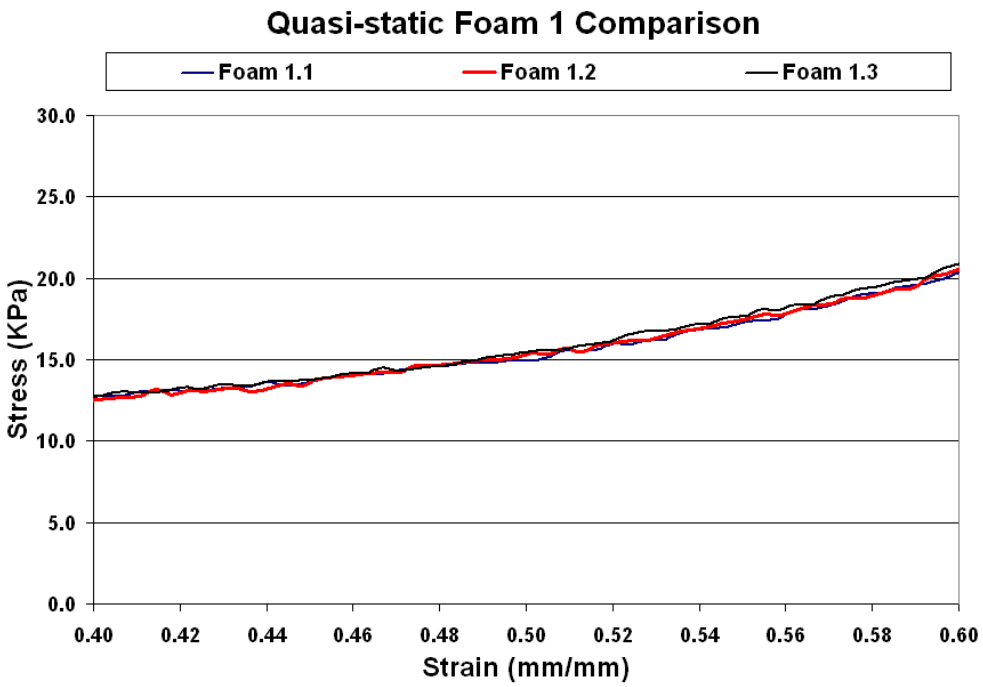

Figure 4.6 Repeat Quasi-static Test Results for Foam 1

The stress-strain curves observed provide an overview of the range of foam stiffness. It is clear that the foams exhibit some modest differences and that foams 2 and 4 occupy the upper and lower ends of the stiffness spectrum respectively. Therefore, further testing was only undertaken for these two foams.

HIGH DEFORMATION RATE COMPRESSION TESTING

High rate testing was undertaken on Foam materials 2 & 4, since they represented the upper and lower bounds, respectively, for the materials considered. Foam samples were cut into 25 mm length by 25 mm diameter cylinders and tested in the Polymeric Split Hopkinson Pressure Bar (PSHPB) apparatus. Initial tests showed that only modest levels of compression (up to 40%) could be achieved, and that the modest elastic wave speed of these materials made it difficulty to achieve dynamic equilibrium, corresponding to uniform axial deformation. This is a fundamental assumption for valid dynamic tests and was determined by comparing the predicted force at the bar ends for the incident and transmitter bars. High-speed video was also investigated but did not provided valuable

results due to the low Poisson's ratio for these foam materials. Based on varying strain rates within the quasi-static range, and additional testing at medium strain rates, it was assumed that strain rate effects were negligible in the early portion of the stress strain curve prior to consolidation of the material. The amount of deformation that can be achieved in a dynamic compression test is directly related to the length of the striker and compression wave within the incident bar. Although the PSHPB achieved high deformations due to the significant length of the bars, the materials could not be compressed to densification while maintaining a representative specimen size. This was addressed through pre-compression of the samples for the high deformation rate tests.

From the quasi-static tests it was determined that compression up to 80% strain was well outside the range of material consolidation, and allowed for valid high deformation rate testing using the Hopkinson technique. As such, the samples were pre-compressed to 80% in the Hopkinson bar prior to testing. In order to determine the stress history over the entire strain path, the quasi-static data was combined with the high rate data to complete the stress-strain curve. It was assumed that the stress in the sample was equivalent at 80% compression during both the quasi-static and high rate tests and so the high rate stress-strain curve was shifted to match the quasi-static curve at 80% strain. The quasi-static and high rate curves can be seen below.

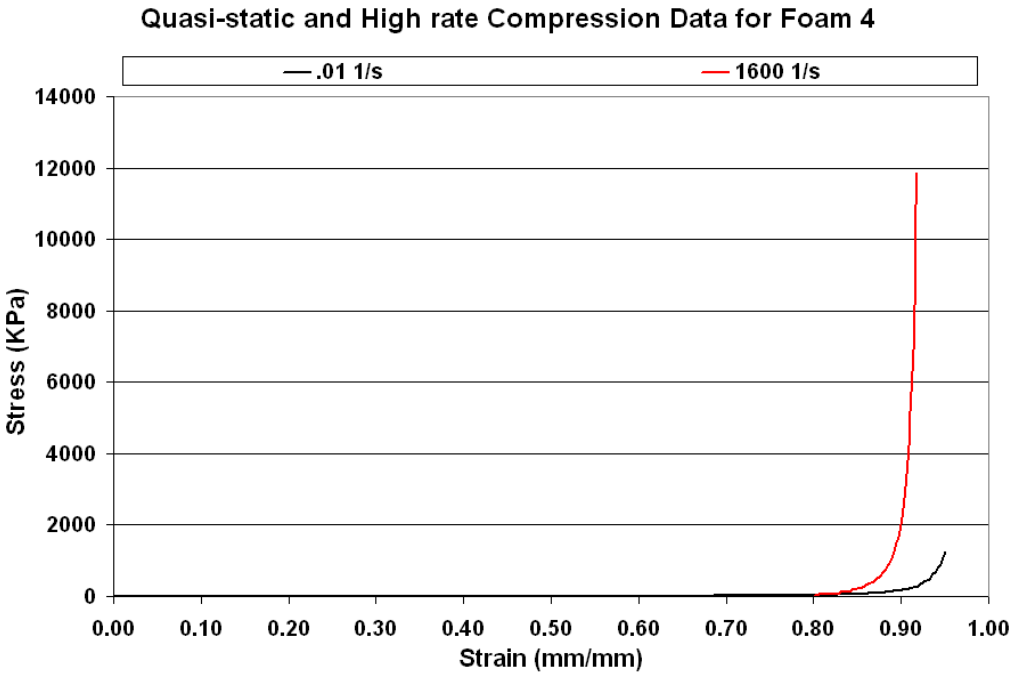

Figure 4.7 Quasi-static and high rate Stress-Strain data for Foam 4

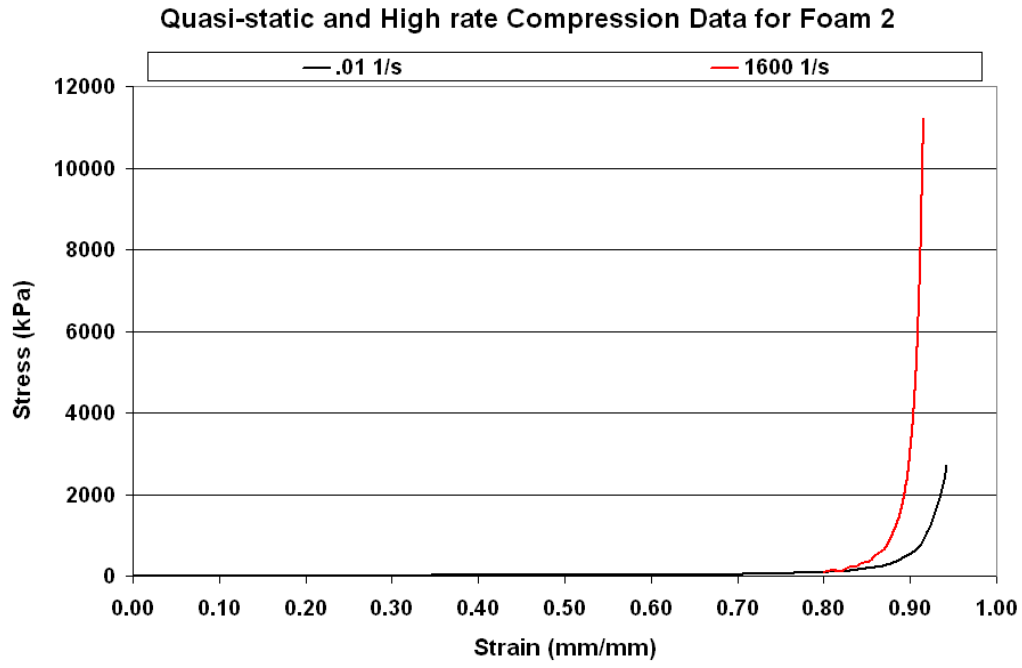

Figure 4.8 Quasi-static and high rate Stress-Strain data for Foam 2

Intermediate Rate Compression Testing

As previously mentioned it was assumed that the stress in the sample was equivalent at 80% compression during both the quasi-static and high rate tests. This assumption has been investigated by performing intermediate strain rate testing using the pendulum impact apparatus shown in Figure 4.9.

Figure 4.9 Pendulum Impact Apparatus

This assumption was validated by pendulum impact tests. The figures below show the quasi-static, intermediate, and high-rate stress-strain curves for Foam 2 and Foam 4.

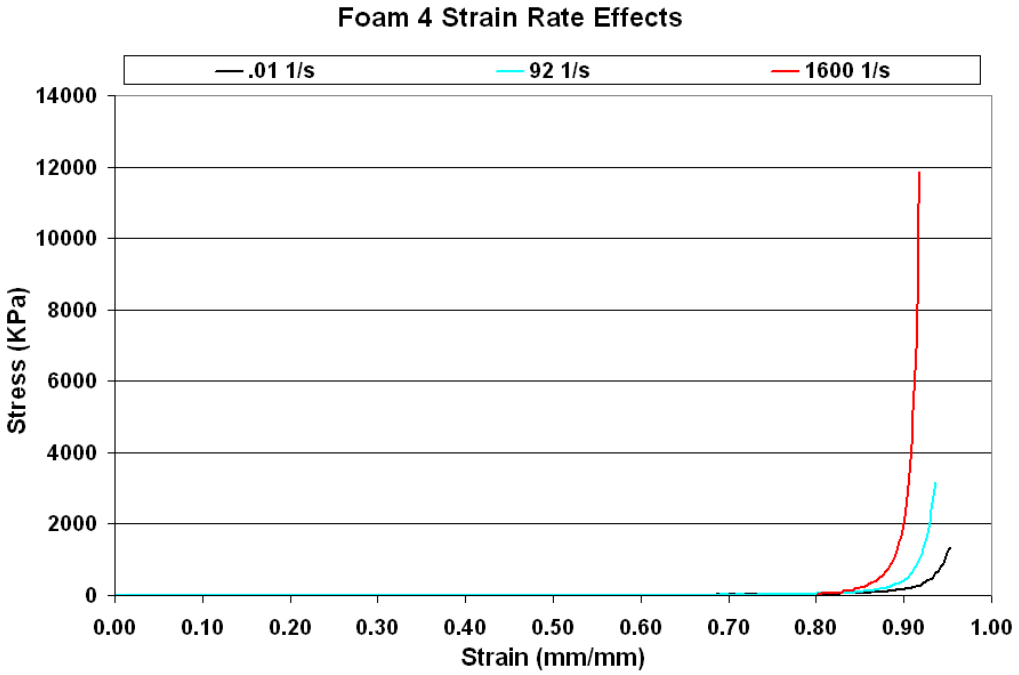

Figure 4.10 Foam 4 Rate Effects

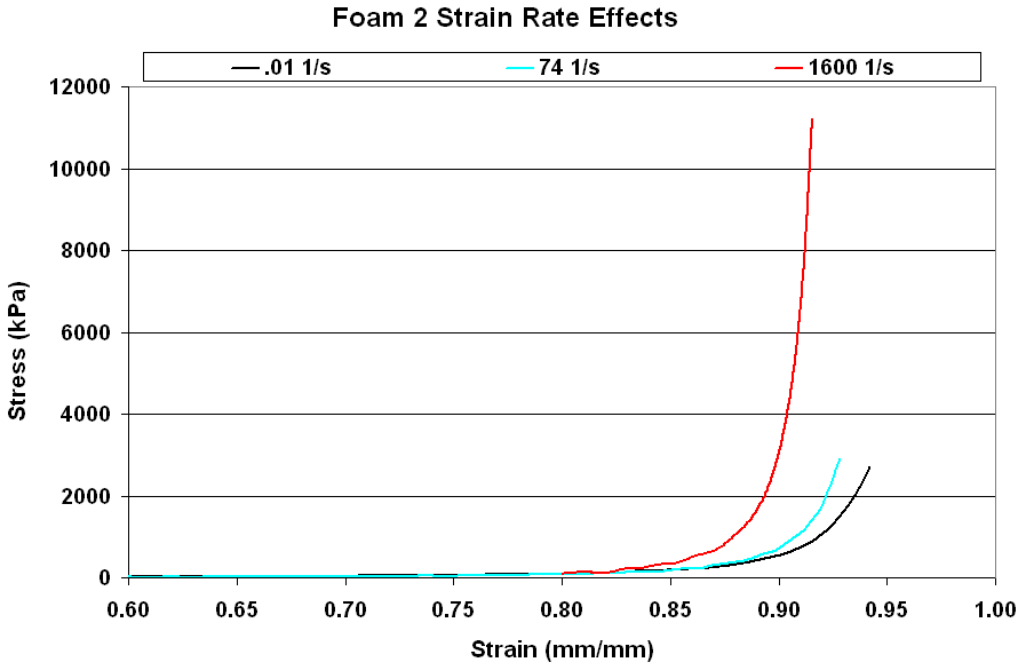

Figure 4.11 Foam 2 Rate Effects

4.2.2 Seat Model

As with the numerical body model, it is ideal to model the seat to the level necessary to achieve the desired results. That is, it is unnecessary to model the seat and its components to such a high degree of accuracy that it becomes too computationally expensive to justify the given results. The seat geometry may become more advanced in the future to obtain more detailed and representative responses. However, initially the seat will consist of the shell element frame components provided in the simplified seat model, and a simple foam seat consisting of the 3-D finite element mesh shown below. The seat pan is based on simplified GM Malibu seat geometry and is composed of rigid shell elements with the properties of steel. Seat foam is modeled using solid elements sharing nodes with the seat pan to maintain contact between the two components.

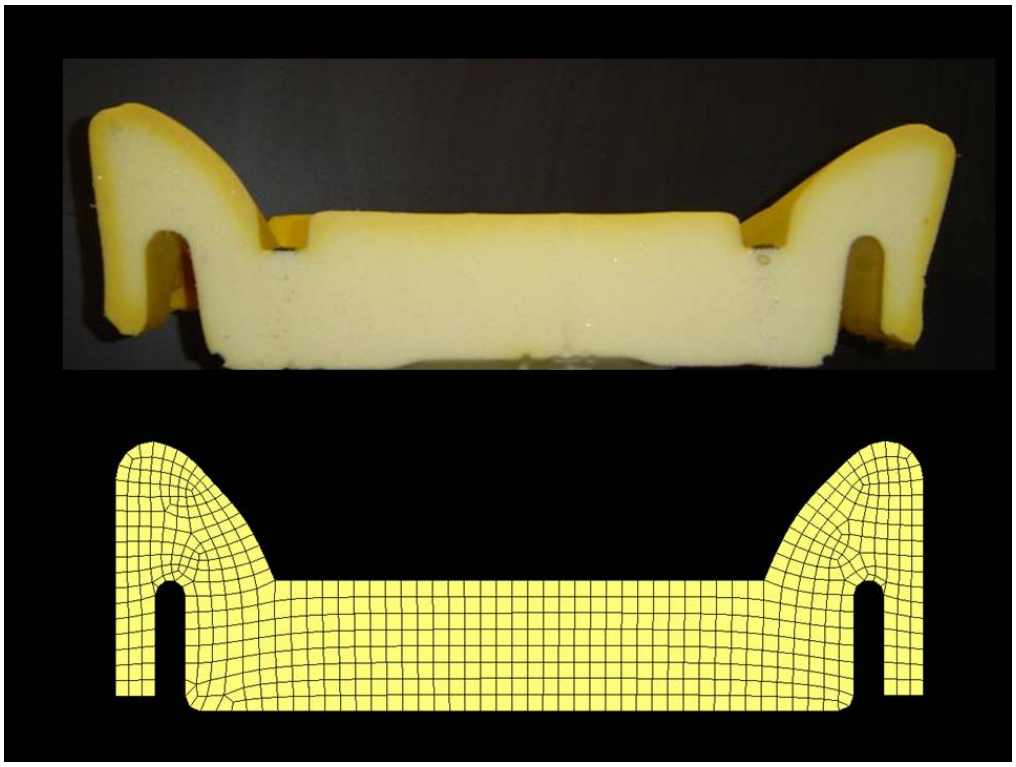

Figure 4.12 Finite Element Seat Bottom Mesh

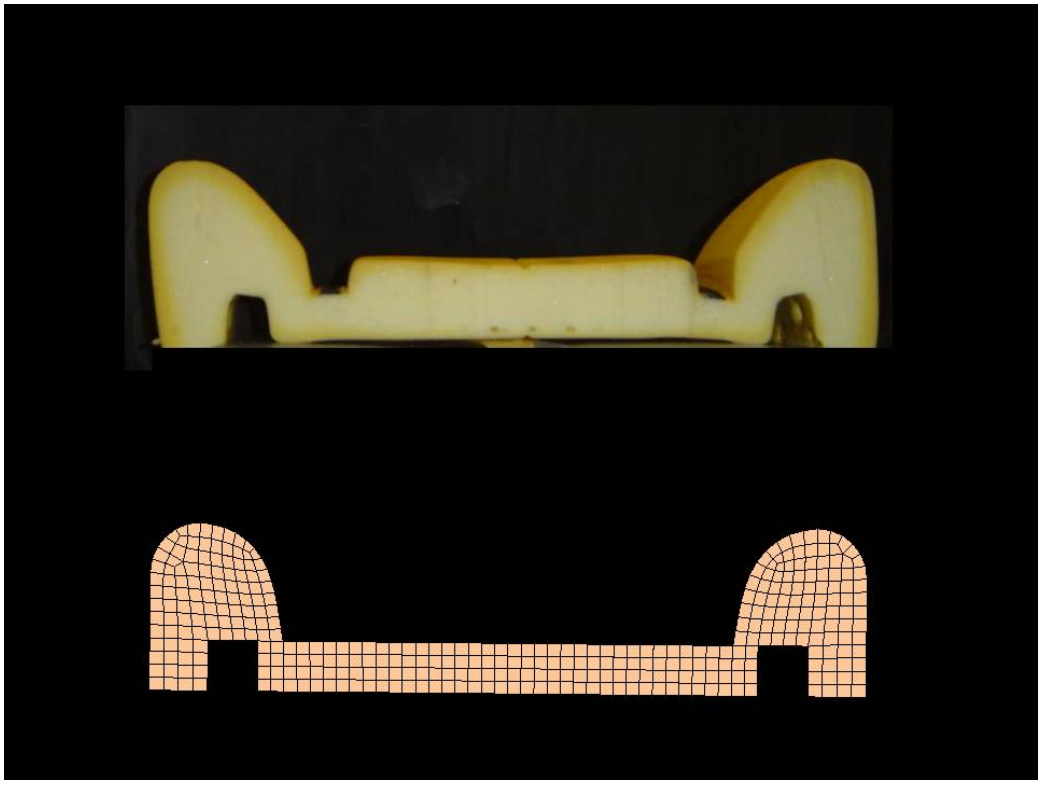

Figure 4.13 Finite Element Seat Back Mesh

Simplifications of the geometry were required to reduce computational time. As a consequence some of the rounded edges have been eliminated reducing the mesh complexity. This will save a significant amount of computational time and may have only modest effect on the quality of results obtained.

Foam material has been modeled using Fu Chang's Material model for low density foams as recommended in the literature (Du Bois, 2004; Serefi et al., 2003). This material model is capable of modeling the rate effects found present in material tests. Below is the *MAT_FU_CHANG card used.

Table 4.2 *MAT_FU_CHANG material card

MID	RO	E	ED	TC	FAIL	DAMP	TBID
2	27.3e-12	175	0	1E20	1	.05	1
BVFLAG	**SFLAG**	**RFLAG**	**TFLAG**	**PVID**	**SRFA**		
0	1	1	0		1		

It should be noted that Fu Chang's Model assumes a poisons ratio of zero. The foam material strain and strain rate responses are decomposed into two parts, linear and non-linear and the material stress is determined as a function of the loading history. The foam model was further enhanced to allow for a material response definition using nominal stress and engineering strain. This version was used for the current study.

In addition to the measured experimental data, extrapolation based on the Young's modulus of solid polyurethane (1.6 GPa) was included from 95% to 98% strain and a near vertical slope was applied between 98% and 99% strain to ensure numerical stability in this region of compression, as recommended by Du Bois (2003).

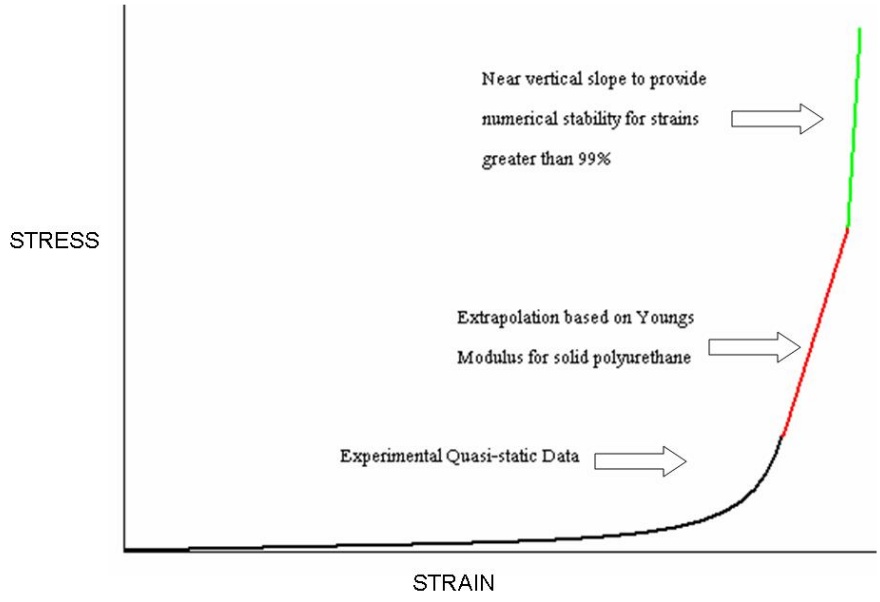

Figure 4.14 Stress-Strain Curve Extrapolation

Numerical simulation and experimental data for the Quasi-static material compression is shown in Figure 4.15 and Figure 4.16 shows the high deformation rate predictions of the numerical model. These curves demonstrate the ability of the modified Fu Chang constitutive model implemented in LS-DYNA to capture the measured experimental response of the foam at quasi-static and high rates.

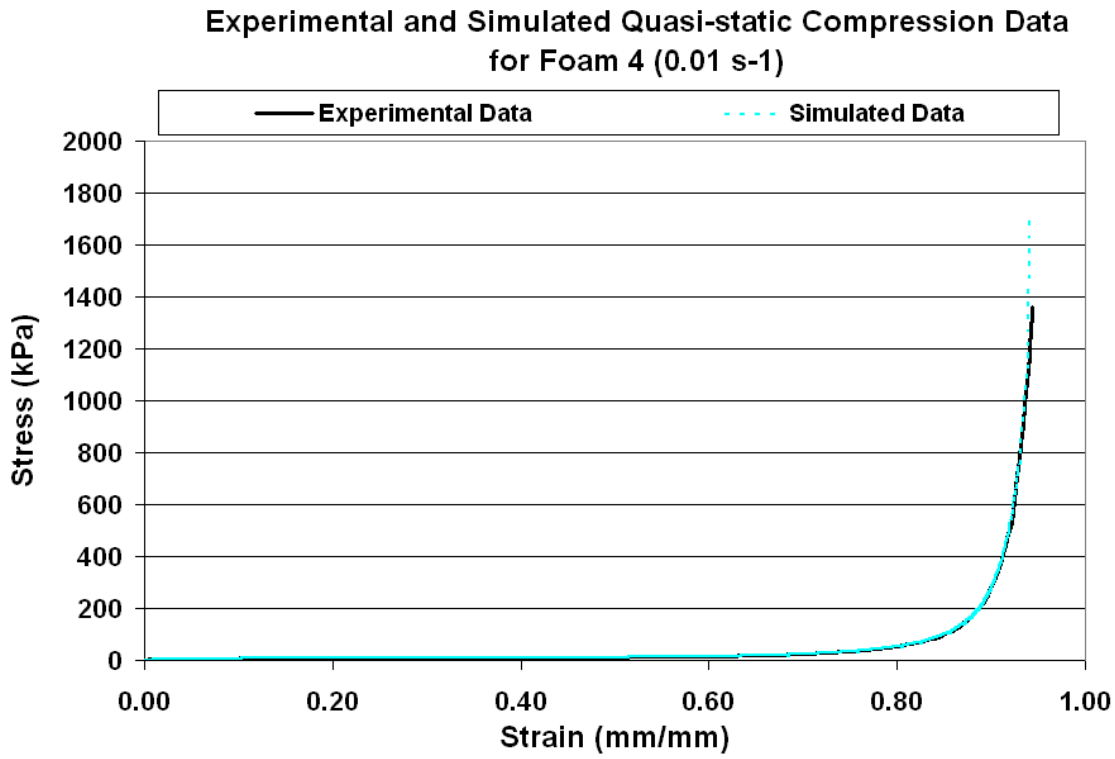

Figure 4.15 Experimental and Simulated Quasi-static Compression Data for Foam 4 (0.01 s^{-1})

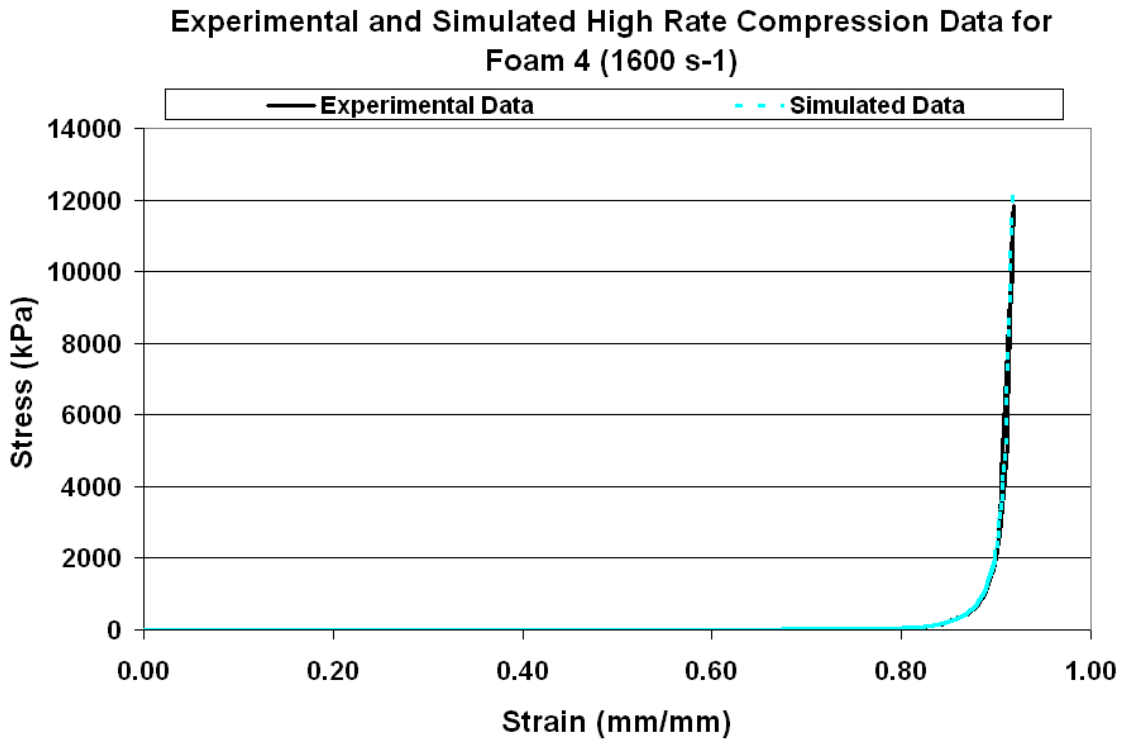

Figure 4.16 Experimental and Simulated High Rate Compression Data for Foam 4 (1600 s^{-1})

Once the Fu Chang material model has been validated for a single element compression it may be applied to modeling automotive seat foam.

The initial position of the occupant will have an effect on occupant motion in collision, and in turn have an impact on thoracic trauma. When the dummy is correctly positioned in the seat, deformations are created in the seat foam causing residual stress and strains to be present. Using the *INITIAL_FOAM_REFERENCE_GEOMETRY card allows the modeling of initial stress and strain in the foam due to a sunk occupant prior to collision.

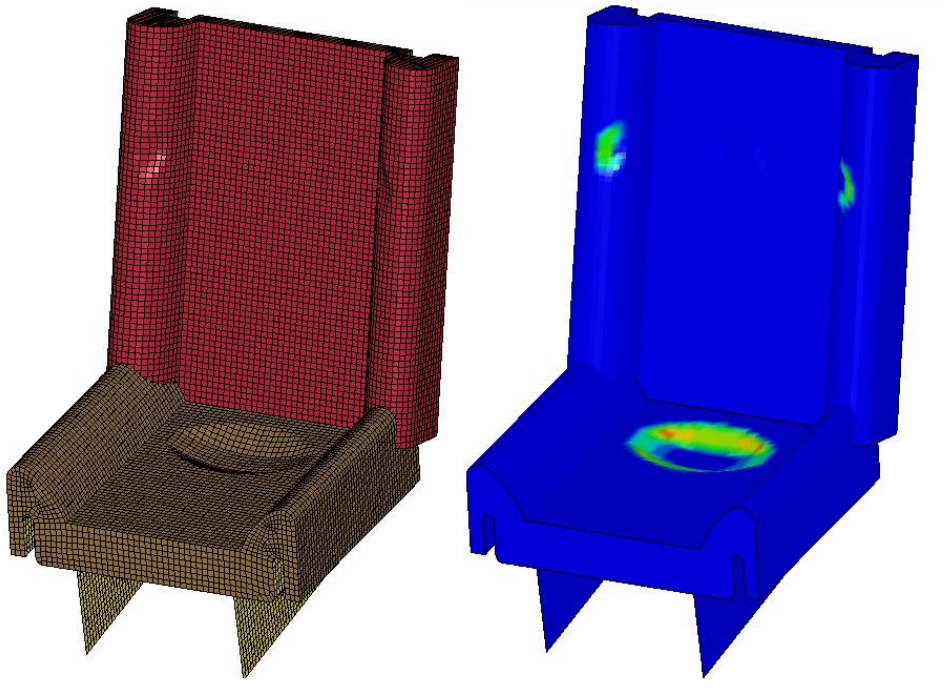

Figure 4.17 Seat Bottom and Back Pre-Deformed Foam

The deformed seat foam geometry is obtained by "sinking" the occupant into the seat using gravity until the occupant has reached a position of equilibrium. This step is performed separate from the side impact simulations as it is a computationally expensive process and requires many hours to run. Alternative methods exist, which involve, forming the seat foam around the pre-positioned occupant. However, this method deformed elements in a non-physical manner thereby creating unrealistic initial stresses in the seat foam.

4.3 Door Model

An extremely important factor and area of focus in this study is the door to occupant interaction. To understand the effects of the door two models have been developed. The first model is simply a rigid plate used to provide a baseline test and understanding of side impact crash at a basic level. The second door model is a simplified door in terms of its geometry, but is representative of automotive door compliance. Similar studies have

been performed by modeling the components of the door including the trim, inner panel, outer panel, and armrest (Deng and Tzeng, 1996). However, for this study a simplified approach was taken to reproduce door geometry and compliance in order to minimize model development and computational time.

Door geometry was based on a cross section of a Ford Taurus model door as seen in Figure 4.18 (NHTSA Website, 2007). The door was sectioned through the area that had the greatest armrest depth in order to produce a conservative door model.

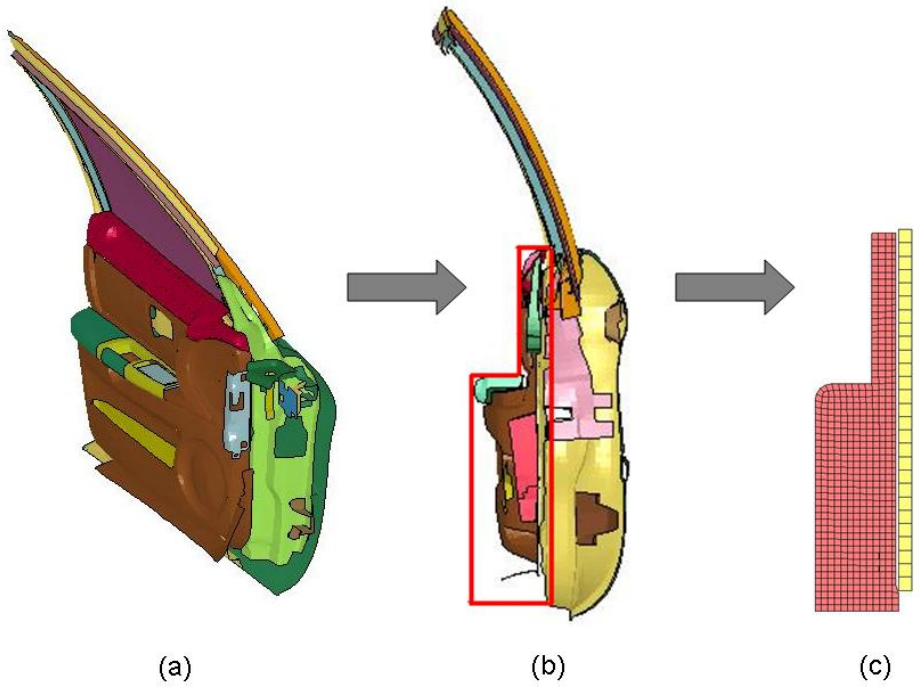

Figure 4.18 Door Model Geometry (a) Ford Taurus Door Model (b) Ford Taurus Door Section (c) Side Impact Simulation Door Model (NHTSA Website, 2007)

The simplified method of door model development requires a prescribed response that will generate the general response of the door components. To determine the general characterization of the door interior, Deng and Ng (1993) developed a test apparatus which quasi-statically crushes the door interior using a SID pelvis and thorax form. However, full scale crash testing indicates a large degree of exterior door crush prior to occupant contact (Deng and Ng, 1993). This pre-crush increases the door stiffness as it

reduces the space between the outer and inner door panels. Deng and Ng developed a test fixture to account for the effects of exterior crush prior to door interior testing by pressing the door against a stationary barrier until the desired crush was reached. The interior crush was then performed to characterize a pre-crushed door. Force-deflection data is recorded for the pelvis and thorax forms in Figure 4.19 (Deng & Ng, 1993).

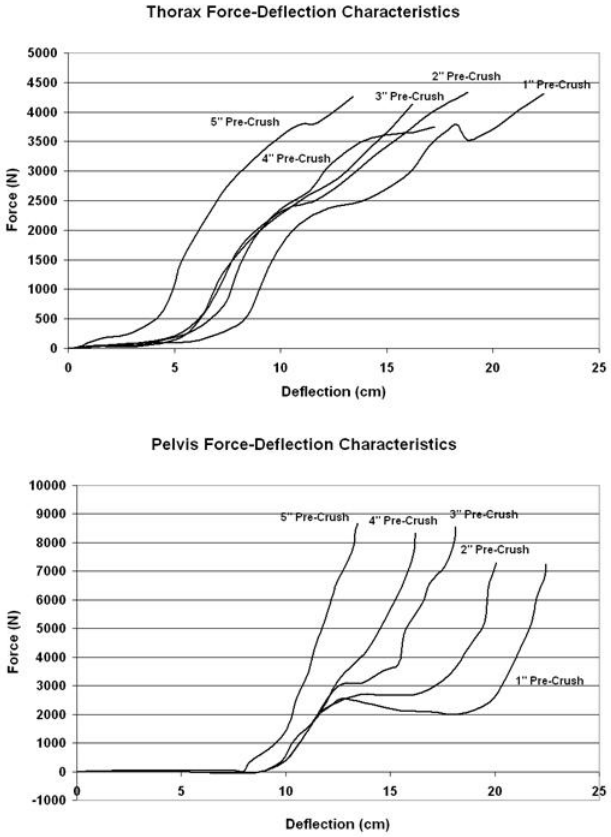

Figure 4.19 Force-Deflection Characteristics of Door Interior (Deng and Ng, 1993)

Since the stiffness tends to increase with increased exterior pre-crush, the side impact simulation door model uses data from a 5" pre-crush to be conservative. Also, it is likely that the exterior door will crush 5" prior to the inner panel contacting the occupant (Deng and Ng, 1993).

The door is modeled using the *Mat_Crushable_Foam model in LS DYNA. However, force-deflection data provided by Deng and Ng cannot be directly applied to the material model because it evaluates thoracic and pelvic force-deflection response rather than the actual material response of the door. Therefore, to determine the material characteristics to input into the material model a simple simulation representing the interior crush test performed by Deng and Ng has been developed using a SID dummy profile (Figure 4.20). This simulation was repeated while adjusting the material load curve used for the door model until the desired force-deflection response was fitted to the experimental response observed by Deng and Ng (Figure 4.21).

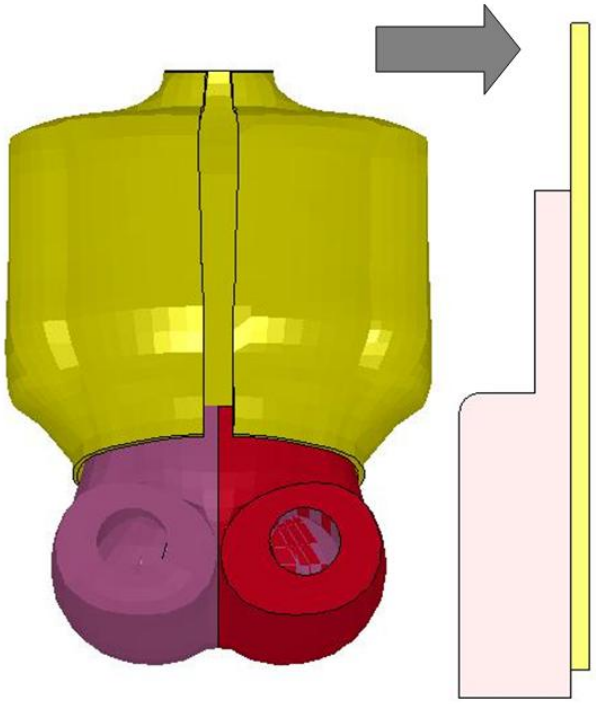

Figure 4.20 Simulated Door Interior Crush Test

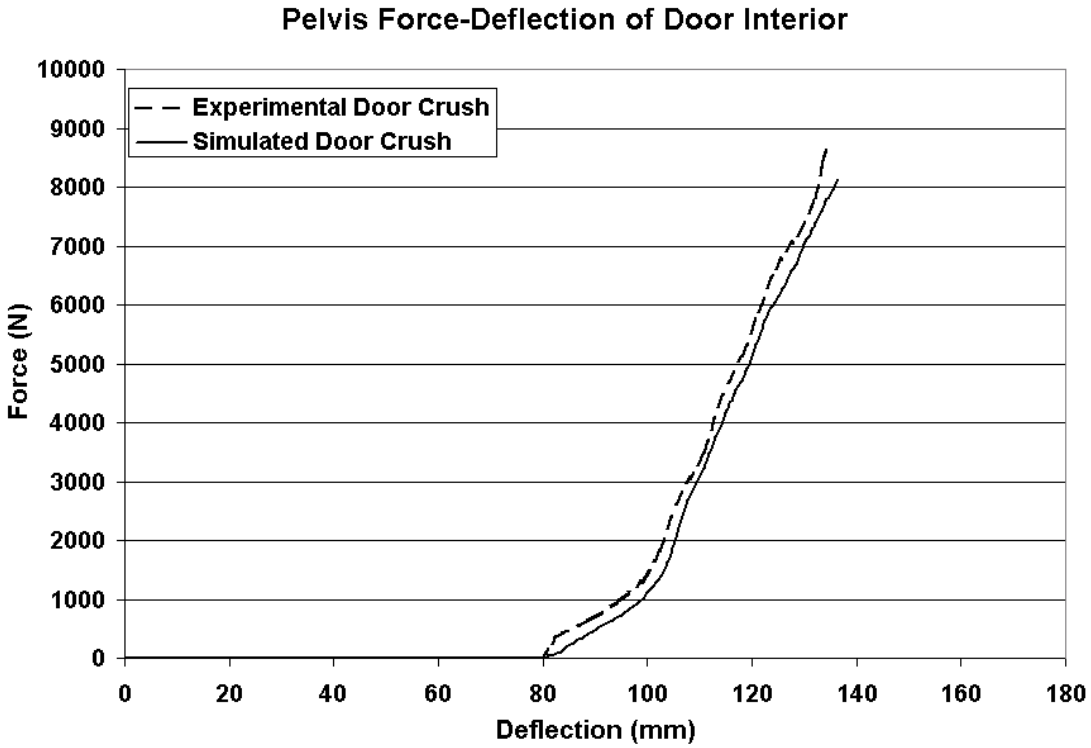

Figure 4.21 Force-Deflection Characterization of Door Model

4.4 Restraint System

The restraint system consists of a shoulder belt, lap belt, slip ring, buckle, retractor, and pretensioner (Cronin et al., 2004). The lap and shoulder belt are fitted to the occupant using the BeltFit function found in LS-PREPOST (LS-PREPOST Online Documentation, 2009). This function allows the user to select a starting node, middle node on the occupant, and an end node, as well as the geometry to fit the belt around.

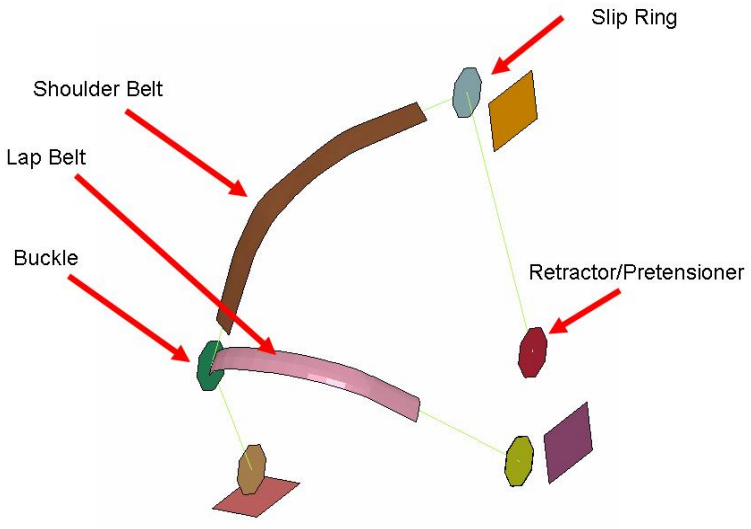

Figure 4.22 Restraint System

Seatbelt retractors operate by paying out belt material when unlocked, or reeling in belt material under constant tension, and finally locking after a user defined fed length has been paid out. Load curves defined to control the seatbelt retractor are defined in the following figures:

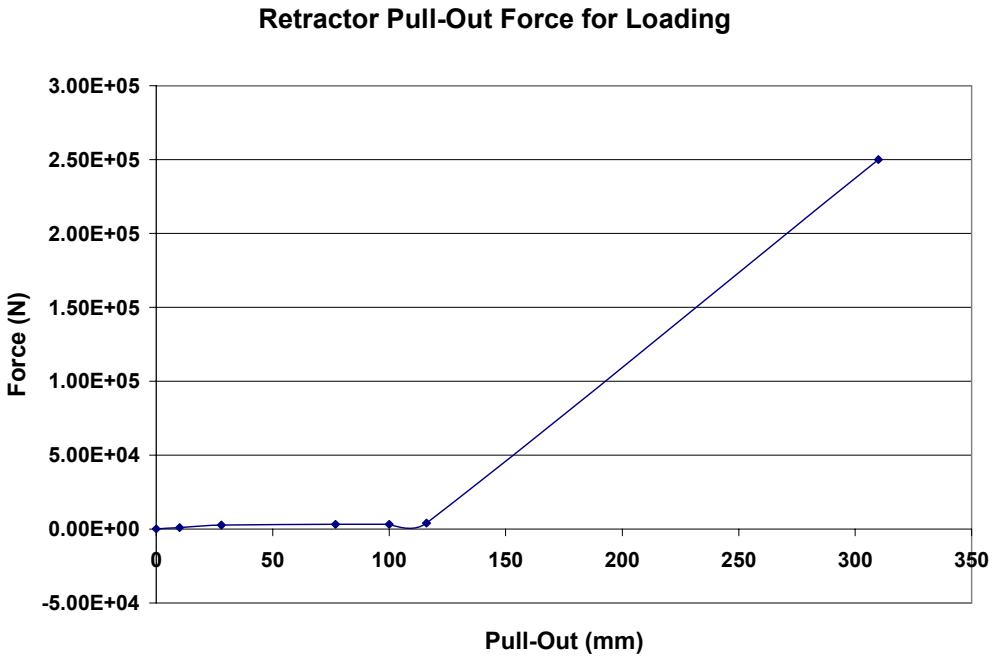

Figure 4.23 Retractor Pull-Out Force for Loading (Cronin et al., 2004)

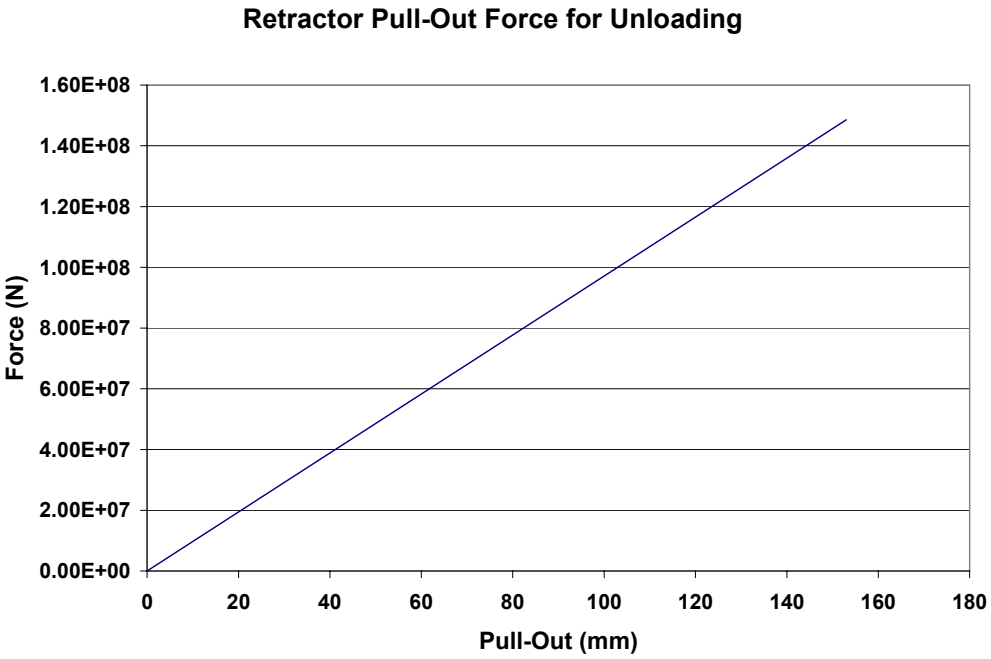

Figure 4.24 Retractor Pull-Out Force for Unloading (Cronin et al., 2004)

The pretensioner allows the tightening of the belt during initial onset of collision by pyrotechnic activation. The pretensioner is defined by the Pull-In vs time curve defined below.

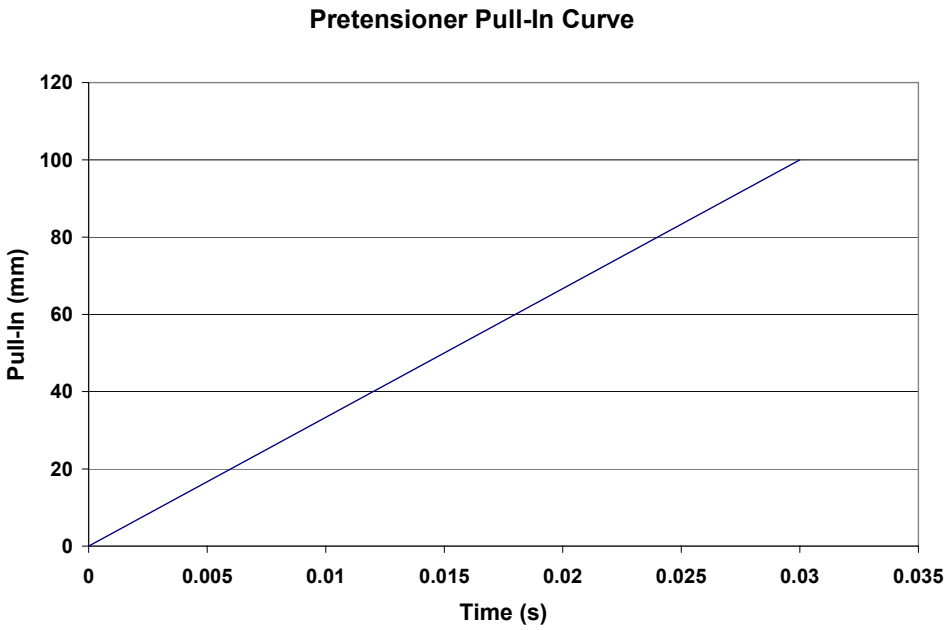

Figure 4.25 Pretensioner Pull-In Curve (Cronin et al., 2004)

The seatbelt has been modeled using a combination of *MAT_SEATBELT and *MAT_FABRIC material models. Tension tests were performed on seatbelt material to determine load curves as required by the *MAT_SEATBELT card.

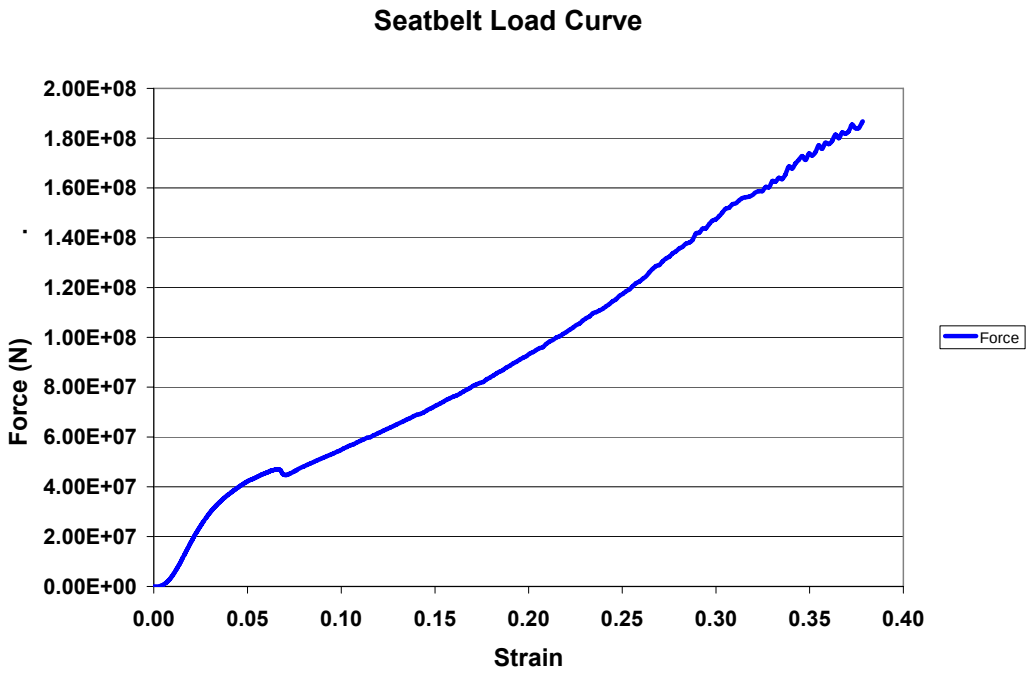

Figure 4.26 Seatbelt Material Load Curve

-- CHAPTER 5 --

Side Impact Model Validation

5.1 Introduction

The side impact model has been developed based on the material properties and geometries previously described and as determined by the literature. The side impact model including the human body model is shown in Figure 5.1 below.

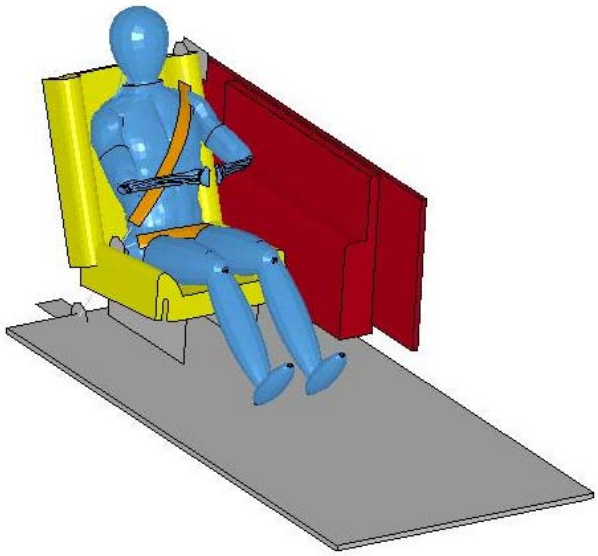

Figure 5.1 Side Impact Model

The model has been validated by comparing the simulated occupant response to values measured in full-scale vehicle tests. Velocity profiles obtained from full-scale side impact tests (MGA Ford Taurus, 2000; MGA Nissan Maxima, 2001) for the vehicle CG, seat base, and inner door panel were used as input velocites to the sled base, seat, and door respectively (Figure 5.2).

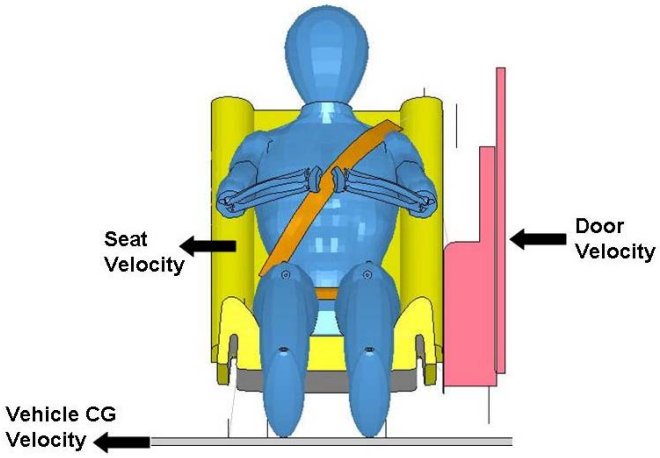

Figure 5.2 Side Impact Model with Input Velocities

It should be noted that velocity inputs from two specific cases were selected and the side impact model was modified to represent a FMVSS 214 test of a Ford Taurus and an IIHS test of a Nissan Maxima. These two test cases were selected for several reasons. First, accurate velocity profiles for the vehicle CG, seat, and door were required to provide input conditions for the side impact model. However, door accelerometers are not regularly included in side impact test procedures, therefore narrowing the test cases to those tests that do include door accelerometers. Second, current and past research using the human body model has focused on VC response to predict injury. However, typical side impact test procedures use a Side Impact Dummy (SID) with TTI injury criteria based on accelerations. This further narrowed the available side impact tests to those that use the ES-2 since VC is used as the injury criteria. Finally, two test types (FMVSS 214 and IIHS) with different test procedures were selected to validate the side impact model under differing test conditions. Test parameters and conditions are further discussed below.

5.2 Side Impact Model Input Profiles

Based on information for similar sled tests in the literature (Teng et al., 2007; Morris et al., 1998; Deng & Tzeng, 1996), input velocities for the sled, seat, and door are determined by the integration of accelerations recorded by uniaxial accelerometers positioned at the vehicle CG, driver seat track, and inner door panel respectively. Full-scale crash data has been obtained from a FMVSS 214 and an IIHS test. However, these tests used a 50th percentile ES-2 dummy, as opposed to the SID used in standard tests. Therefore, comparison of the simulated occupant response to the ES-2 response is based on rib deformation displacement, velocity, and viscous criterion. Input pulses for the FMVSS 214 and IIHS tests are shown in Figure 5.3 and Figure 5.4.

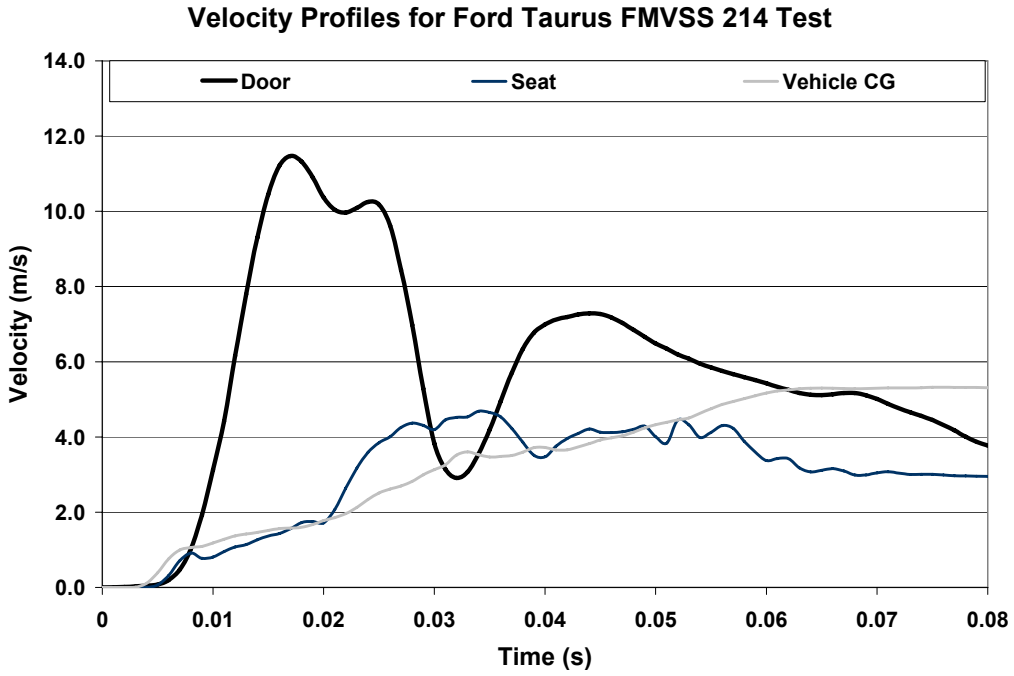

Figure 5.3 Ford Taurus v3522 Velocity Profile (MGA Ford Taurus, 2000)

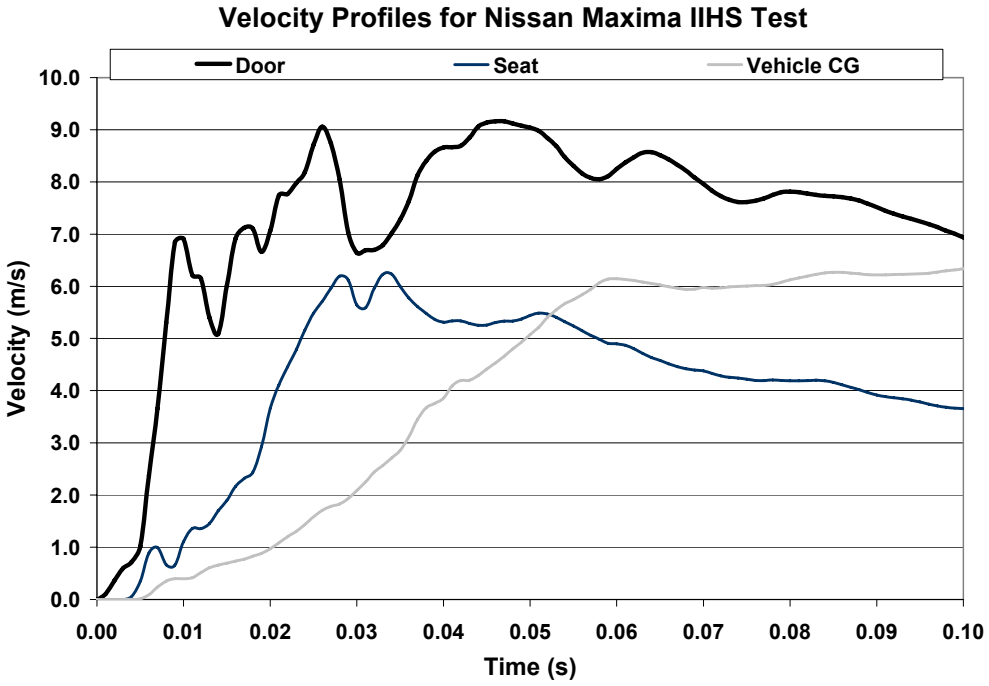

Figure 5.4 Nissan Maxima v3668 Velocity Profile (MGA Nissan Maxima, 2001)

It should be noted that vehicles are equipped with several accelerometers; however, the exact location often varies from vehicle to vehicle. Also, because the door is directly impacted by the intruding MDB, sensors may rotate during the collision. This can result in inaccuracy since the acceleration will not be measured with respect to the expected coordinate system. However, for the purposes of this study, it is assumed that the accelerometer data is accurate and any significant rotation occurs after injury is predicted to occur, at approximately 50 msec.

The door pre-crush, discussed in the development of the simplified door model, is accounted for by the location of the door accelerometers. Since the accelerometers were located on the inner door panel they provided the velocity of the inner door panel which would only begin its motion after the outer skin of the door panel was crushed as done in the door force-deflection experimentation performed by Deng and Ng (1993).

5.2.1 Door Placement

The door was positioned in accordance with vehicle specifications as determined by FMVSS standards and NHTSA test reports. According to the Ford Taurus test report (MGA Ford Taurus, 2000) the ES-2 dummy was positioned 115 mm from the door (Arm to Door or AD distance) as seen in Figure 5.5. To make use of this positioning in the side impact model, the center of the human body model to the door was used as a reference. This distance for the Ford Taurus door has been determined to be 351 mm as shown in the following figure:

$$\text{Center Occupant to Door} = \text{Half Arm-to-Arm Distance} + \text{AD Distance} \quad \textbf{(5.1)}$$

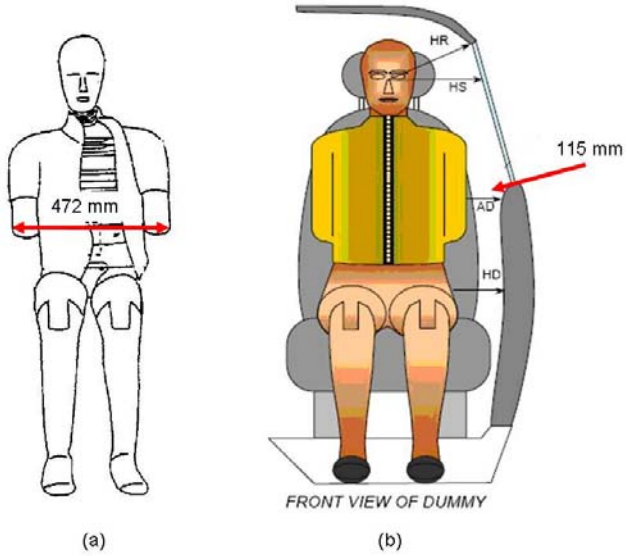

Figure 5.5 Door Positioning (a) ES-2 Arm Width (b) AD Distance (MGA Ford Taurus, 2000)

$$\text{Center Occupant to Door} = 472*.5 + 115 = 351 \text{ mm} \quad \textbf{(5.2)}$$

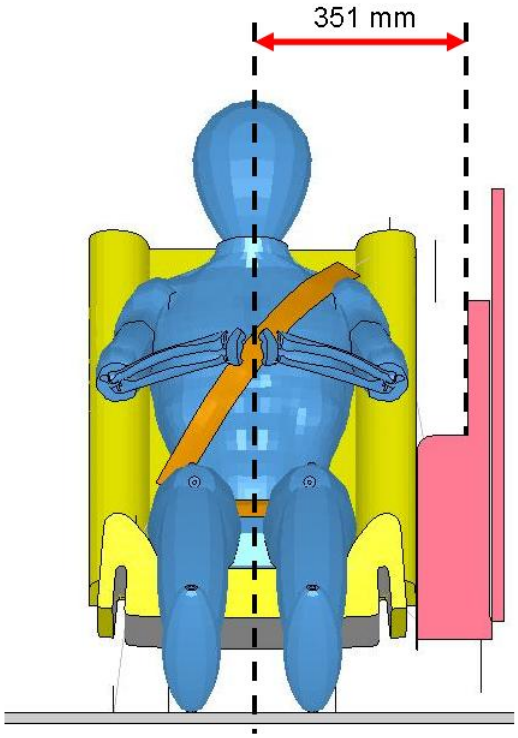

Figure 5.6 Dummy Center to Door Distance

5.3 Validation Results

The ES-2 records numerous acceleration, displacement, and force responses throughout the duration of a crash event. However, for this study, only the lower, middle, and upper rib responses were evaluated for comparison with the human body model. For the purposes of comparison, three levels have been selected on the human body model, representing anatomically equivalent areas to the lower, middle, and upper ribs of the ES-2 (Figure 5.7).

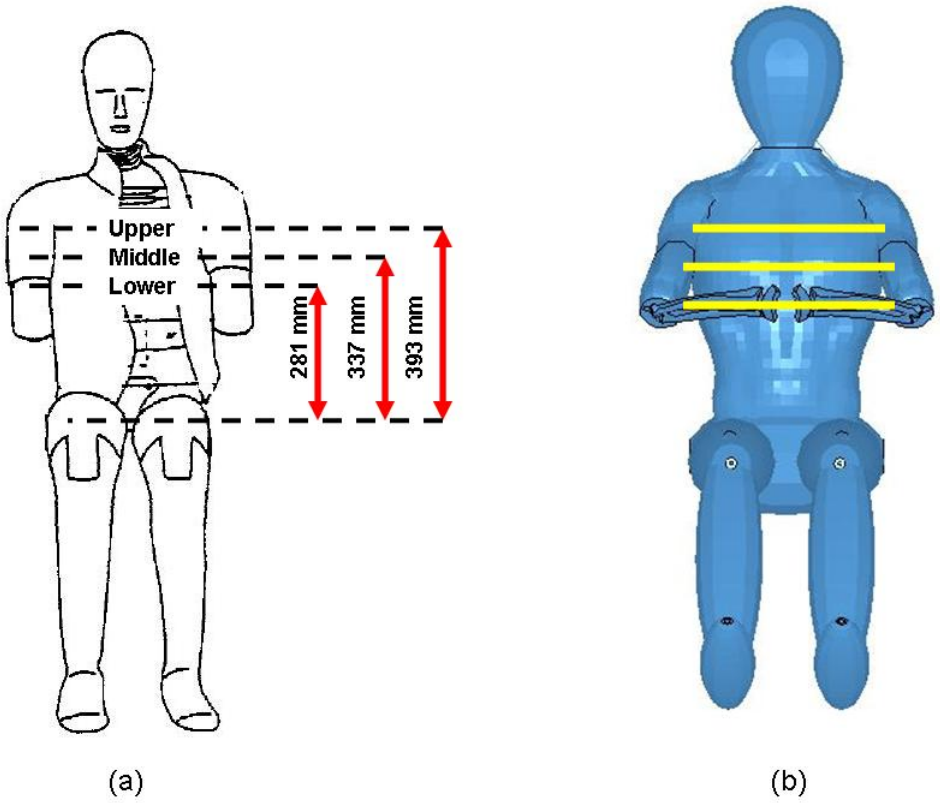

Figure 5.7 Response Locations (a) ES-2 Rib Location (b) Model Chest Levels

The ES-2 calculates thoracic deflection based on the half thorax deflection by measuring the displacement of the ribs on the struck side. Therefore, to ensure comparable results the response of the human body model was also based on half thoracic deflection.

The injury criteria developed for the ES-2 is based on measurements taken from PMHS sled tests and ES-2 response in similar tests (Viano et al., 1995; Pintar et al.,1997; Kuppa, 2004). Currently the European Union Side Impact Standard uses a ES-2 dummy with a rib deflection injury threshold of 42mm or 30% compression (ES-2 half chest width of 140mm) and a VC threshold of 1.0 m/s. As previously discussed, Viano (1989b) determined injury tolerances of 33.9% compression or 55mm deflection (average chest width of 326mm) and a VC of 1 m/s to predict 50% risk of AIS 3+. However, the rib deflection injury criteria developed based on PMHS tests could not be directly applied to the ES-2 dummy because of differences in measured response. Therefore, only the

viscous response of the ES-2 and human body model can be used for direct comparison as they each have the same VC injury threshold value. However, the compression, velocity, and VC are displayed to compare the timing and shape of the response curves.

A similar method to that used in the analysis of chest band data from PMHS testing will be used to evaluate the half thoracic response of the human body model. A description of the methods used to evaluate full and half thoracic deflection using chest band data is shown in Figure 5.8.

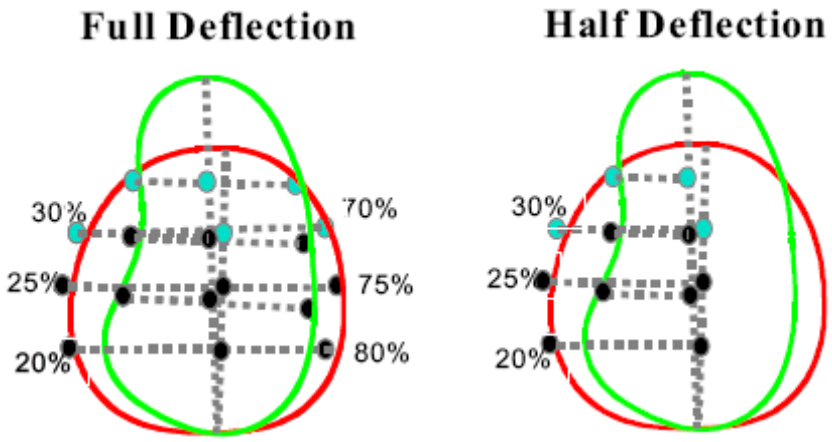

Figure 5.8 Chest Deflection Measurement Methods (a) Full (b) Half (Samaha et al., 2001)

Full Thoracic deflection is determined by selecting six locations starting at the spine and moving clockwise at 20%, 25%, 30%, 70%, 75%, and 80% of the chest circumference (Samaha et al., 2001). The distance between pairs 30% and 70%, 25% and 75%, and 20% and 80% are evaluated at a specified time interval and averaged to determine the average chest deflection.

The half thoracic deflection is measured using three locations starting at the spine and moving clockwise at 20%, 25%, and 30%. Points are selected at the spine and sternum to represent the torso centerline. The distance between each point and the centerline is measured and averaged to determine the average chest deflection. This process is repeated for every time step to produce the half thoracic deflection-time history.

In the case of the numerical human body model, chest deflection is evaluated in much the same way as described above. However, in this case it is evaluated by determining the intersect of two lines created by the line drawn between the 25% and 75% location and the mid-sagittal line between the spine and sternum as shown in Figure 5.9. The deflection is then determined as the distance between the point at 25% chest circumference and the intersection point, measured along the 25%-75% line.

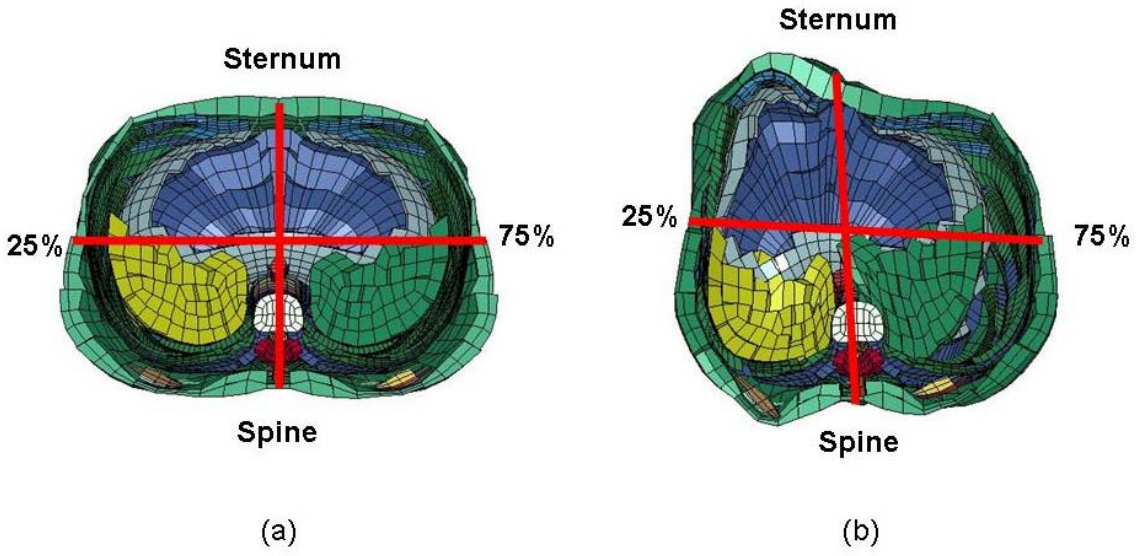

Figure 5.9 Chest Deflection Calculation (a) Uncompressed Chest (b) Compressed Chest

This process is repeated for each time step of the simulation to obtain the deflection-time history of the response. The deflection-time history is normalized by dividing the response by the initial chest width and velocity can be obtained by differentiating the deflection response.

5.3.1 Measureable Response

The compression, velocity, and VC response was used to compare the human body model to the ES-2. NHTSA side sled tests previously performed to compare the response of ES-2 dummies to PMHS were used as the basis for the comparison of the human body model to the ES-2 (Maltese et al., 2002; Rhule et al., 2002). Thoracic compression, velocity, and VC were calculated from the deflection vs time response provided in the literature

(Maltese et al., 2002; Rhule et al., 2002). A simulation representing a low speed rigid flat wall (6.67 m/s) NHTSA sled test, as shown in Figure 3.15, was performed to validate the human body model to the ES-2 thoracic response observed in the literature (Forbes, 2005; Rhule et al., 2002; Maltese et al, 2002). Figure 5.10 compares the upper thoracic deflection found in the low speed sled tests with ES-2 dummies performed by Rhule et al. (2002) to corridors and average PMHS response determined though similar tests performed by Maltese et al. (2002).

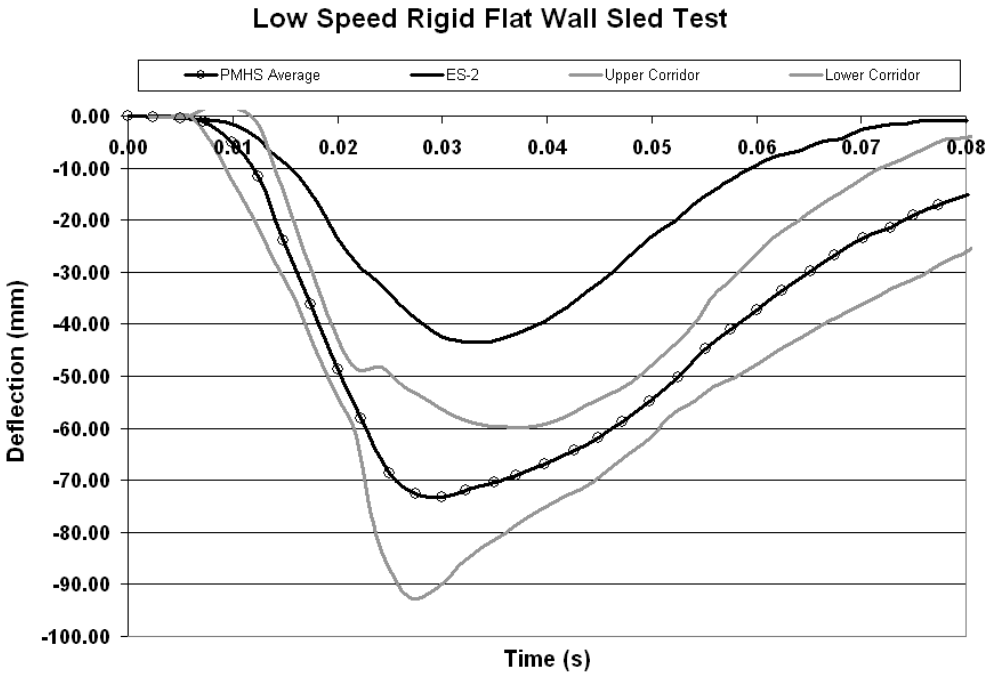

Figure 5.10 Upper Half Thoracic Deflection Response for a Low Speed Rigid Flat Wall NHTSA Sled Test (Rhule et al., 2002; Maltese et al, 2002)

The thoracic compression, velocity, and VC response for the upper chest band location is shown below to justify comparison of the human body model response in the side impact model to the ES-2 response from full-scale crash tests. It should be noted that the timing of the signal is adjusted for uniformity according to methods applied by Maltese et al. (2002), whereby time-zero is determined by the initiation of arm contact with the thoracic plate.

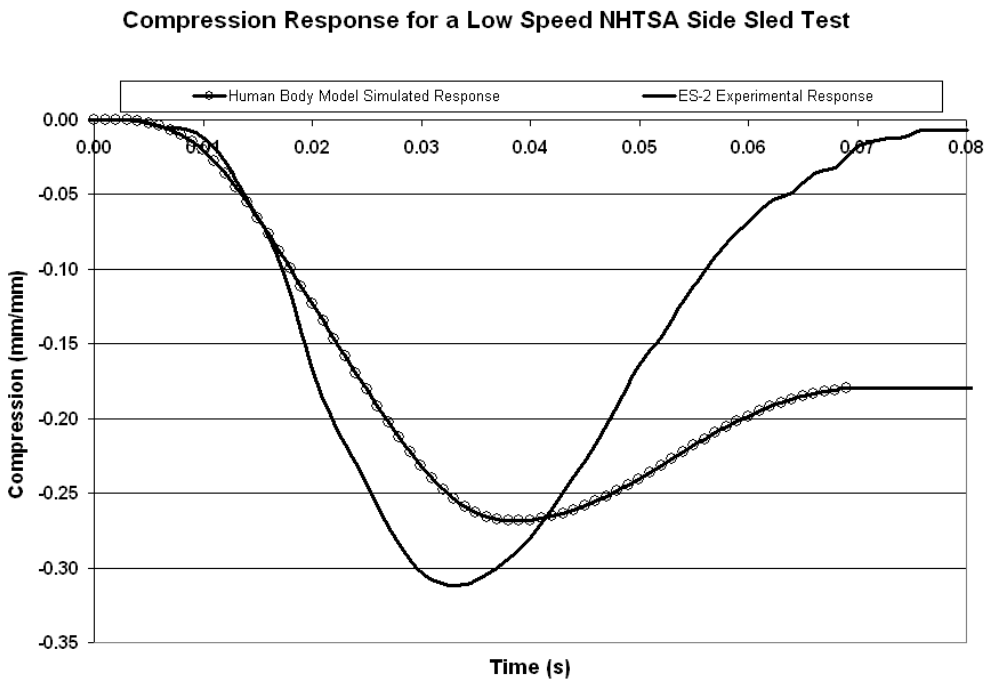

Figure 5.11 Low Speed Sled Test Upper Band/Rib Compression Response (Rhule et al., 2002)

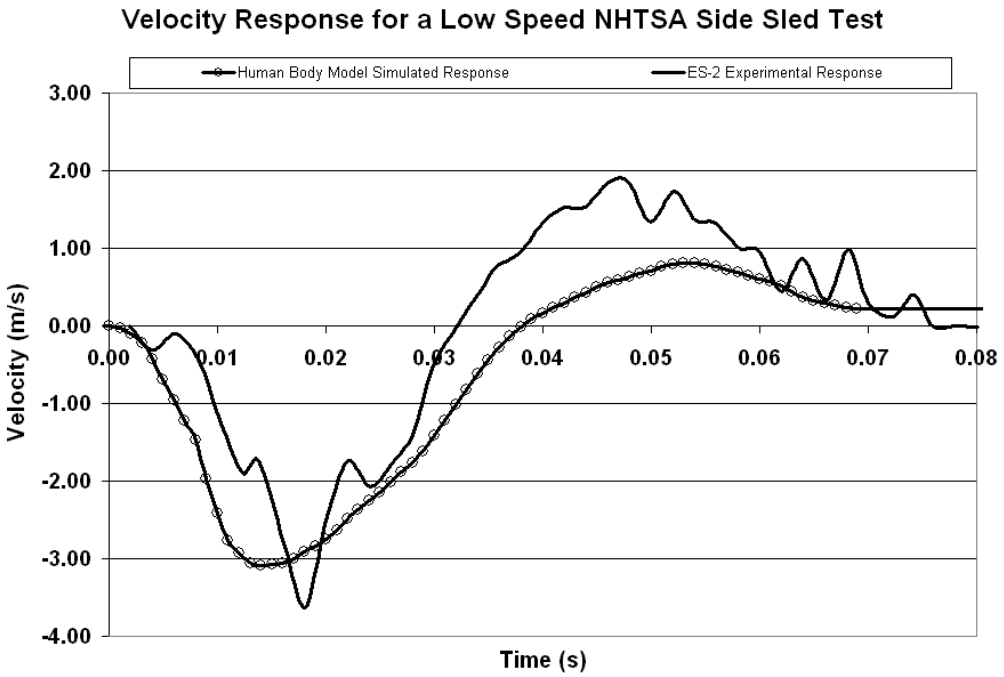

Figure 5.12 Low Speed Sled Test Upper Band/Rib Velocity Response (Rhule et al., 2002)

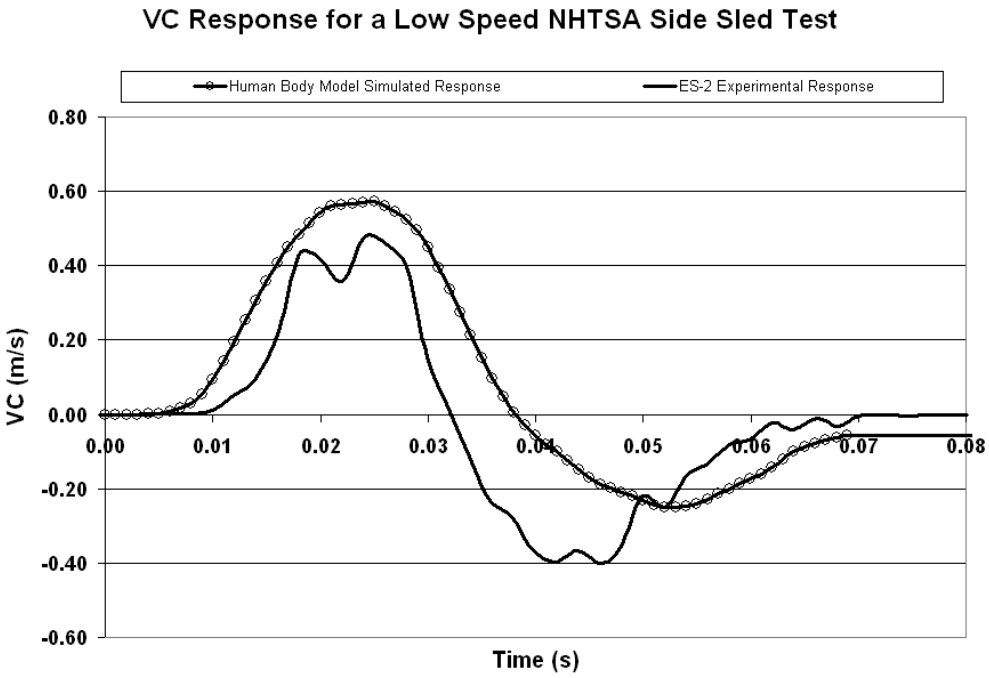

Figure 5.13 Low Speed Sled Test Upper Band/Rib VC Response (Rhule et al., 2002)

Model assessment was undertaken following the methods used by Forbes. The predicted thoracic response was compared to ES-2 based on data for loading, peak, and unloading. The following qualitative measures as applied in previous validation of the human body model (Forbes, 2005) have been used to compare the simulated response to the experimental response.

- Good — Falling close to the experimental response at the discretion of the author.
- Reasonable — Falling reasonably close to the experimental response at the discretion of the author.
- Poor — Falling significantly far from the experimental response at the discretion of the author.

Table 5.1 Low Speed Sled Test Comparison between Human Body Model and ES-2 Response

CHEST BAND	IMPACT PHASE	CORRELATION		
		Compression (mm/mm)	**Velocity (m/s)**	**VC (m/s)**
Upper Rib	**Loading**	Good	Reasonable	Good
	Peak	Reasonable	Reasonable	Reasonable
	Unloading	Poor	Reasonable	Reasonable

Based on the qualitative descriptions in Table 5.1, the ES-2 and human body model present *good* or *reasonable* correlation to each other, thereby, validating the response comparison of the human body model used in the side impact model to the ES-2 in full-scale crash testing.

To validate the side impact model, it was modified to represent a FMVSS 214 test of a Ford Taurus and an IIHS test of a Nissan Maxima. The compression, velocity, and VC were used to compare the timing and overall response of the human body model to the ES-2 dummy.

5.3.2 Ford Taurus FMVSS 214 Simulation

The human body side impact simulation response during an impact with velocity profiles (Figure 5.3) and AD distance as determined by the FMVSS 214 side impact testing of a Ford Taurus is shown in Figure 5.14.

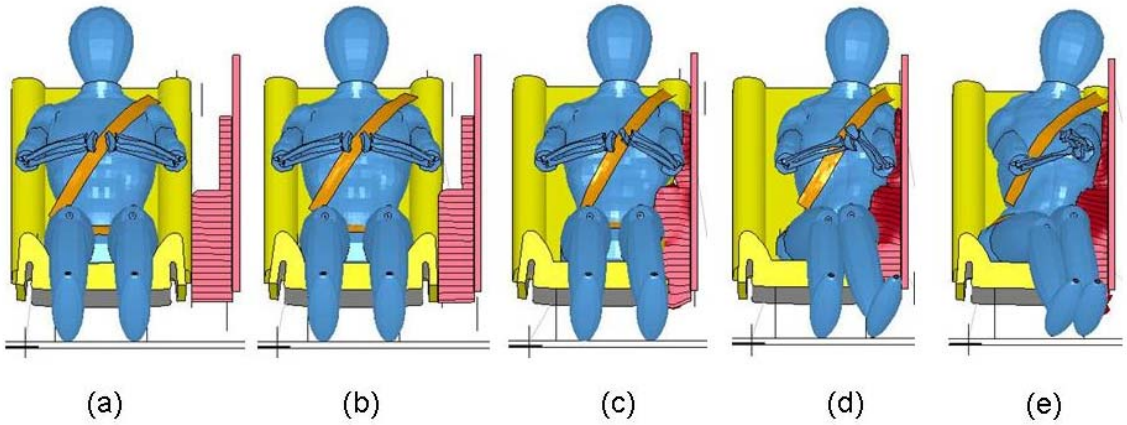

Figure 5.14 Impact Sequence of Ford Taurus Side Impact Simulation (a) t=0 ms (b) t=15ms (c) t=30ms (d) t=45ms (e) t=60ms

The simulated compression, velocity, and VC response for the three locations described in Figure 5.7 is compared to the ES-2 response obtained from a full-scale FMVSS 214 crash test in the figures below.

Upper Rib Response

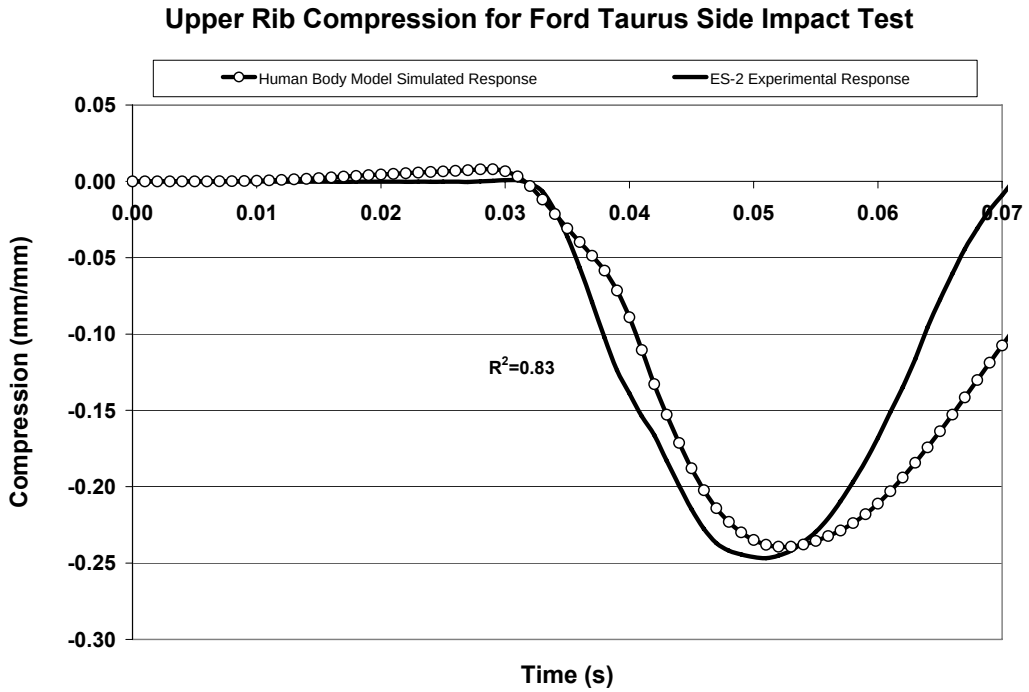

Figure 5.15 Upper Rib Compression Response for the Side Impact Model with Ford Taurus Inputs

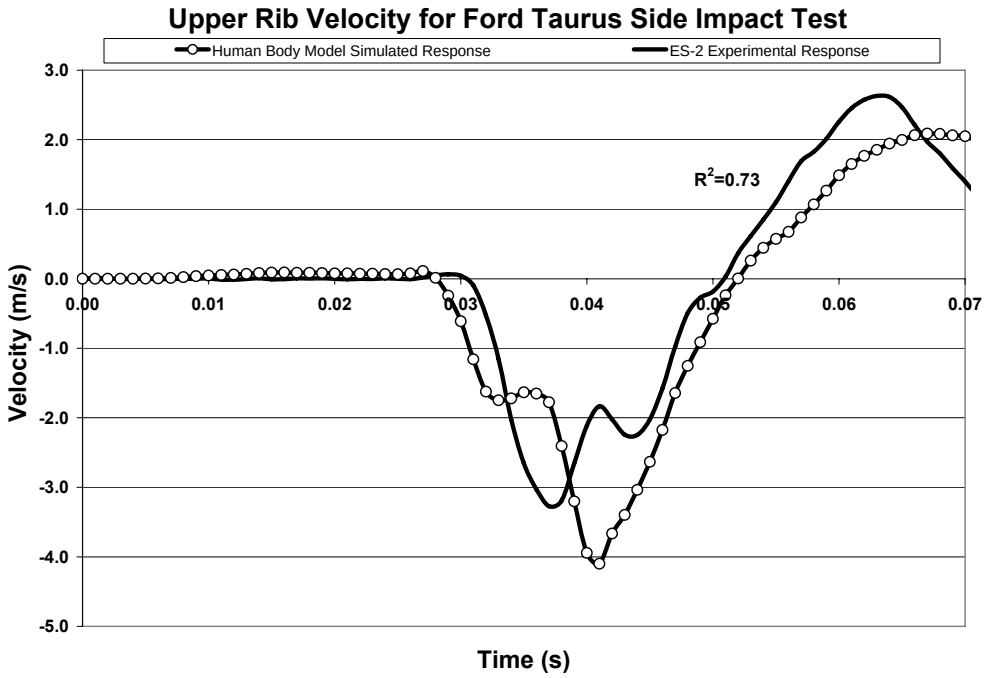

Figure 5.16 Upper Rib Velocity Response for the Side Impact Model with Ford Taurus Inputs

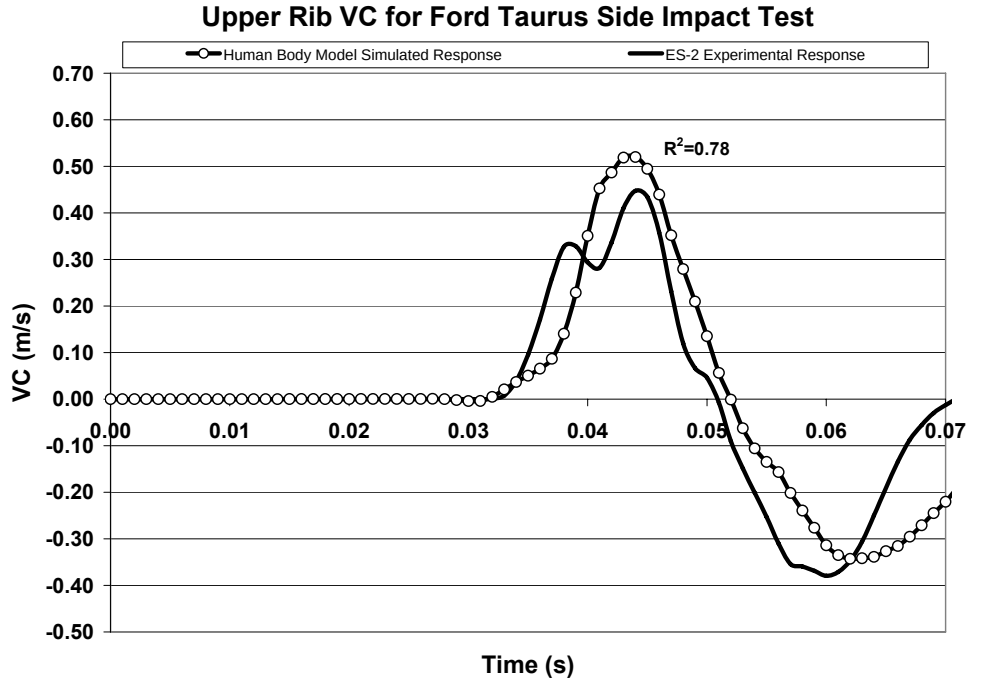

Figure 5.17 Upper Rib VC Response for the Side Impact Model with Ford Taurus Inputs

Middle Rib Response

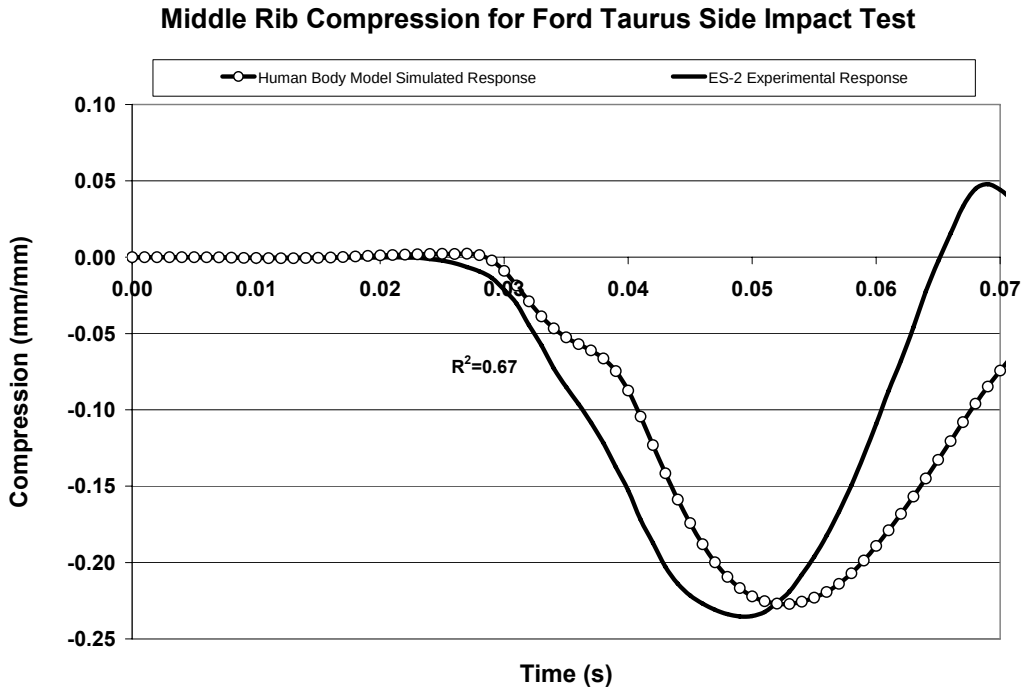

Figure 5.18 Middle Rib Compression Response for the Side Impact Model with Ford Taurus Inputs

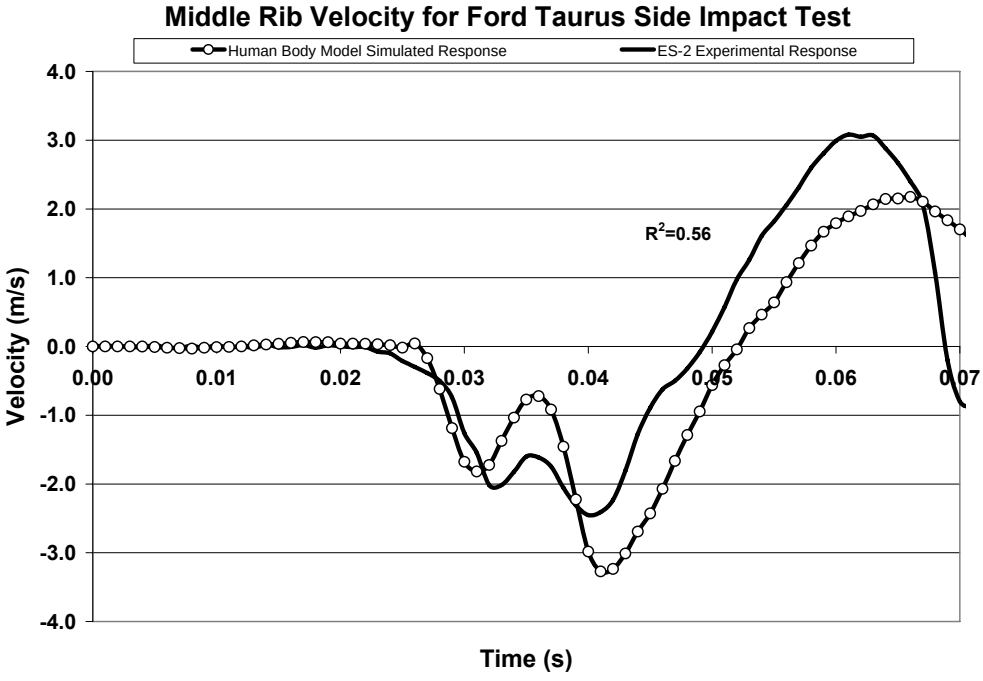

Figure 5.19 Middle Rib Velocity Response for the Side Impact Model with Ford Taurus Inputs

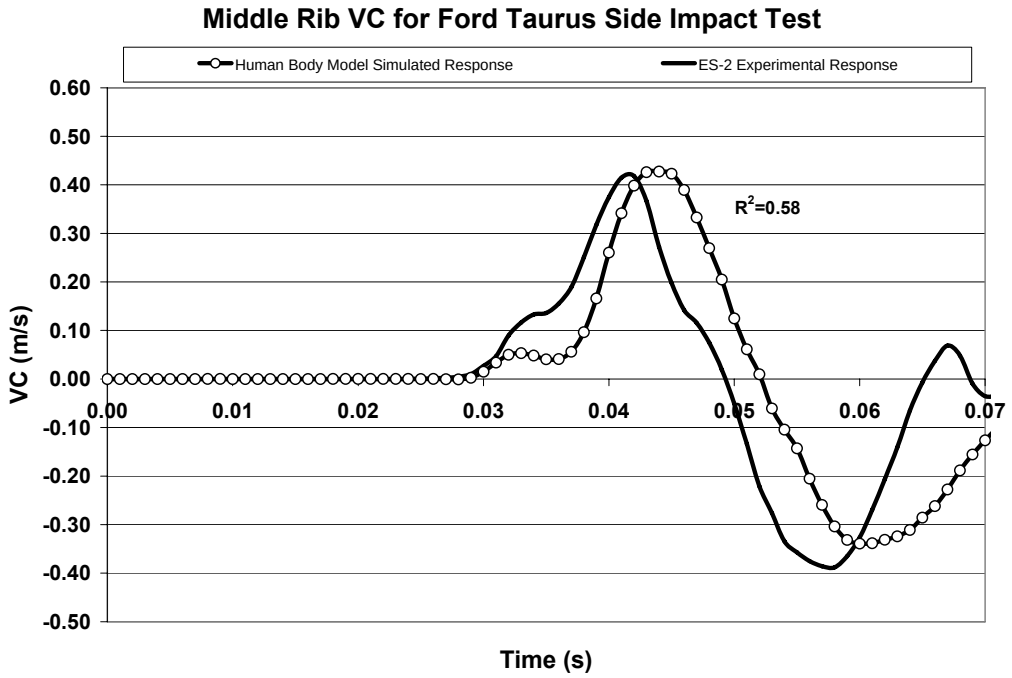

Figure 5.20 Middle Rib VC Response for the Side Impact Model with Ford Taurus Inputs

Bottom Rib Response

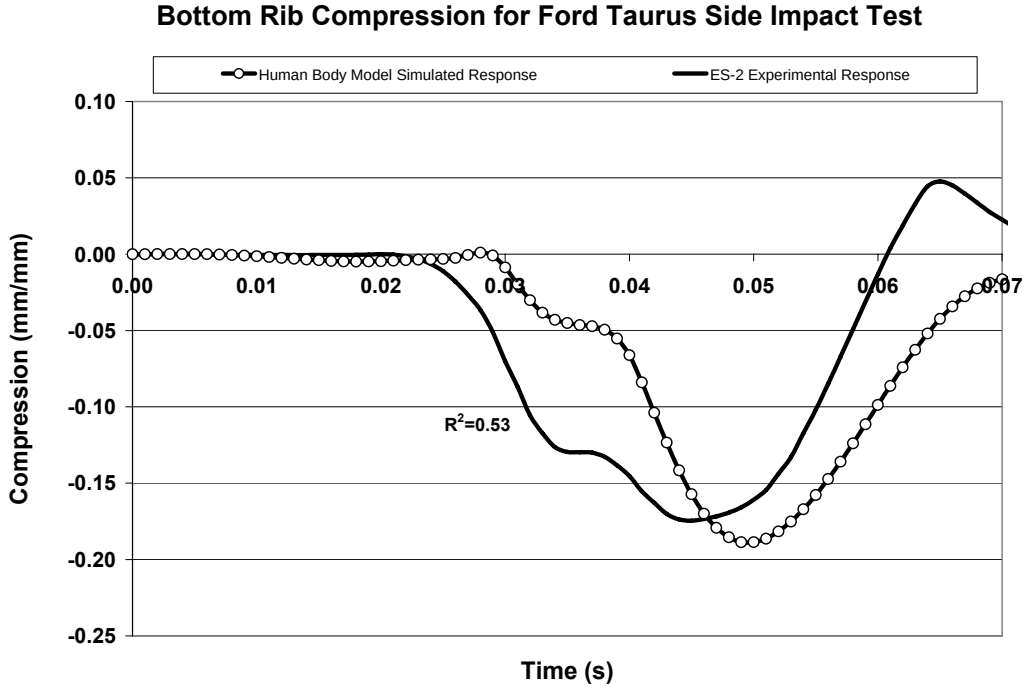

Figure 5.21 Bottom Rib Deflection Response for the Side Impact Model with Ford Taurus Inputs

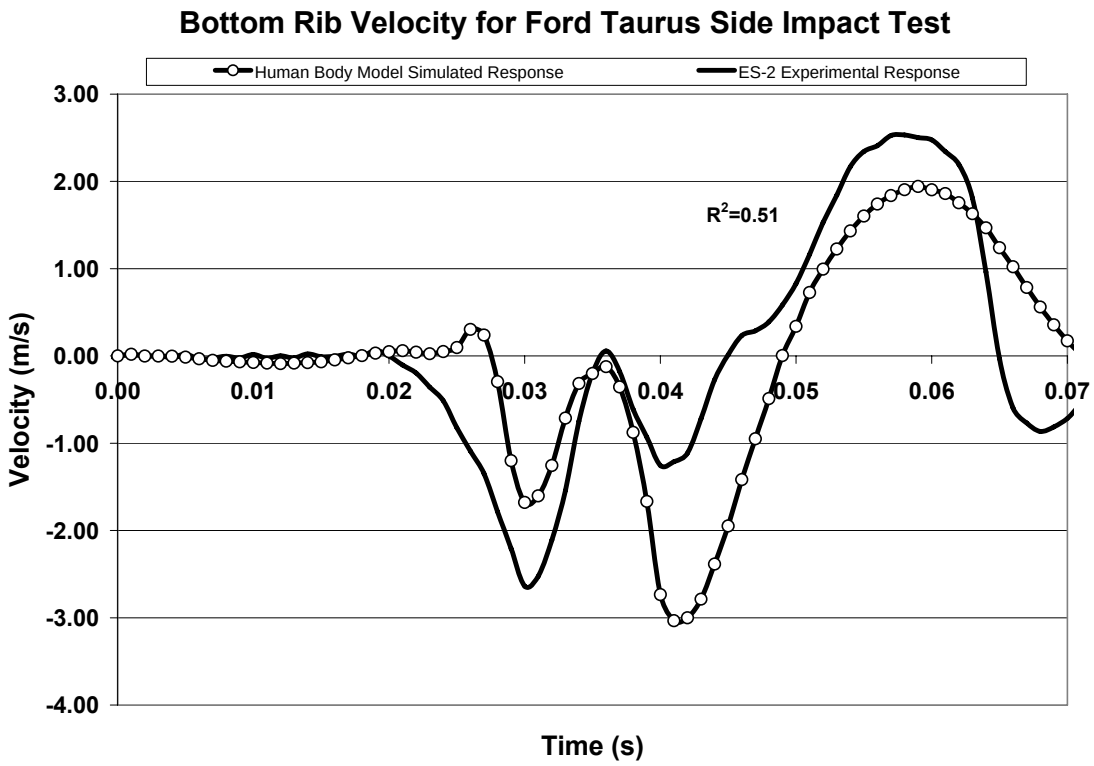

Figure 5.22 Bottom Rib Velocity Response for the Side Impact Model with Ford Taurus Inputs

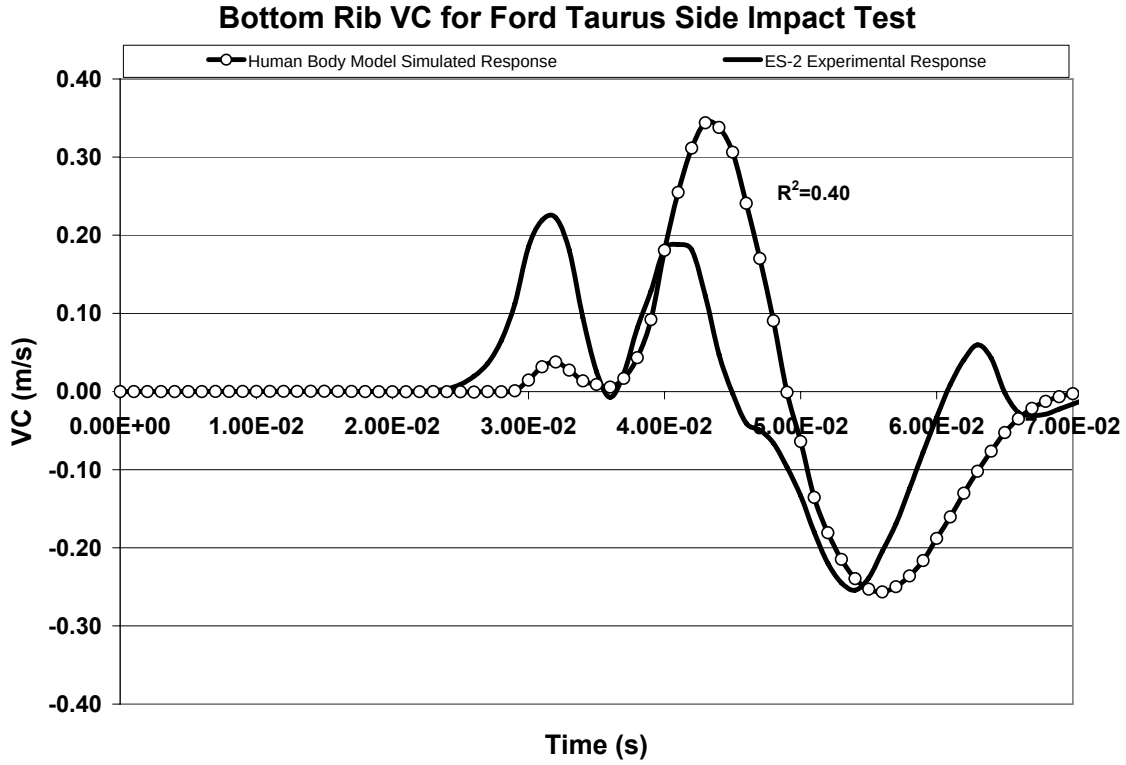

Figure 5.23 Bottom Rib VC Response for the Side Impact Model with Ford Taurus Inputs

Table 5.2 Side Impact Simulation vs Ford Taurus v3522 Injury Response Correlation

CHEST BAND	IMPACT PHASE	CORRELATION						
		Compression (mm/mm)	Velocity (m/s)	VC (m/s)	VCmax (m/s)		VCmax Time (s)	
					Sim	ES-2	Sim	ES-2
Upper Rib	**Loading**	Good	Reasonable	Good	.52	.45	.044	.044
	Peak	Good	Reasonable	Reasonable				
	Unloading	Reasonable	Good	Good				
	R^2	0.83	0.73	0.78				
Middle Rib	**Loading**	Good	Good	Good	.43	.42	.044	.042
	Peak	Good	Good	Good				
	Unloading	Reasonable	Reasonable	Reasonable				
	R^2	0.67	0.56	0.58				
Bottom Rib	**Loading**	Reasonable	Reasonable	Poor	.34	.22	.043	.032
	Peak	Reasonable	Poor	Poor				
	Unloading	Reasonable	Reasonable	Reasonable				
	R^2	0.53	0.51	0.40				

Based on the information above it is apparent that the side impact model closely reproduces the timing and injury response of the Ford Taurus FMVSS 214 test. The model has been found to produce '*good*' to '*reasonable*' response when compared to the ES-2 response in the Ford Taurus test case based on the qualitative description previously discussed. Discrepancies may be attributed to minor differences in occupant positioning,

door positioning and compliance, or geometric differences between the ES-2 and human body model at the specified chest band locations.

5.3.3 Nissan Maxima IIHS Simulation

The human body side impact response during an impact with velocity profiles (Figure 5.4) and AD distance as determined by the IIHS side impact testing of a Nissan Maxima is shown in Figure 5.24.

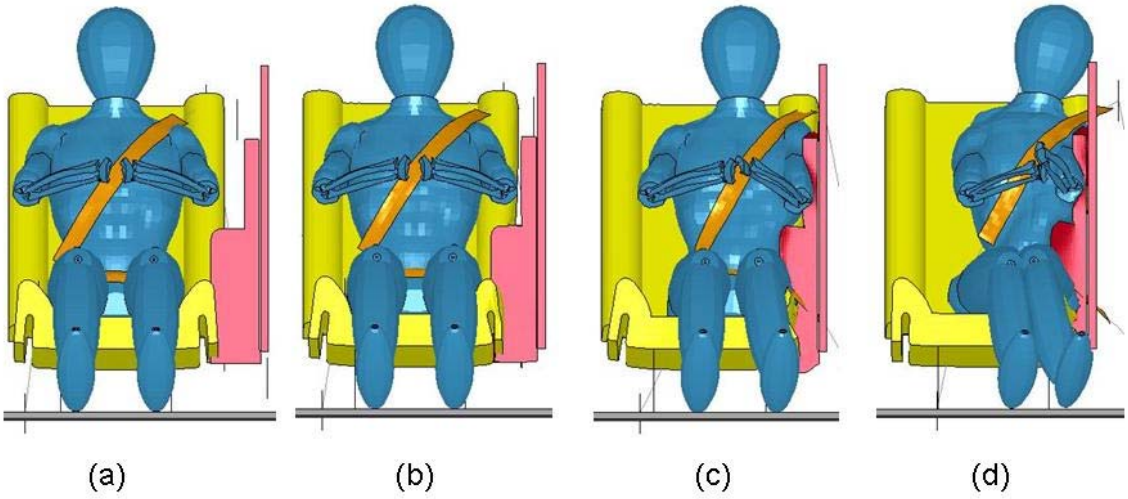

Figure 5.24 Impact Sequence of Side Impact Simulation (a) t=0 ms (b) t=15ms (c) t=30ms (d) t=45ms

The simulated compression, velocity, and VC response for the three locations described in Figure 5.7 is compared to the ES-2 response obtained from a full-scale IIHS crash test in the figures below.

Upper Rib Response

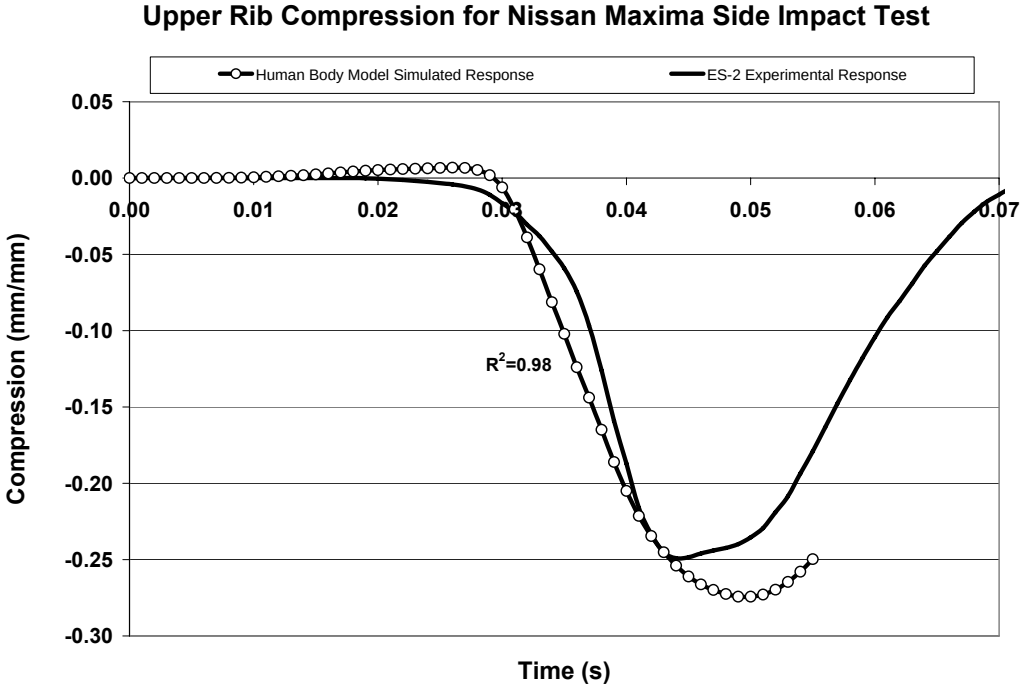

Figure 5.25 Upper Rib Compression Response for the Side Impact Model with Nissan Maxima Inputs

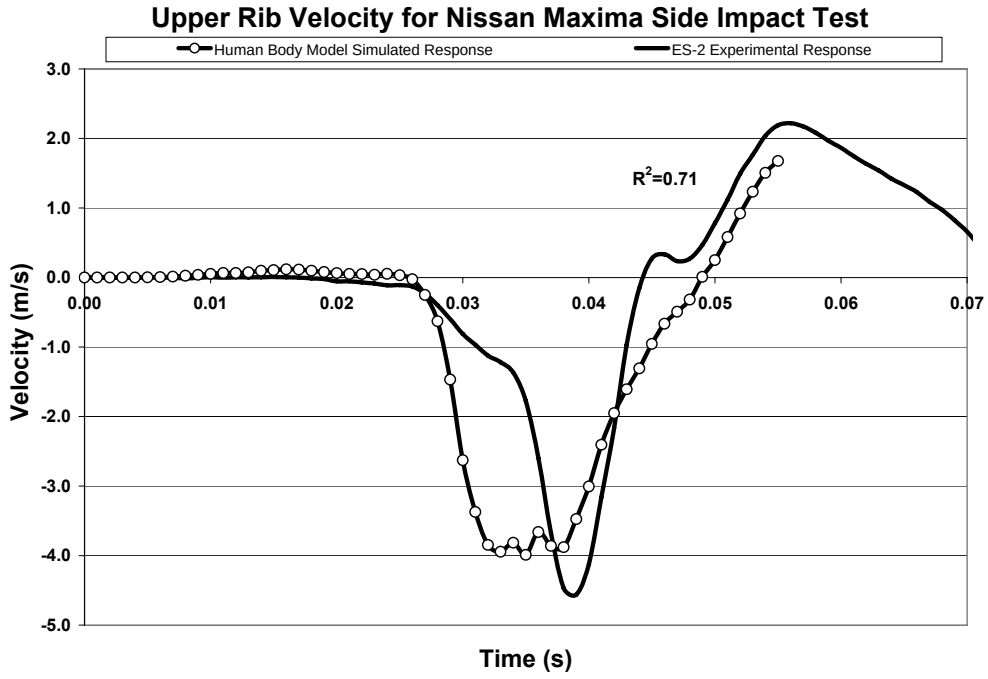

Figure 5.26 Upper Rib Velocity Response for the Side Impact Model with Nissan Maxima Input

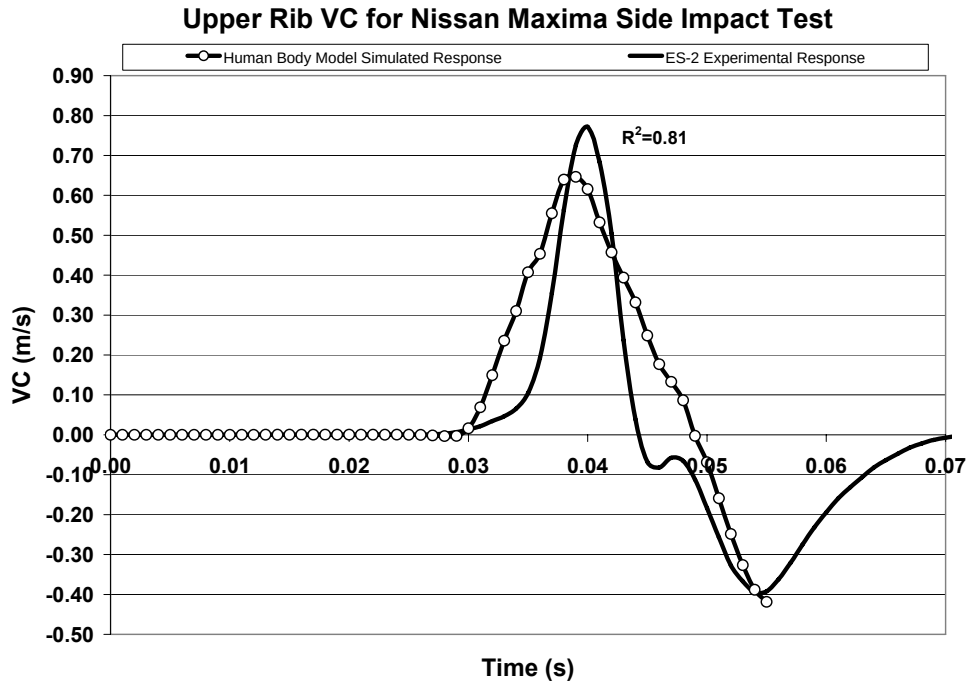

Figure 5.27 Upper Rib VC Response for the Side Impact Model with Nissan Maxima Inputs

Middle Rib Response

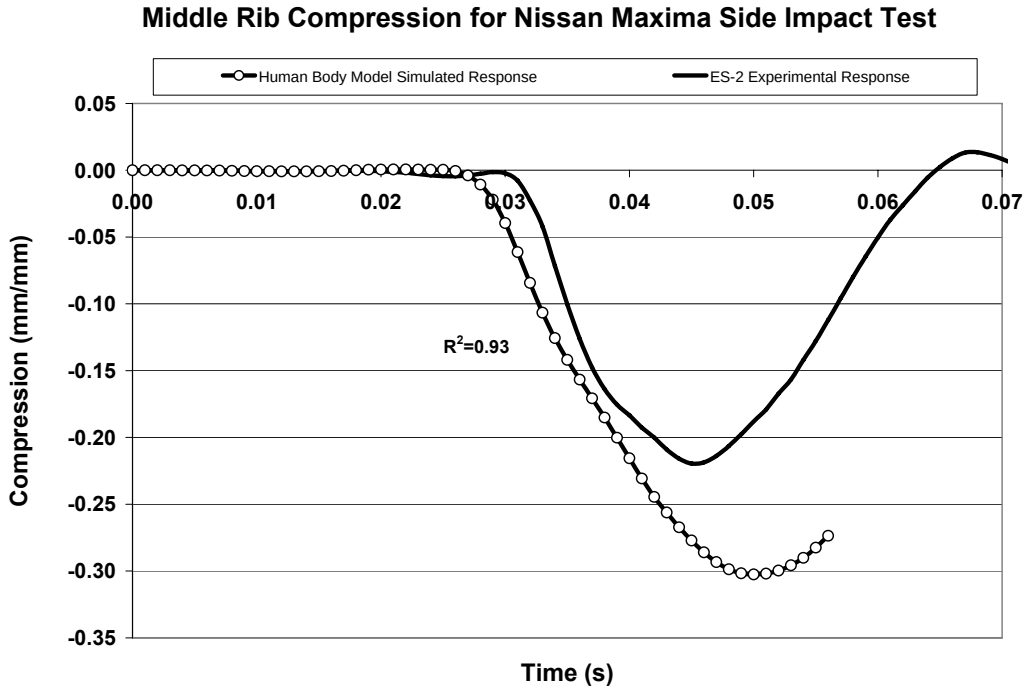

Figure 5.28 Middle Rib Compression Response for the Side Impact Model with Nissan Maxima Inputs

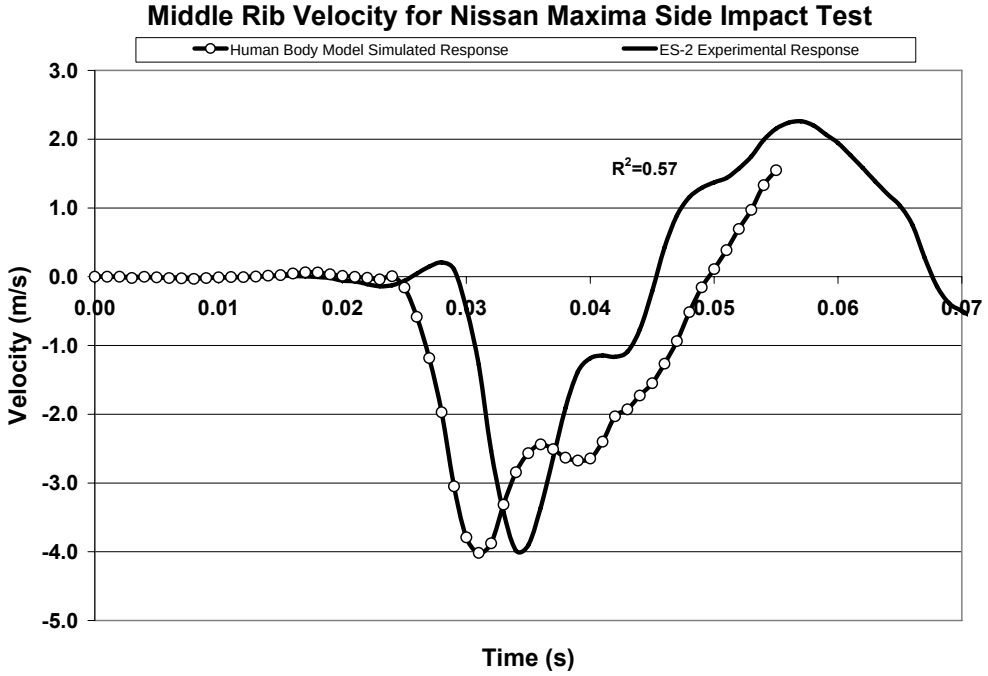

Figure 5.29 Middle Rib Velocity Response for the Side Impact Model with Nissan Maxima Inputs

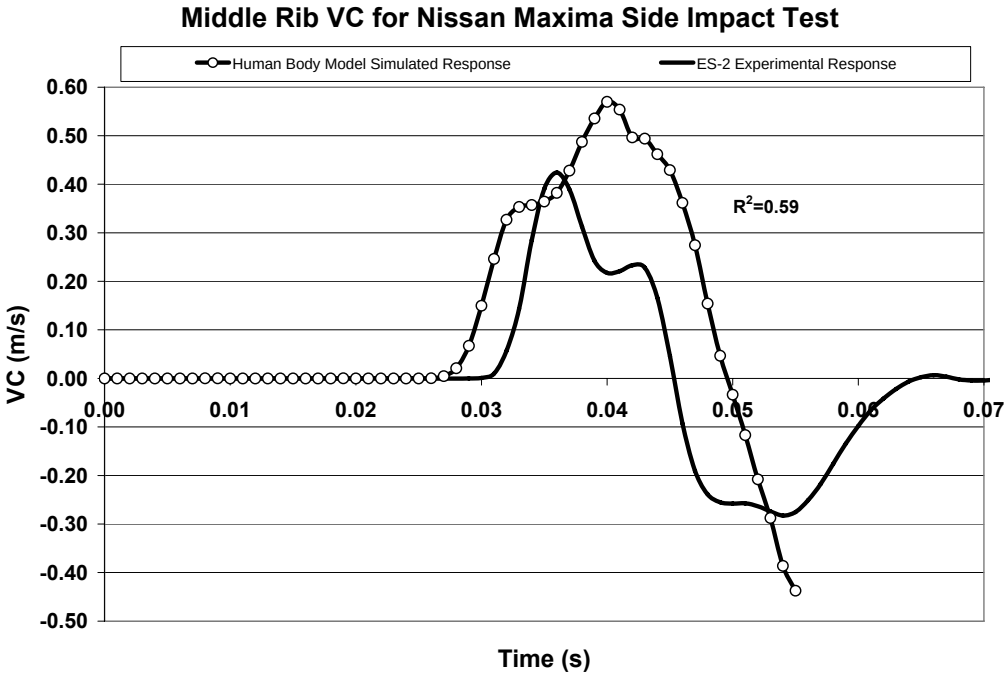

Figure 5.30 Middle Rib VC Response for the Side Impact Model with Nissan Maxima Inputs

Bottom Rib Response

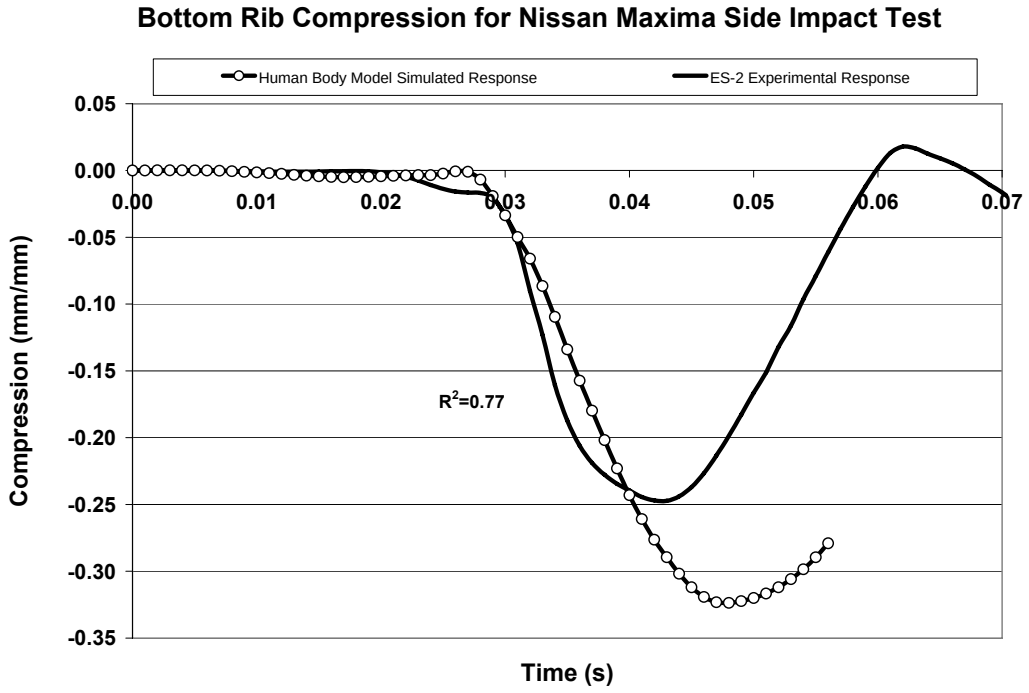

Figure 5.31 Bottom Rib Deflection Response for the Side Impact Model with Nissan Maxima Inputs

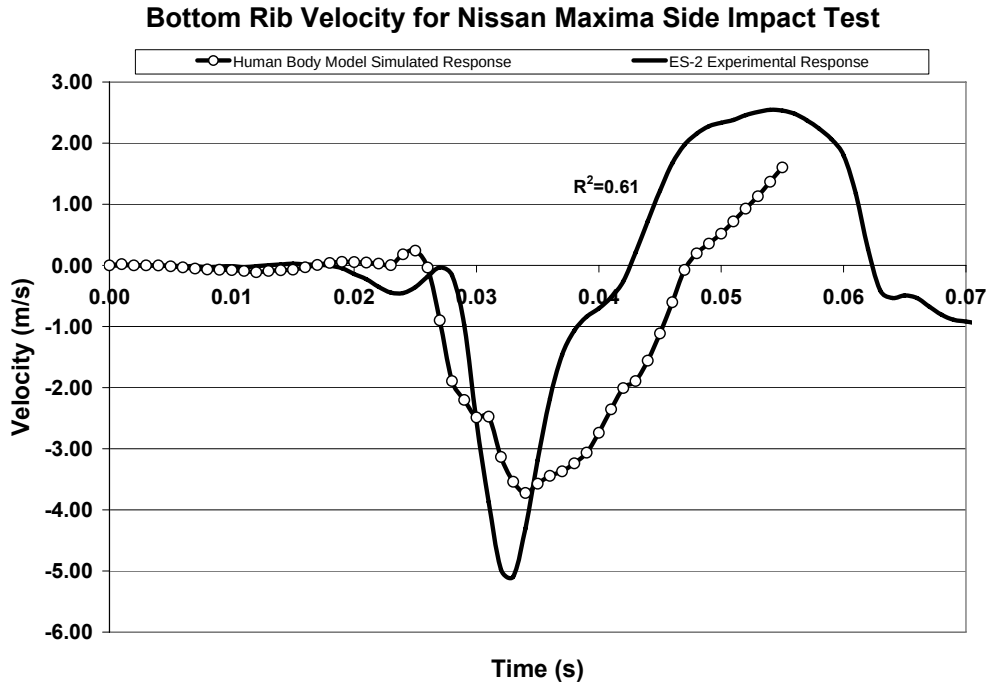

Figure 5.32 Bottom Rib Velocity Response for the Side Impact Model with Nissan Maxima Inputs

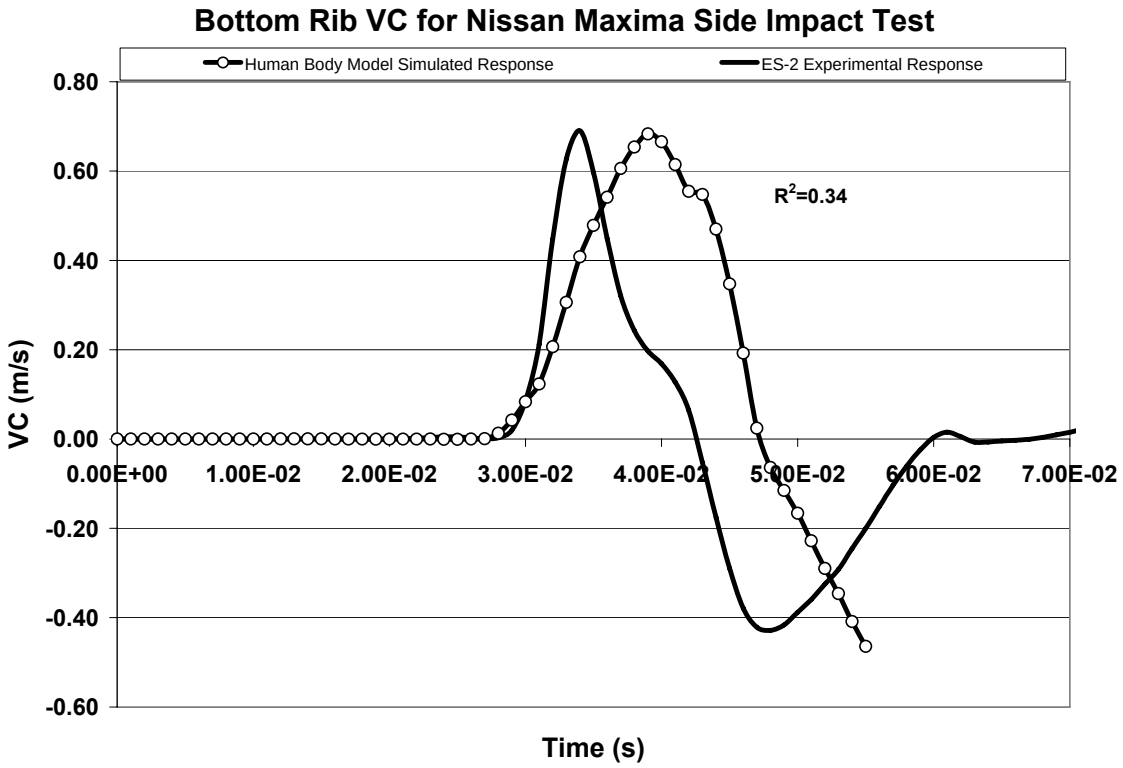

Figure 5.33 Bottom Rib VC Response for the Side Impact Model with Nissan Maxima Inputs

Table 5.3 Side Impact Simulation vs Nissan Maxima v3668 Injury Response Correlation

CHEST BAND	IMPACT PHASE	CORRELATION						
		Compression (mm/mm)	Velocity (m/s)	VC (m/s)	VCmax (m/s)		VCmax Time (s)	
					Sim	ES-2	Sim	ES-2
Upper Rib	Loading	Good	Poor	Reasonable	0.65	0.77	0.039	0.040
	Peak	Reasonable	Reasonable	Good				
	Unloading	N/A	Reasonable	Reasonable				
	R^2	0.98	0.71	0.81				
Middle Rib	Loading	Good	Reasonable	Reasonable	0.57	0.42	0.040	0.036
	Peak	Poor	Reasonable	Poor				
	Unloading	N/A	Reasonable	Reasonable				
	R^2	0.93	0.57	0.59				
Bottom Rib	Loading	Good	Good	Good	0.68	0.69	0.039	0.034
	Peak	Reasonable	Poor	Reasonable				
	Unloading	N/A	Poor	Poor				
	R^2	0.77	0.61	0.34				

As in the case of the Ford Taurus it can be seen that the side impact model closely reproduces the timing and injury response of the Nissan Maxima IIHS test. The model has been found to produce '*good*' to '*reasonable*' response when compared to the ES-2 response in the Nissan Maxima test case based on the qualitative description previously discussed. Again, discrepancies may be attributed to minor differences in occupant positioning, door positioning and compliance, or geometric differences between the ES-2 and human body model at the specified chest band locations.

5.4 Side Impact Model Validation Summary

The side impact model, discussed in the previous chapters, was developed based on the geometry, material properties, and boundary conditions gathered by experimental testing as well as information provided in the literature. The side impact model has been shown to produce '*good*' to '*reasonable*' injury response with respect to the full-scale FMVSS 214 side impact test of a Ford Taurus, as well as the IIHS side impact test of a Nissan Maxima based on the qualitative descriptions previously stated. Therefore, the side impact model response presented above validates the accuracy of the side impact model and encourages its use to predict thoracic trauma under varying conditions. The following chapter will present the application of the side impact model to investigate the effect of various input conditions on thoracic trauma.

-- CHAPTER 6 --

Side Impact Simulation - Parametric Study Results

6.1 Introduction

The previous chapters have discussed the development and validation of the side impact model. The intent of this chapter is to gain further insight into the mechanisms governing thoracic trauma in side impact collisions. A parametric study investigating the effect of several different conditions on thoracic trauma is presented to provide a detailed understanding of side impact collisions and the factors that contribute to injury response based on the evaluation of thoracic compression, velocity, and VC response.

6.2 Measuring Thoracic Response

In the previous chapter injury response was evaluated in such a way to facilitate comparison to the ES-2 dummy using half thoracic measurements. The chest band locations were determined to correspond to the location of the lower, middle, and upper ribs on the ES-2. Also, the half thoracic deflection and VC were measured using the numerical human body model to compare to the half thoracic response of the ES-2. However, the thoracic response in this chapter will be measured using the same chest band locations implemented by Forbes (2005) to ensure consistency with prior human body model usage and PMHS testing in the literature (Forbes, 2005; Pintar, 1997).

Throughout this chapter thoracic response is measured using upper, middle, and lower chest bands located at the lateral level of the 4^{th} rib, level of the xiphoid process, and the level of the 10^{th} rib respectively (Figure 6.2). Also, it has been found that the half thoracic deflection is significantly lower than the full thoracic deflection (Maltese et al., 2002). This indicates that a considerable amount of deformation is occurring on the non-struck side, which is unaccounted for when using the half thoracic response. Table 6.1 presents research performed by Maltese et al. (2002) comparing the half thoracic deflection to the full thoracic deflection. Maltese et al. clearly show that the half thoracic deflection often approximates 60% of the full thoracic deflection, thus indicating a significant amount of deflection on the non-struck side. Similar differences between full and half thoracic deflection were found for the human body model as seen in Figure 6.1.

Table 6.1 Maximum of the mean deflection time history for the full and half-upper thorax, lower thorax, and abdomen (Maltese et al., 2002)

		DEFLECTION			
Test Condition		Rigid High Speed Flat Wall	Padded High Speed Flat Wall	Rigid Low Speed Flat Wall	Padded Low Speed Flat Wall
Measurement Location					
Upper Thorax	Full (mm)	95	89	110	85
	Half (mm)	58	60	72	56
	% Half/Full	**61.1 %**	**67.4%**	**65.5%**	**65.9%**
Lower Thorax	Full (mm)	93	100	82	82
	Half (mm)	58	55	51	52
	% Half/Full	**62.4%**	**55.0%**	**62.2%**	**63.4%**
Abdomen	Full (mm)	n/a	118	86	98
	Half (mm)	n/a	78	86	98
	% Half/Full	**n/a**	**66.1%**	**60.5%**	**59.2%**

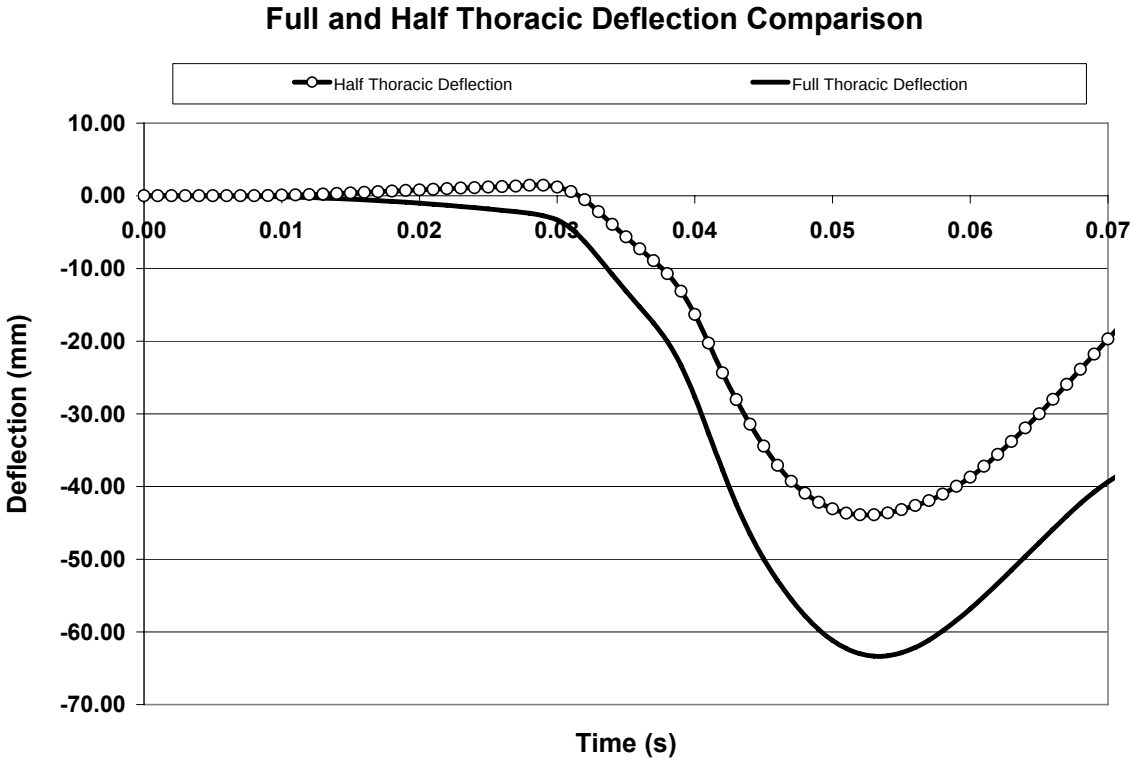

Figure 6.1 Human Body Model Full and Half Thoracic Deflection Comparison for Ford Taurus Simulation.

The full thoracic response will be used for the remainder of this chapter to ensure the maximum thoracic response is observed. Chestband locations (Figure 6.2a) consistent with prior human body model usage and PMHS testing in the literature (Forbes, 2005; Pintar, 1997) will be used to determine thoracic compression, velocity, and VC.

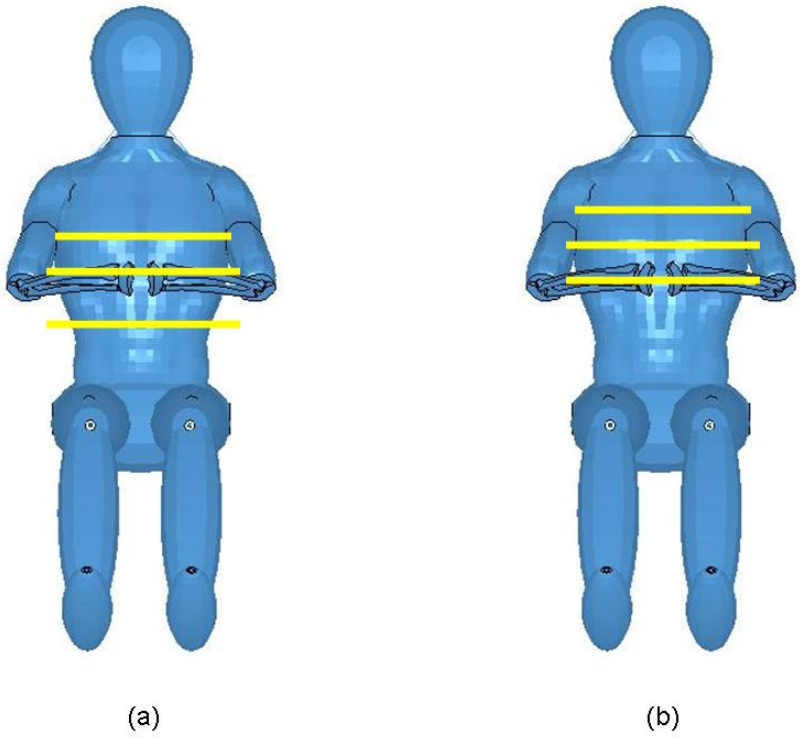

Figure 6.2 Chest band location (a) Parametric Study Location (b) Validation Location

6.3 Side Impact Model Baseline Conditions

The velocity profiles, door compliance, and position determined for the validation of the side impact model for the Ford Taurus FMVSS 214 test were used as the baseline for the parametric study presented in this chapter. The Ford Taurus test was selected as the baseline because it was a validated scenario representative of a typical side impact collision (Figure 6.3). Full-scale side impact tests typically result in door intrusion velocity profiles that consist of three common characteristics; first peak, valley, and second peak (Morris et al., 1998). The first peak occurs immediately after the barrier

contacts the door causing the door velocity to rapidly increase to its initial peak. The door velocity then decreases to its valley as the vehicle side structure transfers load to the main structure of the vehicle (Payne et al, 1997). The second peak in door velocity is caused by stiffening of the barrier prior to slowing to its final velocity. It has been found that the overall kinematics of the door is essentially unaltered by the interaction with the occupant (Chung et al., 1997).

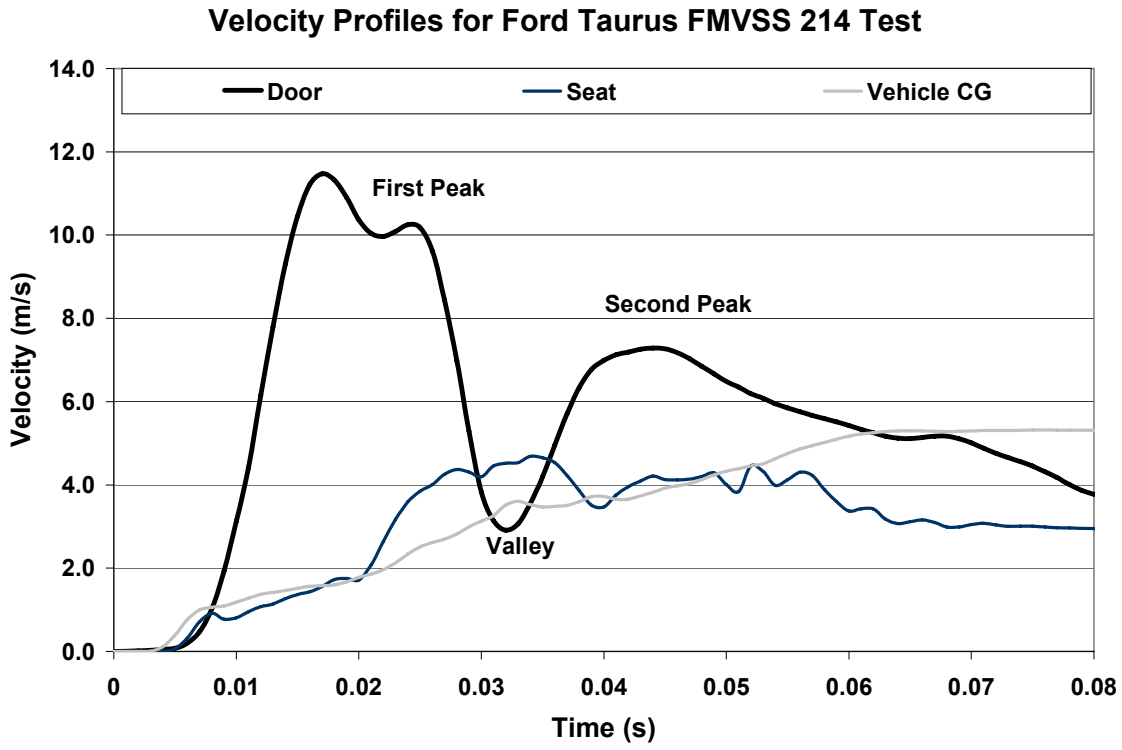

Figure 6.3 Side Impact Model Baseline Velocity Profiles

The parametric study varies several factors to investigate their effect on thoracic response during side impact collisions. Factors investigated include; AD distance, door intrusion velocity profile, arm rest height, seat foam, arm position, and restraint systems. The baseline case uses the velocity profile (Figure 6.3) and AD distance of 115mm as in the Ford Taurus FMVSS test.

6.4 The Effect of Varying Door to Occupant Distance

Improving the vehicles structural integrity to limit intrusion into the occupant compartment under loads observed in side impact collisions has been an area of focus for the past 30 years (NHTSA, 2004). This study investigates the effect of the door to occupant distance by using two door types; a rigid plate and a representative door with armrest (Figure 6.4). The AD spacing used in this study was selected to cover a range as determined by the maximum and minimum values found in FMVSS 214 test reports (NHTSA database, 2008).

One would expect that increasing the spacing between the occupant and the intruding door would reduce occupant injury. The amount of space between the occupant and the door has a direct effect on the contact velocity as well as the contact timing with respect to the velocity profile (Morris et al, 1998). The effect of the occupant to door spacing was investigated by varying the spacing of an intruding rigid door and armrest in the side impact model. As previously discussed, the velocity profiles applied to the side impact model were controlled by the crushing of the vehicle structure and were independent of occupant positioning. Therefore, the velocity profiles for the baseline case were applied for each AD distance in this study.

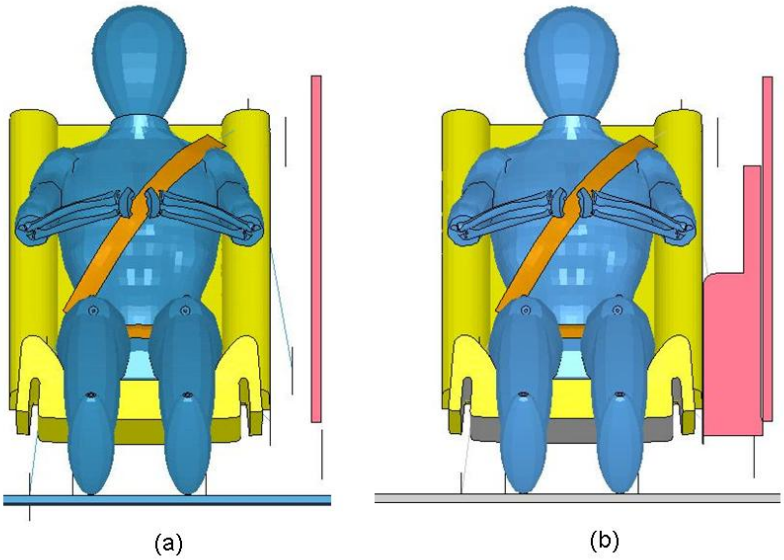

Figure 6.4 Door Type (a) Rigid Door (b) Armrest.

Two cases were used to investigate the effects of door to occupant spacing. First, a rigid door as seen in Figure 6.4a was used to investigate the effect of varied AD distance excluding effects caused by armrest geometry and compliance. Second, the same AD study was performed to investigate differences in thoracic response caused by the presence of an armrest in comparison to a flat rigid door.

6.4.1 Varying AD Distance for a Rigid Door

Intuitively, one would expect that increasing the spacing between the occupant and the intruding door would reduce occupant injury. The AD spacing directly effects the contact velocity and contact timing with respect to the velocity profile, thereby having a significant impact on VC response. The effect of the occupant to door spacing was investigated by varying the spacing of a non-intruding and intruding rigid door in the side impact model (Figure 6.4a). Figure 6.5 shows the relationship between injury and occupant spacing for several AD distances. Trend lines are included to track VCmax for varying AD spacings.

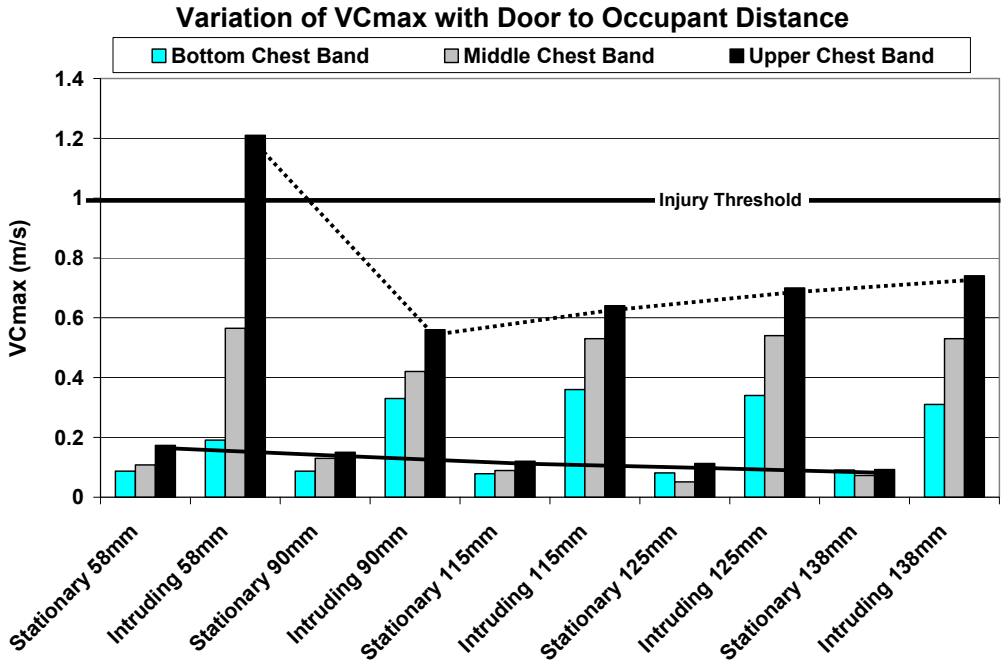

Figure 6.5 Variation of VCmax with AD Distance for a Stationary and Intruding Door

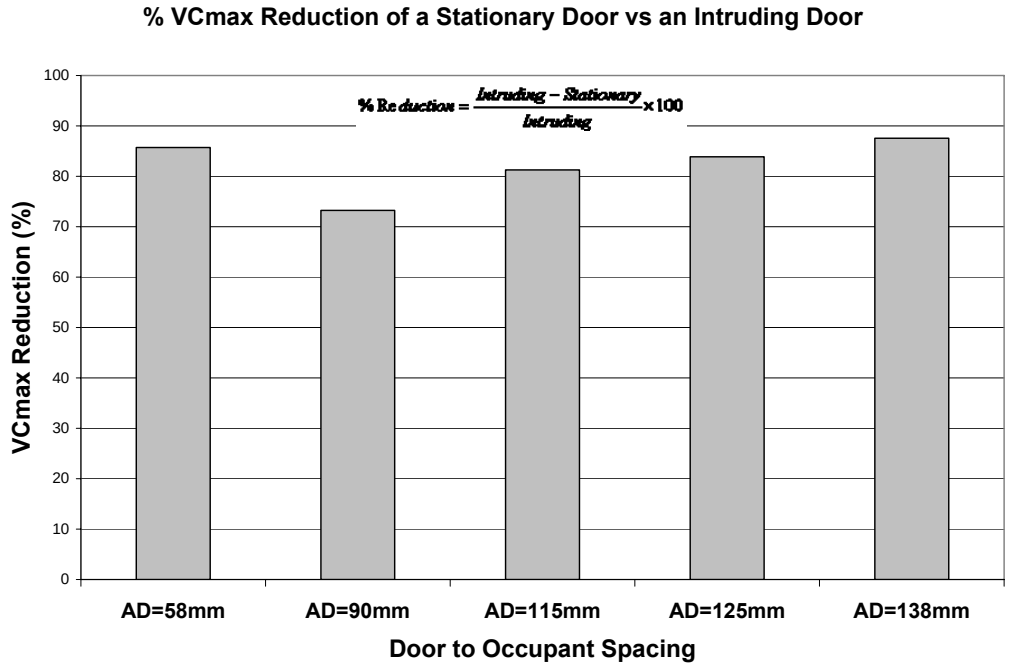

Figure 6.6 % VCmax Reduction of a Stationary Door vs an Intruding Door

The AD spacings used in this study were selected to cover a range determined by the maximum and minimum values found in FMVSS 214 reports (NHTSA database, 2008). The effect of door intrusion and occupant to door distance can be seen in Figure 6.5. It is clear that occupant injury is minimized when intrusion into the occupant compartment is eliminated, reducing VCmax by 73 to 88 percent (Figure 6.6). The injury observed in side impact simulations with no intrusion is a result of the motion of the occupant relative to the seat and door caused by the occupant's inertia.

The occupant response for a side impact with a stationary door can be seen in Figure 6.7.

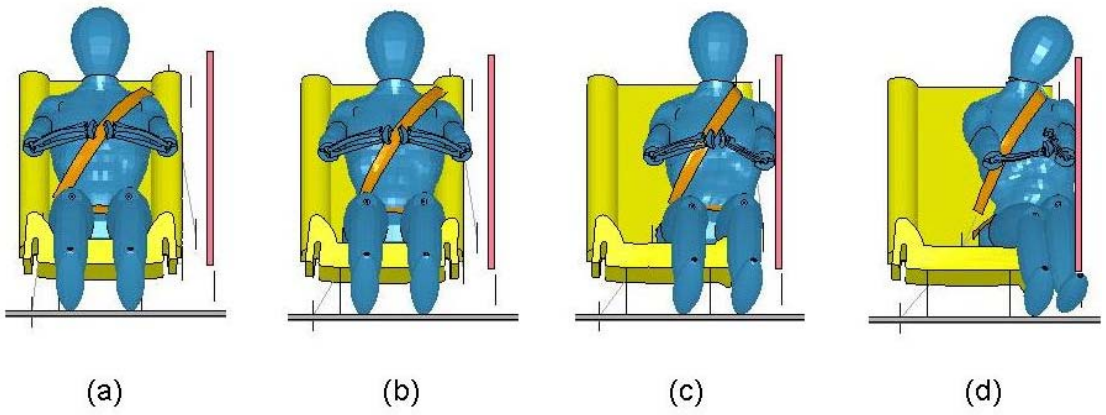

Figure 6.7 Impact Sequence of Stationary Rigid Door Side Impact Simulation (a) t=0 ms (b) t=30 ms (c) t=60 ms (d) t=90 ms

The upper band compression, velocity and VC response for an intruding rigid door is shown in the figures below.

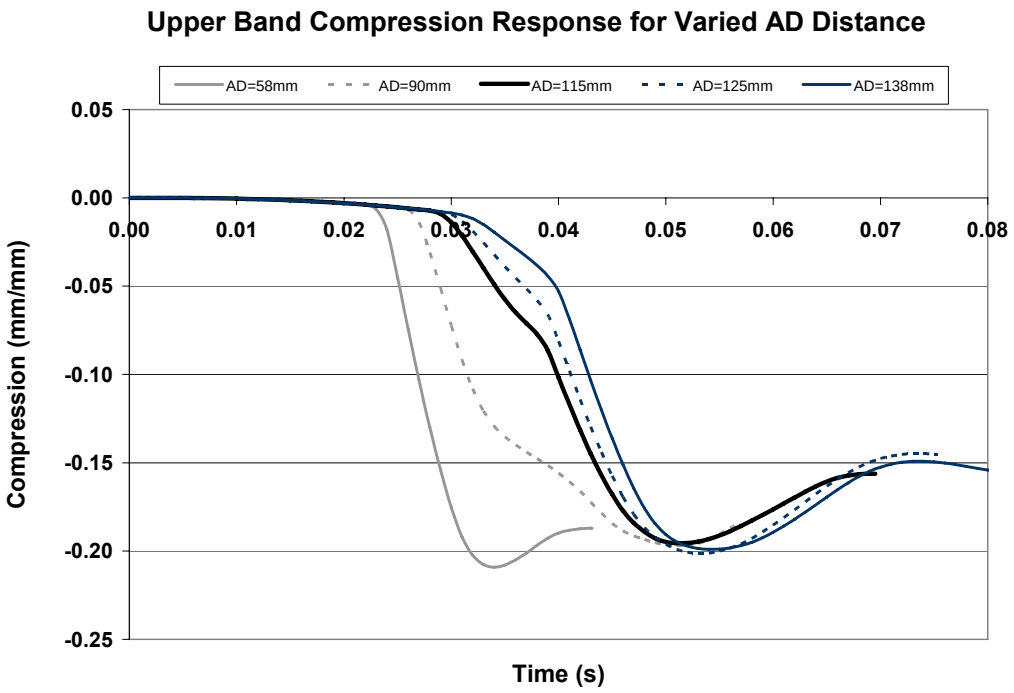

Figure 6.8 Upper Band Compression Response for Varied AD Distance of a Rigid Door

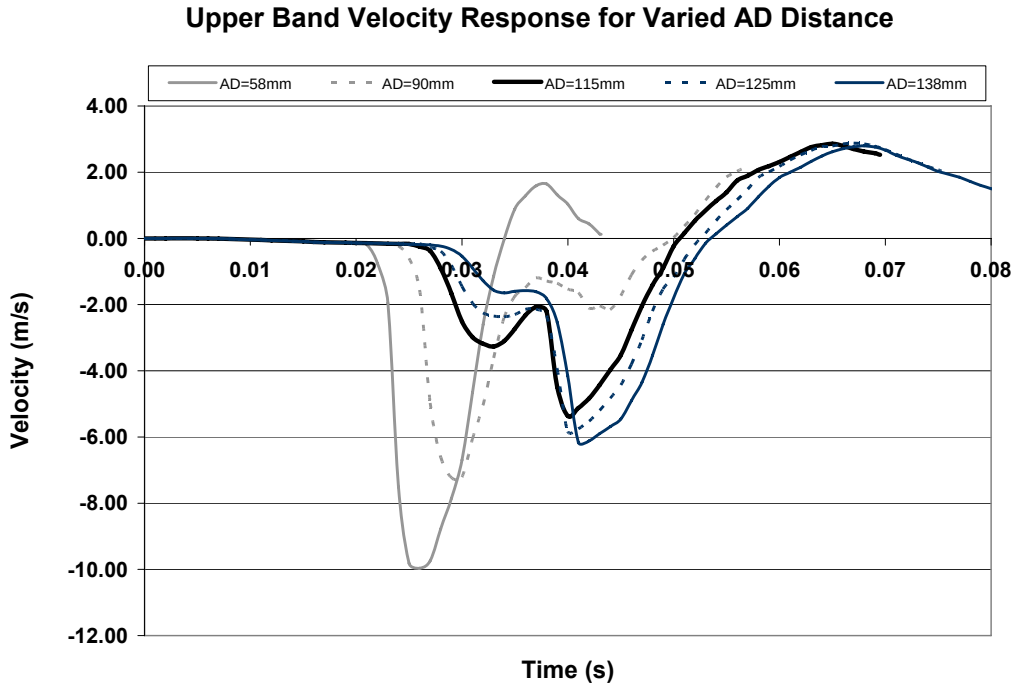

Figure 6.9 Upper Band Velocity Response for Varied AD Distance of a Rigid Door

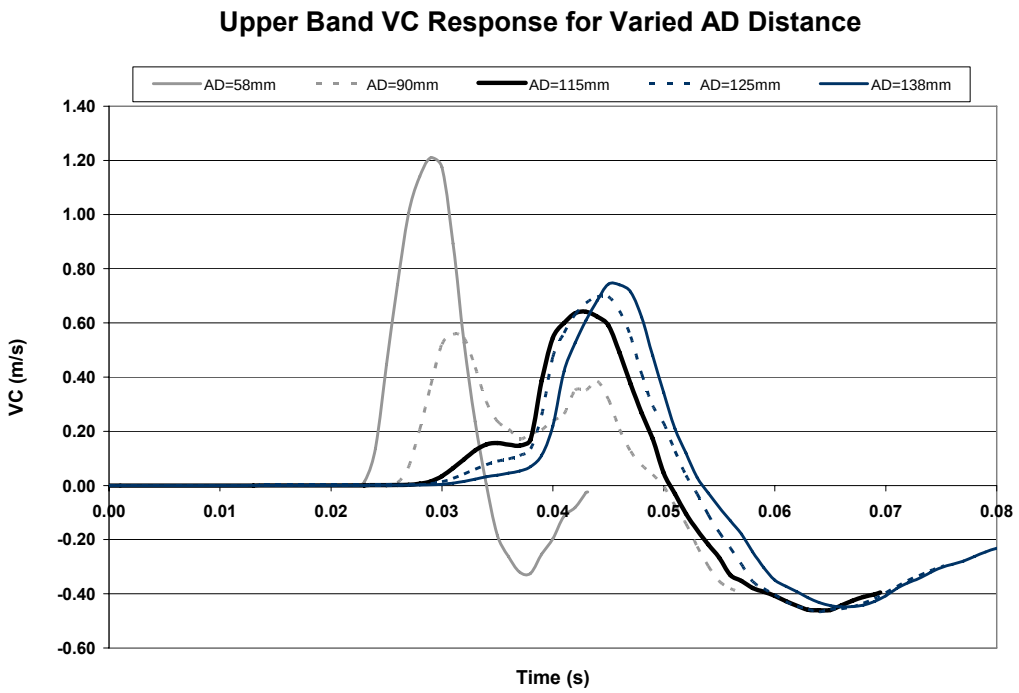

Figure 6.10 Upper Band VC Response for Varied AD Distance of a Rigid Door

Investigating the VC response shown in Figure 6.10 can provide some insight into the timing of injury and the role of the occupant to door distance. Two curves (58mm & 90mm) have their peak injury response occurring just after the first peak in the door intrusion velocity profile (Figure 6.11). The remaining three scenarios (115mm, 125mm, and 138mm) have their maximum injury response closely coinciding in time with the second peak of the door velocity profile. Further insight may be provided by examining the contact timings of the door to chest as determined by the upper band velocity response shown in Figure 6.12.

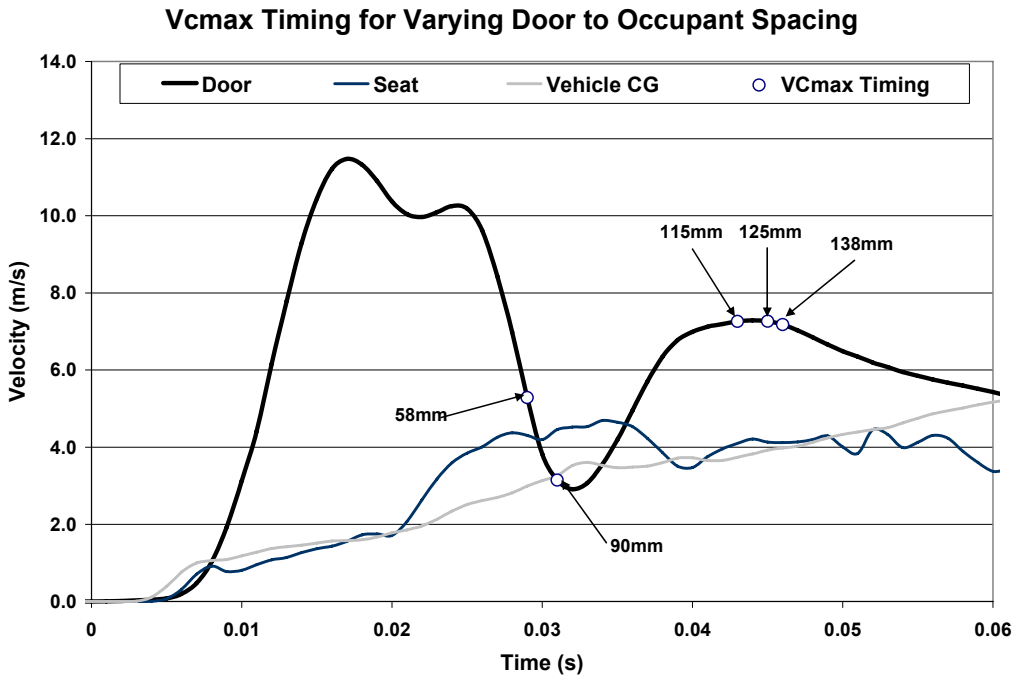

Figure 6.11 VCmax Timing for Varying Door to Occupant Spacing

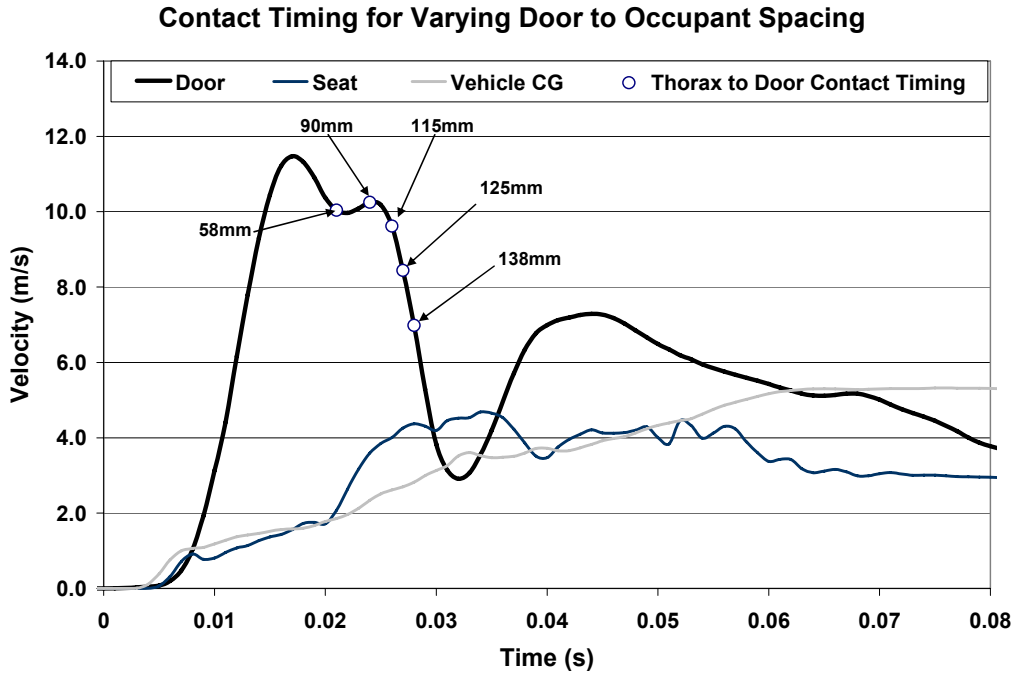

Figure 6.12 Contact Timing for Varying Door to Occupant Spacing

The contact timings for the five AD spacing's discussed occur within 7 ms of each other, but have a significant influence on occupant injury despite the minor differences in contact timing. The variance in injury responses may be explained by examining the occupant motion relative to the sled base by tracking the velocity of the center of the occupant chest relative to the sled floor (Figure 6.13).

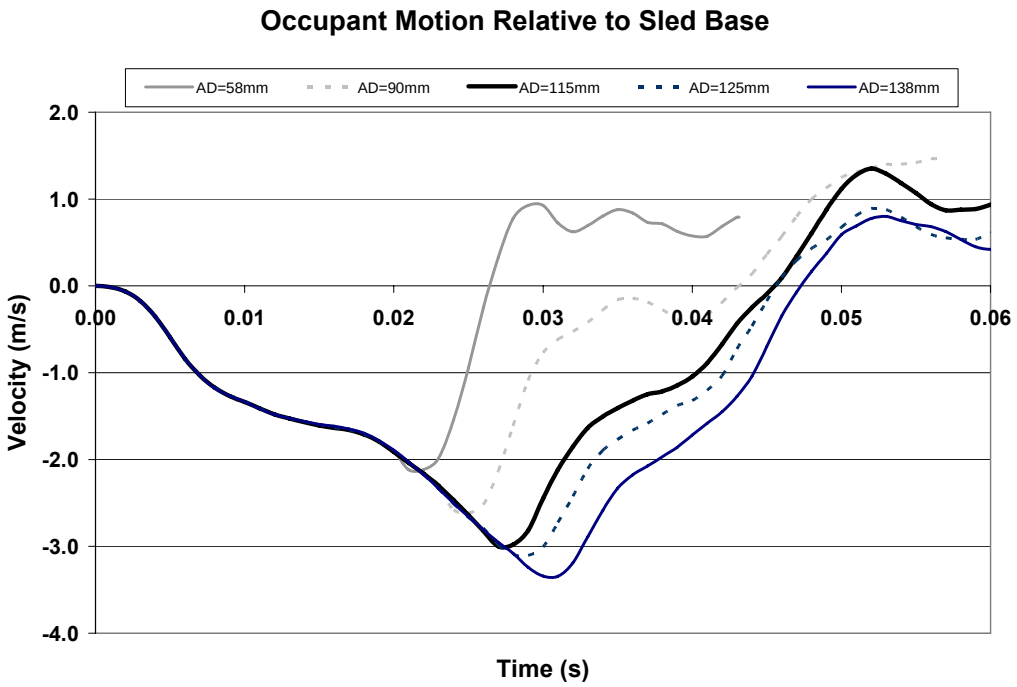

Figure 6.13 Occupant Motion Relative to Sled Base for Varied Door to Occupant Spacing

The occupant response relative to the sled base in Figure 6.13 essentially consists of a decrease in occupant velocity relative to the sled floor prior to door contact followed by an increase in occupant velocity after contact. Therefore, the decreasing relative velocity actually represents the sled floor moving while the occupant remains relatively still due to its inertia. When contact with the door occurs the occupant velocity begins to catch-up to and surpass the velocity of the sled floor.

The variation in VC response was investigated by examining the compression, velocity, and VC curves, and the effect of contact timing and the relative occupant motion on occupant response. The following table summarizes the findings of the varied AD study performed.

Table 6.2 Summary of Injury Response for Varied Door to Occupant Distance

AD Distance	VCmax (m/s)	VCmax Time (s)	Peak Control	Contact Time (s)	Compression Prior to 2nd Peak (%)	Velocity Prior to 2nd Peak (m/s)	Occupant Motion Relative to Sled Base Prior to 2nd Peak (m/s)
58mm	1.21	.029	First	.021	20.9	-.0168	-.804
90mm	.558	.031	First	.024	12.9	-2.39	.278
115mm	.641	.043	Second	.026	4.9	-3.10	1.5
125mm	.696	.044	Second	.027	3.2	-2.39	1.9
138mm	.743	.045	Second	.028	1.9	-1.65	2.58

Intuitively, one would expect that thoracic trauma would inversely correlate to AD distance, such that an increase in AD distance would cause a decrease in injury. This inverse correlation does occur to some extent in the scenario presented and would likely occur for all AD distances if not for the second peak in the door velocity profile.

For a door to occupant distance of 58mm, the VC response is controlled by the first peak and occurs just before the door velocity profile valley. The thoracic compression present at the onset of the second peak in door velocity is 20.9% and is the maximum compression observed in the study. The velocity of chest compression at the onset of the second peak is near zero, confirming that the chest has in fact reached the maximum compression and is beginning to expand. The occupant motion relative to the sled base prior to the second peak suggests that the occupant has surpassed the velocity of the sled floor due to the aggressive impact with the intruding door.

The 90mm door to occupant scenario can be described in much the same way as the 58mm case. However, the 115mm case differs as it is controlled by the second peak in the door velocity profile. The first peak does produce minor thoracic response as observed in the VC response shown in Figure 6.10, but is superseded by the injury produced by the second peak. This response can be largely explained by the time of contact and occupant response prior to the second peak. As seen in Figure 6.12, the contact timing for an AD of 115mm occurs as the door is decelerating to its valley, which decreases the time for the door to compress the chest and accelerate the occupant. In this case, the chest compression is only 5% prior to the second peak. Also, the occupant velocity relative to the sled base suggests that the occupant is beginning to accelerate due to contact with the intruding door, but is still moving considerably slower than the sled floor. These factors significantly increase the effect of the second peak because the occupant has not been accelerated enough to minimize the impact of the second peak.

The same reasoning can be applied to the final two cases (125mm and 138mm). Injury in both cases is highly influenced by the second peak due to the time of contact with the intruding door. As intuition would suggest, the first peak response continually decreases as AD distance increases, but this decrease in first peak response causes an increase in the effects of the second peak, thus creating the VC response observed in Figure 6.10. The later contact time reduces the ability of the first peak to accelerate the occupant, thereby causing the second peak to be far more injurious than observed in scenarios with smaller AD distances.

Based on the VC response produced, one would expect that minimal injury would occur with a door to occupant distance of approximately 100mm in this special case. This study has been performed and the results are presented in Figure 6.14. Although, the 100m AD scenario produces relatively low VCmax, the idealized AD distance should produce two equal VC peaks to minimize VC response.

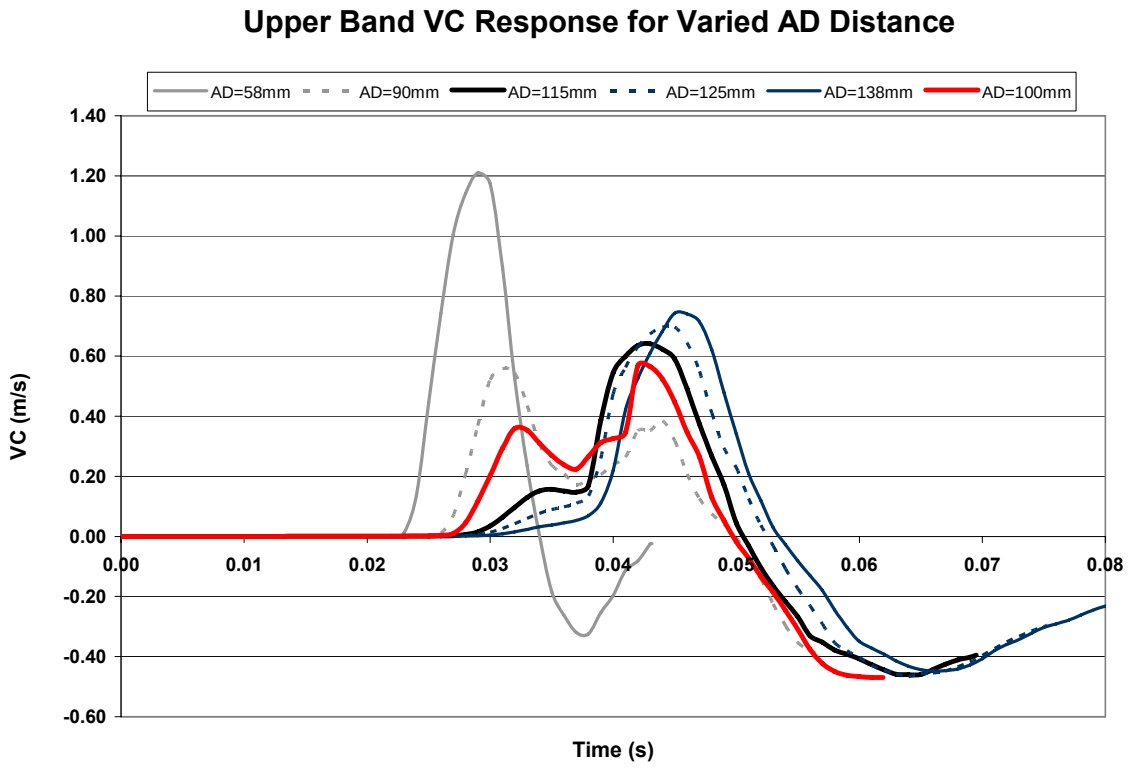

Figure 6.14 Upper Band VC Response for Varied AD Distance

6.4.2 Varying AD Distance with a Deformable Door

The next progression in the parametric study investigates the effect of the door to occupant distance with a representative door and armrest (Figure 6.15). The study utilized the same AD spacing's as the previous study examining the effect of occupant to door spacing with a rigid door. Recall from Equation 5.2, that the door spacing was measured with respect to the center of the human body model. Therefore, the spacing required for an AD distance of 115mm is 351mm from occupant center to door.

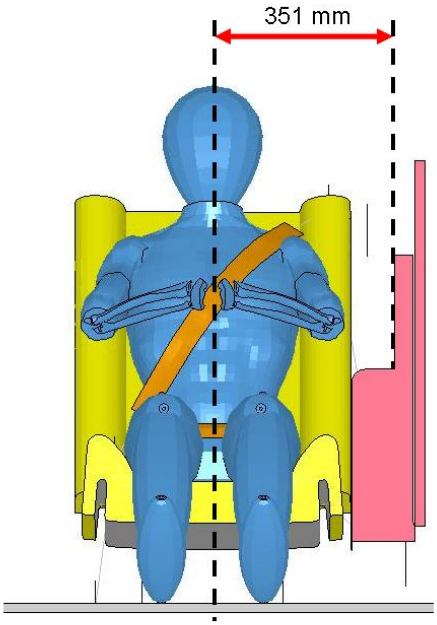

Figure 6.15 Side Sled Model with Simplified Door and Armrest

The VCmax of an occupant for varied AD spacing's of a simplified door including an armrest is compared to that of a rigid flat door in the following bar chart (Figure 6.16). Trend lines are included to track VCmax for varying AD spacings.

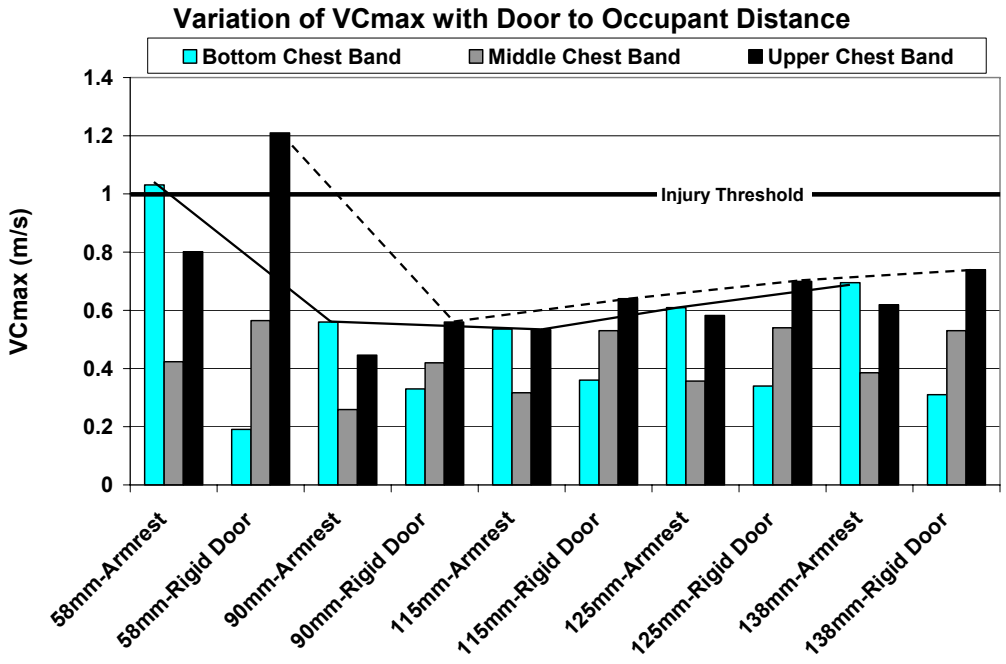

Figure 6.16 Variation of VCmax with Door to Occupant Distance

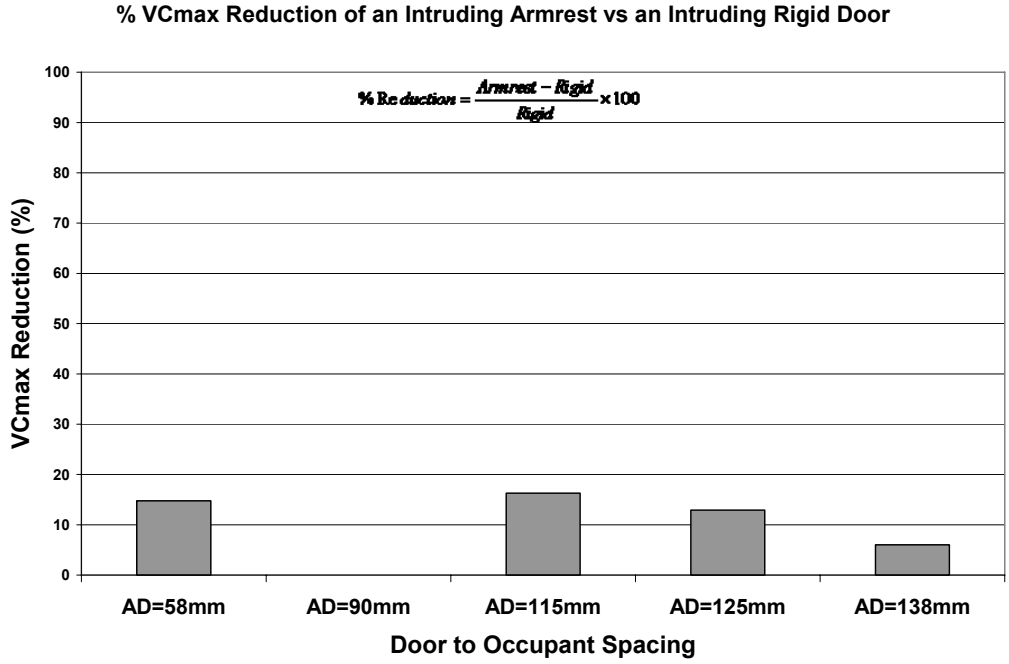

Figure 6.17 VCmax Reduction of an Intruding Armrest vs an Intruding Rigid Door

As one would expect, the presence of an armrest tends to increase the injury response at the level of the lower chest band in comparison to the rigid door. This response can be

attributed to an earlier time of contact with the thorax due to the geometry of the armrest effectively reducing the door to occupant spacing. Also, the armrest causes the localized deformation of the thorax, therefore resulting in higher levels of compression and VC response. VCmax in the previous study regarding varied AD distance with an intruding rigid door was dominated by the upper chest band due to the geometry of the occupant. However, VCmax in this study is highly influenced by the lower chest band due to contact with the armrest. Although the peak VC response observed does not change drastically, the maximum injury is found at the level of the lower chest band when an armrest is present. The presence of an armrest reduces the VCmax observed by a maximum of 16% compared to the VC response caused by an intruding rigid door (Figure 6.17). The compression, velocity, and VC response of the upper chest band is presented in Figure 6.18, Figure 6.19, and Figure 6.20.

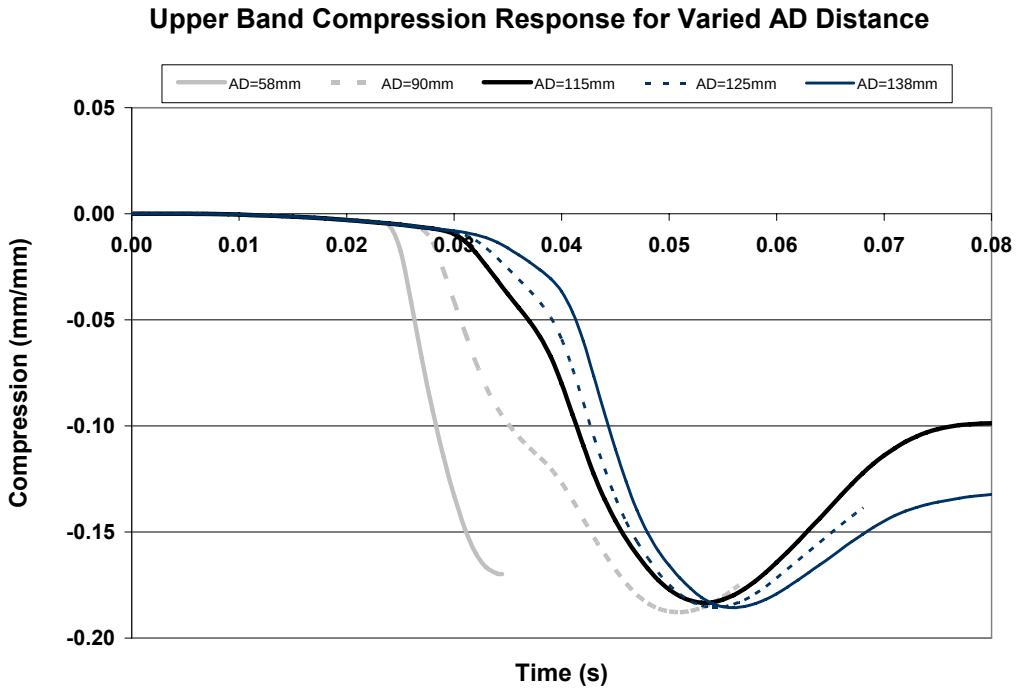

Figure 6.18 Upper Band Compression Response for Varied AD Distance of a Deformable Door

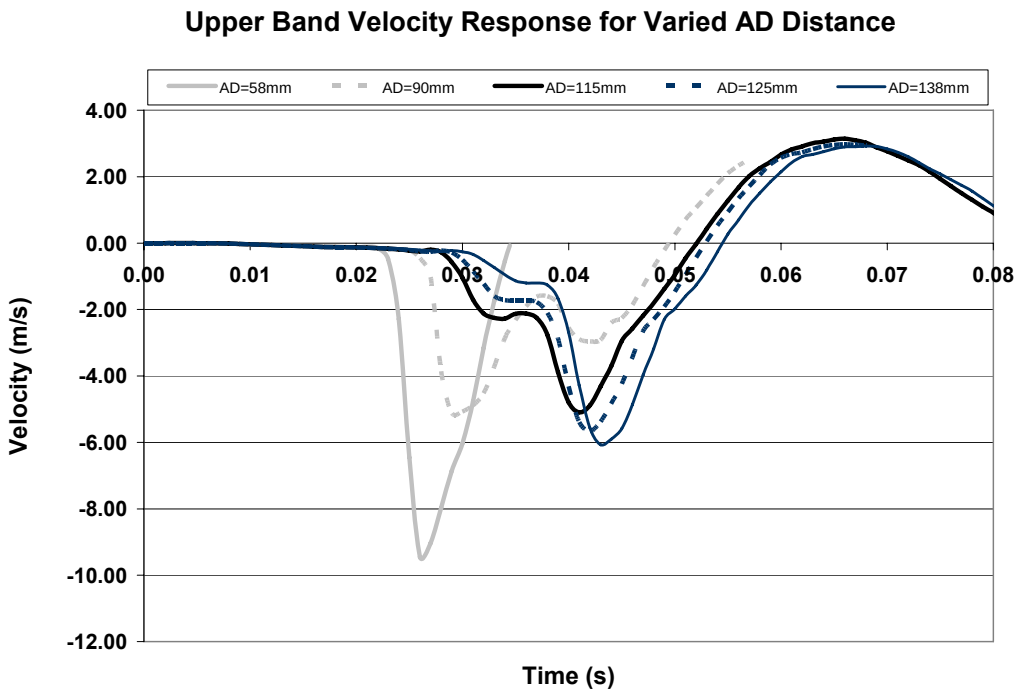

Figure 6.19 Upper Band Velocity Response for Varied AD Distance of a Deformable Door

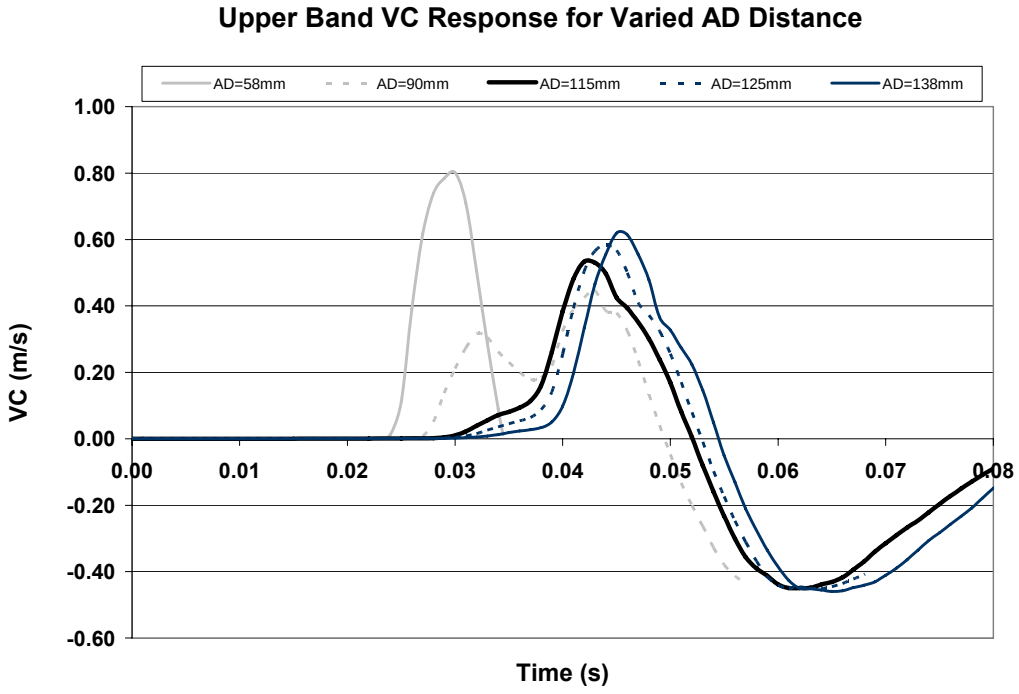

Figure 6.20 Upper Band VC Response for Varied AD Distance of a Deformable Door

6.5 The Effect of Varying Door Intrusion Velocity

Based on information from the literature and the study above it is clear that the door interaction with the occupant is a vital aspect of occupant injury. The occupant to door distance study showed that the AD distance is an important factor in determining thoracic response, but the relationship between VCmax and AD distance was not linear. This is largely due to the effects of the velocity profile and variation in contact timing. The following study examines the effect of the velocity profile by varying the first and second peak of the velocity profile by +/- 15% as shown in Figure 6.21. This velocity profile study is based on the research performed by Morris et al. (1998) discussed in Figure 2.30. As in the previous case study, it was assumed that the velocity profiles applied to the side impact model were independent of occupant positioning and in this case would be possible as a result of structural changes made to the vehicle.

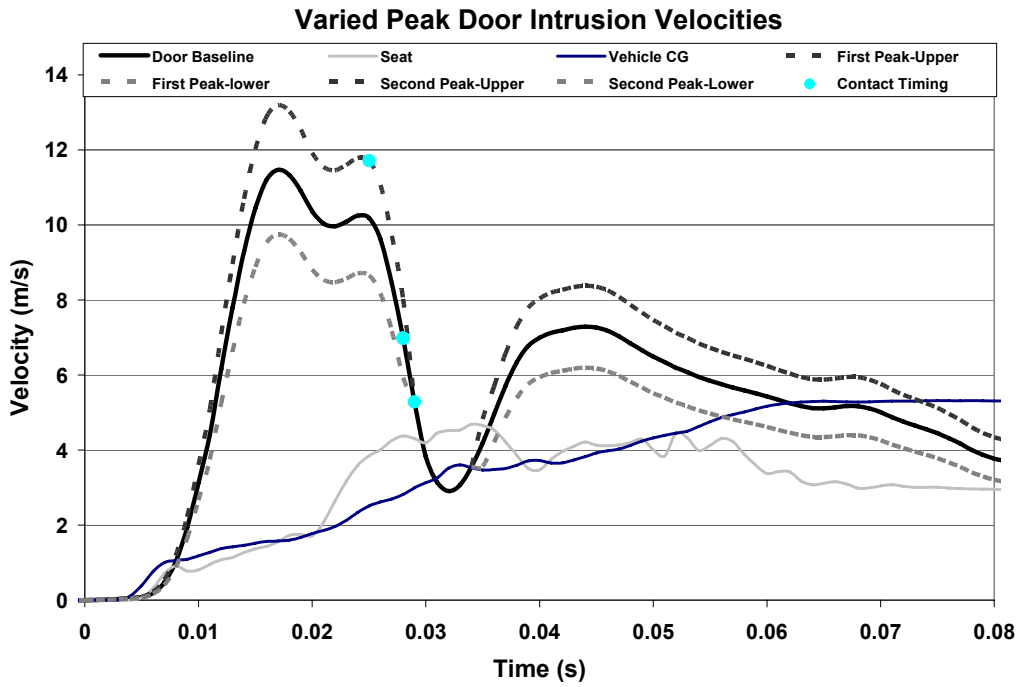

Figure 6.21 Varied Door Intrusion Velocity Profile & Contact Times

Figure 6.22 shows the relationship between injury and velocity profile for variations in first and second peak velocity.

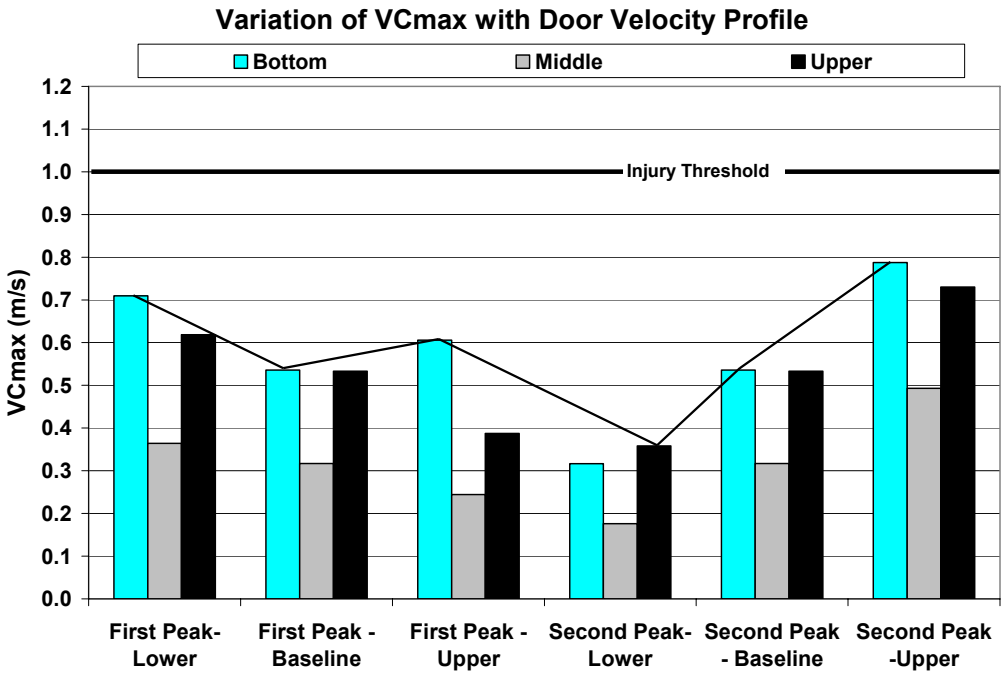

Figure 6.22 Variation of VCmax with Door Velocity Profile

The compression, velocity, and VC responses for the upper chest band are shown below. As expected, the variation in velocity profile has a significant effect on occupant response.

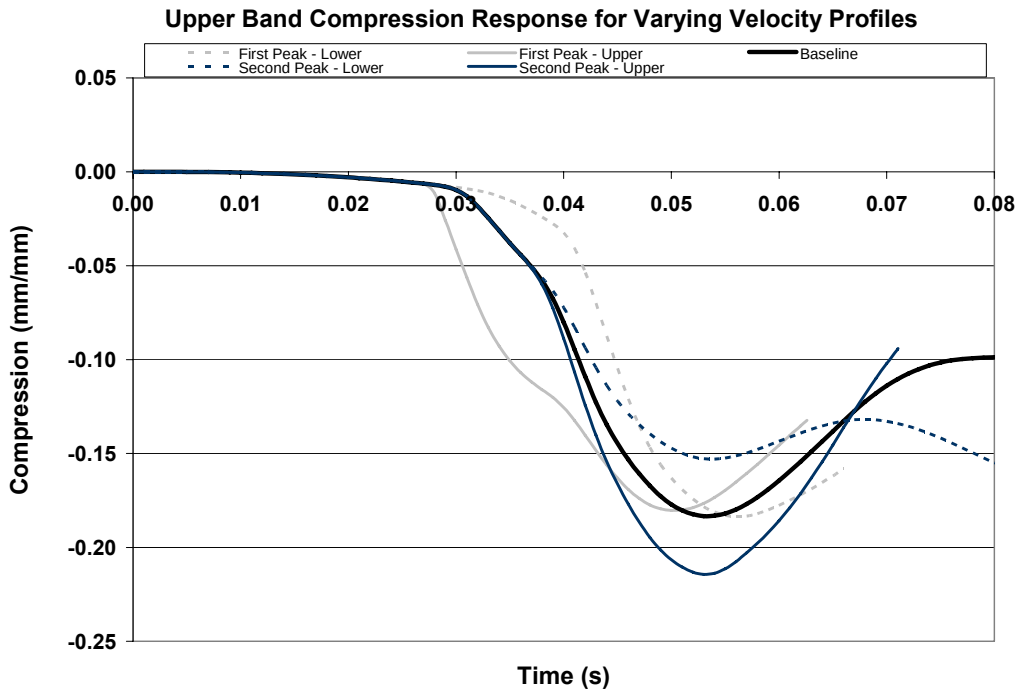

Figure 6.23 Upper Band Compression Response for Varying Velocity Profiles

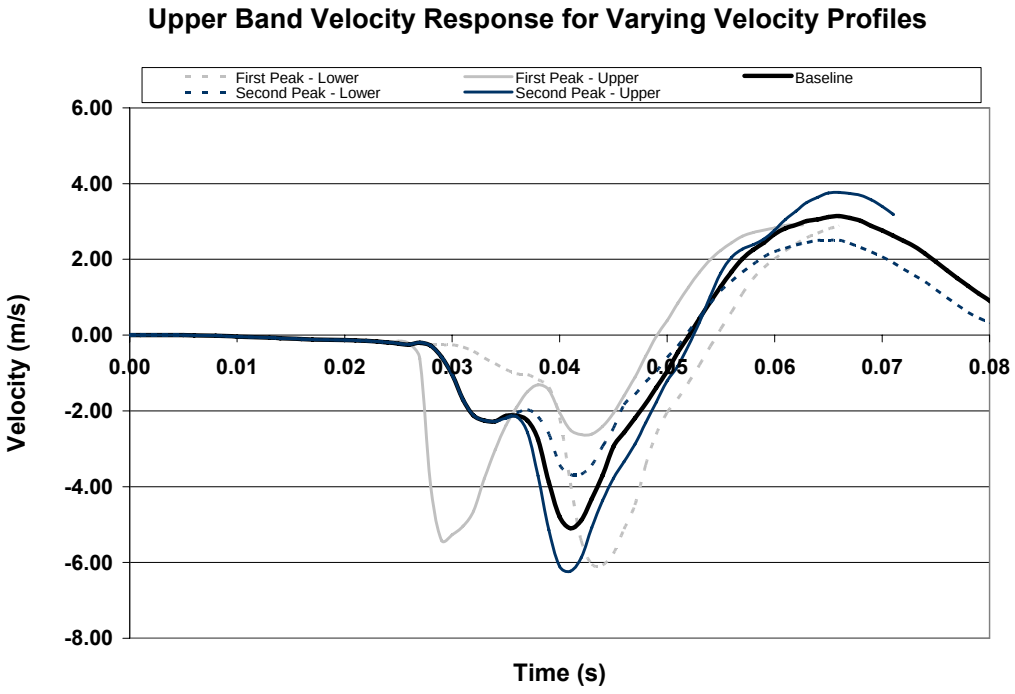

Figure 6.24 Upper Band Velocity Response for Varying Velocity Profiles

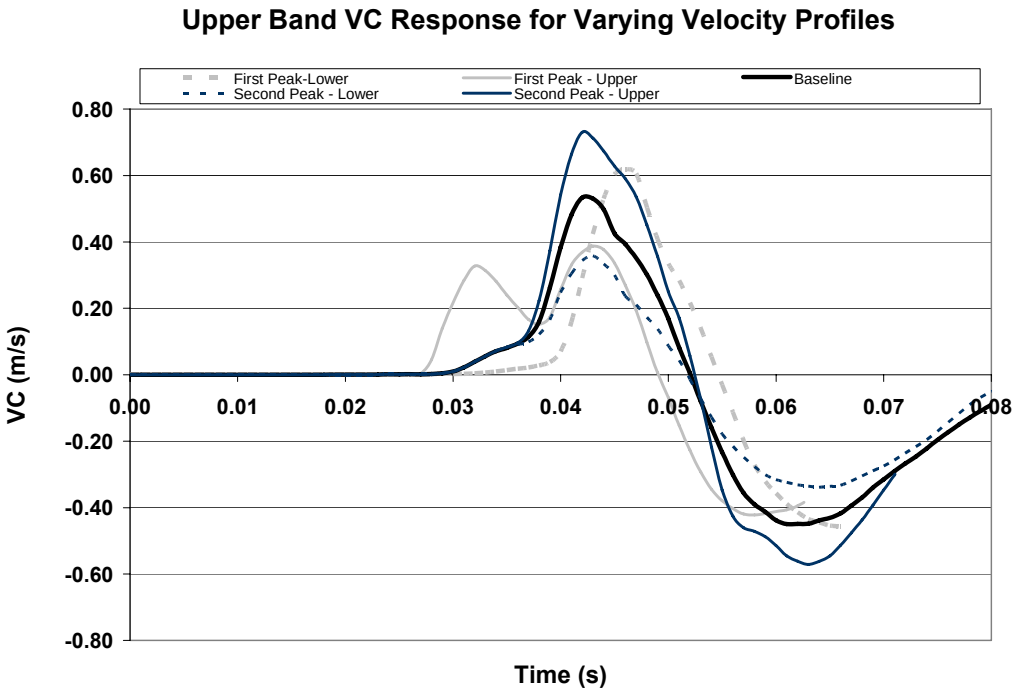

Figure 6.25 Upper Band VC Response for Varying Velocity Profiles

Figure 6.25 shows that the peak VC response in each scenario corresponds in time with the second peak of the door velocity profile. However, varying the first peak has a significant impact on the magnitude of VC response produced by the second peak. This can be explained by investigating the occupant motion relative to the sled base (Figure 6.26). As it has been shown that VC response is largely dependant on the second peak in velocity profile, therefore increasing the velocity of the second peak will clearly increase thoracic response and a decrease in peak velocity will result in a decreased VC response.

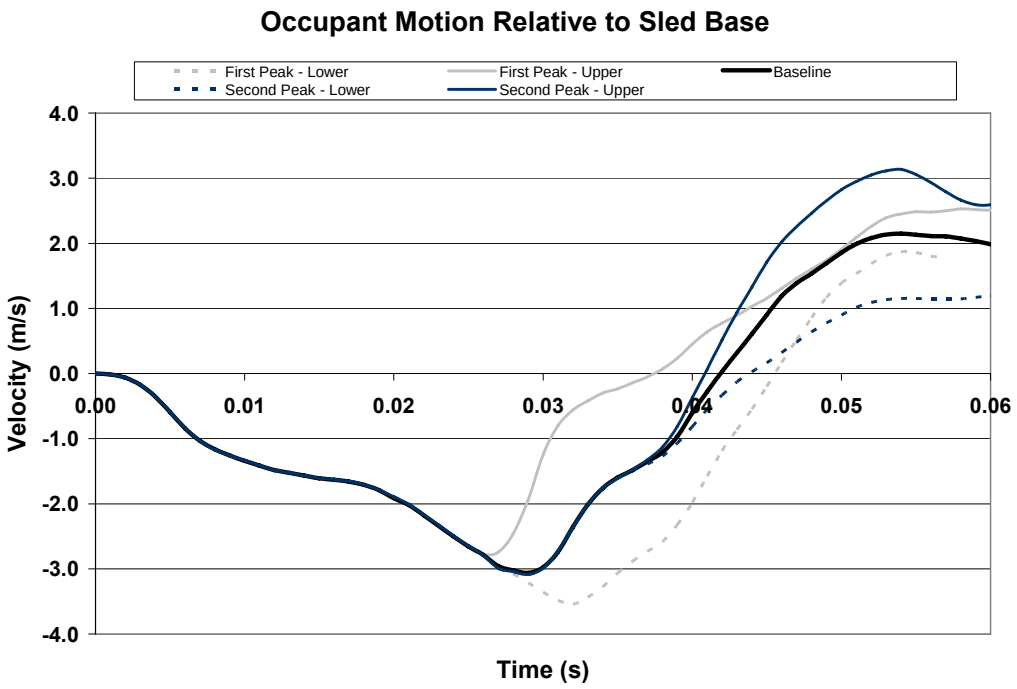

Figure 6.26 Occupant Motion Relative to Sled Base for Varied Door Intrusion Velocity Profile

Again, the variation in VC response was investigated by examining the compression, velocity, and VC curves, and the effect of contact timing and occupant motion relative to the sled base on occupant response. The following table summarizes the findings of the varied velocity profile study performed.

Table 6.3 Summary of Injury Response for Varied Velocity Profile

Velocity Profile	VCmax (m/s)	VCmax Time (s)	Peak Control	Contact Time (s)	Compression Prior to 2nd Peak (%)	Velocity Prior to 2nd Peak (m/s)	Occupant Velocity Relative to Sled Base Prior to 2nd Peak (m/s)
Baseline	.533	.042	Second	.028	3.13	-2.27	-1.76
First - Lower	.618	.046	Second	.030	-.75	-2.39	-3.27
First - Upper	.387	.043	Second	.026	-3.03	-3.10	-.299
Second-Lower	.358	.043	Second	.028	3.13	-2.27	-1.76
Second-Upper	.730	.042	Second	.028	3.13	-2.27	-1.76

Similar to the previous study on varied AD distance, variation in velocity profile has a somewhat counter-intuitive effect on occupant injury. Although VC response in the current scenario corresponds in time with the second velocity peak for all cases, the first peak directly contributes to the degree at which the second peak influences VC.

For the baseline case and therefore the cases varying the second peak velocity, the effect of the first peak is the same in terms of chest compression, velocity of compression, VC, and occupant motion relative to the sled base. Since the conditions prior to the second peak are known and constant for the baseline, upper second peak, and lower second peak it is possible to understand the effect of the second peak velocity irrespective of the effects of the first peak. It is clear that the second peak of the door intrusion velocity profile follows the expectations that intuition would suggest, such that an increase in velocity will cause an increase in injury and a decrease in velocity will cause a subsequent decrease in injury.

However, the first peak does not contribute to injury in the same manner as the second peak in the current study. Instead the first peak acts as a means to accelerate the occupant following contact with the door, thereby increasing the occupant velocity and minimizing the impact of the second peak. An increase in first peak velocity will reduce the effect of the second peak, while a decrease in first peak will increase the influence of the second peak. This effect can be observed by comparing the occupant motion relative to the sled base (Figure 6.26) and VC response (Figure 6.25) for the baseline, upper first peak, and lower first peak.

Figure 6.27 shows that increasing the first peak velocity by 15% can reduce the Upper Band VCmax by 27% and decreasing the first peak velocity by 15% can increase the Upper Band VCmax by 16%. However, increasing the second peak velocity by 15% increases the Upper Band VCmax by 37% and decreasing the second peak velocity by 15% causes a 33% reduction of the Upper Band VCmax.

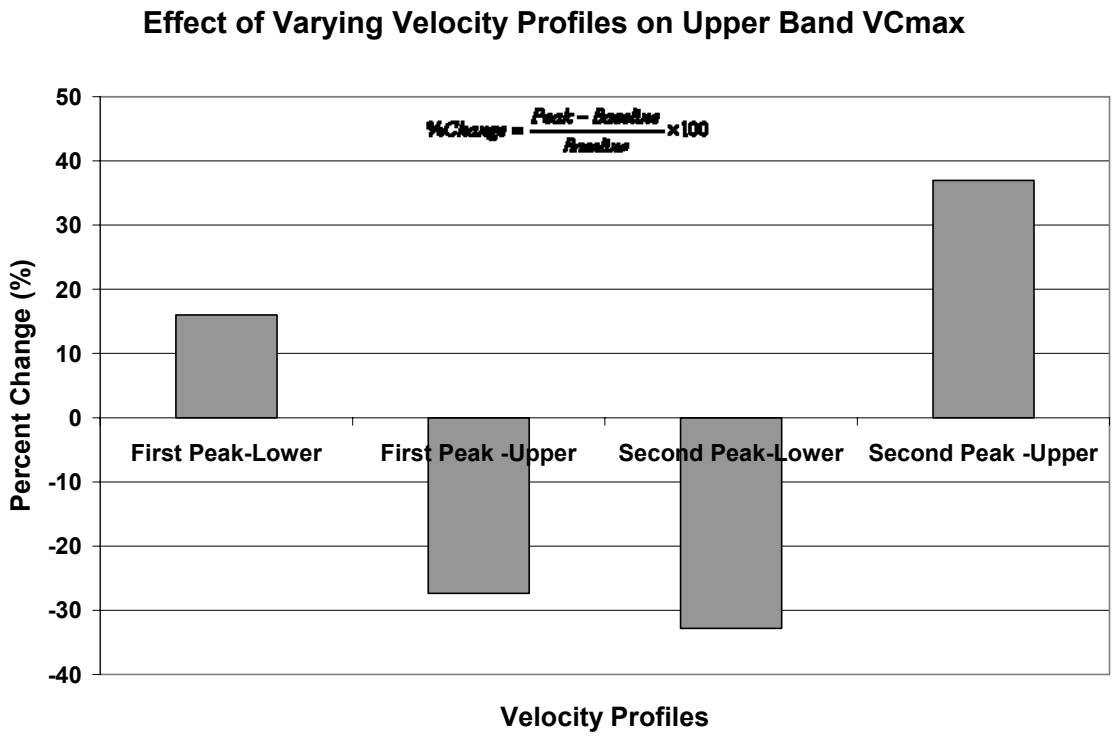

Figure 6.27 The Effect of Varying Velocity Profiles on Upper Band VCmax

The middle chest band follows the same tendencies as the upper band in response to varied velocity profiles. However, the response of the lower chest band does not follow the same trend as the middle and upper band for the case of an increase in first peak velocity (Figure 6.22). This discrepancy is due to the high contact velocity at the lower chest band caused by the reduced door to occupant distance due to the armrest geometry.

As shown in Figure 6.28, the Lower Band VCmax occurs at the first peak in its response. Although the first peak does not control injury for the middle and upper chest bands in this study, a greater increase in first peak velocity would result in injury being dominated by the first peak, similar to the response of the lower chest band.

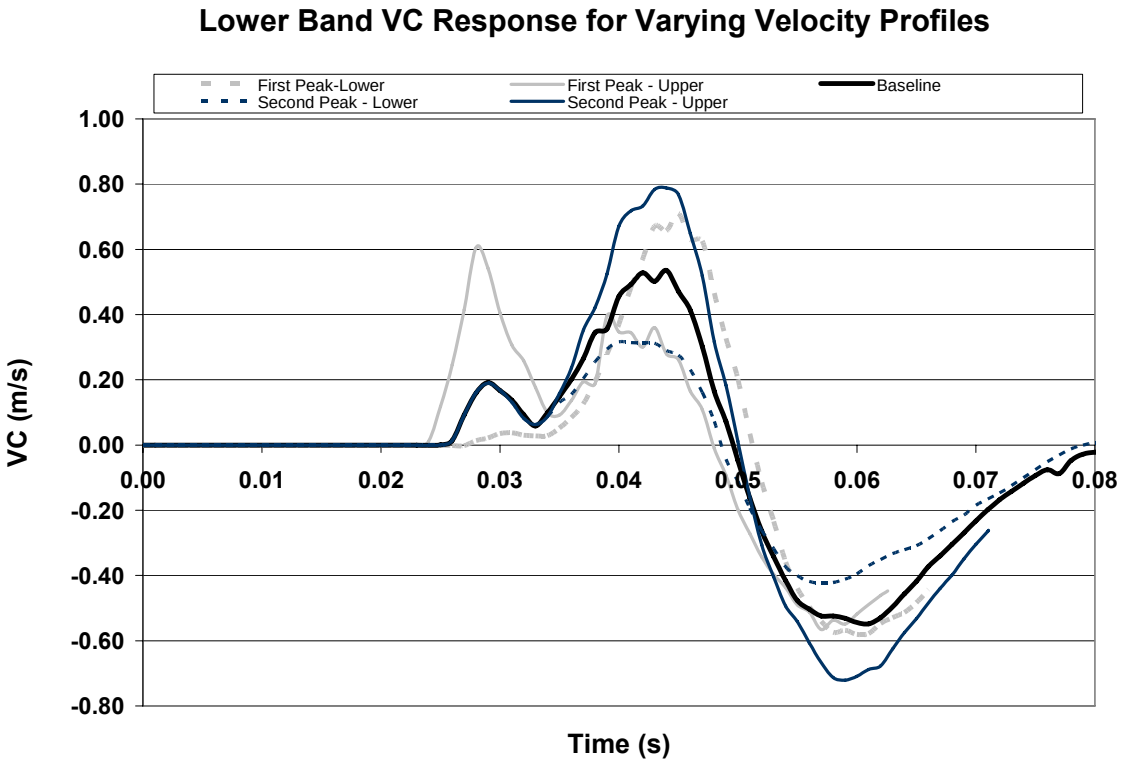

Figure 6.28 Lower Band VC Response for Varying Velocity Profiles

6.6 The Effect of Varying Armrest Height

Based on the previous two studies, it is clear that occupant interaction with the intruding door has a significant impact on thoracic trauma. The following study was used to determine the relevance of armrest position on occupant injury. The variation in armrest position can be seen below for +/- 25mm and 50mm in the vertical direction from the baseline position (Figure 6.29). Figure 6.30 shows the relationship between VCmax and armrest height for each chest band.

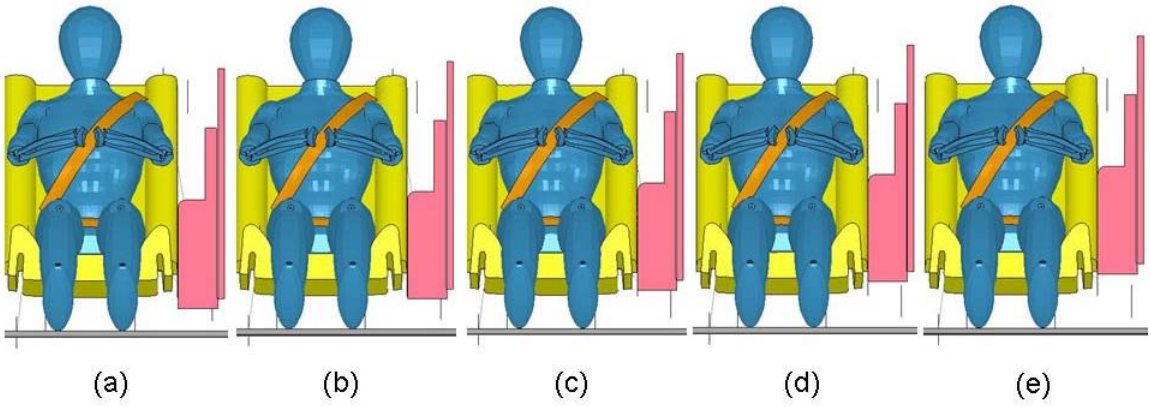

Figure 6.29 Varied Armrest Height (a) Minus 50mm (b) Minus 25mm (c) Baseline (d) Plus 25mm (e) Plus 50mm

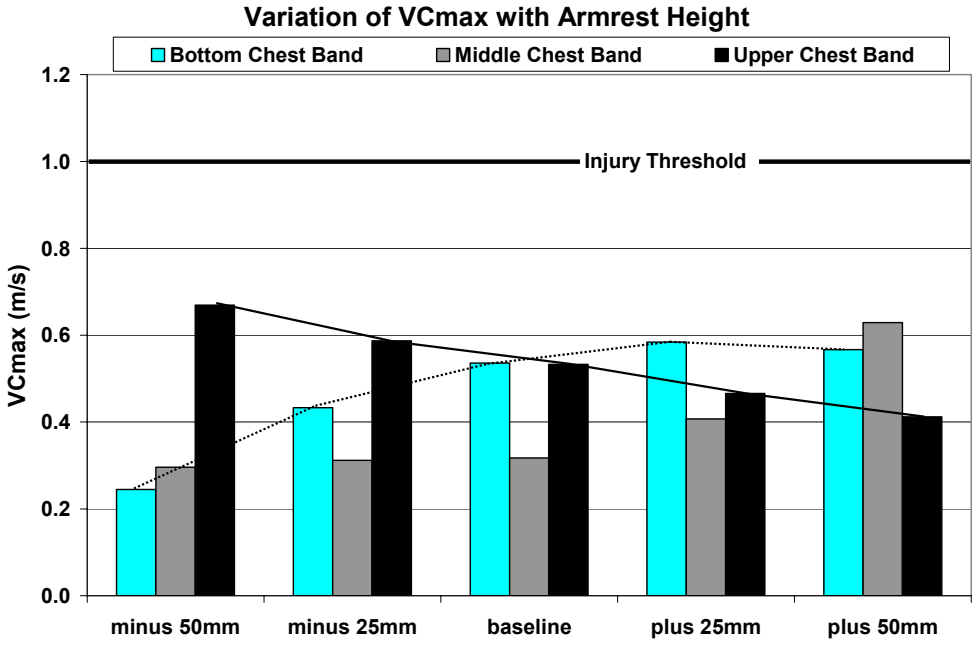

Figure 6.30 Variation of VCmax with Armrest Height

By observing the information presented in the bar chart above, it is clear that the armrest position has considerable influence on injury as it can significantly increase the injury response of one chest band while simultaneously reducing the injury of another.

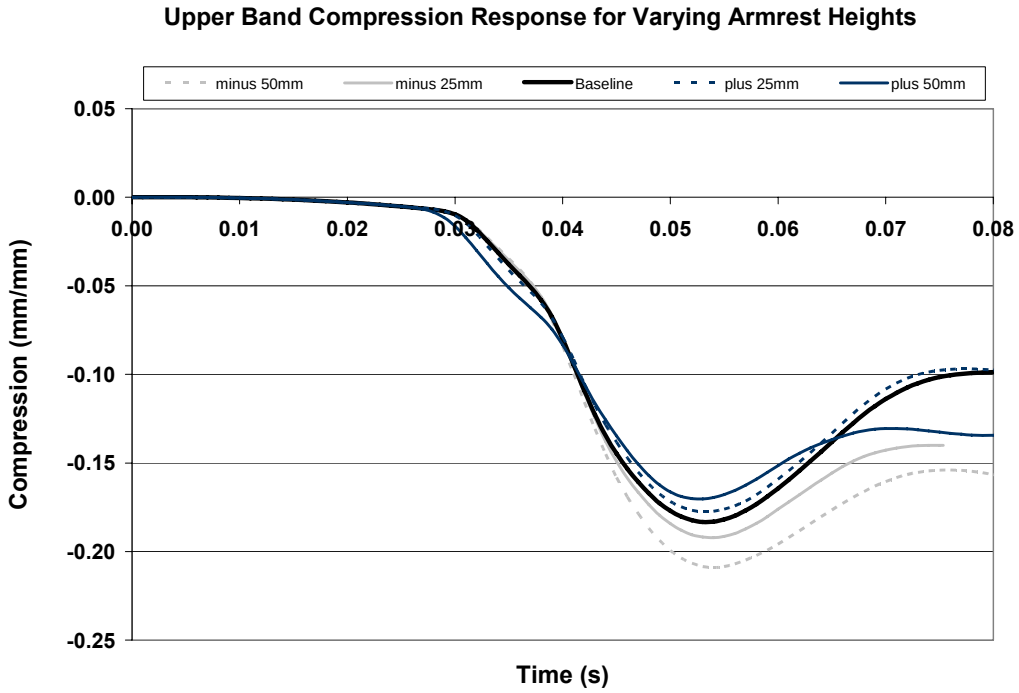

Figure 6.31 Upper Band Compression Response for Varying Armrest Heights

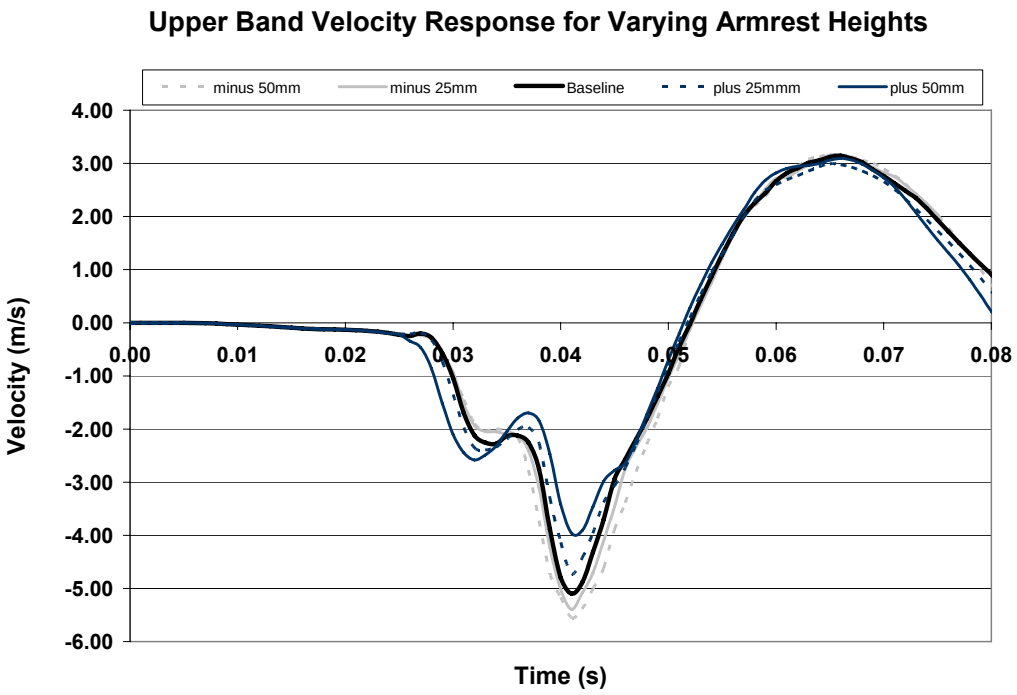

Figure 6.32 Upper Band Velocity Response for Varying Armrest Heights

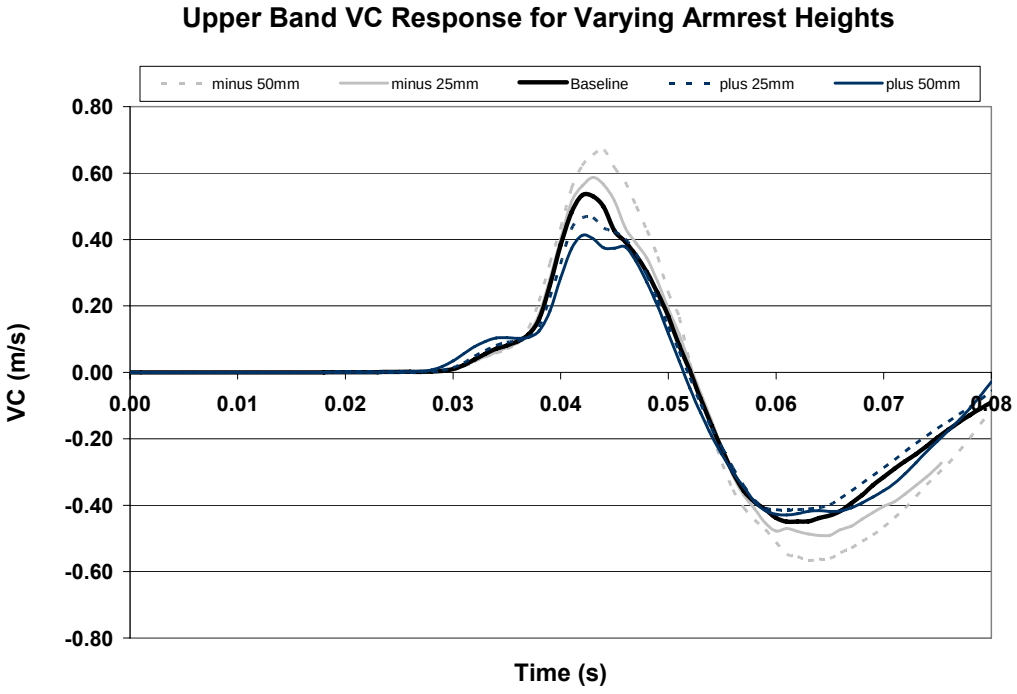

Figure 6.33 Upper Band VC Response for Varying Armrest Heights

The upper band VC response is opposite to the response of the lower and mid bands as the armrest height changes. This difference may be explained by observing the occupant deformation during contact with the armrest for each armrest location (Figure 6.34).

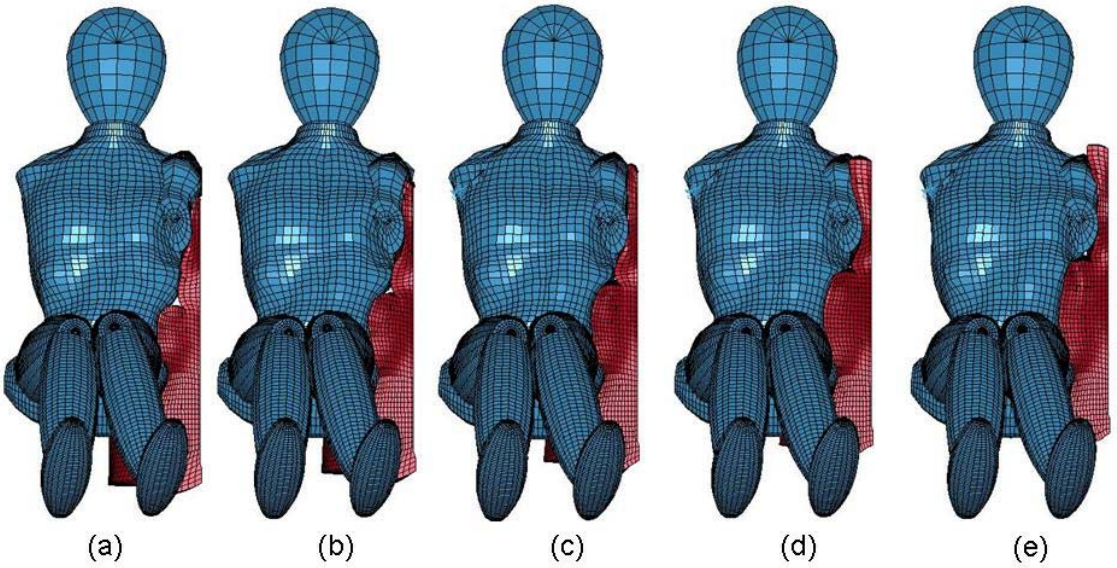

Figure 6.34 Door to Occupant Contact for Varied Armrest Height (a) Minus 50mm (b) Minus 25mm (c) Baseline (d) Plus 25mm (e) Plus 50mm

Interestingly, the injury response at the upper band is reduced as the armrest height is increased. Figure 6.31 shows a decrease in thoracic compression at the level of the upper chest band with the incremental increase in armrest height. This reaction can also be observed by viewing the occupant response shown in Figure 6.34. The reduction of thoracic compression due to contact with the arm can be explained by examining the occupant motion relative to the sled base (Figure 6.35).

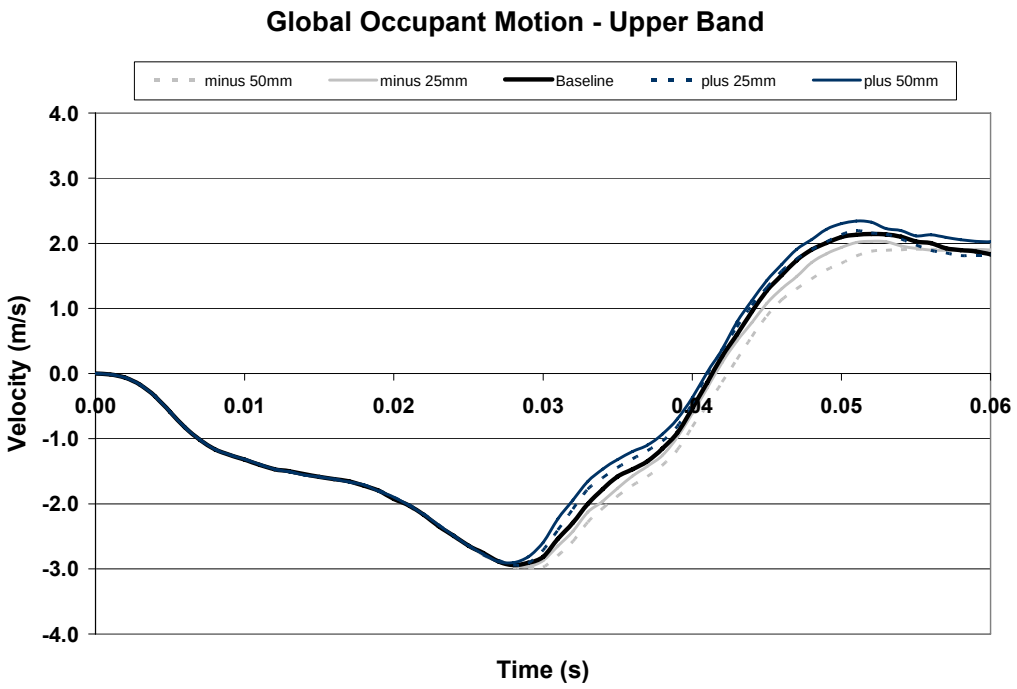

Figure 6.35 Occupant Motion Relative to Sled Base for Varied Door Intrusion Velocity Profile

As the armrest height increases the surface area contacting the occupant also increases and the time of contact occurs earlier due to the location of the armrest with respect to the occupant profile. These two effects cause an increase in occupant velocity relative to the sled with increasing armrest height (Figure 6.35). The increase in occupant velocity relative to the sled minimizes the relative velocity between the occupant and the door, thereby reducing the injury caused as a result of the upper arm contacting the thorax, which is evident in the upper band response.

Although the injury response found at the level of the upper band decreases with an increase in armrest height, the VC at the lower and mid bands increases. The compression, velocity, and VC response for the lower and mid bands is presented in Figure 6.36 and Figure 6.37 below.

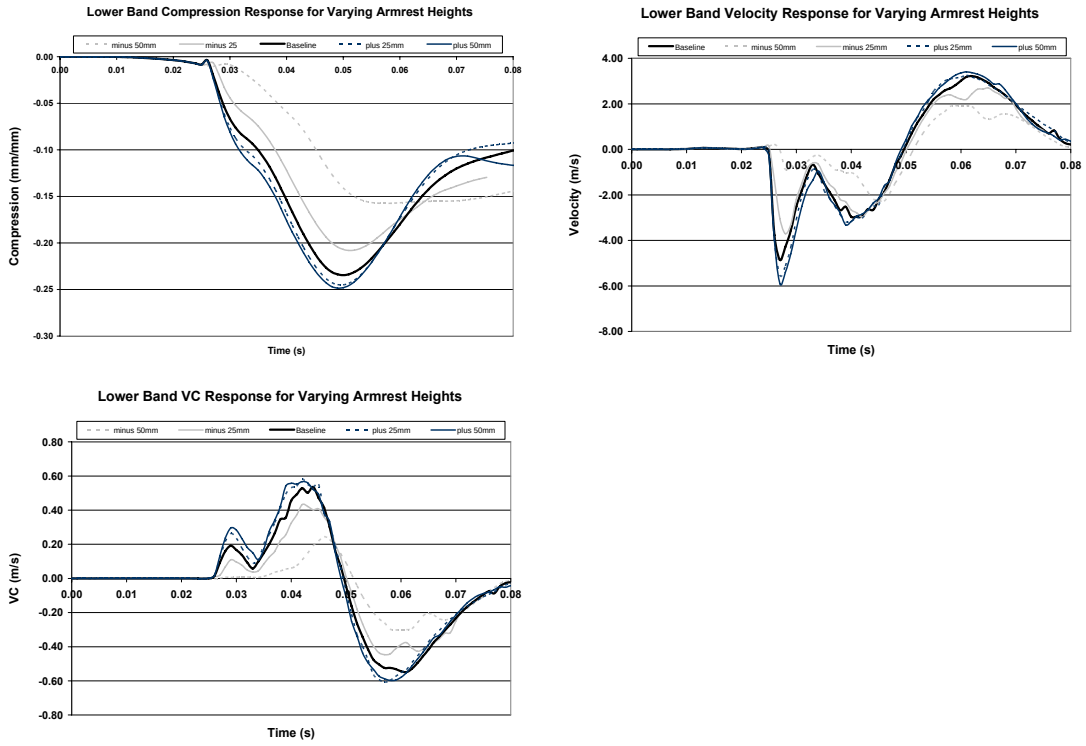

Figure 6.36 Lower Band Response for Varying Armrest Heights

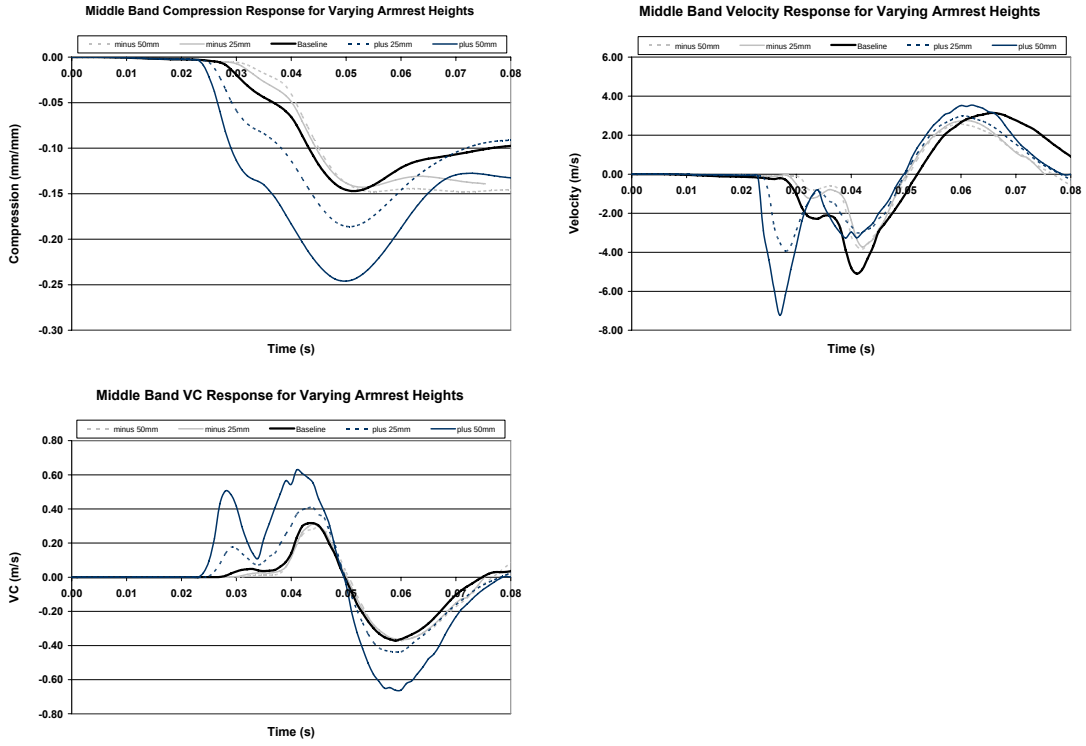

Figure 6.37 Middle Band Response for Varying Armrest Heights

The increase in injury response observed at the low and mid bands is caused by effectively reducing the door to occupant spacing as armrest height is increased. The protrusion of the armrest causes a localized deformation of the thorax and the height has a significant effect on the time of contact due to the geometry of the occupant (Figure 6.38).

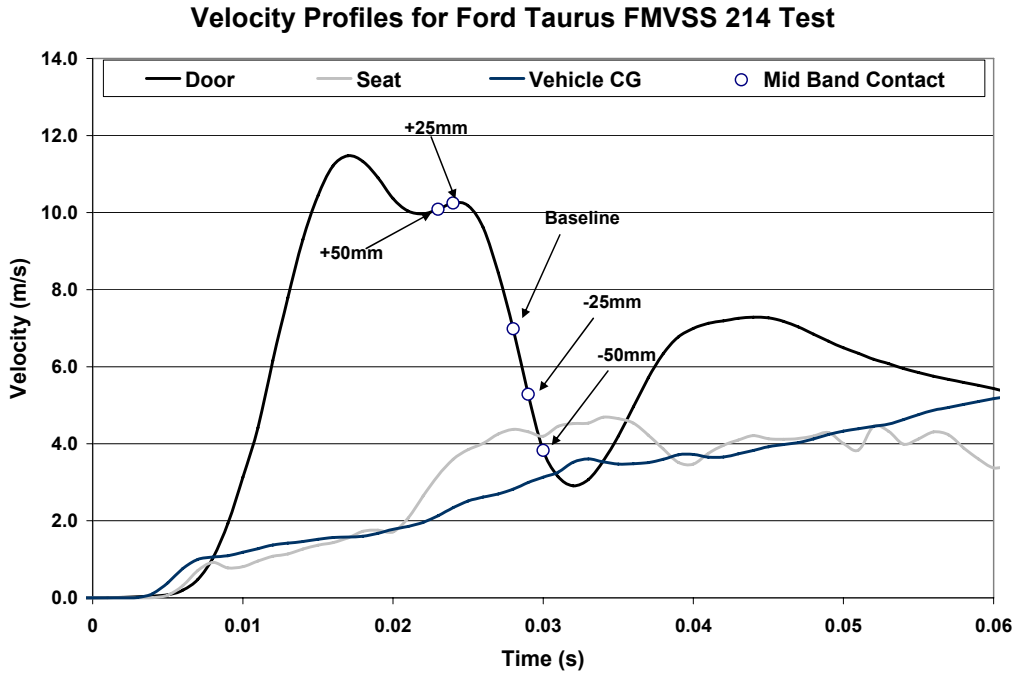

Figure 6.38 Contact Times Between Occupant and Door for Varied Armrest Height

Although armrest position has a significant effect on the thoracic response of each chest band, the baseline case has the lowest VCmax overall for all three chest bands. Figure 6.39 shows that increasing or decreasing the armrest height will cause an increase in VCmax by 9-25% when selecting the highest value of VCmax observed for all three chest bands. Although increasing armrest height was shown to reduce the upper band thoracic response, it simultaneously increased the VC response of the lower and middle chest bands. Therefore, the variation in armrest position has been shown to shift maximum VC response between the three chest bands, but the baseline position produces the lowest VC response.

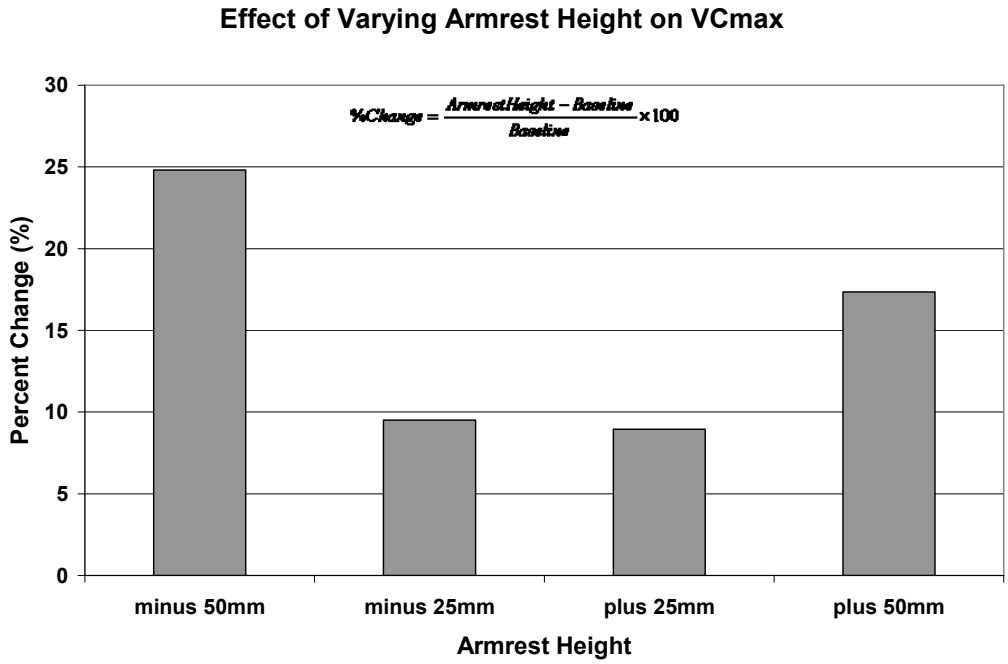

Figure 6.39 The Effect of Varying Armrest Height on VCmax

6.7 The Effect of Varying Seat Foam on Thoracic Trauma

The seat acts as a primary point of interaction between the occupant and the vehicle, although seat foam is predominately used as a means of improving occupant comfort. While the mechanical properties of common seat foams fall in a relatively small range, their impact on occupant injury can be significant despite being largely developed for comfort rather than safety. This study presents the relevance of seat foam in side impact by comparing the occupant response in a seat modeled using Foam 2 and Foam 4 characterized for varying rates of strain in Chapter 4. The results are summarized in the bar chart presented in Figure 6.40.

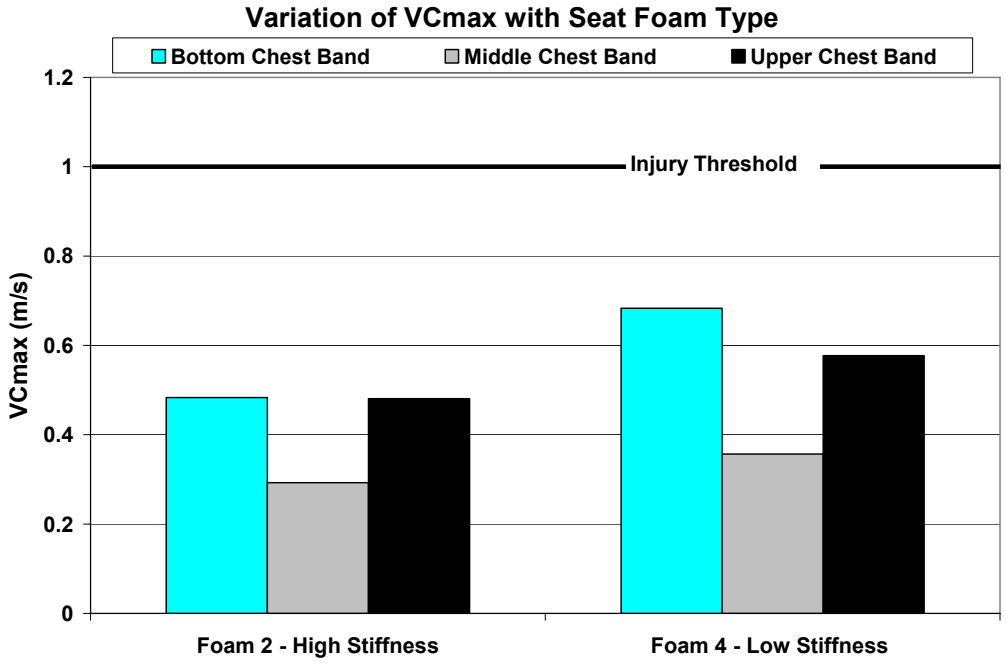

Figure 6.40 Variation of VCmax with Seat Foam Type

Despite modest differences in mechanical properties, seat foam clearly plays a significant role in side impact occupant safety. Figure 6.40 shows that using the low stiffness foam instead of the high stiffness foam causes a 41% increase in the predicted VCmax value.

The compression, velocity, and VC responses for Foam 2 and Foam 4 are compared in Figure 6.41, Figure 6.42, and Figure 6.43 below.

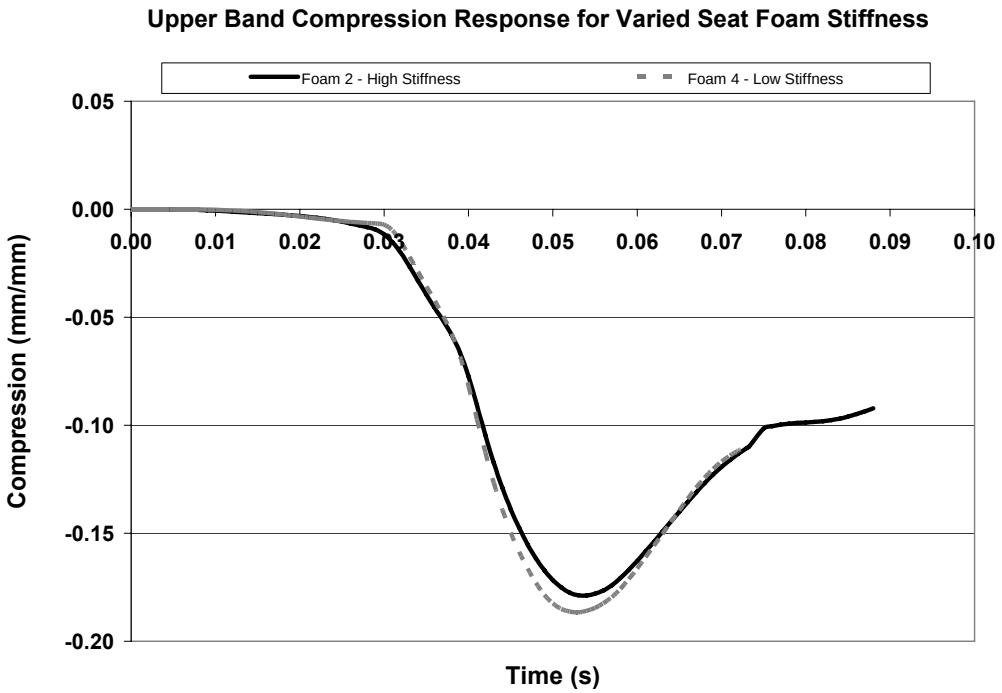

Figure 6.41 Upper Band Compression Response for Varied Seat Foam Stiffness

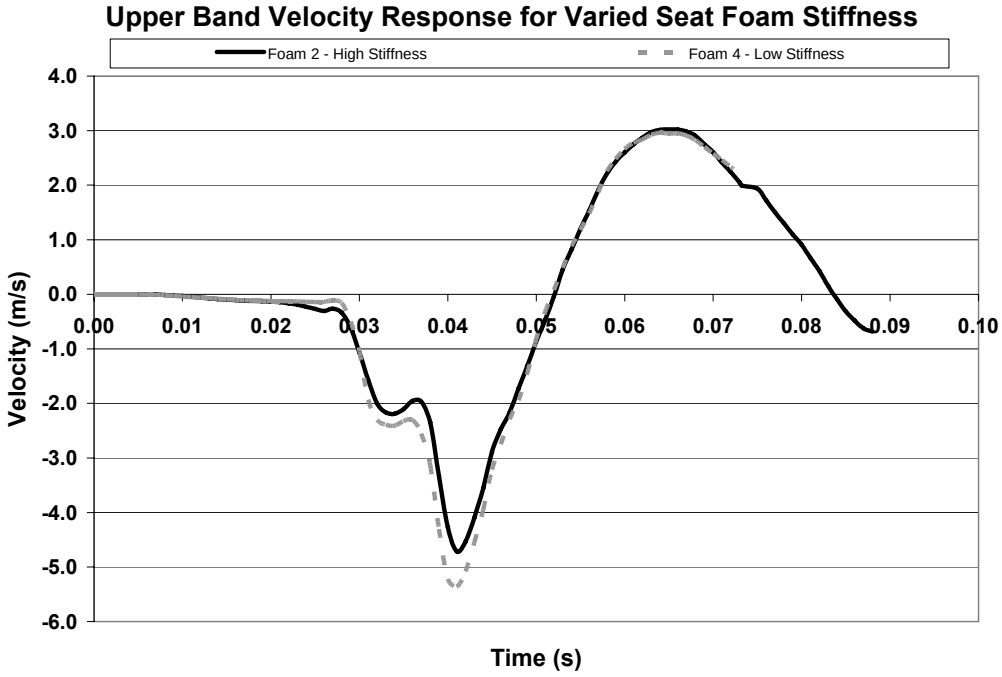

Figure 6.42 Upper Band Velocity Response for Varied Seat Foam Stiffness

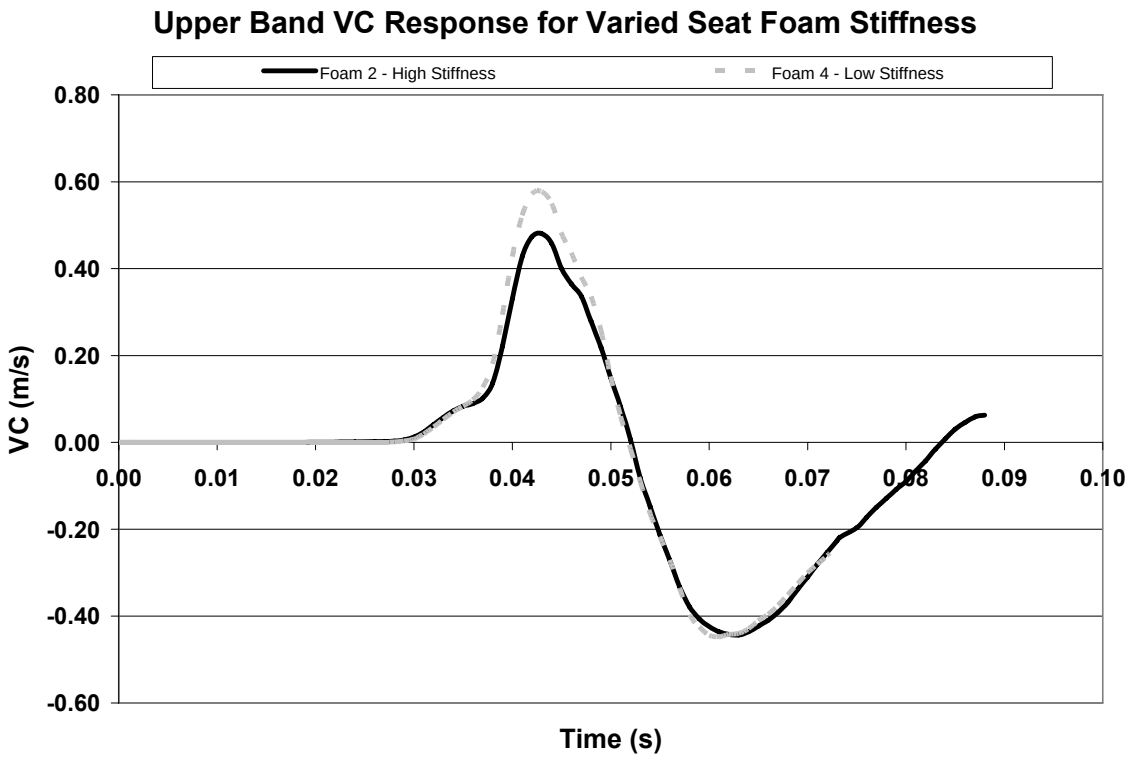

Figure 6.43 Upper Band VC Response for Varied Seat Foam Stiffness

The three bands shown are comparable in terms of their shape and timing, however the peak response observed when using Foam 4 is elevated for the compression, velocity, and VC. This variation in response may be explained by comparing the occupant motion relative to the sled base for each seat foam (Figure 6.44).

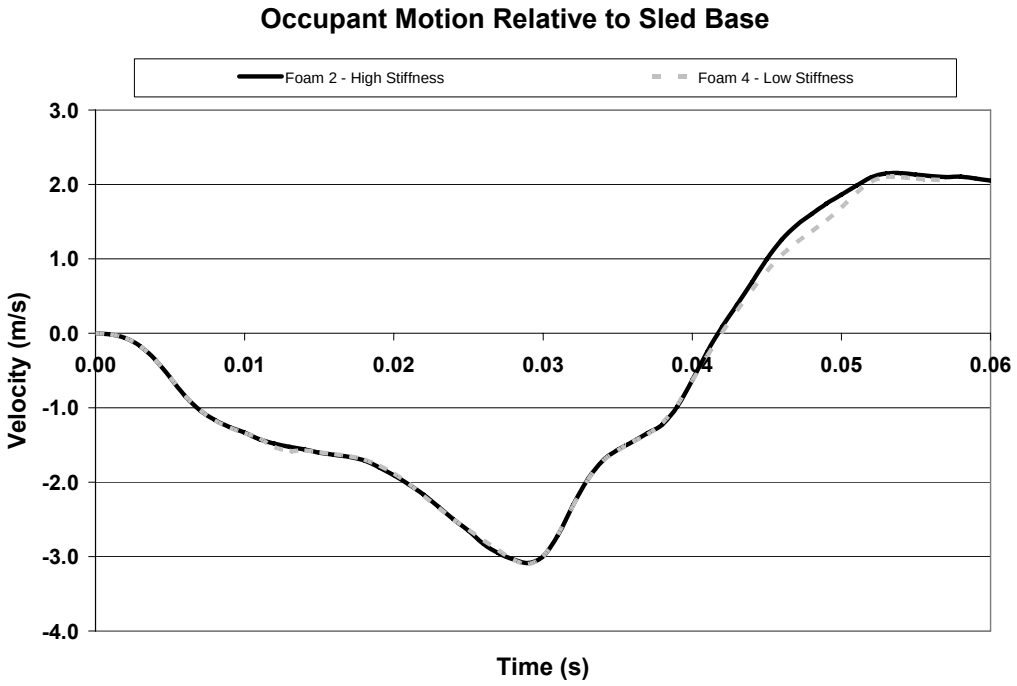

Figure 6.44 Occupant Motion Relative to Sled Base for Varied Foam Stiffness

It can be seen that seat foam has minimal effect on occupant motion relative to the sled base, however the minor differences observed translate to considerable differences in viscous response. The variation in occupant velocity relative to the sled base is the result of differences in foam stiffness. A stiffer foam, such as Foam 2 in this case, is more capable of applying a load to the occupant, thus increasing the occupants velocity and reducing the effect of the intruding door.

Although the differences between the seat foams compared in this study are relatively small the effect on thoracic response is noteworthy. Stiffer seat foams and more encompassing side bolsters may have the potential to significantly reduce injury.

6.8 The Effect of Arm Position on Thoracic Trauma

The literature has provided many studies regarding thoracic trauma under various loading conditions, however few of them have investigated the effect of arm position on thoracic injury in side impact scenarios. This study investigates the effect of the arms positioned at 45 degrees and parallel to the thorax for the conditions described for the baseline case. The arms positioned at 45 degrees are in accordance with the ES-2 arm positioning procedure as recommended in FMVSS tests. It should be noted that the arms positioned in the 'down' position are not typical of a drivers arm position, but represent the extreme case of arm position. The arm positions used in this study can be seen in Figure 6.45.

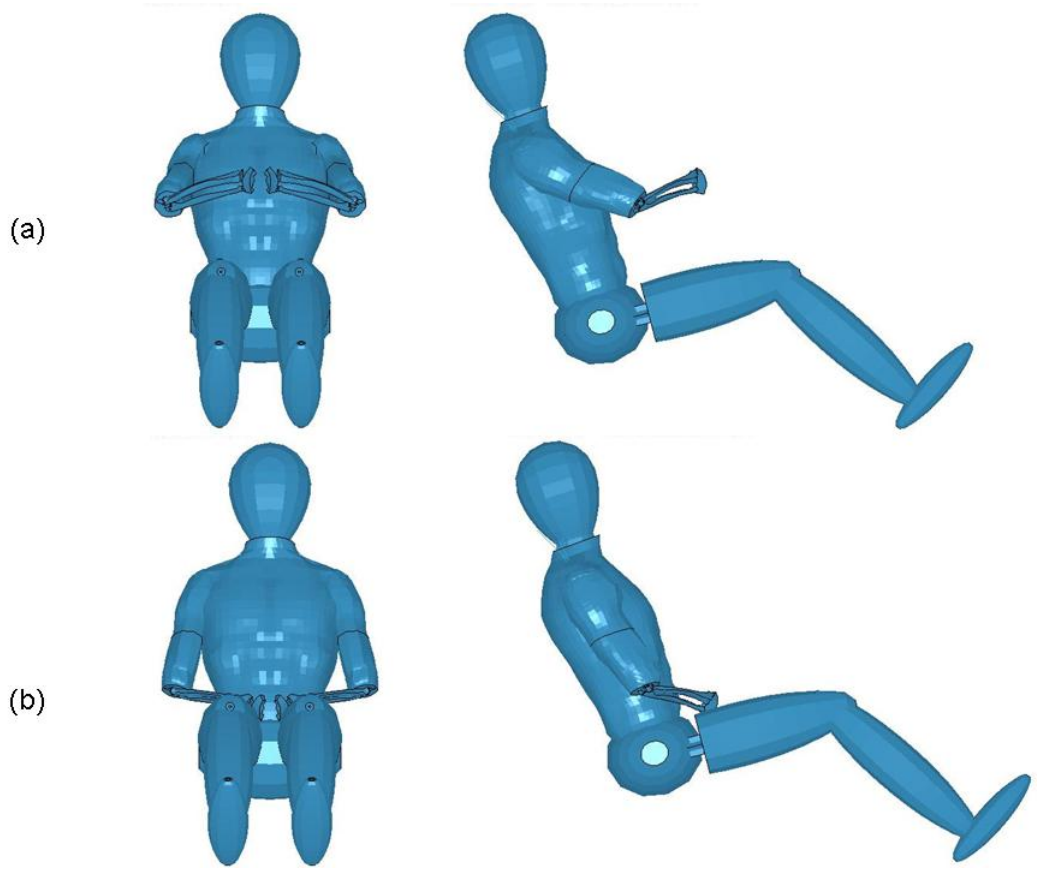

Figure 6.45 Arm Position (a) Baseline (b) Arms Down

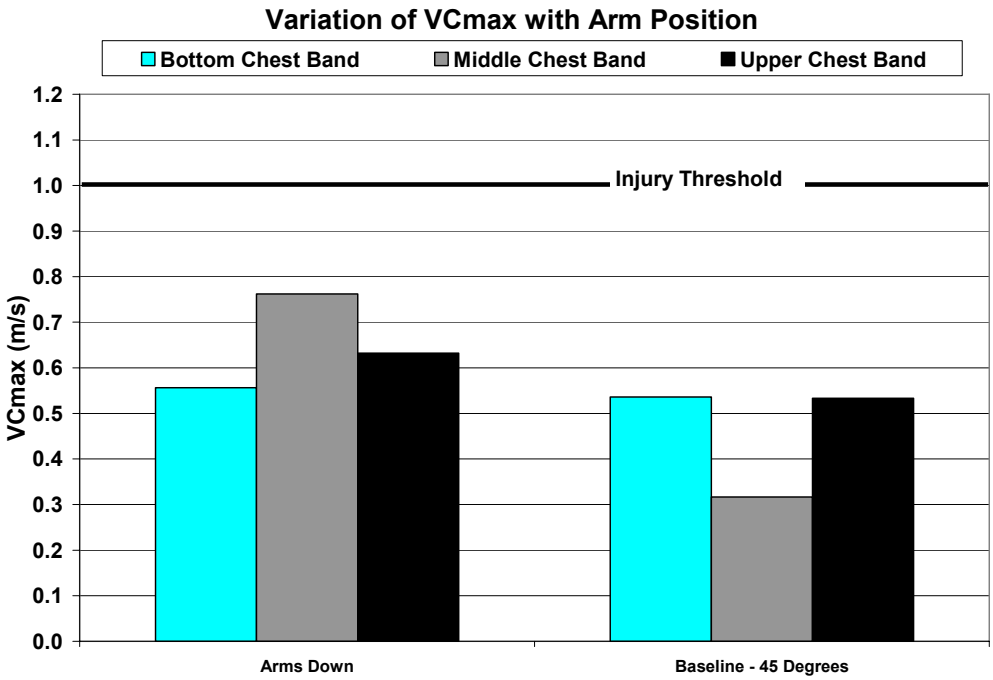

Figure 6.46 Variation of VCmax with Arm Position

Figure 6.46 shows that positioning the arms parallel to the thorax cause a 42% increase in the observed VCmax value compared to the baseline position with arms positioned at 45 degrees. The thoracic compression, velocity, and VC responses for each arm position are presented in Figure 6.47, Figure 6.48, and Figure 6.49.

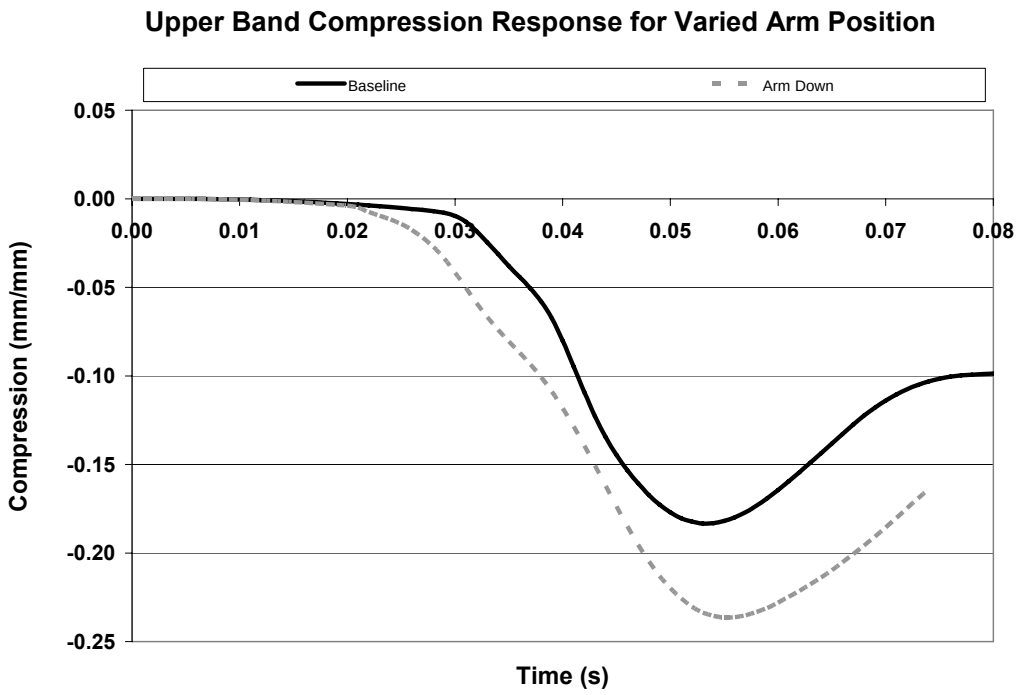

Figure 6.47 Upper Band Compression Response for Varied Arm Position

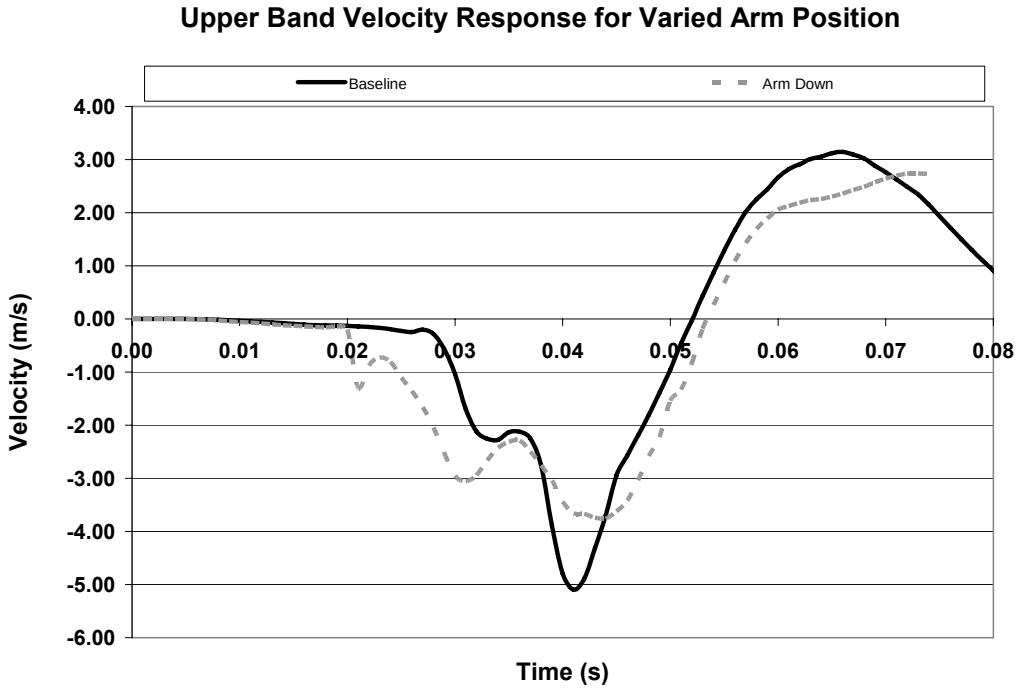

Figure 6.48 Upper Band Velocity Response for Varied Arm Position

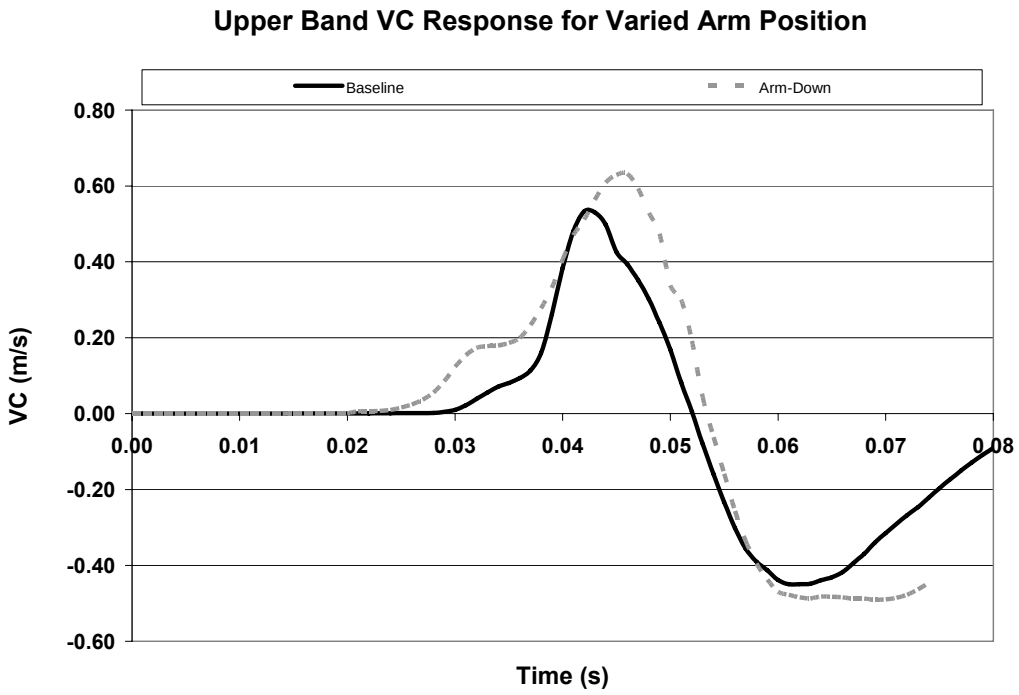

Figure 6.49 Upper Band VC Response for Varied Arm Position

Rotating the occupant arm position down effectively reduces the spacing between the occupant and the intruding door causing significantly earlier onset of thoracic compression (Figure 6.47, Figure 6.50). Also, because the arms are aligned with the thorax, they tend to intrude directly into the thorax for the duration of the collision, where as the arms placed in the "up" position are more likely to slide in front of the chest thereby minimizing chest compression. This effect can be observed in Figure 6.51.

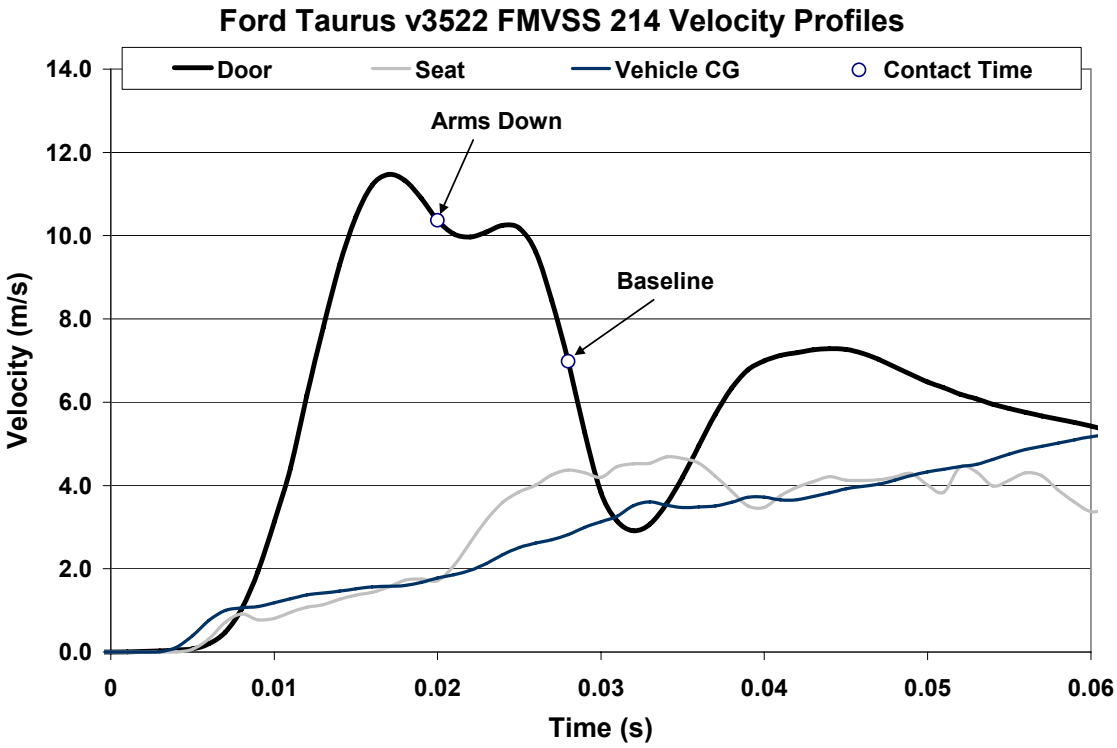

Figure 6.50 Contact Timing for Varied Arm Position

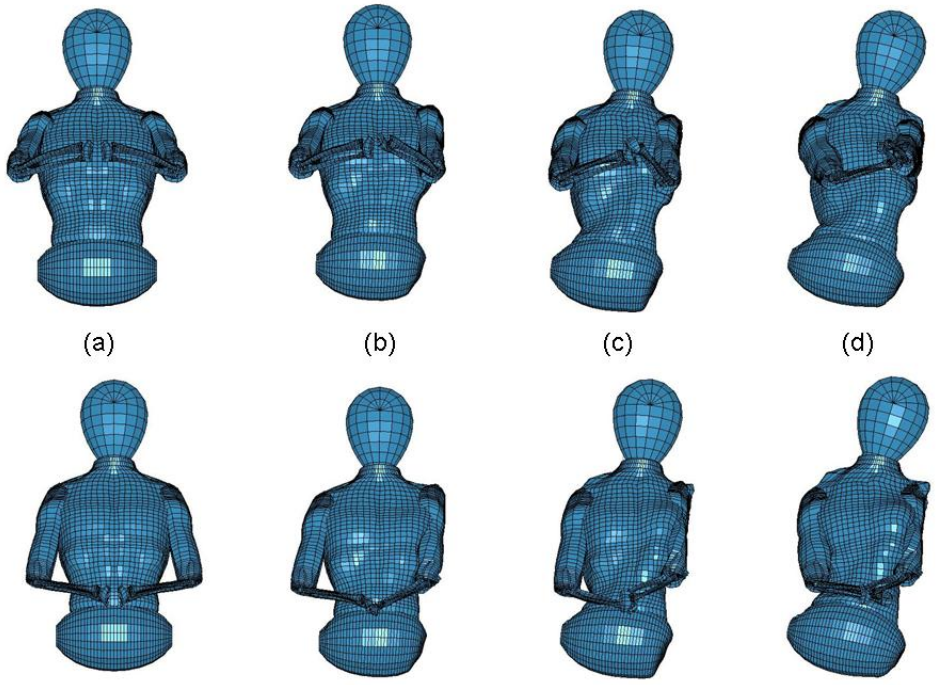

Figure 6.51 Arm Position (a) 0 s (b) 0.030 s (c) 0.045 s (d) 0.060 s

Although the door to occupant distance is significantly reduced as a result of the "Arms Down" position, the physical response is quite different in terms of the location of trauma (Figure 6.46). In the case of small AD distances the armrest is much closer to the occupant and inflicts the greatest amount of trauma. However, for the "Arms Down" position, the arm is pressed into the thorax by the intruding door causing a localized increase in VC response.

6.9 The Effect of Restraint Systems on Thoracic Trauma

The effect of restraints on the reduction of occupant trauma in frontal collisions is well-known. However, the effect of restraints in side impact is not as clear. According to a study performed by NHTSA (NHTSA, 2000; NHTSA, 2007), the reduction of fatalities in near-side impacts as a result of restraint systems is a mere 5 percent. In comparison, the fatality reduction as a result of seat belt usage was 39 percent in farside impacts, 50 percent in frontals, and 74 percent in rollovers.

However, because of inconsistencies in crash scenarios it is difficult to quantify the effect of restraints in side impact. The study performed in this section compares the thoracic trauma of a belted and un-belted occupant under identical crash conditions to determine the effect of restraints. A summary of the results is presented in the bar chart in Figure 6.52.

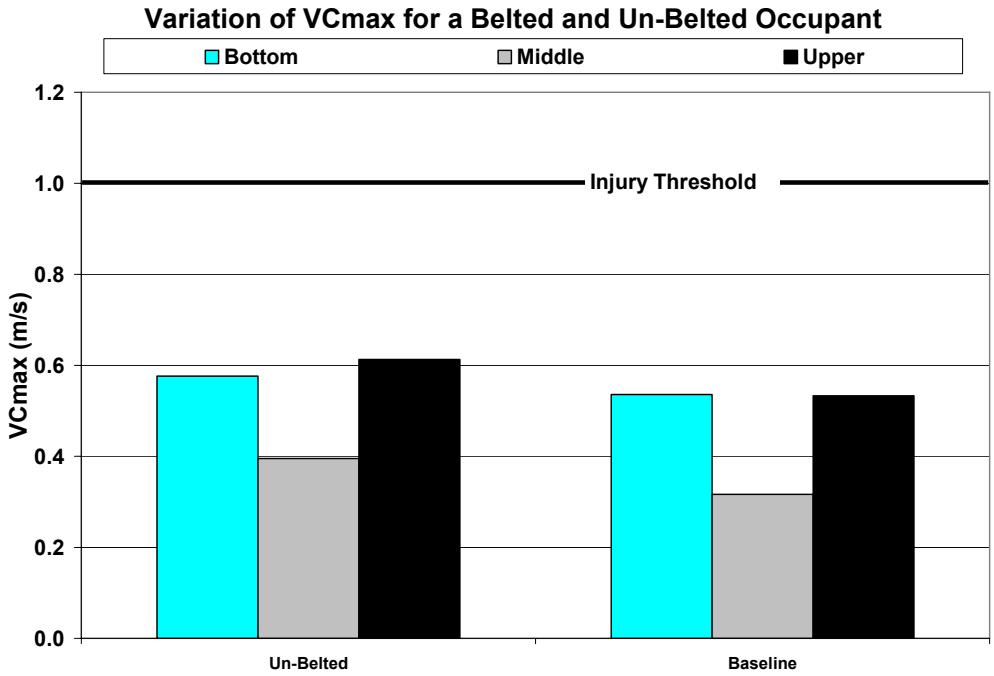

Figure 6.52 Variation of VCmax for a Belted and Un-Belted Occupant

The small spacing between the occupant and the intruding door makes energy dissipation difficult and contact inevitable. However, it is clear that the presence of restraints reduces the thoracic trauma at each chest band level and can reduce VCmax by up to13% compared to an un-belted occupant. The thoracic compression, velocity, and VC response is presented in Figure 6.53, Figure 6.54, and Figure 6.55.

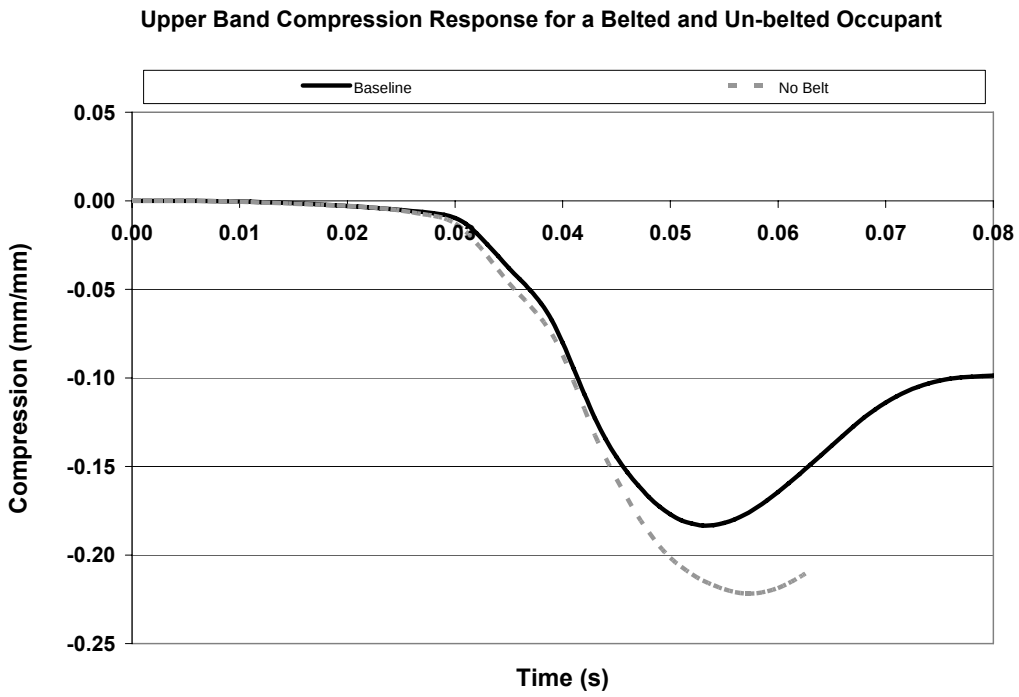

Figure 6.53 Upper Band Compression Response for a Belted and Un-Belted Occupant

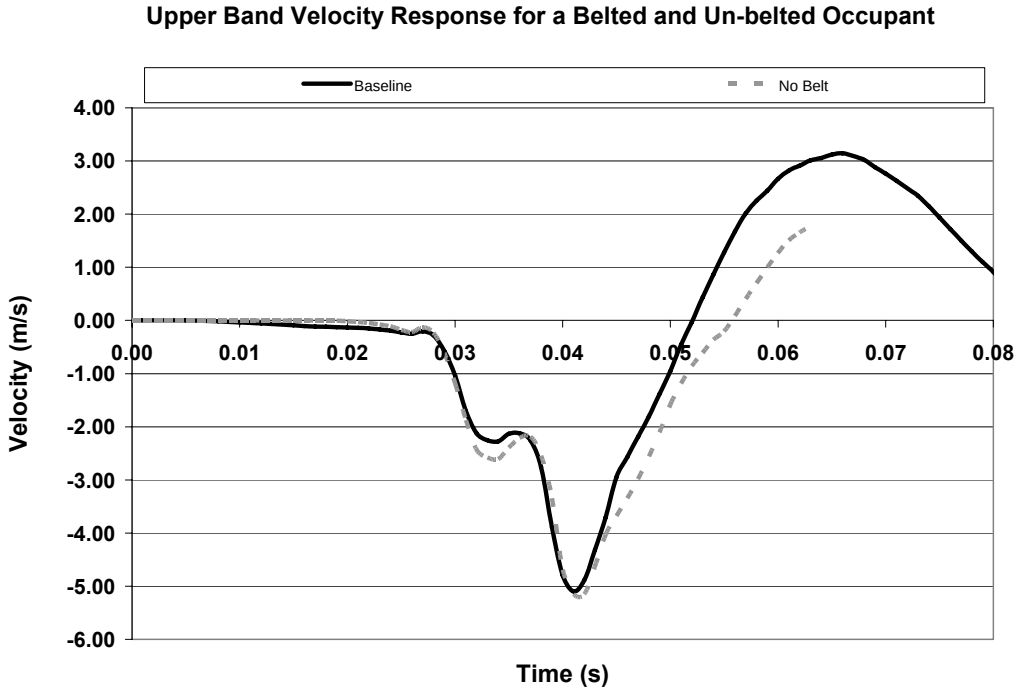

Figure 6.54 Upper Band Velocity Response for a Belted and Un-Belted Occupant

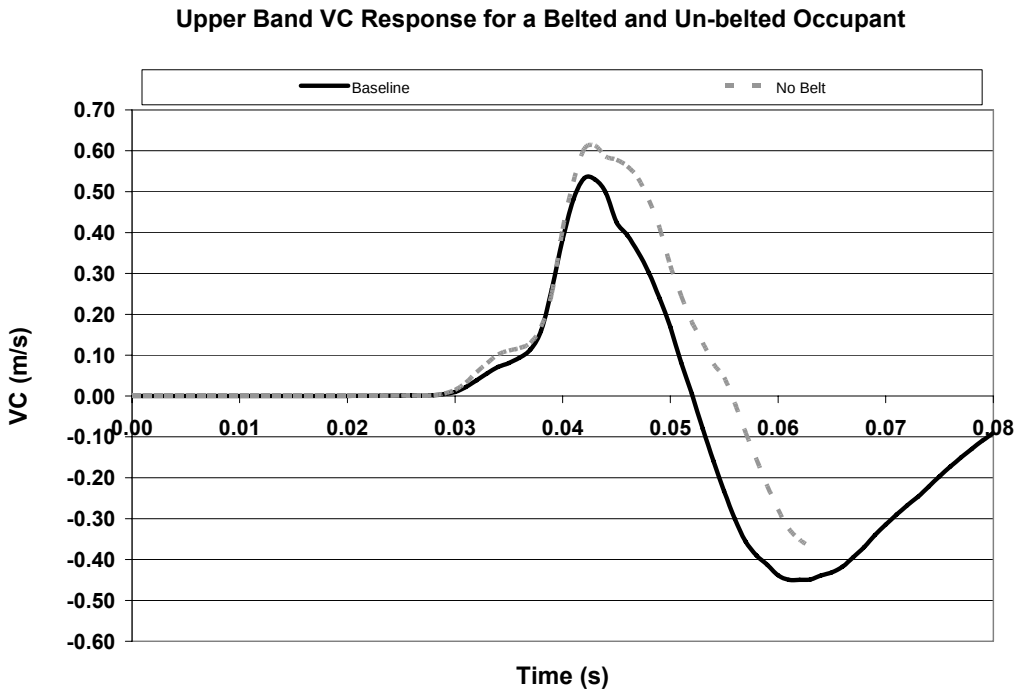

Figure 6.55 Upper Band VC Response for a Belted and Un-Belted Occupant

The compression, velocity, and VC response for the un-belted occupant is slightly elevated in comparison to the belted occupant. The modest difference in thoracic trauma may be explained by investigating the occupant motion relative to the sled base (Figure 6.56).

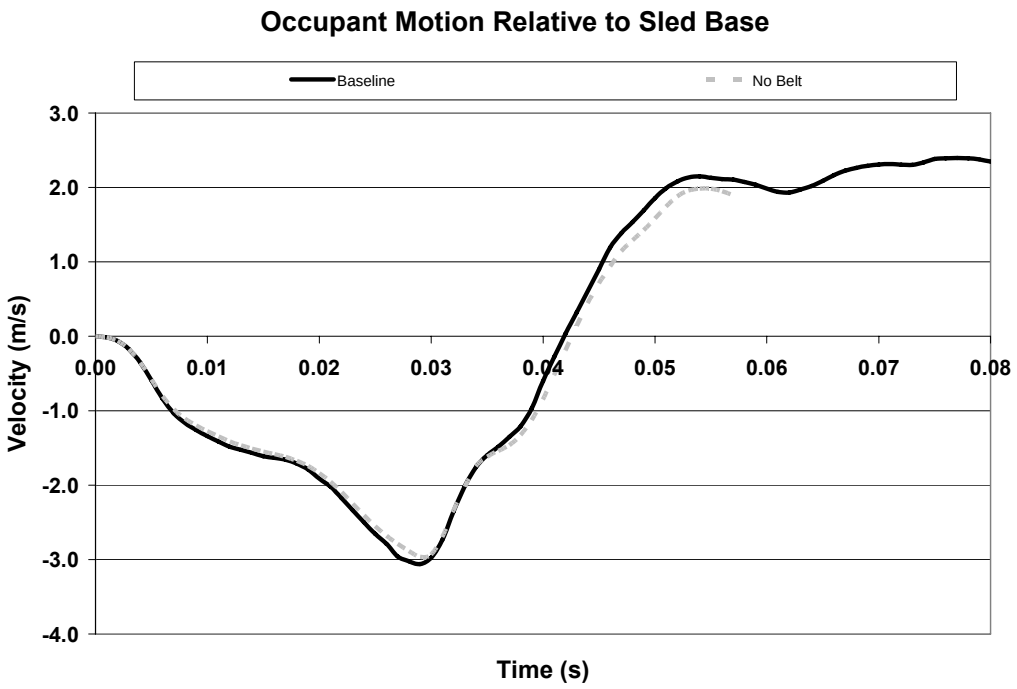

Figure 6.56 Occupant Motion Relative to Sled Base for a Belted and Un-Belted Occupant

The presence of a seatbelt appears to accelerate the occupant slightly more than in the case of the un-belted occupant, thereby reducing the impact of the intruding door. It is likely that the increase in occupant velocity relative to the sled base is due to an increased interaction with the seat, facilitated by the restraint system. Although, the presence of the a restraint system reduced thoracic injury in this case, it will undoubtedly reduce the risk of further injuries incurred in a collision by restraining the occupant in their seat and minimizing occupant motion in the occupant compartment.

6.10 Parametric Study Summary Discussion

The parametric study presented above provides some insight and understanding into the mechanisms governing thoracic trauma in side impact collisions. It is clear that occupant protection in side impact scenarios is a difficult task. The small door to occupant spacing associated with typical vehicles provides minimal stand-off for the occupant and makes it challenging for engineers to include safety features.

Based on the information gathered from the studies performed on AD distance, armrest height, and intrusion velocity, side impact safety is extremely dependant on small changes in several factors. This chapter provides evidence that side impact safety is truly a function of millimeters and milliseconds. These minor measures can result in significant safety improvements or detriments depending on the situation. Some of these measures are extremely difficult to control, such as the door to occupant distance, because of variation in occupant size and out of position scenarios. However, it is clear that there are ways of improving occupant safety.

Thoracic response can be reduced by altering the structural properties of the vehicle to minimize door intrusion or in order to idealize the door intrusion velocity profile. The study comparing the effect of an intruding rigid door to a stationary rigid door showed that thoracic response can be significantly reduced (73-88%) by eliminating door intrusion. Also, the presence of an armrest instead of a rigid door can reduce VCmax by up to 16% as shown in Figure 6.16. However, it was found that adjusting the height of the armrest simply tends to shift the maximum thoracic response between the three chest bands. Although increasing armrest height was shown to reduce the upper band thoracic response, it simultaneously increased the VC response of the lower and middle chest bands.

Developing seats better suited for crash safety by increasing the stiffness of the foam and improving the side bolsters is one area that may contribute to better safety. The seat foam study showed that using the low stiffness foam instead of the high stiffness foam can cause a 41% increase in the observed VCmax value. Although this study investigates seat foams in a relatively limited range of material characteristics, seat foam has been shown to be an extremely relevant parameter in influencing thoracic response.

The occupant arm position has been shown to have a large effect on thoracic response. Positioning the arms in the "down" position, parallel to the thorax, resulted in a 42% increase in VCmax when compared to the arms positioned at 45 degrees. Although it is a difficult parameter to control, it is an area that may significantly improve occupant safety if approached.

This study has shown that pre-tensioning restraint systems can reduce VC by improving the contact between the occupant and the seat. The improved occupant to seat contact minimizes the impact of the intruding door by accelerating the occupant with the seat, thereby reducing the relative velocity between the occupant and intruding door causing a 13% decrease in VCmax in this study.

-- CHAPTER 7 --

Conclusions and Recommendations

7.1 Conclusions

This study was performed to provide an understanding of the mechanisms governing thoracic trauma in side impact auto crash. Thoracic trauma ranks as the primary cause of fatalities and serious injuries in lateral collisions, thus warranting research regarding the mechanisms of side impact injury. Although progress has been made in side impact safety, lateral impact fatalities still comprise a large percent of total fatalities. A detailed understanding of thoracic injury mechanisms is required in order to provide feasible solutions to the problem of thoracic trauma in lateral impacts, thus justifying this study.

The study presented in this thesis builds upon an advanced numerical human body model with focus on a detailed thorax previously developed by Forbes (2005). The numerical human body model was previously validated using available PMHS test data for pendulum and side sled impact tests (Forbes, 2005).

A numerical side impact model was then developed to investigate factors and crash conditions present in full scale crash tests. The model was developed to account for several important factors that contribute to occupant response including the relative velocities between the seat and door, the occupant to door distance, as well as door shape and compliance.

The seat geometry was based on a GM Malibu and foam characterization was determined through a series of compressive tests for varying rates of strain. Foam material was modeled using Fu Chang's material model for low density foams as recommended in the literature. Initial stresses present in the foam due to deformations caused by the occupant were accounted for by pre-sinking the occupant into the seat prior to initiation of the side impact simulation.

The door and armrest model was simplified in terms of geometry, but is representative of automotive door compliance. Door geometry was based on a cross section of a Ford Taurus model door sectioned through the area possessing the greatest armrest depth in order to produce a conservative door model. The simplified door geometry required the door to be characterized as one solid material. Material properties required to produce the door response observed in the literature was determined by a series of simple simulations reproducing the experiments used to evaluate door compliance.

Validation of the side sled model was done by reproducing the crash conditions present in FMVSS 214 and IIHS side impact tests and comparing the thoracic response determined by the model to the response of the ES-2 dummy used in the crash tests. The side impact model was shown to produce '*good*' to '*reasonable*' injury response with respect to the full-scale FMVSS 214 side impact test of a Ford Taurus, as well as the IIHS side impact test of a Nissan Maxima.

The side impact model was then used to investigate the effects of door to occupant spacing, door velocity profile, armrest height, seat foam, restraint system, and arm position. It was found that the Viscous Criterion was controlled by both the first and

second peaks typically found in door velocity profiles, but the influence of each varies depending on the situation.

The parametric study presented in this thesis has provided valuable insight into the factors influencing thoracic trauma in side impact collisions. Clearly, occupant protection in side impact scenarios is a difficult task due to the limited door to occupant spacing associated with lateral collisions. The study performed has shown that thoracic injury is largely dependant on relatively small changes in a number of factors such as AD distance, armrest height, and door intrusion velocity. The information presented proves that side impact safety is truly a function of millimeters and milliseconds and that minor variance in the factors discussed can result in significant safety improvements or detriments depending on the situation.

The side impact model has been validated and proven to be a useful tool for determining the influential factors on thoracic trauma. Although some of factors discussed are difficult to control due to differences in occupant size and collision specific characteristics, there are areas for improvement.

The structural properties of the vehicle can be altered to minimize door intrusion or in order to idealize the door intrusion velocity profile. The parametric study performed has shown that if door intrusion is entirely eliminated the thoracic response can be reduced by 73-88%. Also, the presence of an armrest instead of a rigid door can reduce VCmax by up to16%, showing that door geometry and compliance plays a roll in safety. However, it was found the height of the armrest simply tends to shift the maximum thoracic response between the three chest bands as shown in Figure 6.30.

The seat foam study performed has shown that using the low stiffness foam instead of the high stiffness foam can cause a 41% increase in the observed VCmax value. This is based on the investigation of seat foams falling in a relatively limited range of material properties. Clearly, seat foam plays an important role in crash safety and improving side bolsters and increasing foam stiffness may contribute to better side impact safety.

Although it is a difficult parameter to control, the occupant arm position has been shown to significantly influence thoracic response, and is an area worth investigating. The parametric study performed has shown that positioning the arms in the "down" position, parallel to the thorax, resulted in a 42% increase in VCmax when compared to the arms positioned at 45 degrees.

Although the effect of pre-tensioning restraint systems are limited in side impact crash, this study has shown that they reduce VC by improving the contact between the occupant and the seat. The improved occupant to seat contact minimizes the impact of the intruding door by accelerating the occupant with the seat, thereby reducing the relative velocity between the occupant and intruding door. Thus causing a 13% decrease in VCmax in this study.

The current study is limited to velocity profiles obtained from a specific FMVSS 214 test and therefore results and observations are restricted to the confines of the input conditions used. Also, although based on vehicle geometries, the side impact model has been developed using simplified geometries for the seat, armrest, and restraints and may not fully encompass all vehicle designs. However, the side impact model developed is a useful tool for evaluating factors influencing side impact and can be used to determine occupant response in any side impact crash scenario when the appropriate input conditions are provided.

7.2 Recommendations and Current Progress

Following the development of the numerical human body model, Forbes (2005) identified several key areas for improvement, including; the high level of chest compression found in side impact response, geometric differences between the abdomen and pelvis, and inaccurate frontal impact response. Current research is in progress to resolve these issues as well as efforts to further the thoracic models ability to capture localized injuries, specifically pulmonary contusion. Since the conclusion of this study, the thorax model has been improved by implementing new lung and diaphragm FE models. The heart has also been repositioned to be more anatomically correct. These refinements have furthered the biofidelity and overall robustness of the thoracic model.

The author has noted a few key areas requiring improvement or further study. First, differences in geometry and thoracic compliance exist between the human body model and the ES-2, therefore contributing to some error in validating the side sled model. Although, the side sled model was validated by the comparison of the human body models thoracic response to ES-2 thoracic response found in FMVSS 214/IIHS tests, more accurate and conclusive validation may be performed by implementing a numerical ES-2 model in the future.

Second, the current study did not include the use of side airbags in the scope of this research although they are a common form of side impact safety device. The effect of side airbags on occupant injury is likely highly dependant on the injury criteria used. However, differing injury criteria exist for thoracic trauma and much of the investigation regarding the influence of side airbags has been performed with SID dummies using acceleration based criteria. Side airbags may have an adverse effect on the viscous response of the occupant by prolonging contact with the intruding door, effectively reducing the door to occupant distance, or contacting the occupant at a different point in the velocity profile of the intruding door. Including side airbags in the side sled model would provide interesting insight into their impact on occupant safety and may offer potential methods for improving air bag use to further side impact safety.

References

Abbreviated Injury Scale (AIS), 1990 Revision, American Association for Automotive Medicine, Morton Grove, Illinois

Abbreviated Injury Scale (AIS), 2005 Revision, American Association for Automotive Medicine, Barrington, Illinois

Aekbote K., Sundararajan S., Chou C.C., Lim G.G., Prater J.A.., 1999, A New Component Test Methodology Concept for Side Impact Simulation, SAE 1999-01-0427

Aekbote K., Sobick J., Zhao L., Abamcyk J.E., Maltarich M., Stiyer M., Bailey T., 2007, A Dynamic Sled-to-Sled Test Methodology for Simulating Dummy Responses in Side Impact, SAE 2007-01-0710

Andriacchi, T., Schultz, A., Belytschko, T., Galante, J., 1974, A Model for Studies of Mechanical Interaction Between the Human Spine and Ribcage, Journal of Biomechanics, Vol. 7, pp. 497-507

Blincoe, L., Seay, A., Zaloshnja, E., Miller, T., Romano, E., Luchter, S., Spicer, R., 2000, The Economic Impact of Motor Vehicle Crashes, 2000, U.S. Department of Transportation National Highway Traffic Safety Administration, DOT HS 809 446

Campbell, B.M., Cronin, D.S., Salisbury, C.P, 2007, High Rate Characterization of Automotive Seat Foams, Society of Experimental Mechanics Conference, Springfield, MA

Cavanaugh, J.M., Walilko, T.J., Malhotra, A., Zhu, Y., King, A.I., 1990, Biomechanical Response and Injury Tolerance of the Pelvis in Twelve Sled Side Impacts, Proceedings of the 34th Stapp Car Crash Conference, 902305

Cavanaugh, J.M., Walilko, T.J., Malhotra, A., Zhu, Y., King, A.I., 1990, Biomechanical Response and Injury Tolerance of the Thorax in Twelve Sled Side Impacts, Proceedings of the 34th Stapp Car Crash Conference, 902307

Cavanaugh, J.M., Zhu, Y., Huang, Y., King, A.I., 1993, Injury and Response of the Thorax in Side Impact Cadaveric Tests, Proceedings of the 37th Stapp Car Crash Conference, 933127 175

Cavanaugh, J.M., Walilko, T., Walbridge, A., Huang, Y., King, A.I., 1994, An Evaluation of TTI and ASA in SID Side Impact Sled Tests, Proceedings of the 38th Stapp Car Crash Conference, 942225

Chang, F., 2001, The Development of a Finite Element Human Thorax Model for Impact Injury Studies, Proceedings of the 2001 ASME International Mechanical Engineering Congress and Exposition, AMD Vol. 251, 2001, pp. 103-111

Chung J., Cavanaugh J.M., Mason, M., King, A.I., 1997, Development of a Sled-to-Sled Subsystem Side Impact Test Methodology, Society of Automotive Engineers, 970569

Cronin, D., Forbes, P., Panzer, M., 2004, Human Body Model Development and Impact Simulation, Progress Report, University of Waterloo, Waterloo, Ontario, Canada

Cronin, D., Campbell, B., Yuen, K., 2006, Detailed Thorax Human Body and Vehicle Model Integration, Progress Report, University of Waterloo, Waterloo, Ontario, Canada

Cronin, D., Campbell, B., Moulton, J., Watson, B., Yuen, K., 2008, Detailed Thorax Human Body and Vehicle Model Integration, Progress Report, University of Waterloo, Waterloo, Ontario, Canada

Cronin, D.S., Salisbury, C.P., Horst, C.R.,2006, High Rate Characterization of Low Impedance Materials Using a Polymeric Split Hopkinson Pressure Bar, Society of Experimental Mechanics, University of Waterloo, Waterloo, Ontario, Canada

de Lange, R., van Rooij, L., Mooi , H., Wismans, J., 2005, Objective Biofidelity Rating of a Numerical Human Occupant Model in Frontal to Lateral Impact, Proceedings of the 49th Stapp Car Crash Conference, 2005-22-0020

Deng, Y.C., 1989, The Importance of the Test Method in Determining the Effects of Door Padding in Side Impact, Proceedings of the 33rd Stapp Car Crash Conference, 892429

Deng, Y.C., Kong, W., Ho, H., 1999, Development of A Finite Element Human Thorax Model for Impact Injury Studies, SAE International Congress and Exposition, Detroit, Michigan, SAE Paper 1999-01-0715

Deng Y.C., P Ng, 1993, Simulation of Vehicle Structure and Occupant Response in Side Impact, SAE 933125

Deng Y.C., Tzeng B., 1996, Side Impact Countermeasure Study Using a Hybrid Modeling Technique, SAE 962413

Deng, Y.C., Chang, F., 2000, F8B: Development of a Finite Element Human Thorax

Doman, D., Cronin, D.S., Salisbury, C.P., 2006,Characterization of polyurethane rubber at high deformation rates, Experimental Mechanics 46:3 June 2006.

Du Bois, P.A., 2003, A Simplified Approach to the Simulation of Rubber-Like Materials

Under Dynamic Loading, 4th European LS_DYNA Users Conference, Material I

Du Bois, P.A., 2004, Crashworthiness Engineering Course Notes, Livermore Software Technology Corporation

Du Bois, P.A., Generation of Foam Material Input Data for LS-DYNA law 83

Eiband, A.M., 1959, Human Tolerance to Rapidly Applied Acceleration. A Survey of the Literature, NASA Memo No. 5-19-59E., National Aeronautics and Space Administration, Washington, D.C.

Eppinger, R.H., Marcus, J.H., Morgan, R.M., 1984, Development of Dummy and Injury Index for NHTSA's Thoracic Side Impact Protection Research Program, SAE Publication No. 840885, Government/Industry Meeting and Exposition, Washington, D.C.

Fatality Analysis Reporting System (FARS), 2008, http://www-fars.nhtsa.dot.gov

Federal Motor Vehicle Safety Standards and Regulations, Motor Vehicle Safety Standard No. 208, "Occupant Crash Protection." U.S. Department of Transportation, National Highway Safety Bureau, Effective October 1, 2002
176

Forbes, P. A., 2005, Development of a Human Body Model for the Analysis of Side Impact Automotive Thoracic Trauma, MASc Thesis, University of Waterloo, Waterloo, Ontario, Canada

Forbes, P.A, Cronin, D.S., Deng, Y.C., 2005, Multi-Scale Human Body Model to Predict Side Impact Thoracic Trauma, IJCrash 2006 Vol 11 No. 3 pp. 203-216

Forbes, P.A., Cronin, D.S., Deng, Y.C.,2006, Numerical Human Body Model to Predict Human Shoulder Impact Response, 5th World Congress of Biomechanics, Munich, Germany, July 29-August 4, 2006. Citation: Journal of Biomechanics 2006; Vol. 39 Suppl. 1, page S161.

Forman, J., Lessley, D., Shaw, C.G., Evans, J., Kent, R., Rouhana, S.W., Prasad, P., 2006, Thoracic Response of Belted PMHS, the Hybrid III, and the THOR-NT Mid-Sized Male Surrogates in Low Speed Frontal Crashes, Proceedings of the 50th Stapp Car Crash Conference, 2006-22-0009

Fung, Y.-C., Tong, P., Patitucci, P., 1978, Stress and Strain in the Lung, ASCE Journal of the Engineering Mechanics Division, Vol. 104, No. 1, pp. 201-223

Gadd, C.W., Patrick, L.M., 1968, Systems Versus Laboratory Impact Tests for Estimating Injury Hazard, SAE paper 680053, Society of Automotive Engineers,

New York

Guccione, J.M., McCulloch, A.D., Waldman, L.K., 1991, Passive Material Properties of Intact Ventricular Myocardium Determined From a Cylindrical Model, Journal of Biomechanical Engineering, Vol. 113, pp. 42-55

Guccione, J.M., McCulloch, A.D., 1991, Finite Element Modeling of Ventricular Mechanics, in Theory of Heart, Glass, L., Hunter, P., McCulloch, A., Springer-Verlag, New York, pp. 121-137

Happee, R., Hoofman, M., van den Kroonenberg, A.J., Morsink, P., Wismans, J., 1998, A Mathematical Human Body Model for Frontal and Rearward Seated Automotive Impact Loading, Proceedings of the 42nd Annual Stapp Crash Conference, 983150

Huang, Y., King, A.I., Cavanaugh, J.M., 1994a, Finite Element Modeling of Gross Motion of Human Cadavers in Side Impact, Proceedings of the 38th Stapp Car Crash Conference, 942207

Huang, Y., King, A.I., Cavanaugh, J.M., 1994b, A MADYMO Model of Near Side Human Occupants in Side Impact, Journal of Biomechanical Engineering, ASME, Vol. 116

Iwamoto, M., Miki, K., Mohammad, M., Nayef, A., Yang, K.H., Begeman, P.C., King, A.I., 2000, Development of a Finite Element Model of the Human Shoulder, Proceedings of the 44th Stapp Car Crash Conference

Kallieris, D., Mattern, R., Schmidt, G., Eppinger, R.H., 1981, Quantification of Side Impact Response and Injuries, Proceeding of the 25th Annual Stapp Car Crash Conference, 811009

Kroell, C.K., Schneider, D.C., Nahum, A.M., 1971, Impact Tolerance and Response of the Human Thorax, Proceedings of the 15th Stapp Car Crash Conference, 710851

Kroell, C.K., Schneider, D.C., Nahum, A.M., 1974, Impact Tolerance and Response of the Human Thorax II, Proceedings of the 18th Stapp Car Crash Conference, 741187

Kroell, C.K., Pope, M.E., Viano, D.C., Warner, C.Y., Allen, S.D., 1981, Interrelationship of Velocity and Chest Compression in Blunt Thoracic Impact to Swine, Proceedings of the 25th Stapp Car Crash Conference, 811016

Kuppa, S., Eppinger, R.H., McKoy, F., 2003, Development of Side Impact Thoracic Injury Criteria and Their Application to the Modified ES-2 Dummy with Rib Extensions (ES-2re), Proceedings of the 47th Annual Stapp Car Crash Journal, 2003-22-0010

Kuppa S., 2004, Injury Criteria Development for the ES-2 Dummy, NHTSA

Kuppa S., Eppinger R.H, McKoy F., Nguyen T., Pintar F.A., Yoganandan N., 2004, Development of Side Impact Thoracic Injury Criteria and Their Application to the Modified ES-2 Dummy with Rib Extensions (ES-2re), Proc. Fourty-seventh Stapp Car Crash Conference, pp. 189-210, SAE, Warrendale, PA.

Lau, I.V., Viano, D.C., 1981, Influence of Impact Velocity on the Severity of Non-Penetrating Hepatic Injury, Journal of Trauma, Vol. 21, pp. 115-123

Lau, I.V., Viano, D.C., 1985, Thoracic Impact: A Viscous Tolerance Criterion, Proceedings of the Tenth Experimental Safety Vehicle Conference, Oxford, England

Lau, I.V., Viano, D.C., 1986, The Viscous Criterion - Bases and Applications of an Injury Severity Index for Soft Tissues, Proceedings of the 30th Stapp Car Crash Conference, 861882

Lobdell, T.E., Kroell, C.K., Schneider, D.C., Hering, W.E., Nahum, A.M., 1973, Impact Response of the Human Thorax, Proceedings of the Symposium from Human Impact Response Measurement and Simulation, New York, London, Plenum Press, pp. 201-245

LS-PREPOST Online Documentation, 2009, http://www.lstc.com/lspp/content/pages/5/beltfit/beltfit.shtml

LSTC (Livermore Software Technology Corp.), "LS DYNA Keyword User's Manual, Version 971", May, 2007

Maltese M., Eppinger R., Rhule H., Donnelly B., Pintar F., Yoganandan N., 2002, Response Corridors of Human Surrogates in Lateral Impacts, Proc. Fourty-sixth Stapp Car Crash Conference, pp. 321-351, SAE, Warrendale, PA.

McCulloch, A.D., Omens, J.H., 1991, Non-Homogeneous Analysis of Three-Dimensional Transmural Finite Deformation in Canine Ventricular Myocardium, Journal of Biomechanics, Vol. 24, No. 7, pp. 539-548

McElhaney, J.H., 1966, Dynamic Response of Bone and Muscle Tissue, Journal of Applied Physiology, Vol 21 pp. 1231-1236

Mertz, H.J., Gadd C.W., 1971, Thoracic Tolerance to Whole-body Deceleration, Proc. Fifteenth Stapp Car Crash Conference, pp. 135-157, SAE, Warrendale, PA.

MGA Research Corporation, Nissan Maxima v3668, 2001, NHTSA

MGA Research Corporation, Ford Taurus v3522, 2000, NHTSA

Model, Final Report, General Motors Internal Report

Moore, K.L., Dalley, A.F., 2006, Clinically Oriented Anatomy, Fourth Edition, Lippincott Williams and Wilkins, Baltimore

Morgan, R.M., Marcus, J.H., Eppinger, R.H., 1986, Side Impact - The Biofidelity of NHTSA's Proposed ATD and Efficacy of TTI, Proceedings of the 30th Stapp Car Crash Conference, 861877

Morris R.A, Crandall J.R, Pilkey W.D., 1998, Multibody Modelling of a Side Impact Test Apparatus, IJCrash 1999 Vol 4 No. 1 pp. 17-30

Morton, 1995, Side Impact Test Device

Nahum, A.M., Melvin J.W., 2002, Accidental Injury Biomechanics and Prevention, Second Edition, Springer-Verlag Inc., New York

National Highway Traffic Safety Administration, 2001, A Compilation of Motor Vehicle Crash Data from the Fatality Analysis Reporting System and the General Estimates System, Traffic Safety Facts 2001, DOT HS 809 484

National Highway Traffic Safety Administration, 2006, Traffic Safety Facts

National Highway Traffic Safety Administration, 2004, Federal Motor Vehicle Safety Standards; Side Impact Protection; Side Impact Phase-In Reporting Requirements; Proposed Rule, Federal Register, Part IV, Department of Transportation 49 CFR Parts 571 and 598, Docket No. NHTSA-2004-17694

National Library of Medicine, 2004, The Visible Human Project, National Institutes of Health, slice a_vm1460.

Neathery, R.F., 1974, Analysis of Chest Impact Response Data and Scaled Performance Recommendations, Proceeding of the 18th Stapp Car Crash Conference, 741188
180

Neathery, R.F., Kroell, C.K., Mertz, H.J., 1975, Prediction of Thoracic Injury from Dummy Responses, Proceeding of the 19th Stapp Car Crash Conference, 751151

NHTSA Database, 2008,

NHTSA Side Impact Evaluation, 2004

NHTSA Website, 2007, http://www-nrd.nhtsa.dot.gov/departments/nrd-11/FEA_models.html

Oshita, F., Omori, K., Nakahira, Y., Miki, K., 2002, Development of a Finite Element Model of the Human Body, Proceedings of the 7th International LS-DYNA Users Conference

Patrick, L.M., Kroell, C.K., Mertz, H.J., 1965, Forces of the Human Body in Simulated Crashes, Proceedings of the 9th Stapp Car Crash Conference, 650961

Payne, A.R., Mohacsi, R., Allan-Stubbs, B., 1997, The Effects of Variability in Vehicle Structure and Occupant Position on Side Impact Dummy Response Using the MIRA M-SIS Side Impact Technique., Society of Automotive Engineers, 970571

Pintar, F.A., Yoganandan, N., Hines, M.H., Maltese, M.R., et al., 1997, Chestband Analysis of Human Tolerance to Side Impact, Proceedings of the 41st Annual Stapp Car Crash Conference, 973320

Plank, G.R., Eppinger, R.H., 1989, Computed Dynamic Response of the Human Thorax From a Finite Element Model, Proceedings of the 12th International Technical Conference of Experimental Safety Vehicle

Plank, G.R., Eppinger, R.H., 1991, An Improved Finite Element Model of the Human Thorax, Proceedings of the 13th International Technical Conference of Experimental Safety Vehicle

Plank, G.R., Eppinger, R.H., 1994, Finite Element Modeling and Analysis of Thorax/Restraint System Interaction, Proceedings of the 14th International Technical Conference of Experimental Safety Vehicle

Rhule H., Maltese M., Donnelly B., Eppinger R., Brunner J., Bolta J., 2002, Development of a New Biofidelity Ranking System for Anthropomorphic Test Devices, Fourty-sixth Stapp Car Crash Conference, pp. 477-512, SAE, Warrendale, PA

Ruan, J., El-Jawahri, R., Chai, L., Sarbat, S., Prasad, P., 2003, Prediction and analysis of a human thoracic impact responses and injuries in cadaver impacts using a full human body finite element model, Proceedings of the 47th Stapp Car Crash

Salisbury, C., 2001 Spectral Analysis of Wave Propagation Through a Polymeric Hopkinson Bar, Masters Thesis, University of Waterloo

Samaha et al., 1998, Comparative Performance Testing of Passenger Cars Relative to FMVSS 214 and the EU 96/EC/27 Side Impact Regulations, 98-S8-O-08, NHTSA

Samaha R., Maltese M., Bolte J., 2001, Evaluation of the ES-2 Dummy in Representative Side Impacts, Seventeenth International Technical Conference on the Enhanced Safety of Vehicles, Paper No. 486, NHTSA

Schönpflug, M., von Merten, K., Mester, M., Wernicke, P., 2004, Numerical Simulation of Human Kinematics and Injuries in Side Crash Scenarios, SAE, 2004-01-2161

Schuster, P., Franz, U., Stahlschmidt, S., Pleshberger, M., Eichberger, A. (2004), 'Comparison of ES-2re with ES-2 and USSID Dummy – Consideration for ES-2re model in FMVSS Tests' LS-DYNA Forum 2004 Proceedings

Serifi, E., Hirth, A., Matthaei, S., Mullerschon, H., 2003, Modeling of Foams using Mat83-Preparation and Evaluation of Experimental Data, 4th European LS-DYNA Users Conference

Severy, D.M., Blaisdell, D.M., Kerkhoff, J.F., 1976, Automotive Seat Design and Collision Performance, Society of Automotive Engineers, SAE 760810

Shah, C.S., Yang, K.H., Hardy, W., Wang, H.K., King, A.I., 2001, Development of a Computer Model to Predict Aortic Rupture Due to Impact Loading, Proceedings of the 45th Stapp Car Crash Conference, 2001-01-0007

Stapp, J.P., 1951, Human Exposure to Linear Decelerations, Part 2: The Forward Facing Position and the Development of a Crash Harness, AFTR 5915, Wright-Patterson AFB, Dayton, Ohio

Stapp, J.P., 1957, Human Tolerance to Deceleration, American Journal of Surgery, Apr; 93(4): 734-740

Stapp, J.P., 1970, Voluntary Human Tolerance Levels, Impact Injury and Crash Protection, Ed: Gurdjian, E.S., Lang, W.A., Patrick, L.M., Thomas, L.M., pp. 308-349, Charles C. Thomas, Springfield, IL.

States, J.D., 1969, The Abbreviated and the Comprehensive Research Injury Scales, Proceedings of the 13th Stapp Car Crash Conference, 690810

Sundaram, S.H., Feng, C.C., 1977, Finite Element Analysis of the Human Thorax, Journal of Biomechanics, Vol. 10, pp. 505-516

Teng, Tso-Liang, Chang, Kuan-Chun and Wu, Chien-Hsun, 2007, Development and validation of side-impact crash and sled testing finite-element models,Vehicle System Dynamics,45:10,925 — 937

Van Sligtenhorst, C.R., Cronin, D.S., Brodland, W.G., 2003, High Strain Rate Compressive Properties of Soft Tissue, American Society of Mechanical Engineers, Bioengineering Division BED, Vol. 55

Vawter, D. L., 1980, A Finite Element Model for Macroscopic Deformation of the Lung, Journal of Biomechanical Engineering, Vol. 102
182

Viano, D.C., 1987a, Evaluation of the SID Dummy and TTI Injury Criterion for Side Impact Testing, Proceedings of the 31st Stapp Car Crash Conference, 872208

Viano, D.C., 1987b, Evaluation of the Benefit of Energy-Absorbing Material in Side Impact Protection: Part I, Proceedings of the 31st Stapp Car Crash Conference, 872212

Viano, D.C., 1987c, Evaluation of the Benefit of Energy-Absorbing Material in Side Impact Protection: Part II, Proceedings of the 31st Stapp Car Crash Conference, 872213

Viano, D.C., Lau, I.V., 1988, A Viscous Tolerance Criterion for Soft Tissue Injury Assessment, Journal of Biomechanics, Vol. 21, pp. 387-399

Viano D., 1989, Biomechanical Responses and Injuries in Blunt Lateral Impact. Proc. Thirty-third Stapp Car Crash Conference, pp. 113-142, SAE, Warrendale, PA.

Viano, D.C., King, A.I., Melvin, J.W., Weber, K., 1989a, Injury Biomechanics Research: An Essential Element in the Prevention of Trauma, Journal of Biomechanics, Vol. 22, No. 5, pp 403-417

Viano, D.C., Lau, I.V., Asbury, C., King, A.I., Begeman, P., 1989b, Biomechanics of the Human Chest, Abdomen, and Pelvis in Lateral Impact, Proceedings of the 33rd Association for the Advancement of Automotive Medicine

Viano, D.C., 1989, Biomechanical Responses and Injuries in Blunt Lateral Impact, Proceedings of the 33rd Stapp Car Crash Conference, 892432

Viano D., Fan a., Ueno K., Walilko T., Cavanaugh J., King A., 1995, Biofidelity and Injury Assessment in EuroSID I and Biosid. Proc. Thirty-Ninth Stapp Car Crash Conference, pp. 307-326, Society of Automotive Engineers, Warrendale, PA.

Wang, H.K., 1995, Development of a Side Impact Finite Element Human Thoracic Model, Ph.D. Dissertation, Wayne State University

Watson, B., Cronin, D., Campbell, B., 2009, Study of Vehicle Dynamics and Occupant Response in Side Impact Crash Tests, Submitted to 21st International Technical Conference on the Enhanced Safety of Vehicles, Paper No. 09-0016, NHTSA

WorldSID Home Page

Yamada, H., 1970, Strength of Biological Materials, Evans, F.G., ed., Lippincott Williams and Wilkins, Baltimore

Yuen, K.F., Cronin, D.S., Deng, Y.C., 2008, Lung Response and Injury in Side Impact Conditions, Proceedings of the 2008 International Research Council on Biomechanics of Injury (IRCOBI) Conference

Appendix A

Side Impact Model Simulation Data

A.1 The Effect of Varied Door to Occupant Spacing for an Intruding Rigid Door

Lower Chest Band

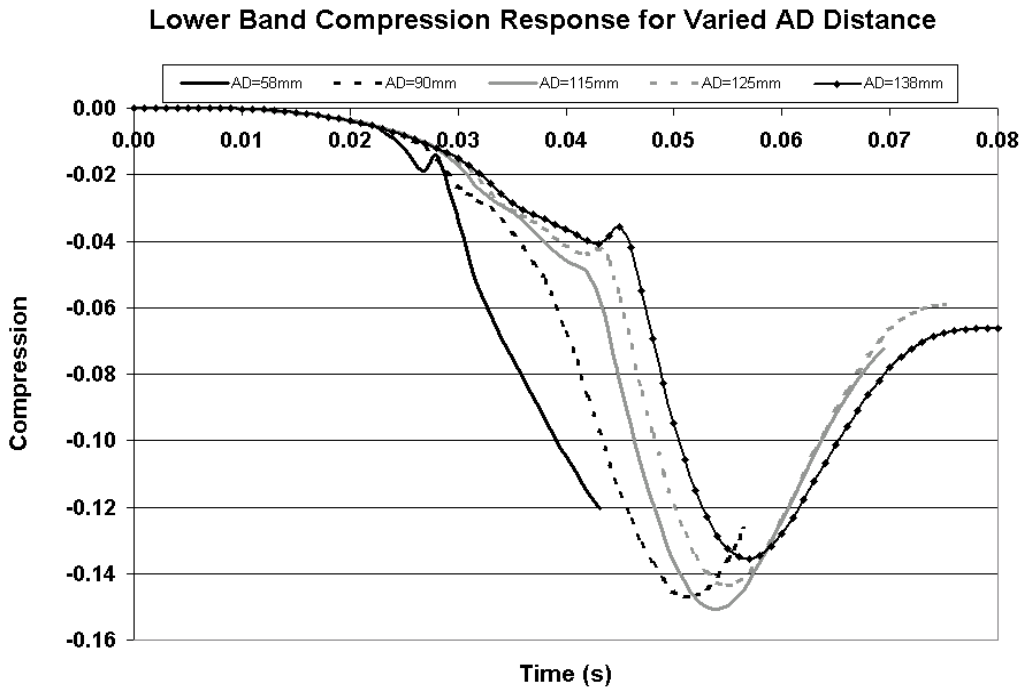

A. 1 Lower Band Compression Response for Varied AD Distance

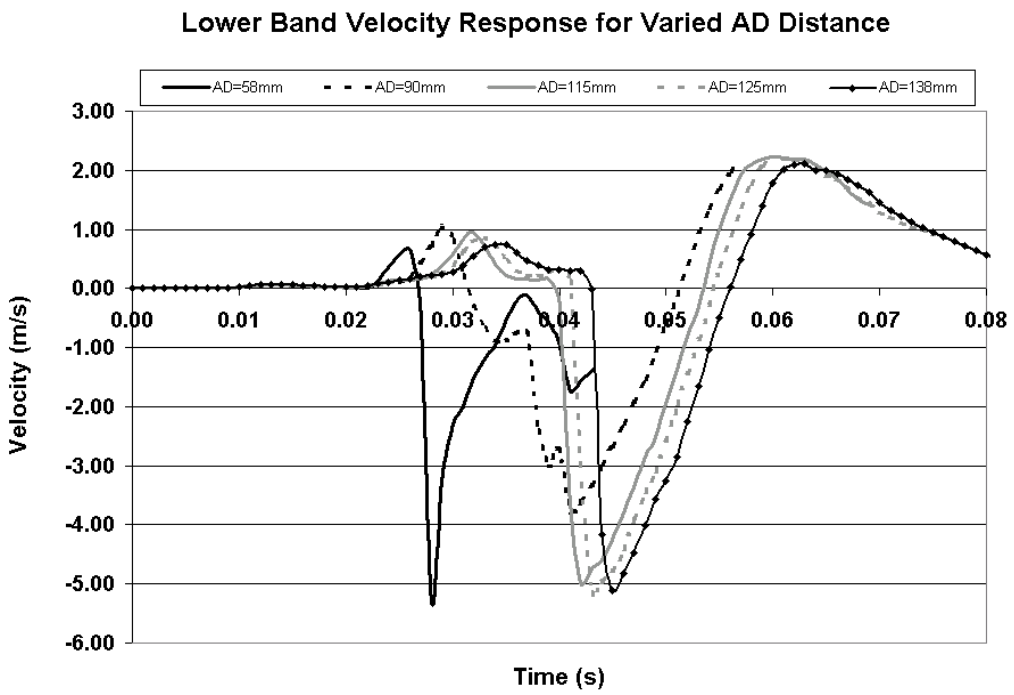

A. 2 Lower Band Velocity Response for Varied AD Distance

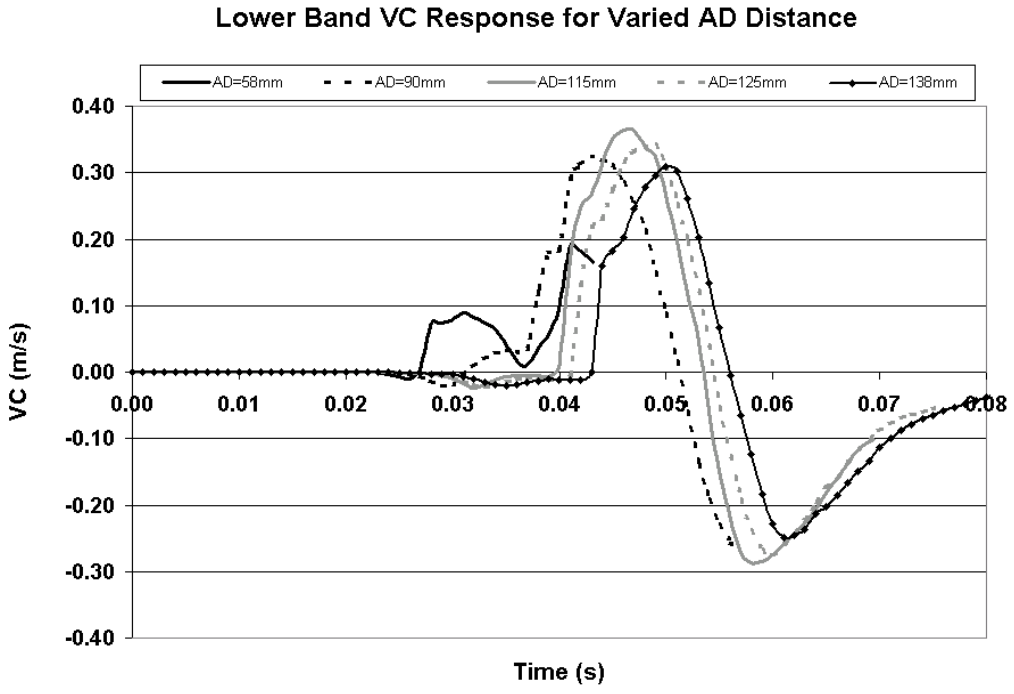

A. 3 Lower Band Velocity Response for Varied AD Distance

Middle Chest Band

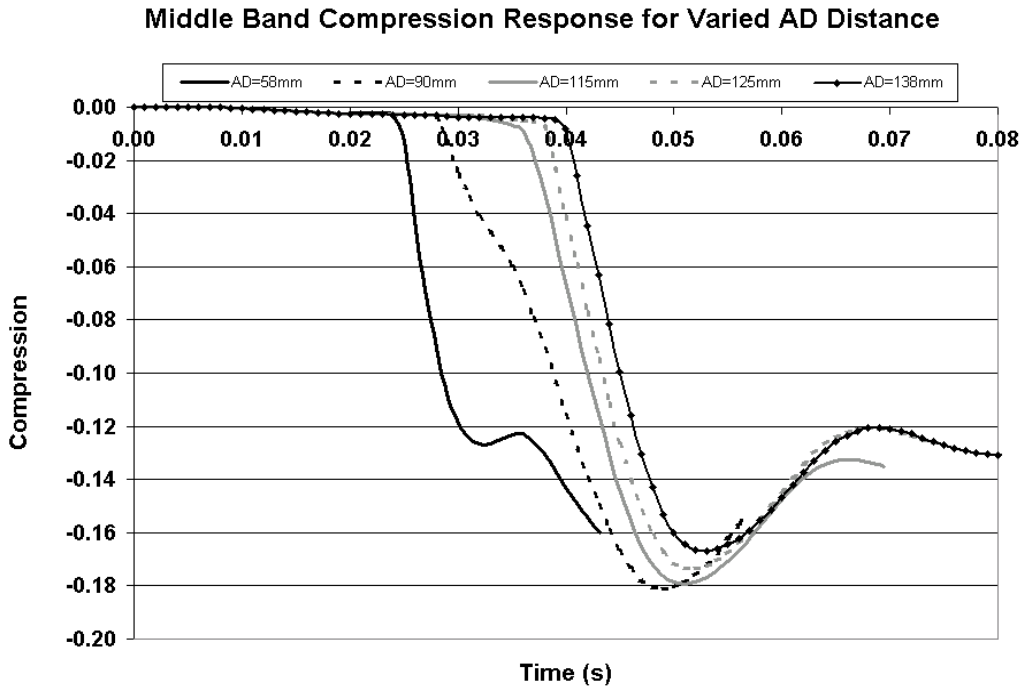

A. 4 Middle Band Compression Response for Varied AD Distance

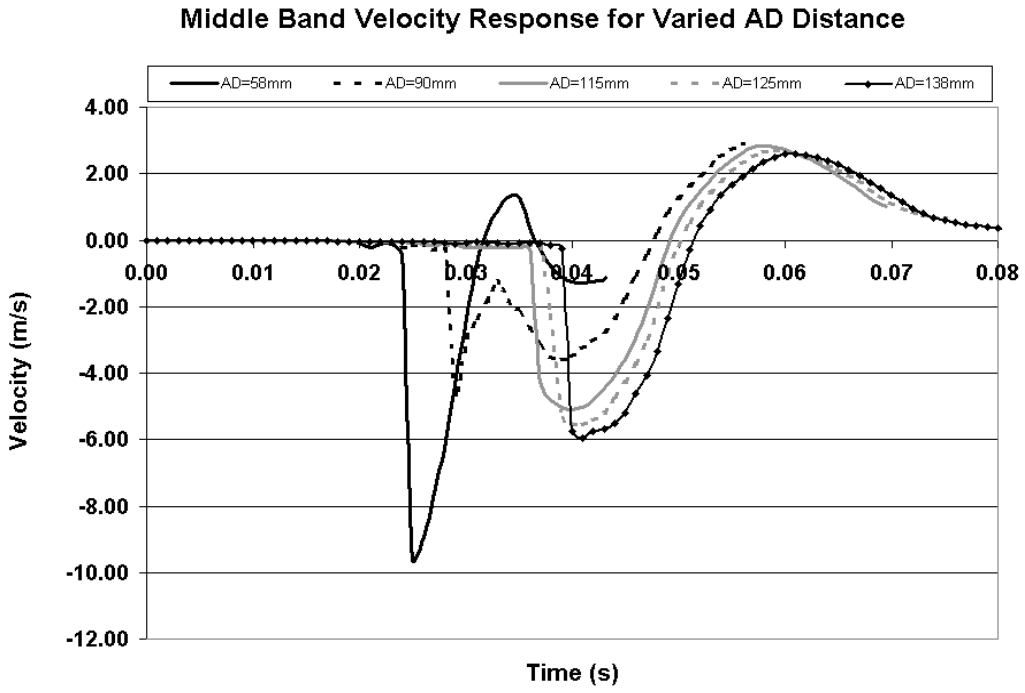

A. 5 Middle Band Velocity Response for Varied AD Distance

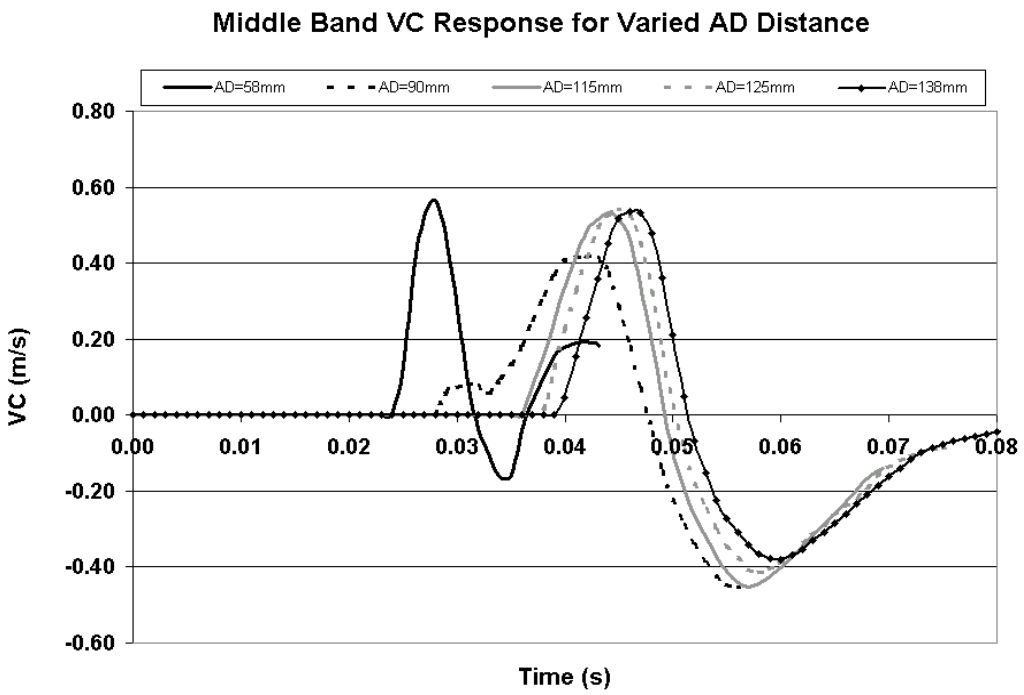

A. 6 Middle Band VC Response for Varied AD Distance

A.2 The Effect of Varied Door to Occupant Spacing for an Intruding Armrest

Lower Chest Band

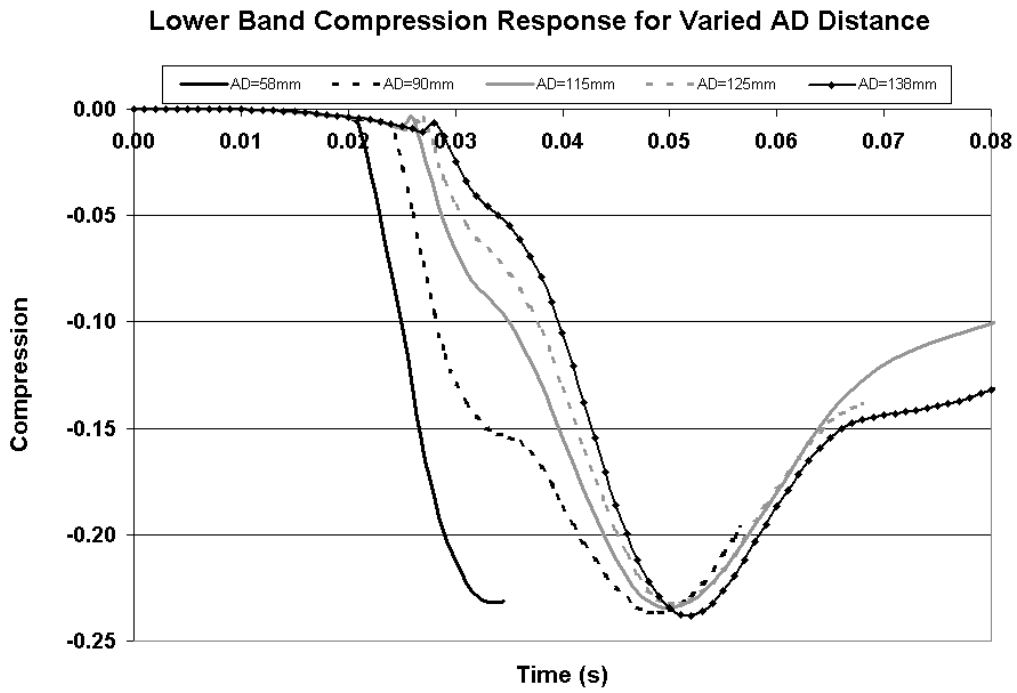

A. 7 Lower Band Compression Response for Varied AD Distance of an Intruding Armrest

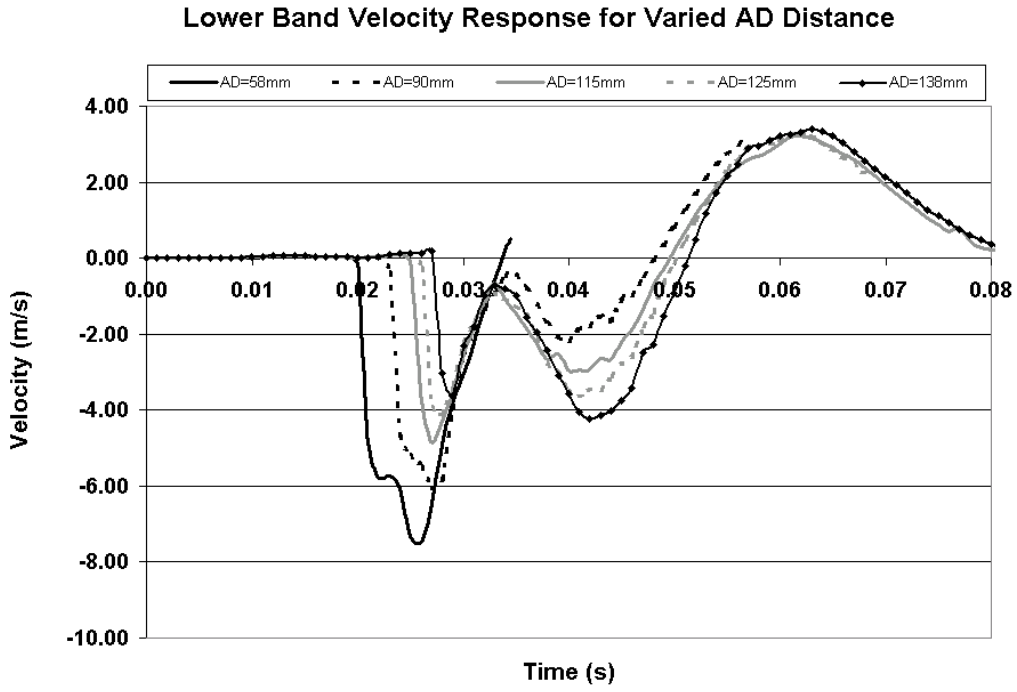

A. 8 Lower Band Velocity Response for Varied AD Distance of an Intruding Armrest

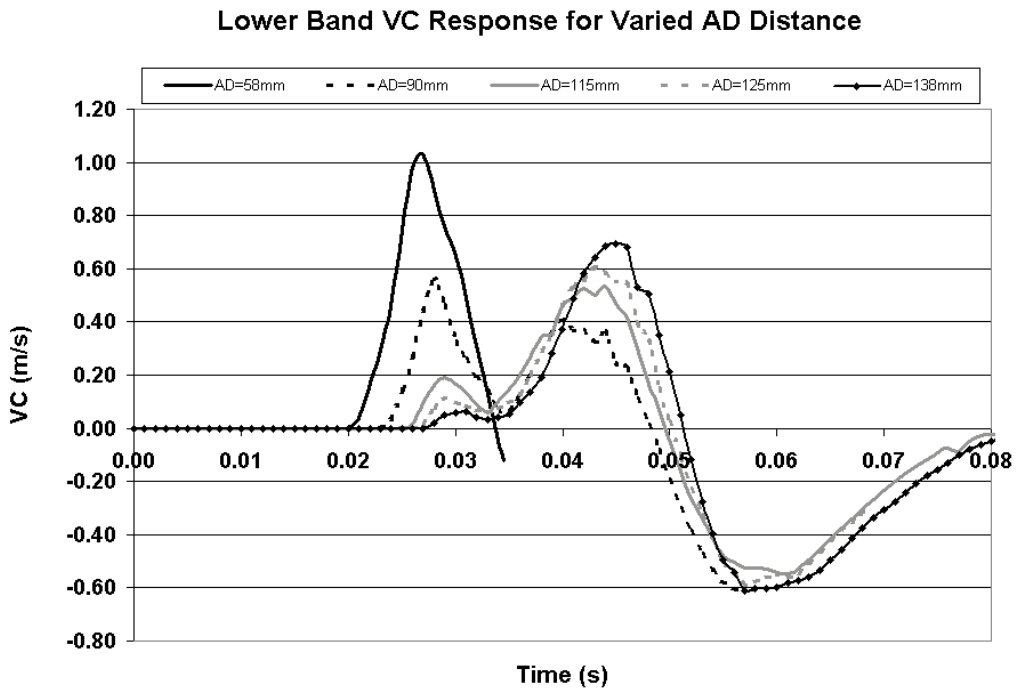

A. 9 Lower Band VC Response for Varied AD Distance of an Intruding Armrest

Middle Chest Band

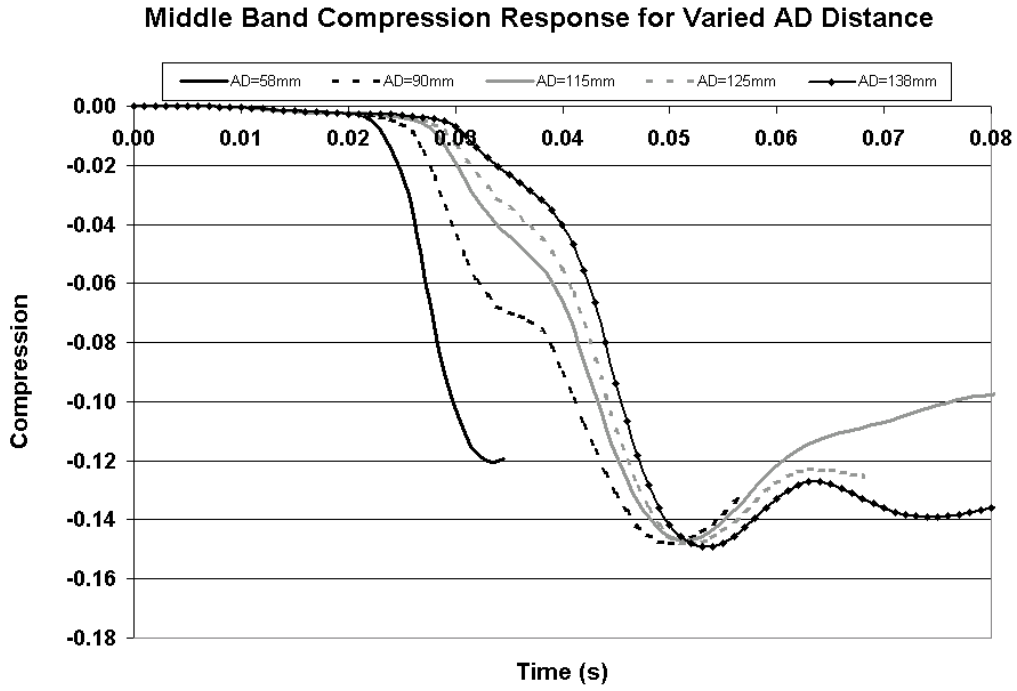

A. 10 Middle Band Compression Response for Varied AD Distance of an Intruding Armrest

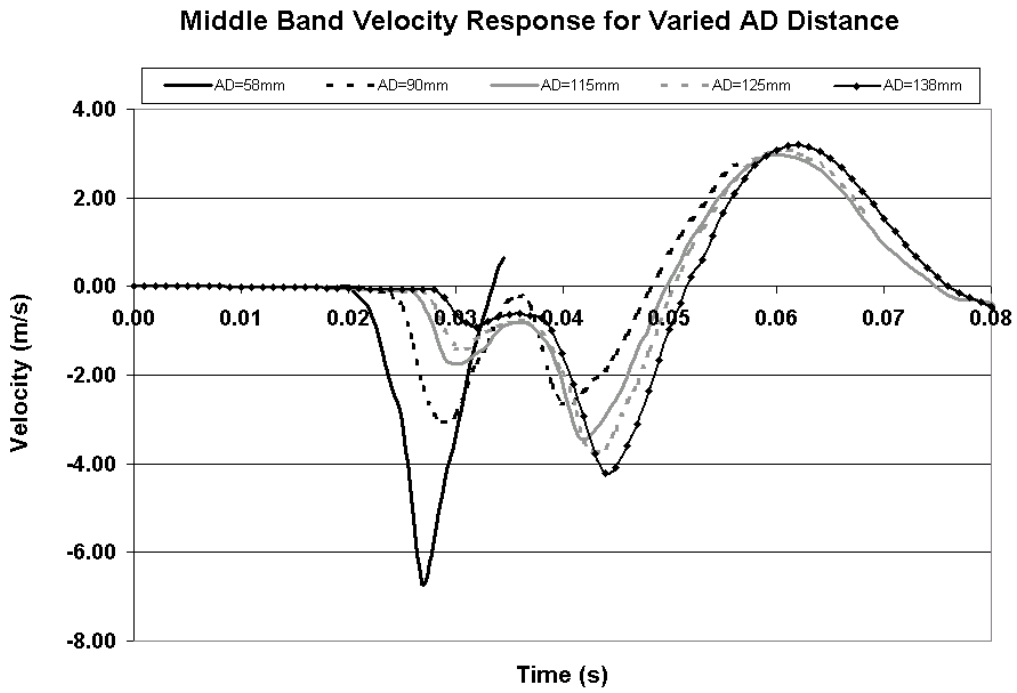

A. 11 Middle Band Velocity Response for Varied AD Distance of an Intruding Armrest

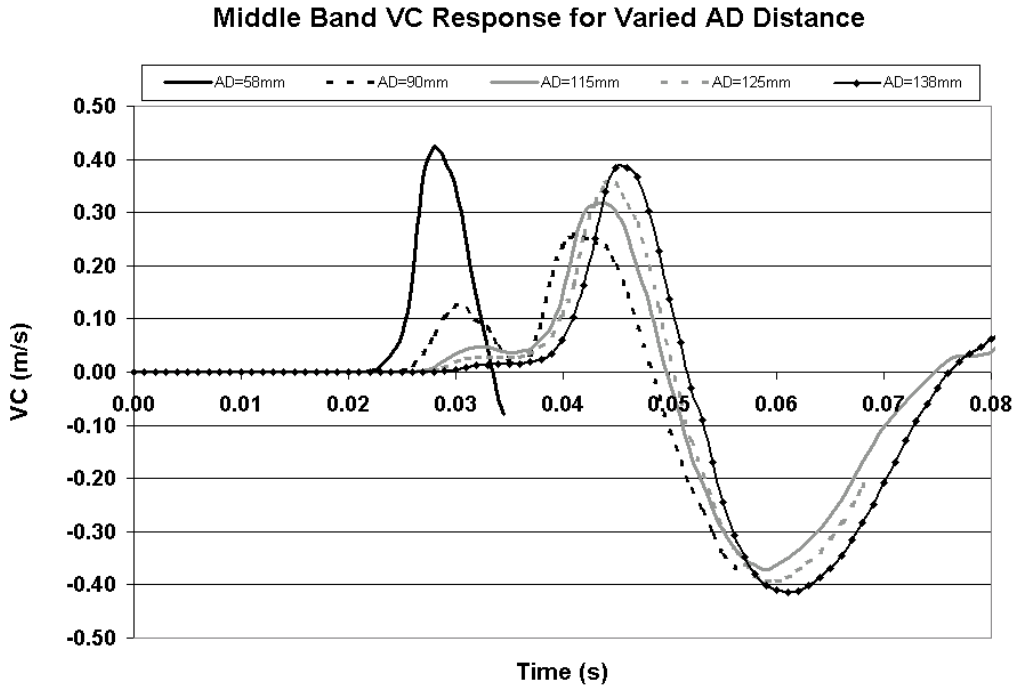

A. 12 Middle Band VC Response for Varied AD Distance of an Intruding Armrest

A.3 The Effect of Varying Door Intrusion Velocity Profile

Lower Chest Band

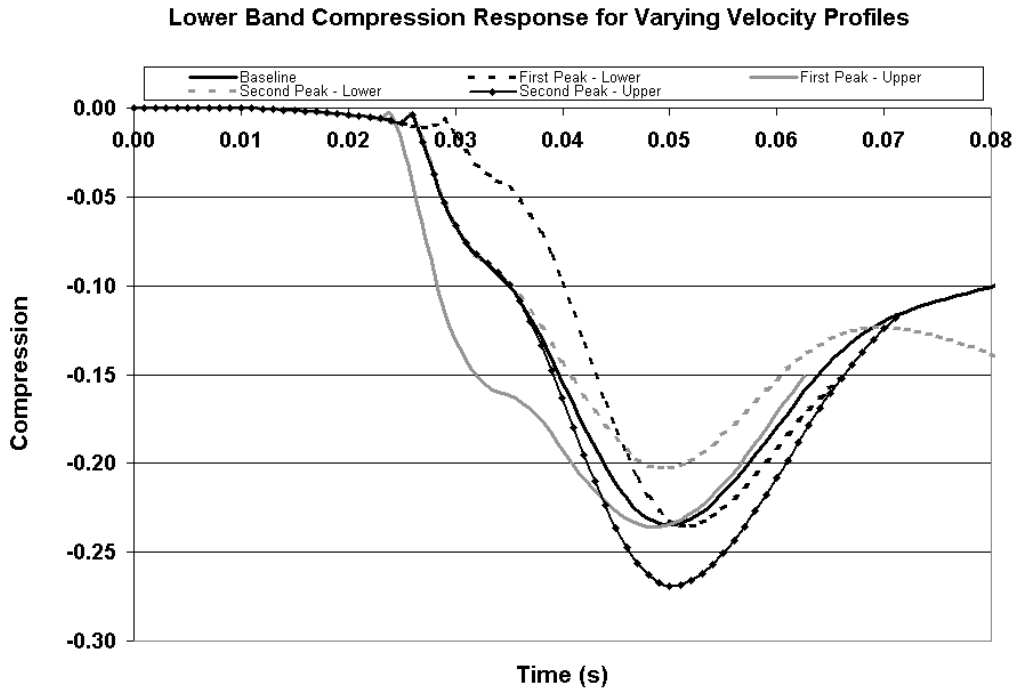

A. 13 Lower Band Compression Response for Varying Velocity Profiles

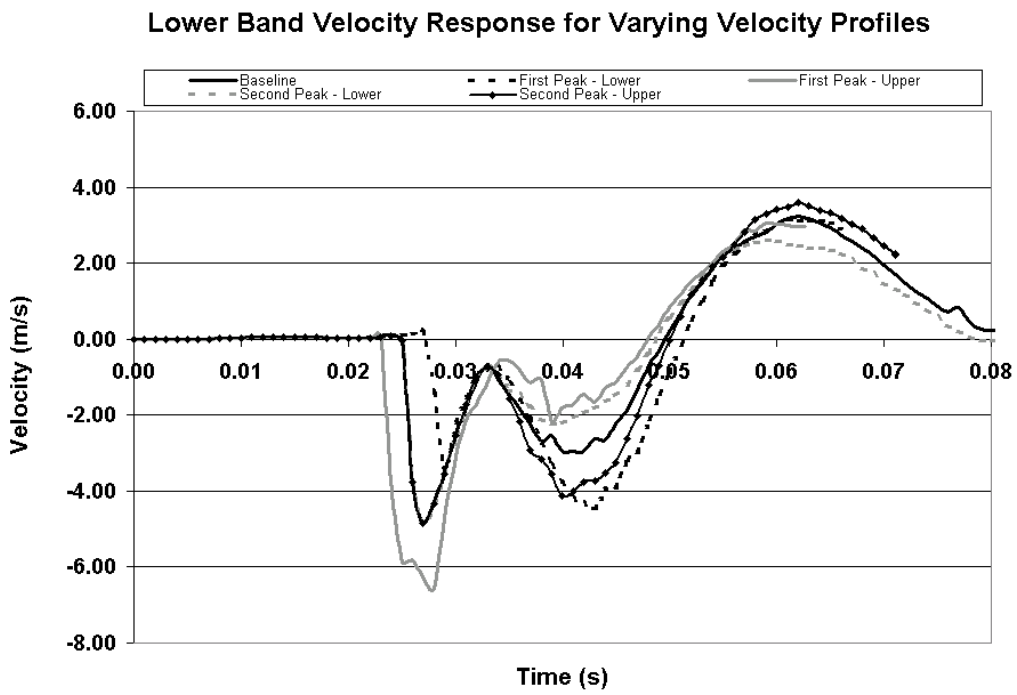

A. 14 Lower Band Velocity Response for Varying Velocity Profiles

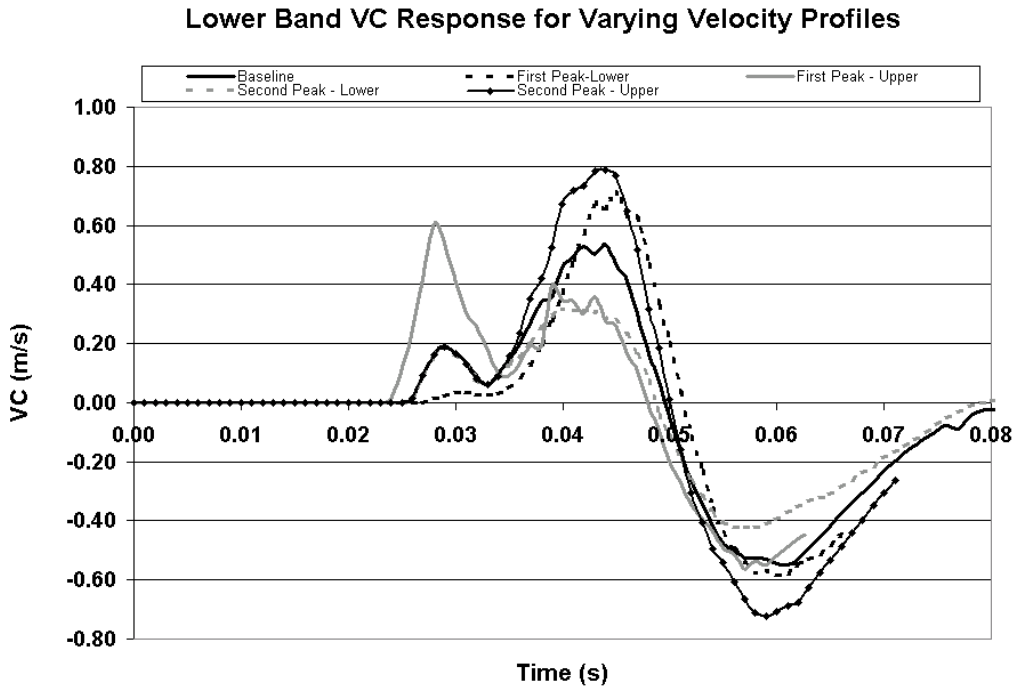

A. 15 Lower Band VC Response for Varying Velocity Profiles

Middle Chest Band

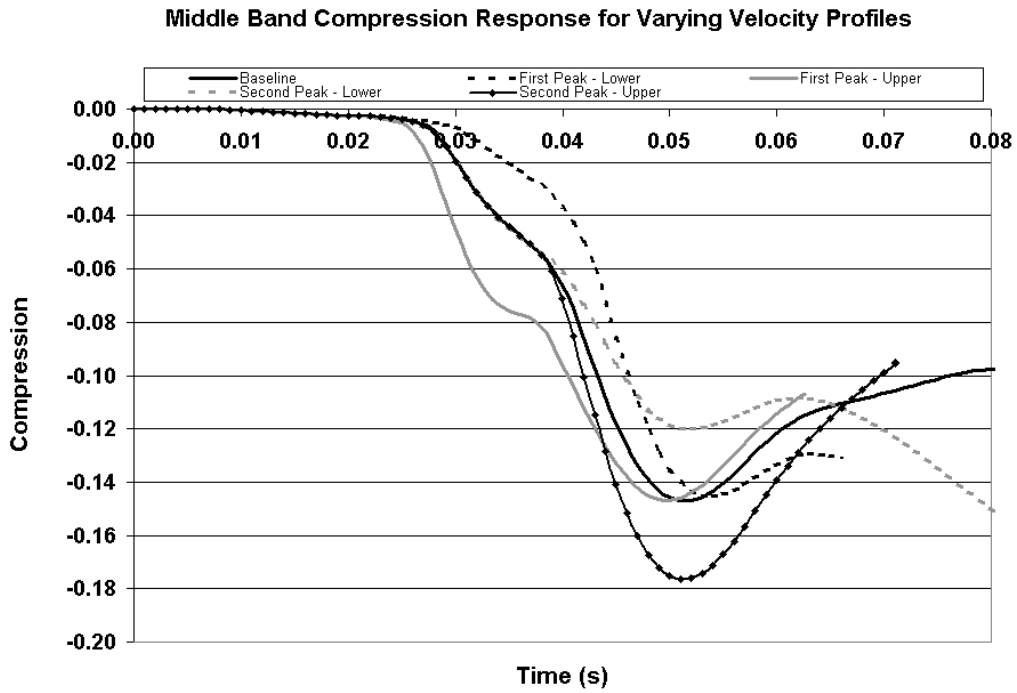

A. 16 Middle Band Compression Response for Varying Velocity Profiles

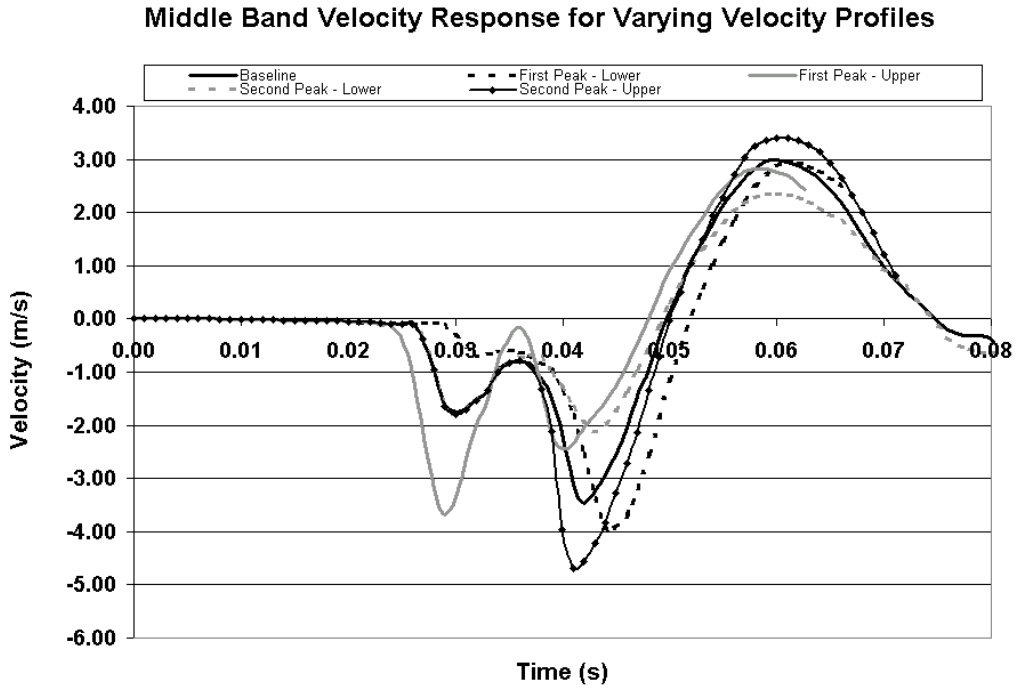

A. 17 Middle Band Velocity Response for Varying Velocity Profiles

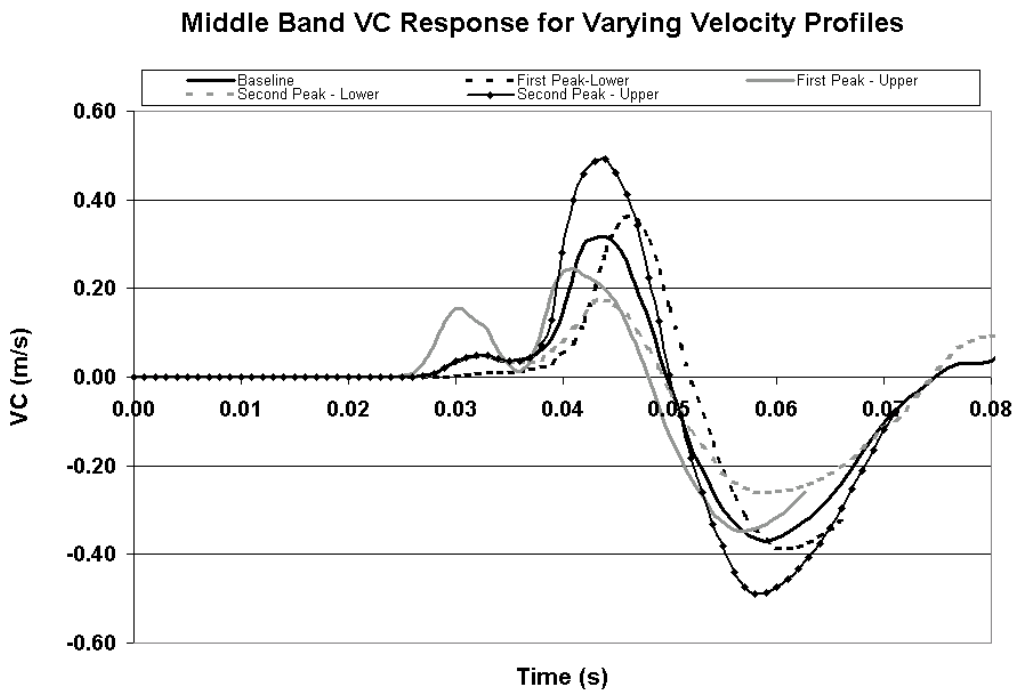

A. 18 Middle Band VC Response for Varying Velocity Profiles

A.4 The Effect of Varying Seat Foam Stiffness

Lower Chest Band

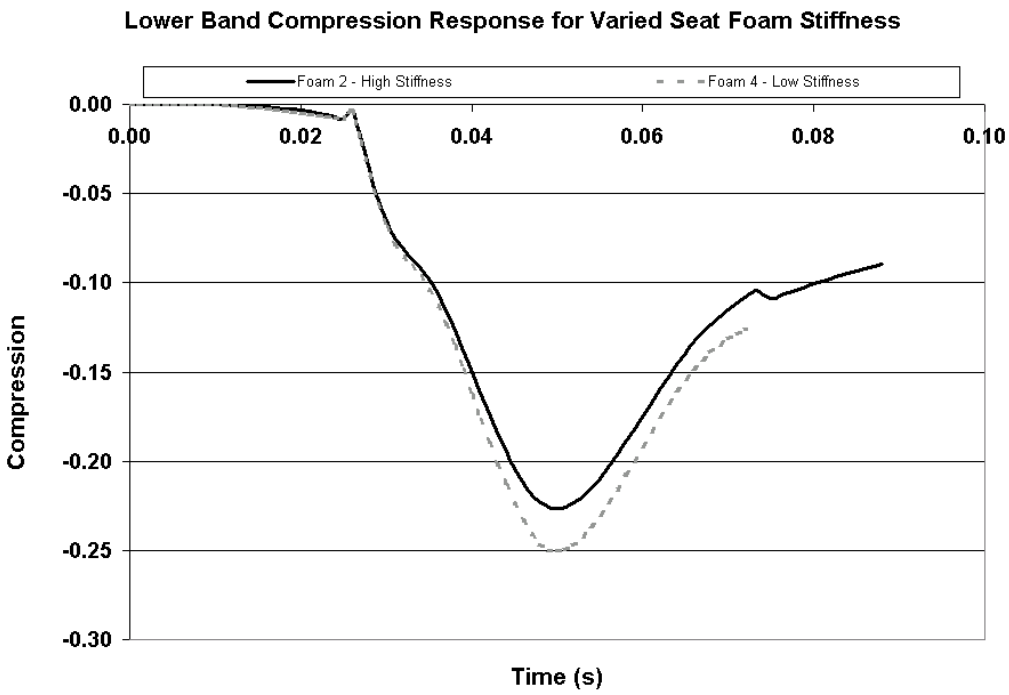

A. 19 Lower Band Compression Response for Varied Seat Foam Stiffness

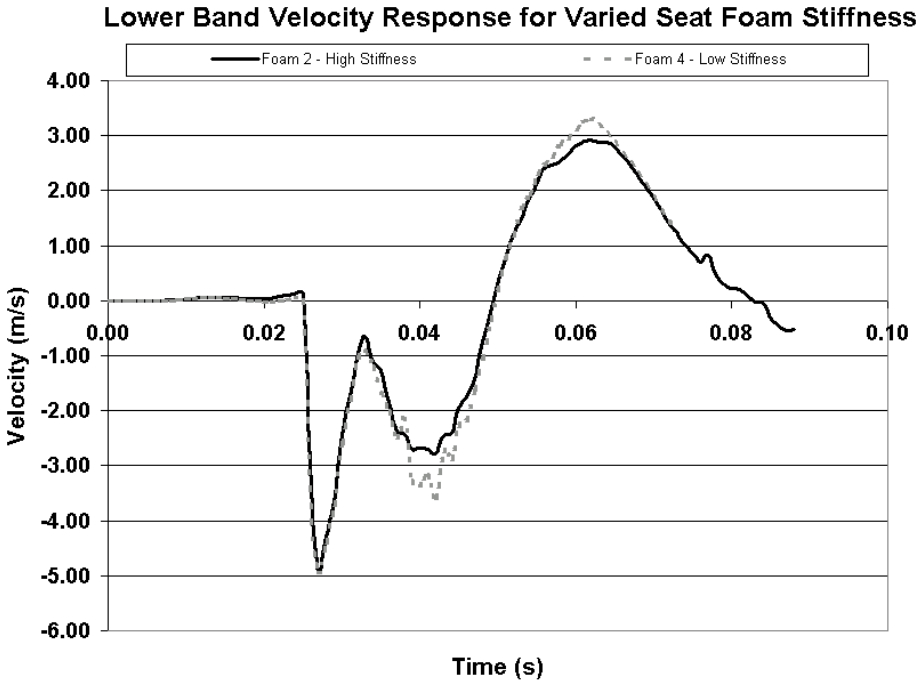

A. 20 Lower Band Velocity Response for Varied Seat Foam Stiffness

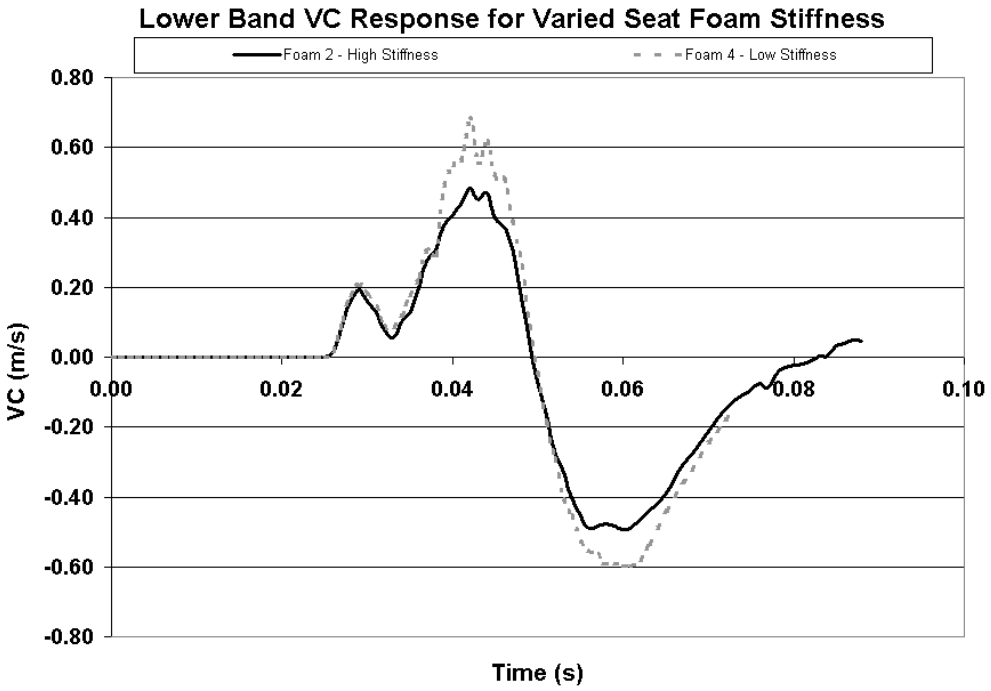

A. 21 Lower Band VC Response for Varied Seat Foam Stiffness

Middle Chest Band

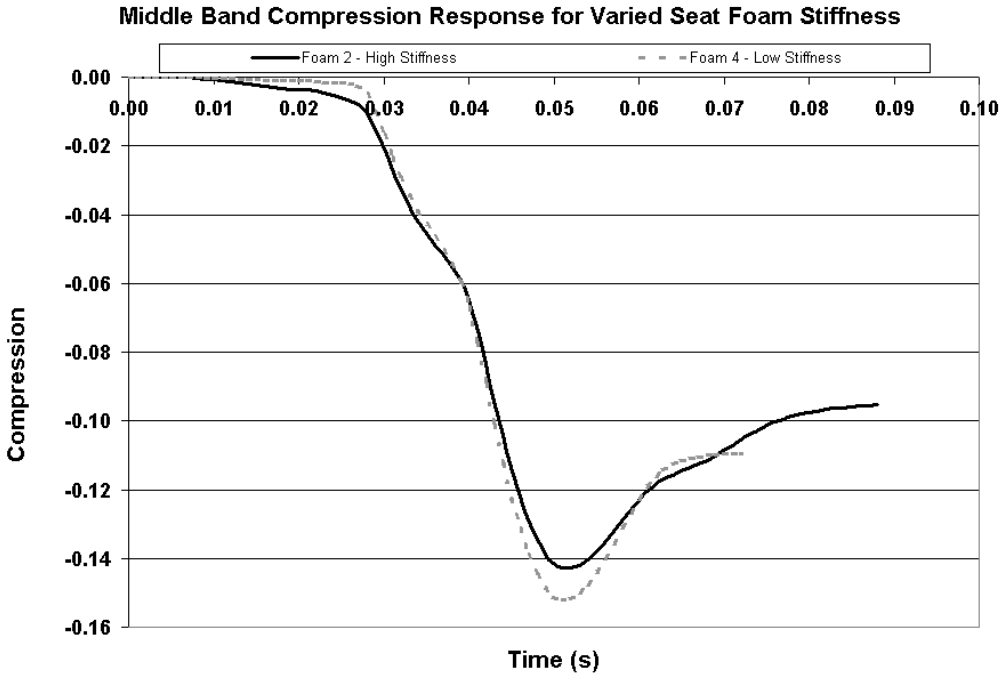

A. 22 Middle Band Compression Response for Varied Seat Foam Stiffness

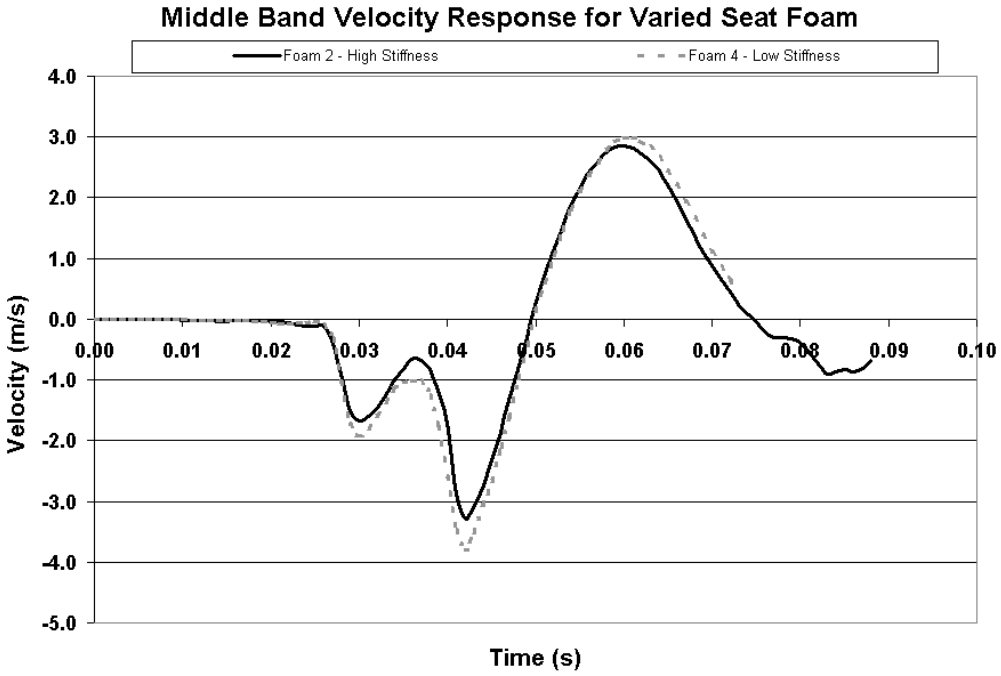

A. 23 Middle Band Velocity Response for Varied Seat Foam Stiffness

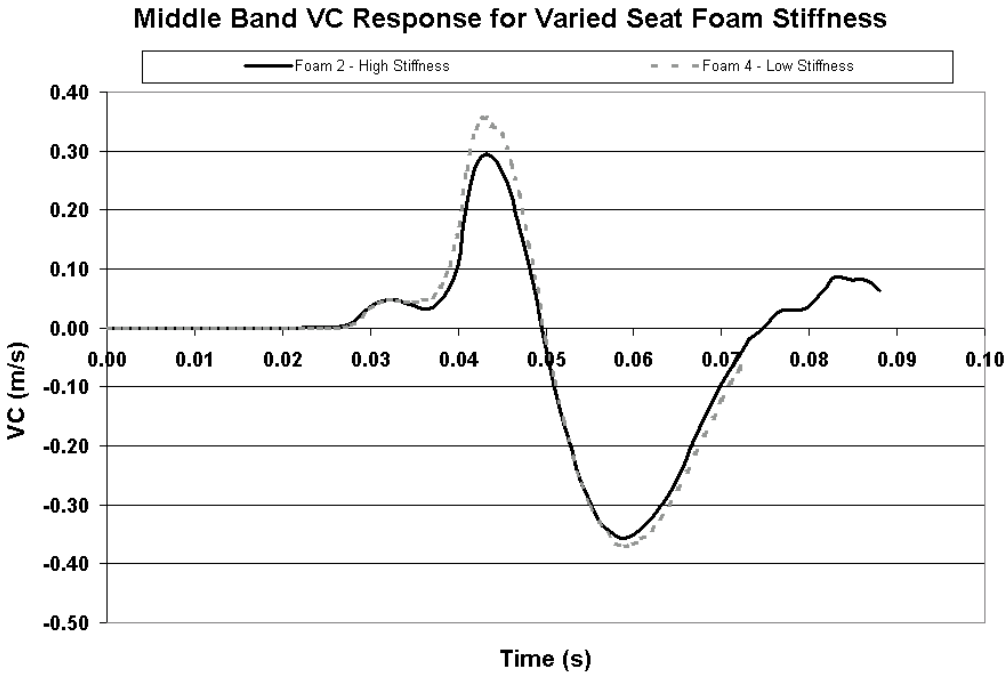

A. 24 Middle Band VC Response for Varied Seat Foam Stiffness

A.5 The Effect of Varying Arm Position

Lower Chest Band

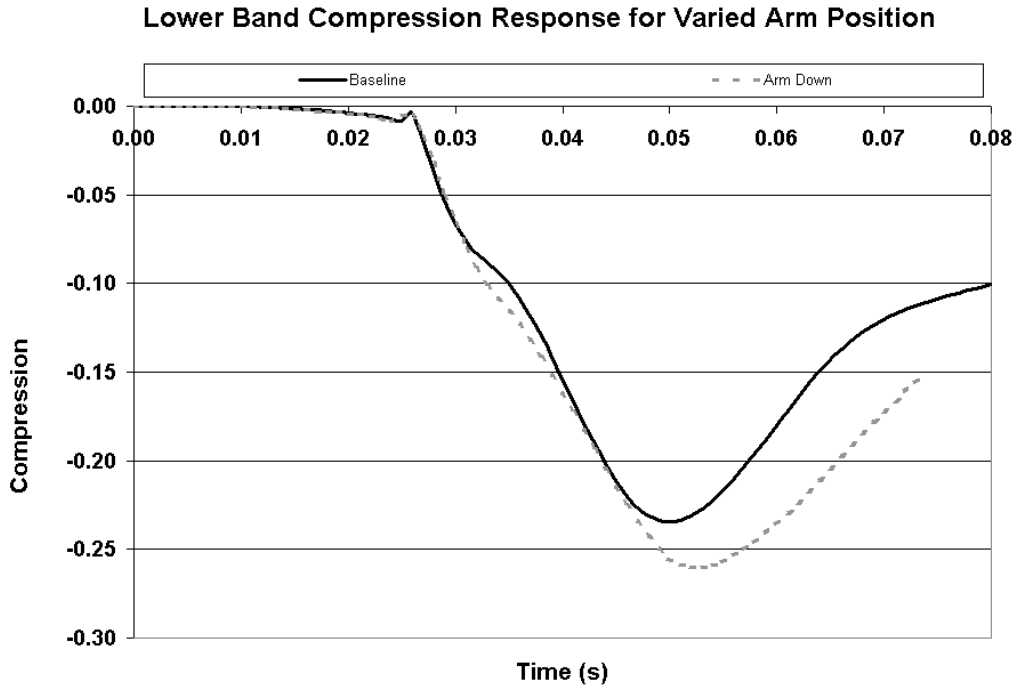

A. 25 Lower Band Compression Response for Varied Arm Position

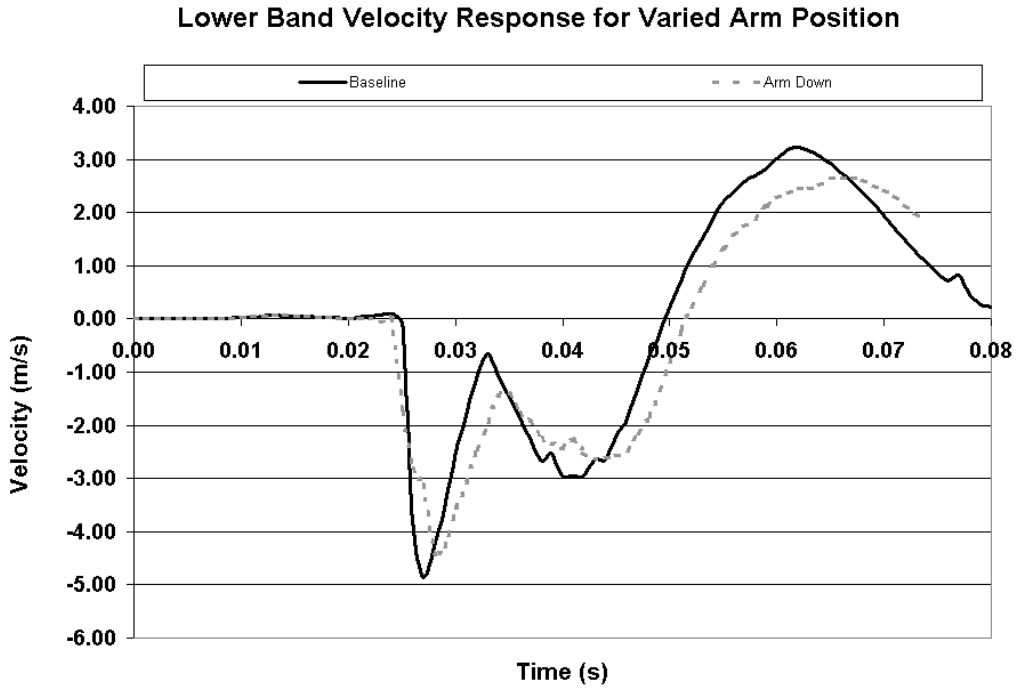

A. 26 Lower Band Velocity Response for Varied Arm Position

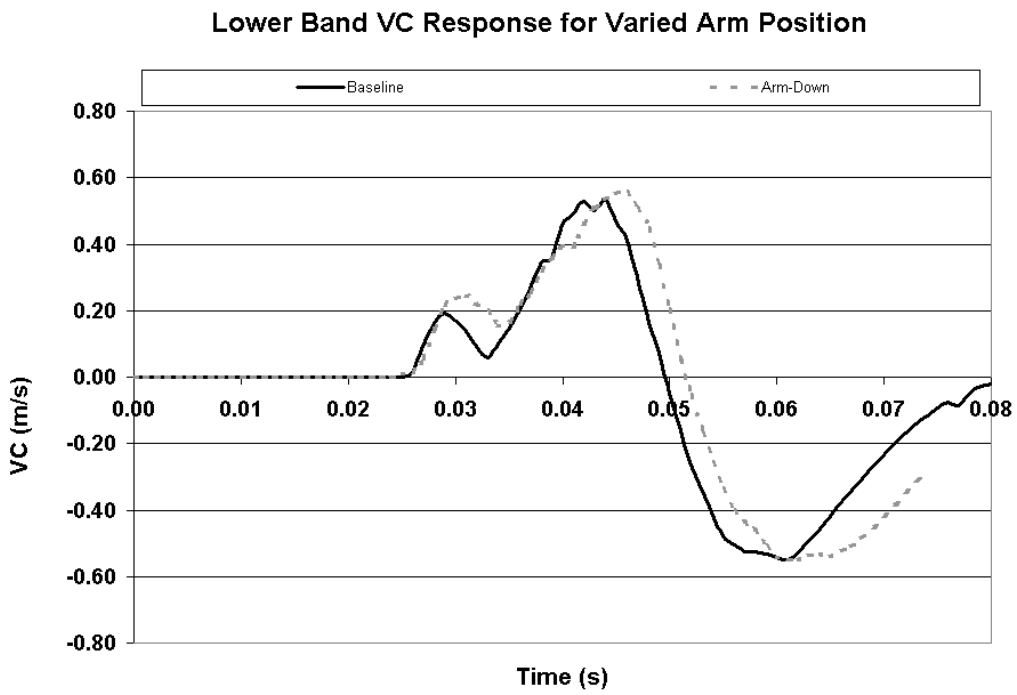

A. 27 Lower Band VC Response for Varied Arm Position

Middle Chest Band

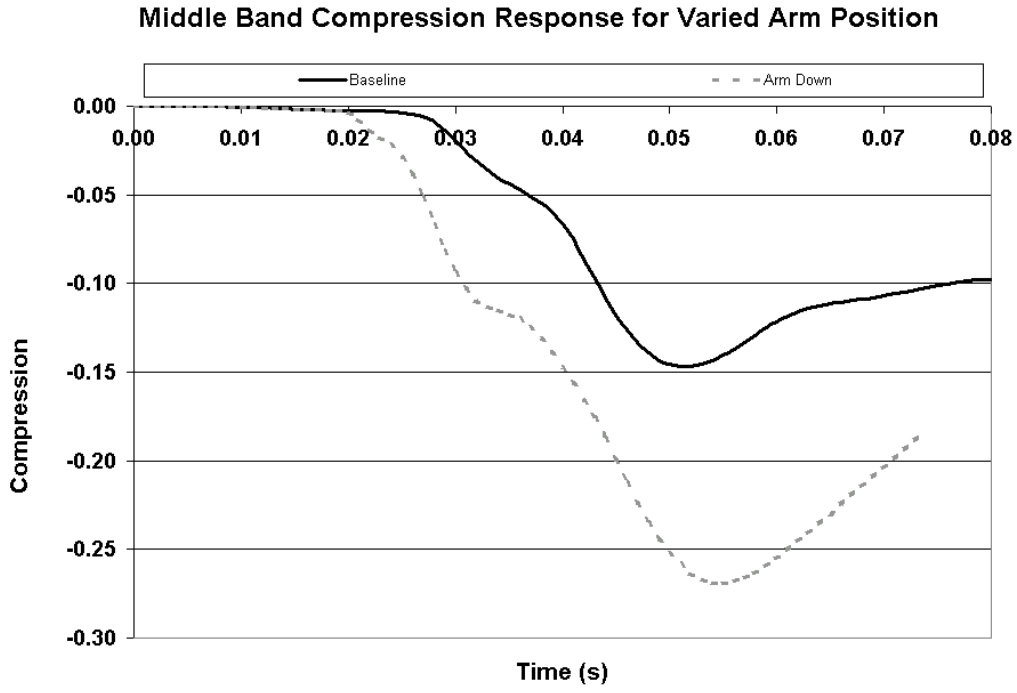

A. 28 Middle Band Compession Response for Varied Arm Position

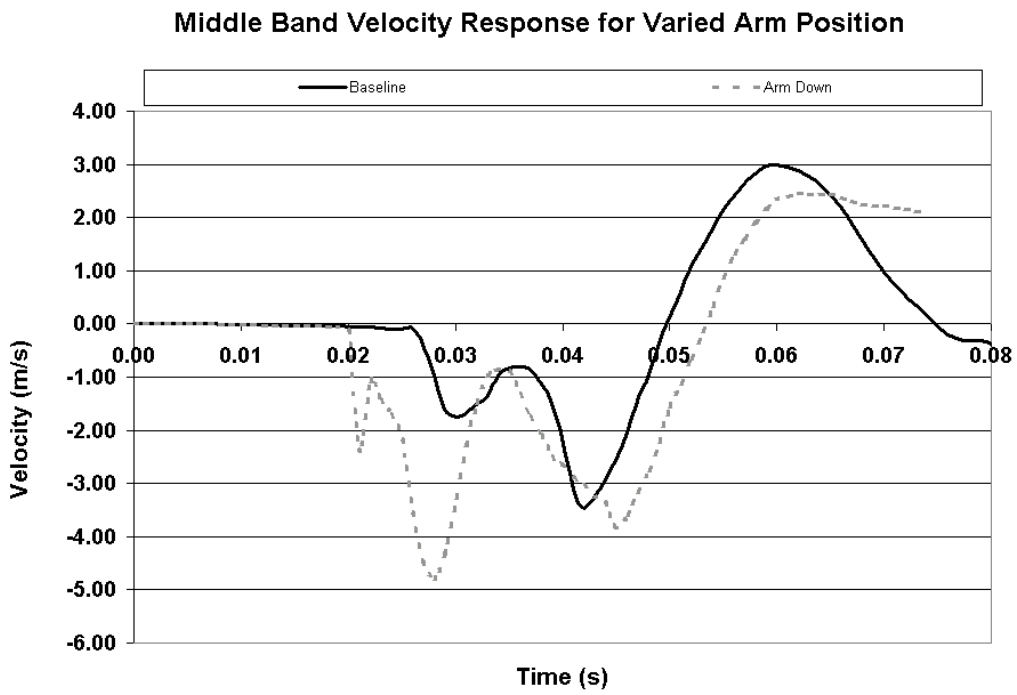

A. 29 Middle Band Velocity Response for Varied Arm Position

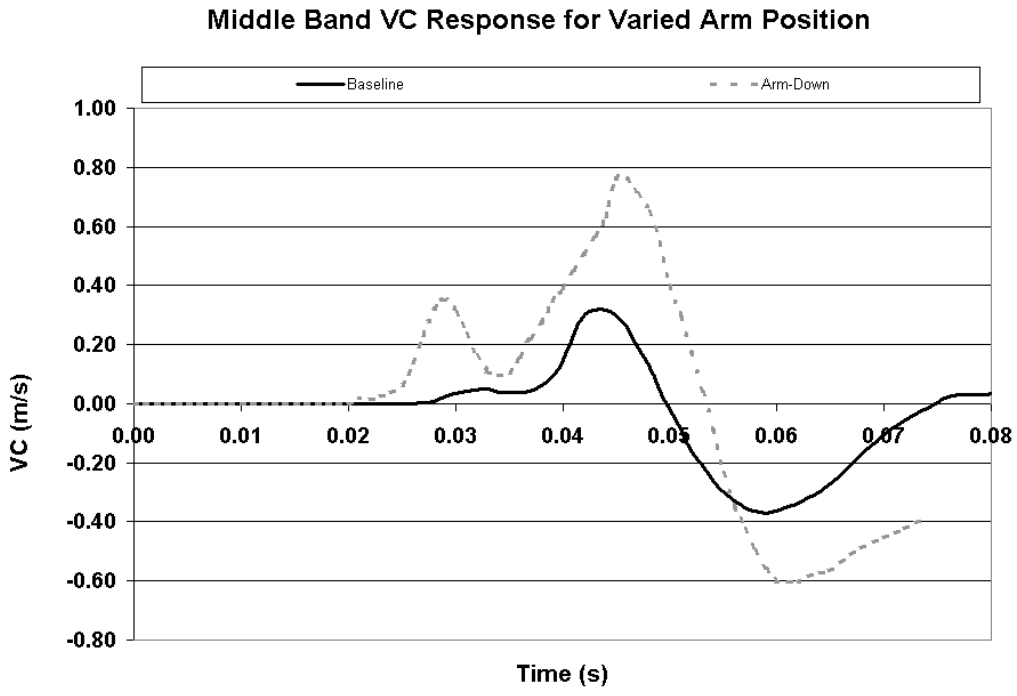

A. 30 Middle Band VC Response for Varied Arm Position

A.6 The Response of Belted and Un-belted Occupants

Lower Chest Band

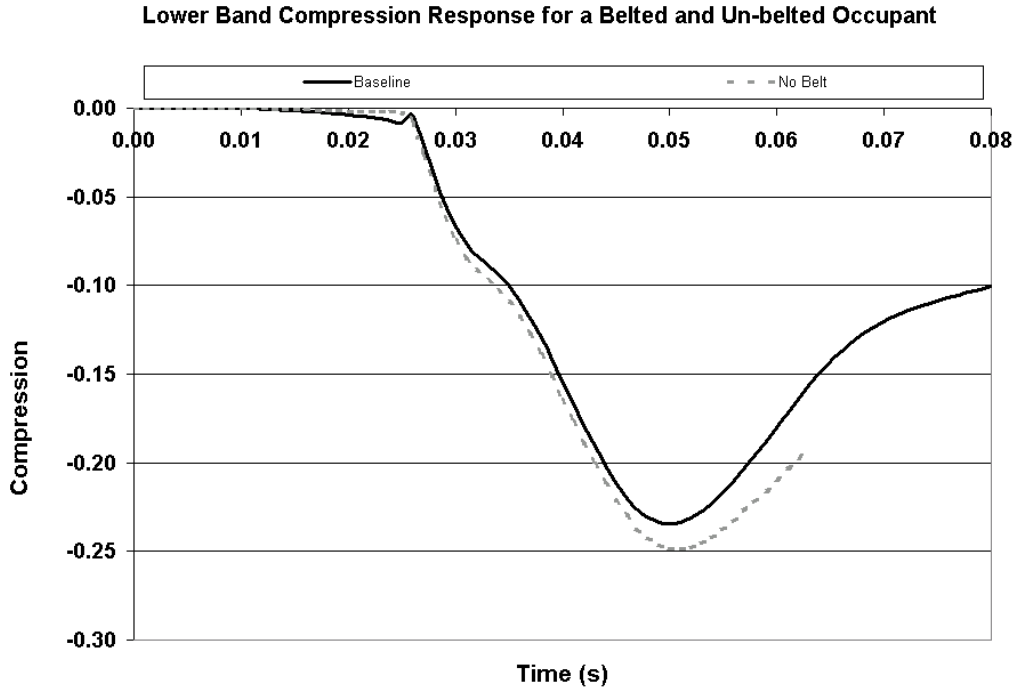

A. 31 Lower Band Compression Response for a Belted and Un-belted Occupant

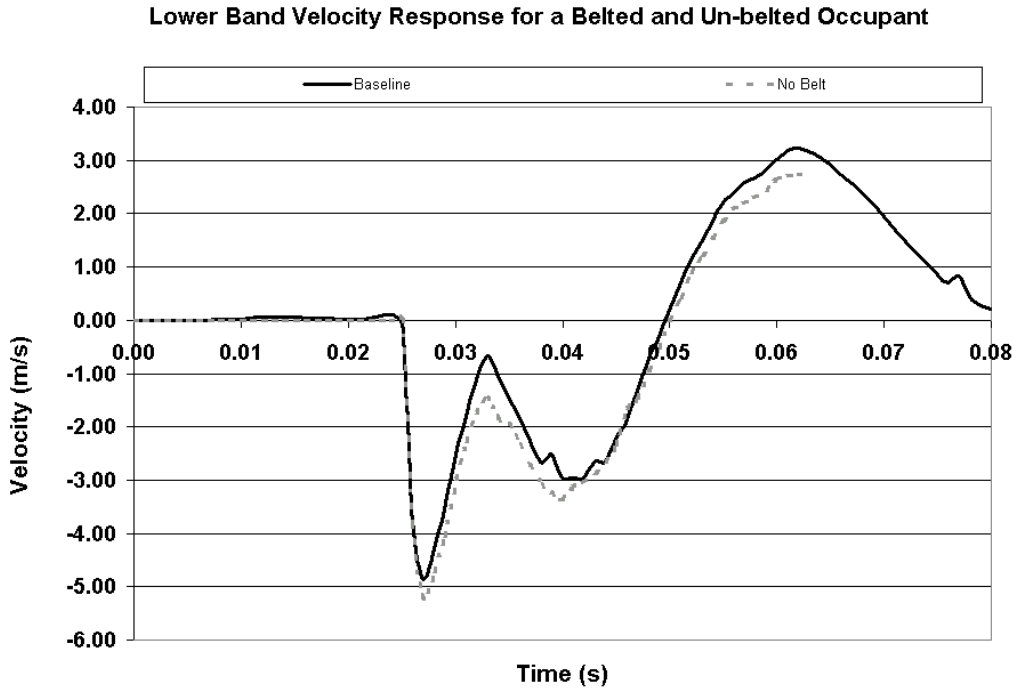

A. 32 Lower Band Velocity Response for a Belted and Un-belted Occupant

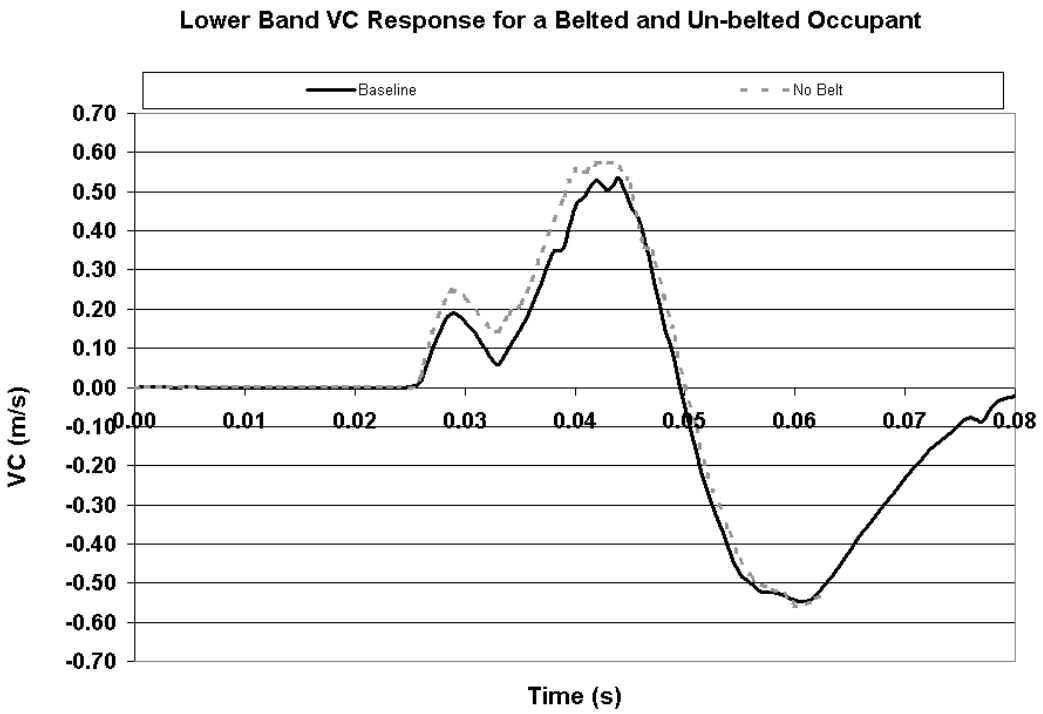

A. 33 Lower Band VC Response for a Belted and Un-belted Occupant

Middle Chest Band

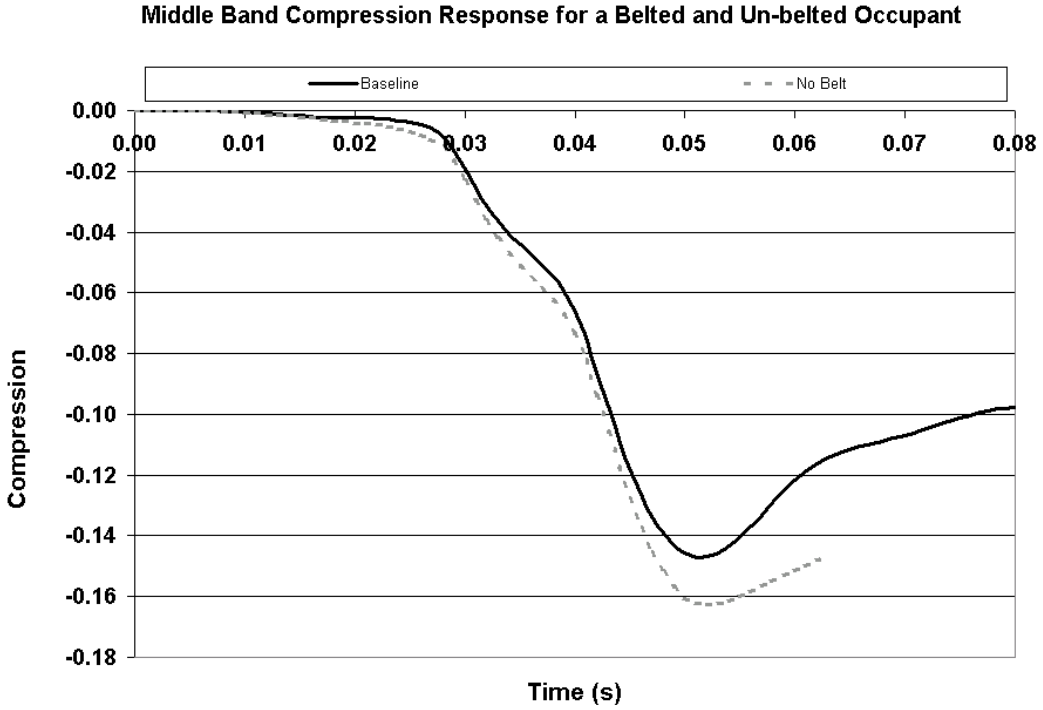

A. 34 Middle Band Compression Response for a Belted and Un-belted Occupant

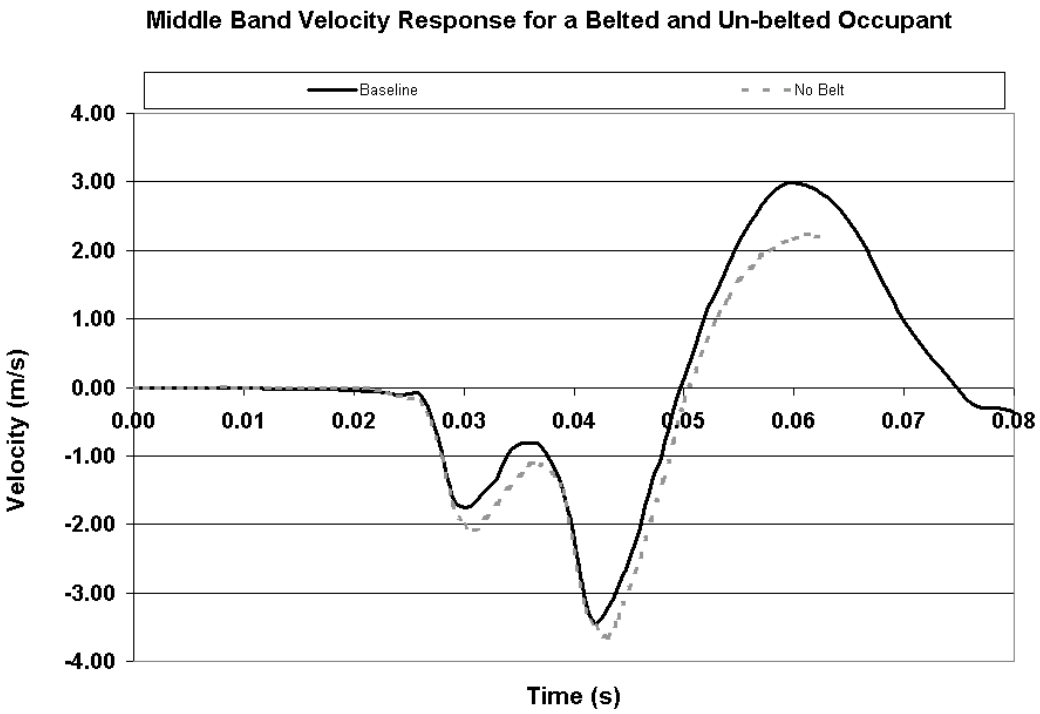

A. 35 Middle Band Compression Response for a Belted and Un-belted Occupant

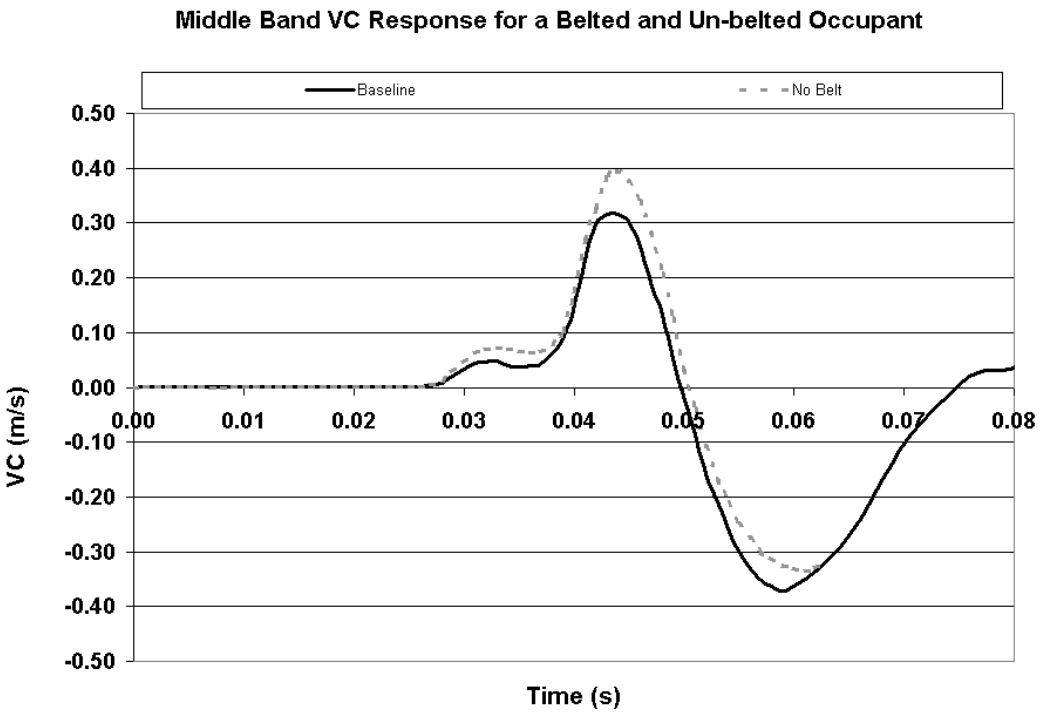

A. 36 Middle Band VC Response for a Belted and Un-belted Occupant